'*In Vivo* Adaptation of Tendon Material Properties in Healthy and Diseased Tendons with Application to Rotator Cuff Disease'

A thesis submitted for the degree of Doctor of Philosophy in Materials Science at the University of Oxford

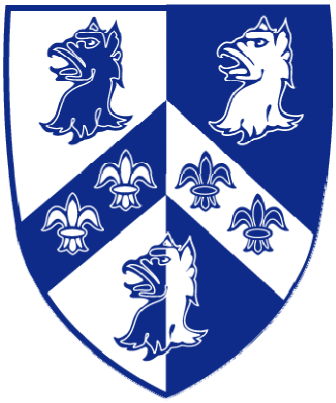

Jennifer Miriam Ruth Tilley

Trinity College, University of Oxford

Trinity Term 2012

***In Vivo* Adaptation of Tendon Material Properties in Healthy and Diseased Tendons with Application to Rotator Cuff Disease**

Jennifer M. R. Tilley, Trinity College. **DPhil Candidate, Trinity Term 2012**

ABSTRACT

Degenerative disorders of the rotator cuff tendons account for nearly 75% of all shoulder pain, causing considerable pain and morbidity. Given the strong correlation between age and tendinopathy, and unprecedented population aging, these disorders will become increasingly prevalent. Improved understanding of tendon degeneration will guide the development of future diagnostic and treatments, and is therefore urgently needed. However, the aetiology and pathology of rotator cuff tendinopathy remain unclear.

The complicated mechanical environment of the rotator cuff is hypothesised to influence the susceptibility of the tendons to degeneration and tearing. Studies have reported biological adaptations in torn cuff tendons indicative of increased compressive loading within the tendon. The material adaptations of healthy and degenerative cuff tendons are largely unreported but will provide further insight into the role of the mechanical environment in rotator cuff aetiology and pathology. This thesis examined the material adaptations of healthy and diseased tendons to explore the role of mechanical loading in rotator cuff pathology. The material adaptations of healthy animal tendons, and healthy and delaminated human cadaveric rotator cuff tendons, in response to different loading environments were characterised. The effects of age, tears, steroid injection and subacromial decompression surgery on the structural adaptations of human cuff tendons were also studied, as was the effect of tendon cell proliferation on the mechanical properties and degradation behaviour of collagen scaffolds.

Loading environment significantly affected the structural adaptations of healthy tendons. Regions exposed to compressive and shear strains exhibited thinner fibres, shorter crimp lengths and thinner, less aligned fibrils compared with regions exposed to tensile strains alone. In healthy rotator cuff tendons, the inhomogeneous loading environment produced topographically inhomogeneous structural adaptations. The tendons of a delaminated rotator cuff exhibited less topographical variation in properties and thinner, less aligned fibrils compared with healthy cuff tendons. Torn cuff tendons exhibited thinner fibrils and shorter crimp lengths compared with control samples. These adaptations were identifiable early in the disease progression, and neither steroid injection nor subacromial decompression surgery significantly influenced these adaptations at seven weeks post-treatment. Significant correlations between decreasing dimensions and increasing tear size were found when age was included as a confounding factor, reflecting the importance of age and tear size in determining the material properties of tendons. Tendon cell proliferation influenced the mechanical properties and degradation behaviour of the collagen scaffolds, emphasising the integral role of cells in the functional adaptation of biological materials.

These results demonstrate the effect of mechanical environment on the material adaptations of tendons. They also indicate the importance of the complicated mechanical environment experienced by the rotator cuff tendons in predisposing the tendons to degeneration and tearing. The observed material adaptations of degenerative and torn tendons suggest that rotator cuff pathology is associated with increased levels of compressive and/or shear strains within the tendon. These changes begin early in the disease progression and neither steroid injection nor sub-acromial decompression surgery are capable of reversing the changes in the timeframe investigated. These findings highlight the urgent clinical need for pre-rupture diagnostic techniques for the detection of early pathological changes in the rotator cuff. They also emphasize the requirement for new intervention strategies that restore the healthy mechanical environment and reverse early pathological adaptations in order to prevent catastrophic failure of the tendons.

Preface

The research presented in this thesis is the result of work carried out in the Department of Materials and the Botnar Research Centre, University of Oxford, under the joint supervision of Dr. Jan Czernuszka (Materials) and Prof. Andrew Carr (Botnar), between October 2008 and April 2012.

No part of this thesis has been previously submitted for a degree at this, or any other, university. Where the work of other authors has been drawn upon, this is referenced or acknowledged in the text. A full list of cited references can be found in the bibliography at the end of thesis.

This work is funded by a doctoral training scholarship from the EPSRC and supported by funding from the NIHR Oxford Biomedical Research Unit. I would also like to acknowledge funding in the form of postgraduate research travel grants from Trinity College.

Jennifer M. R. Tilley
Trinity College, Oxford
24 April 2014

Publications and Conferences

Parts of the work described in this thesis are reproduced from Journal articles with full permission from the publisher, and have been presented at national and international conferences as follows:

Micron 42(5) p.531-535 Atomic Force Microscopy of Bulk Tendon Samples: Affect of Location and Fixation on Tissue Ultrastructure. Tilley, J.M.R., Carr, A.J., Czernuszka, J.T. Copyright (2011). Adapted for use in Chapter Four, Sections 4.1.1.1, 4.1.2.2, 4.1.4.4, 4.2.3, 4.3.1.4, and 4.3.2.1 with permission from Elsevier [DOI: 10.1016/j.micron.2011.01.001]

Journal of Materials Science: Materials in Medicine 23(3) p823-33 Tenocyte proliferation on collagen scaffolds protects against degradation and improves scaffold properties. Tilley, J.M.R., Chaudhury, S., Hakimi, O., Carr, A.J., Czernuszka, C.T. Copyright (2011). Adapted for use in Chapter Ten with kind permission from Springer Science and Business Media [DOI: 10.1007/s10856-011-4537-7]

22nd European Conference on Biomaterials, **Lausanne.** A Collagen Scaffold for Tissue Engineering: Effects of Freeze Drying and Crosslinking on Thermal, Mechanical Enzymatic Degradation Properties and In Vitro-Biodegradation. Yahyouche, A., Tilley, J.M.R., Czernuszka, J.T. (Sep 2009)

3rd International Conference on Mechanics of Biomaterials and Tissues, **Florida.** Mechanical Response of Collagen Scaffolds *In Vitro.* Tilley, J.M.R., Carr, A.J., Czernuszka, J.T. (Dec 2009)

2nd China-Europe Symposium on Biomaterials in Regenerative Medicine, Barcelona. Mechanical Response of Collagen Scaffolds *In Vitro*. Tilley, J.M.R., Carr, A.J., Czernuszka, J.T. (Nov 2009)

British Society of Matrix Biology Spring Meeting, Bristol. Effect of *In Vivo* Stress Distribution on the Structure and Composition of Ovine and Human Rotator Cuff Tendons. Tilley, J.M.R., Chaudhury, S., Carr, A.J., Czernuszka, J.T. (Apr 2011)

International Symposium on Ligaments and Tendons-XII, San Francisco. Effect of Degenerative Rotator Cuff Tears and Subacromial Bursa Steroid Injection on the Structural Properties of the Supraspinatus Tendon. Tilley, J.M.R., Murphy, R.J., Chaudhury, S. Carr, A.J., Czernuszka, J.T. (Feb 2012)

British Society of Matrix Biology Special Meeting: Tendinopathy, Norwich. Structural Adaptations Rotator Cuff Tendons Associated with Degeneration, Tearing and Treatment Highlight the Need for Improved Tendon Diagnostics and Early Intervention Strategies. Tilley, J.M.R. Murphy, R.J. Chaudhury, S. Czernuszka, J.T., Carr, A.J. (Sep 2012)

Acknowledgements

The multidisciplinary nature of the work in this thesis has necessitated working in at least four different departments across two universities. Consequently, there are many people without whose help this research project would be a fragment of what it has become.

Firstly I wish to thank my **supervisors**, Dr. Jan Czernuszka (Head of Biomaterials and Tissue Engineering research group, Department of Materials) and Prof. Andrew Carr (Head of Department, Nuffield Department of Orthopaedics, Rheumatology and Musculoskeletal Sciences), both of whom have provided invaluable support and guidance, whilst allowing me the freedom to develop my own research project within the scope of their research interests. I am incredibly grateful for the opportunities they have provided me with.

As a DPhil student in the **Department of Materials**, University of Oxford, I would like to thank past and present members of the Biomaterials Research group, in particular Asma Yahyouche who provided training in scaffold production and cell work, and Jessica Smith for provision of enzyme-treated tendon samples and for being a lovely Part II student to supervise! I would also like to thank Prof. Chris Grovenor for provision of laboratory space, Prof. Steve Roberts for access to mechanical testing equipment, Dr. David Armstrong and Sophie Godard-Desmarest for training and guidance in nanoindentation, Dr. Keyna O' Reilley for access to differential scanning calorimetery and Nick Rounthwaite for training in its use, Dr. Dan Haley for advice on image analysis and kindly writing the colour thresholding macro and Dr. Matthew Thomas for advice on AFM image processing.

At the **Oxford Materials Characterisation Service (Begbroke)** I would like to thank Dr. Alison Crossley for access to research equipment, Dr. Colin Johnson for spectroscopy training and advice, Dr. Sverre Myhra for training and guidance in Atomic Force Microscopy, Dr. Vanessa Cheel and Clive Dowling for optical microscopy training, and Gabriella Chapman for SEM training.

At the **Botnar Research Centre** I would particularly like to thank members of Prof. Carr's tendon research group, in particular Dr. Osnat Hakimi for provision of cells, guidance in cell work and advice on the cell work chapter, Dr. Richard Murphy for provision of tissue and lessons in dissection and animal anatomy, Dr. Salma

Chaudhury for provision of cells and tissue, Dr. Sarah Franklin for her editing skills, Dr. Hannah Oag for help with cadaveric dissection, and Dr. James Edwards for general advice and support. I would also like to thank Dr. Philippa Hulley for access to laboratory space and histological stains and cell culture advice, Dr. Zhidao Xia for access to cell culture facilities, Dr. Richard Taylor for provision of cells, Dr. Udo Tirlapur for access to optical microscopes, Dr. Clarence Yapp for optical microscopy guidance, Dr. Andrew Judge for advice on statistical analysis, Prof. Amy Zvatsky for access to laboratory facilities. I would also like to express my gratitude to Dr. Cameron Brown, who stepped in at the last minute to help with Raman spectral analysis when a collaboration proved unfruitful.

I would like to thank the staff at the **Oxford Musculoskeletal BioBank** for their help with access to human tissue. In particular, I would like to thank Karolina Kliskey and Matthew Burgess for help with ethics applications and obtaining access to tissues, invaluable guidance on sample preparation and histological procedures, and access to laboratory space. I would also like to thank Prof. John Morris of the **Medical Sciences Teaching Centre** for access to cadaveric material, and Ryan Green for technical support.

Outside of University of Oxford, I would like to thank Prof. Chris Hawes for access to ultra-microtome equipment, Gareth Morgan for microtome and sample processing training and Barry Martin for microtomy support, all of whom are based in the **Plant Sciences Department at Oxford Brookes University**. I would like to thank Dr. Kevin Buckley (**STFC, Rutherford Appleton Laboratory**) for help with processing of Raman spectra.

I would like to thank the many administrative and support staff within the Department of Materials, NDORMS and Trinity College. In particular I would like to express my gratitude to Annabel Ownsworth, Isabel Lough, Alastair Johnston, Sharon Cure, Lyn Richmond, Marion Beckett, Adrian Taylor, Keith Maule and John Royal.

On a personal note, I would like to thank Prof. George Smith and Dr. Mike Jenkins, for the invaluable support and guidance they provided as my college advisors at Trinity College. I would also like to thank friends, old and new, for their patience and friendship over the past 3.5 years. Finally, I wish to thank my parents, my sister, and Graeme Spence for their patience, their love, and their unfailing belief that my best is good enough.

Abbreviations

AFM	Atomic Force Microscopy / Microscope
Ant.	Anterior
DDFT	Deep Digital Flexor Tendon
DFT	Digital Flexor tendon
dH_2O	Distilled H_20
ECM	Extracellular matrix
FA	Formalin / Formaldehyde
FFT	Foot Flexor Tenocyte (a.k.a. Foot Flexor Tendon-derived Cell)
GA	Glutaraldehyde
GAG	Glycosaminoglycan
IMS	Industrial Methylated Spirits
PG	Proteoglycan
Post.	Posterior
SAD	Sub-acromial decompression
SDFT	Superficial Digital Flexor Tendon
SLRP	Small Leucine-Rich Repeat Proteoglycan

Glossary

Abduct[*] to move a limb or any other part of the body away from the midline of the body.
–**abduction** *n.*

Acromion[1] an oblong process at the top of the spine of the scapula.
–**acromial** *adj.*

Adipose tissue[1] fibrous connective tissue packed with masses of fat cells.

Aggrecan a high molecular weight proteoglycan with approximately 100-150 chondroitin sulfate and keratin sulfate side-chains attached to its core protein. Major structural proteoglycan in the extracellular matrix of cartilage.

Aldehyde[†] organic compound that contains the –CH=O group.

Anterior[1] describing or relating to the front (**ventral**) portion of the body or limbs.
c.f. **posterior**

Anterior stabilisation of the shoulder[‡] surgical procedure which aims to tighten and/or repair the over-stretched and damaged ligaments, rim of cartilage and muscle damaged by recurrent dislocation of the shoulder.

Apoptosis[2] programmed cell death.
–**apoptotic** *adj.*

Arthroscopic surgery procedure enabling a surgeon to repair the interior of a joint through a small incision.

Atrophy[1] the wasting away of a normally developed organ or tissue due to degeneration of the cells. This may occur due to undernourishment, disuse, or aging.

Biglycan a small, leucine-rich repeat proteoglycan with two chondroitin sulfate and/or dermatan sulfate side chains found in a range of connective tissues.

Bony process[3] a prominence on a bone.

Bursa[1] a small sac of fibrous tissue that is lined with synovial membrane and filled with fluid.
–**bursal** *adj.*

---

1. Oxford Concise Colour Medical Dictionary, 1st edition (1996). E.A. Martin (Ed.). Oxford University Press, Oxford.
2. Marieb, E.N., (2001). Human Anatomy & Physiology, 5th edition. Edited by.Benjamin Cummings, San Francisco / London.
3. Yeovil Elbow and Shoulder Service (2009). Information for You after Your Operation: Anterior Stabilisation of the Shoulder. Published by Yeovil District Hospital, NHS Foundation Trust. Accessed on 05/05/11. Available from http://www.yeovilhospital.nhs.uk/Downloads/Patient%20information%20leaflets/Orthopaedics/Anterior-stabilisation-of-the-shoulder-post-op.pdf

Bursa-side[1]	on the side of the bursa.
Chondrocyte[3]	mature cell found in cartilage.
Chondroid metaplasia	replacement of differentiated cells in a particular tissue with mature differentiated cells typically found in cartilage.
Chondroitin sulphate[1]	a mucopolysaccharide that forms an important constituent of cartilage, bone and other connective tissues. It is composed of glucuronic acid and N-acetyl-D-galactosamine units.
Chondroitinase ABC	an enzyme that acts to breakdown chondroitin sulfate A, chondroitin sulfate B and chondroitin sulfate C.
Collagen profile	the ratio of different types of collagen present in a particular tissue or organ.
Confounding variable	a variable other than the independent variable in a statistical model that correlates with the dependent and independent variables measured; i.e. a variable which affects the measurements of an experiment such that the experimental results will not solely reflect the correlation between the investigated variables.
Connective tissue[1]	the tissue that supports, binds, or separates more specialised tissues and organs or functions as a packing tissue of the body.
Corticosteroid[1]	any steroid hormone synthesised by the adrenal cortex.
Crimp	characteristic zigzag pattern found in tendon at the microstructural level; can be defined by a length, amplitude and angle.
Critical zone	hypovascular area on the articular-side of the supraspinatus tendon, close to the enthesis.
'D' spacing	characteristic striations that run perpendicular to the long axis of a collagen fibril; thought to be related to the stacking of the tropocollagen molecules within the fibril.
Decorin	a small, leucine-rich repeat proteoglycan with one chondroitin sulfate or dermatan sulfate side chain found in a range of connective tissues; binds to collagen fibrils and is thought to play a role in regulation of collagen fibrillogenesis.
Degeneration[1]	the deterioration and loss of specialised function of the cells or tissues of an organ. -**degenerative** *adj.*
Delamination	separation of the layers in a fibrous composite
Dermatan sulphate	(a.k.a. **Chondroitin sulfate B**) a mucopolysaccharide that forms an important constituent of skin, blood vessels, heart valves, lungs and tendon. Generally no longer classified as a form of chondroitin sulfate.

Distal[1]	situated away from the origin or point of attachment or from the median line of the body. *c.f.* **proximal**
Dorsal*	relating to or situated at or close to the back of the body or to the posterior part of an organ. *c.f.* **ventral**
Enthesis[1]	the junction of tendon and bone.
Enzyme[1]	a protein that, in small amounts, speeds up the rate of a biological reaction without itself being used up in the reaction (i.e. it acts as a catalyst).
Fascicles[1]	(a.k.a **fasciculus**) a bundle, e.g. of nerve or muscle fibres.
Fatty degeneration[1]	deterioration in the health of a tissue due to the deposition of abnormally large amounts of fat in its cells.
Fibrillogenesis	the formation and development of collagen fibrils.
Fibril[1]	a very small fibre or a constituent thread or a fibre. **–fibrillar** *adj.*
Fibroblast[1]	a widely distributed cell in connective tissue that is responsible for the production of both the ground substance and of the precursors of collagen, elastic fibres, and reticular fibres.
Fibrocartilage[1]	a tough kind of cartilage in which there are dense bundles of fibres in the matrix.
Fibronectin[1]	a large glycoprotein that acts as a host defence mechanism.
Fossa[3]	a shallow, basin-like depression in a bone, often an articular surface.
Full thickness rotator cuff tear	a tear spanning the full superior-inferior thickness of one or more rotator cuff tendons.
Glenoid cavity[1]	(a.k.a. **glenoid fossa**) the socket of the shoulder joint.
Glycosaminoglycan[2]	long, linear, highly charged polysaccharide composed of repeating pairs of sugars, one of which is always an amino sugar. Mainly found covalently linked to a protein core in extracellular matrix proteoglycans.
Greater tubercle	the tubercle of the humerus, lateral to the humeral head.
Ground substance[1]	the matrix of connective tissue, in which various fibres and cells are embedded.
Hemiarthroplasty	joint replacement operation.

Humeral head	the head of the humerus.
***In vitro*[1]**	describing biological phenomena that are made to occur outside the living body.
***In vivo*[1]**	describing biological phenomena that occur or are observed occurring within the bodies of living organisms.
Inferior[1]	lower in the body in relation to another structure or surface. *c.f.* **superior**
Infraspinatus[3]	muscle [and associated tendon] named for its scapular location; a rotator cuff muscle. Origin: infraspinous fossa of scapular. Insertion: greater tubercle of humerus, posterior to insertion of supraspinatus.
Inter-fascicle[1]	lying between fascicles.
Inter-fibre[1]	lying between fibres.
Inter-fibrillar[1]	lying between fibrils.
Knock-out model	genetically-engineered animal model in which a particular gene, or genes, is inactivated.
Lateral[1]	1. Situated at or relating to the side of an organ or organism. 2. Relating to the region or parts of the body that are furthest from the medial plane. *c.f.* **medial**
Lipoid degeneration	*(a.k.a.* **fatty degeneration**) deterioration in the health of a tissue due to the deposition of abnormally large amounts of fat in its cells.
Macroscopic[1]	visible to the naked eye.
Matrix metalloproteinase	an enzyme that acts to breakdown extracellular matrix proteins.
Maturation[1]	the process of obtaining full development.
Medial[1]	related to or situated in the central region of an organ, tissue or the body. *c.f.* **lateral**
Micro-trauma	damage and/or injury to the body, an organ, or a tissue on the micrometre scale. *E.g.* tearing of collagen fibrils.
Morbidity[1]	the state of being diseased.
Mucoid degeneration	accumulation of deposits of proteoglycans and glycosaminoglycans in a tissue or organ.

Mucopolysaccharide[1] — one of a group of complex carbohydrates functioning mainly as structural components in connective tissue. Mucopolysaccharide molecules are usually built up of two repeating sugar units, one of which is an amino sugar.

Musculotendinous junction — junction between muscle and tendon.

Nanoindentation — instrumented indentation at nanometre indentation depths.

Partial tear — a tear that does not span the full superior-inferior thickness of one or more rotator cuff tendons.

Phenotype[2] — the observable character of a cell or an organism.

Posterior[1] — situated at or near the back of the body or an organ.
c.f. **anterior**

Proteoglycan[2] — molecule consisting of one or more glycosaminoglycan (GAG) chains attached to a core protein.

Proximal[1] — situated close to the origin or at the point of attachment or close to the medial line of the body.
c.f. **distal**

Scapula[1] — the shoulder blade: a triangular bone, a pair of which form the back part of the shoulder girdle. The spine on its dorsal (back) surface ends at the acromion process at the top of the shoulder.

Senescence[1] — the condition of aging, which is often marked by a decrease in physical and mental abilities.
–senescent *adj.*

Significant difference — the results are statistically different, i.e. result is unlikely to have occurred by chance alone.

Subacromial[1] — below the acromion.

Impingement — narrowing of the gap between the acromion and the rotator cuff causing the acromion to impose on / rub against the subacromial bursa and the rotator cuff tendons.

Subscapularis[3] — muscle [and associated tendon] that passes under the scapular to the front of the shoulder joint; a rotator cuff muscle.
Origin: subscapular fossa of scapular.
Insertion: lesser tubercle of humerus.

Superior[1] — situated uppermost in the body in relation to another structure or surface.
c.f. **inferior**

Supraspinatus[3] — muscle [and associated tendon] named for its location on the posterior aspect of the scapula; a rotator cuff muscle.
Origin: supraspinous fossa of scapula.
Insertion: superior part of greater tubercle of humerus.

Tendinitis[1]	acute inflammation of a tendon. Occurs most commonly after excessive overuse but is sometimes due to bacterial infection or a generalised rheumatic disease.
Tendinopathy	disease of the tendon.
Tendinosis	non-inflammatory (or post-inflammatory) chronic disorder of tendon.
Tendon[1]	a tough whitish cord, consisting of numerous parallel bundles of collagen fibres, that serves to attach a muscle to a bone.
Tenoblast	tendon cell that is ovoid in shape; considered to be immature tenocyte precursor.
Tenocyte	(*a.k.a.* **tendon forming cell, tendon fibroblast**) elongated, specialised fibroblast found in tendon.
Teres minor[3]	small, elongated muscle [and associated tendon]; lies inferior to infraspinatus and may be inseparable from that muscle; a rotator cuff muscle. Origin: lateral border of the dorsal scapular surface. Insertion: greater tubercle of the humerus, inferior to infraspinatus insertion.
Tropocollagen[1]	the molecular unit of collagen; consists of a helix of three collagen molecules.
Ultrastructure	structure of a biological material on a sub-micron scale; i.e. not visible using light microscopy.
Vascular[1]	relating to or supplied with blood vessels.
Ventral[1]	relating to or situated at or close to the front of the body or to the anterior part of an organ. *c.f.* **dorsal**
Wrap-around tendon	tendon which wraps around, and articulates with, a bone.

Table of Contents

List of Figures

PART I

INTRODUCTION

Chapter One

Clinical Motivation

Chronic, non-inflammatory tendon disorders, generally referred to as tendinosis, are widespread and debilitating. These degenerative disorders are associated with failed healing of the tendon after micro-traumas and commonly affect energy storage tendons such as those in the hand, wrist, forearm, elbow, shoulder, knee, and heel often leading to rupture. Conditions such as jumper's knee, tennis elbow, runner's heel, pitcher's shoulder are common amongst athletes: the incidence of runner's heel (Achilles tendinosis) is almost 50% in elite endurance athletes and greater than 10% in soccer players [4, 5], swimmer's shoulder (supraspinatus tendinosis) is reportedly seen in 67% of elite swimmers [6, 7], tennis elbow (lateral epicondylitis) affects up to half of club tennis players over the age of 30 [8-10], and prevalence of jumper's knee (patellar tendinosis) is greater than 10% across the athletic community, affecting almost 50% of elite male volleyball players and up to 40% of basketball players [11-13].

Tendinosis is not limited to the athletic community. Incidence of tendinosis is reportedly 11 per 100,000 workers in the USA [14] while a Swedish study found that approximately 5% of a sample population visiting a rheumatologist were suffering from chronic tendinitis (a common mis-diagnosis of tendinosis) [15]. It has been reported that 6-31% of sedentary people experience Achilles tendinosis during their lifetime [4, 16, 17], while an estimated 3% of the population suffer from lateral epicondylitis, making it the most prevalent elbow condition [18]. Supraspinatus tendinosis, generally referred to as rotator cuff disease, is a particular issue in the general population; shoulder pain affects up to 30% of the population and is most commonly caused (up to 75% of all shoulder pain) by disorders of the rotator cuff tendons [19]. These disorders range from inflammation and tendinitis to full thickness tears and tendinosis of the cuff tendons. Incidence of rotator cuff tears is also reportedly in excess of 20% in the general population [20-23], but is thought to be

higher in older sub-populations [24, 25], and participants in manual labour, particularly those who work at, or above, shoulder height [26].

The aetiology of chronic degenerative tendon disorders is unclear but is considered to be related to tissue degeneration, possibly associated with aging and mechanical loading. As early as 1959, Arner et al proposed that degeneration played a significant role in tendon and ligament ruptures, based on their findings that all of the ruptured tendons they examined contained 'degenerative lesions' [27]. In a seminal study, Kannus et al [28] showed that degenerative changes, such as hypoxic degeneration (oxygen starvation), mucoid degeneration (increased ground substance), lipoid degeneration (fatty degeneration) and calcifying tendinopathy (calcium deposits) are associated with spontaneous rupture, and are also increasingly common in older patients, regardless of pre-rupture symptoms. Subsequent studies have provided further evidence supporting the link between degeneration, tendinosis and rupture [29, 30]. These studies have shown that degeneration and ruptures are also associated with changing collagen and ground substance profiles, decreased metabolism, increased apoptosis and altered enzyme concentrations [31, 32]. Furthermore, tears of the rotator cuff tendons are thought to be associated with alterations in the complex stress distributions within the cuff tendons, with partial tears resulting in larger regions of compressive stresses in the extracellular matrix (ECM) surrounding the tear [33-35]. In agreement with these studies increased concentrations and sizes of proteoglycans and glycosaminoglycans [24, 36] (substances typically associated with compressive stresses [37, 38]), and evidence of chondroid metaplasia [32, 39-41] have been reported in torn cuff tendons.

Since the structure of biological materials is intrinsically related to their loading environment, alterations in loading can be expected to produce structural changes in the extracellular matrix (ECM) of torn cuff tendons [42]. Changes in the thermal stability and structural organisation of torn cuff tendons have previously been reported [43]. However, to date quantitative data regarding the effect of rotator cuff tears on the micro- and ultrastructural properties of the extracellular matrix of the tendons, a characteristic known to be sensitive to the loading environment [44], has not been reported.

Given the strong correlation between patient age and tendon disease [18, 45], and recent levels of population aging [46], tendinosis prevalence is set to increase. Improved understanding and diagnosis of

non-inflammatory tendon disorders is therefore urgently needed to aid clinician decision-making. The primary objective of the research presented in this thesis is therefore to expand current knowledge regarding the material adaptations of rotator cuff tendons in order to elucidate further information regarding the influence of the mechanical environment in the aetiology and pathology of rotator cuff tendinosis. The effectiveness of common treatment modalities and the viability of tissue engineering for treatment of rotator cuff tears will also be investigated in order to provide information that may guide future research and clinical decision-making.

Chapter Two

Thesis Outline

The work presented in this thesis is arranged as follows.

Part II acts as an introduction to the material adaptations of tendon. In Chapter 3 the background literature concerning the material characteristics of tendon, their adaptability to different mechanical environments, and their importance in determining the mechanical properties of tendon is reviewed, with a focus on the adaptations of wrap-around tendons. In Chapter 4 a range of characterisation techniques is used to compare the material adaptations of wrap-around tendons in two animal models. The suitability of each technique for determining the adaptations of the tendon is evaluated in order to establish a portfolio of techniques suitable for characterising the adaptations of the human rotator cuff tendon in health and disease. Concurrently, the adaptations of these tendons as a result of the different loading conditions they experience are characterised. The inter-relation of the compositional and structural adaptations is also investigated.

Part III investigates the material adaptations of the rotator cuff tendons. Chapter 5 gives an introduction to function and anatomy of the rotator cuff and the loading environment experienced by the cuff tendons. The implications of this for the material adaptation of these tendons and the effect of degeneration and tearing on these adaptations are then discussed. In Chapter 6, the topographical adaptations of the cuff tendons in health and disease are compared. The effect of age and tear progression on the structural adaptation of the supraspinatus tendon are then investigated in Chapter 7.

Part IV investigates the relationship between current treatment and structural adaptations, and the suitability of collagen scaffolds for use in a potential new treatment, tissue engineering. Chapter 8 gives a brief outline of current and future treatment modalities, Chapter 9 investigates the effect of treatment on the structural adaptations of torn tendons, and Chapter 10 investigates the influence of tenocyte proliferation on the degradation behaviour and tensile properties of collagen scaffolds.

Finally, important conclusions and suggestions for further work based on the findings in this thesis are outlined in Part V, Chapter 11.

PART II

MATERIAL ADAPTATIONS OF ANIMAL TENDON

Chapter Three

*Background Literature: Form Follows Function**

3.1 INTRODUCTION

Tendons are the fibrous connective tissues that connect muscle to bone. They must therefore be strong and flexible whilst facilitating highly efficient energy storage and return. This functionality is achieved through the use of fibre reinforced composite material with a hierarchical structure, in which elastic collagen fibres provide strength, flexibility and energy storage, and a viscous mucopolysaccharide matrix provides viscoelasticity. As in all biological materials, the design of this rope-like structure is capable of adapting to the loading environment it experiences. This is achieved by the action of the cells of the tissue, which adapt the composition and structure of the surrounding material in order that the form of the tissue is appropriate for its required function. The purpose of this literature review is to give an insight into the key features of tendons, their adaptability to different mechanical environments, and their importance in determining the mechanical properties of tendon.

3.2 TENDON FUNCTION

Tendons provide structural support whilst facilitating transmission of the muscle contraction forces. Concurrently, they act as shock absorbers, absorbing some of the energy associated with the muscle contraction force in order to prevent damage to the bone, and then returning this energy to the muscle as required [47]. Tendons are thus designed to allow highly efficient energy storage and recovery, greatly increasing the force-generating capacity of the associated muscle [48]. It is important to emphasise that there is a clear distinction between tendon and ligament. While there are similarities between the two tissues, they perform different functions: tendons connect muscle to bone and facilitate force transmission

* Sections of text in this chapter are adapted from **Atomic Force Microscopy (AFM): Principles, Modes of Operation and Limitations 1(6),** H. Yang (Editor). Characterisation of Tendons at Different Length Scales Using Atomic Force Microscopy and Polarised Light Microscopy May Provide Insight into Tendon Disease, J. M. R. Tilley A. J. Carr and J. T. Czernuszka, copyright (2014), with permission from Nova Science Publishers, Inc.

within joints, whereas ligaments connect bone to bone and act to 'prevent excessive or abnormal movements occurring in joints' [49]. In other words, while tendons facilitate joint motion, ligaments prevent it. Consequently, there are distinct biological differences between the two tissues [49-52], and ligament literature will not be included in this review.

3.3 TENDON FORM AND MATERIAL PROPERTIES

To achieve high stiffness and strength coupled with a high degree of flexibility and energy absorption, tendon has evolved to be a fibre composite composed of elastic collagen fibres embedded in a viscous acid mucopolysaccharide matrix. Being biological, this composite material has a far more complicated, hierarchical structure than typical engineering composites, as discussed below (Section 3.3.1).

3.3.1 Collagen Backbone

Thorough reviews of the hierarchical structure of tendon (depicted in Figure 3:1) have already been performed, and will not be repeated in detail here [53, 54]. Briefly, collagen protein triple helices are arranged in a quarter-stagger array, forming tropocollagen molecules with regular striations along their length, the most pronounced of which is termed the 'D' spacing and is thought to correspond to the gap region within the array [55] (Hierarchical level 2, Figure 3:1). These tropocollagen molecules are wound together into fibrils (Hierarchical level 3, Figure 3:1). The fibrils also display the characteristic 'D' spacing, although the manner in which the molecules pack together in order to reproduce the 'D' spacing at this hierarchical level is not known. Fibrils are then wound together to form fibres ((Hierarchical level 4, Figure 3:1), which in turn are wound together to form fascicles (Hierarchical levels 5, 6, Figure 3:1). Alignment of the fascicles parallel to the loading axis therefore gives tendon its tensile strength [56], and the strength and stability of the structure is improved by crosslinking the tropocollagen molecules together via specific lysyl, hydroxylysyl and allysine residues on the telepeptides [57]. As an in-built safety factor, the unloaded fibres contain a crimp pattern (Figure 3:1, Hierarchical level 4), a wave-like formation that must be removed before load is applied directly to the fibres. The average period of this crimp varies with function, loading and collagen type [58]. The vast majority of the collagen present in tendon is type I collagen [59], although some type III and type IV may also be present [51, 60-63].

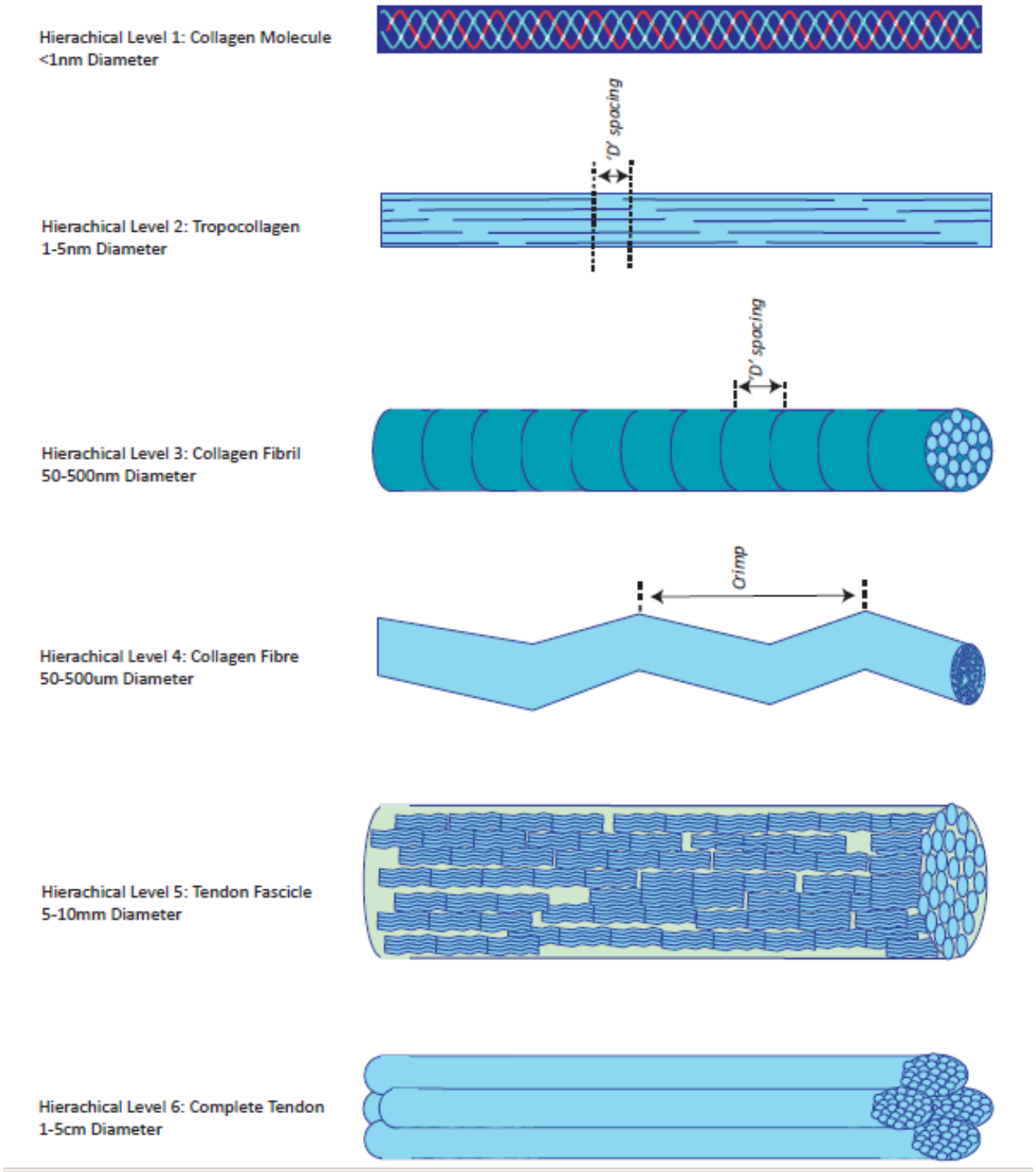

Figure 3:1 Hierarchical Structure of Collagen Architecture in Tendon. Original artwork inspired by previous illustrations by Lakes [64] and Kastelic et al [65].

The characteristic stress-strain curve of tendon, shown in Figure 3:2, can be explained with reference to this hierarchical structure as follows; initially, under tensile loading, the crimp stretches and disappears, giving rise to a low stiffness (low strain Tensile modulus), illustrated in Figure 3:2. Once the crimp has been removed, the tendon reaches the heel point in the curve defined by characteristic heel stress and heel strain as shown on Figure 3:2. Once this point is exceeded, all the load is transmitted directly along the longitudinal axis of the collagen fibres and fascicles, giving an increased stiffness (high strain Tensile modulus), the value of which is determined by stretching and sliding of the fibres and fibrils [66-69]. Finally, the applied load overcomes the forces between the collagen chains, fibrils and fibres and, as the chains begins to slide past each other, the tendon yields and finally fails. It is interesting to note that once the failure point has been exceeded, the stress born by the tendon gradually decreases with increasing extension. This feature of the stress-strain curve of tendon, shown in Figure 3:2, is not often commented upon but may suggest that, as in engineering fibre composites, fibre pull-out from the matrix is an important feature of the failure mechanism of tendon.

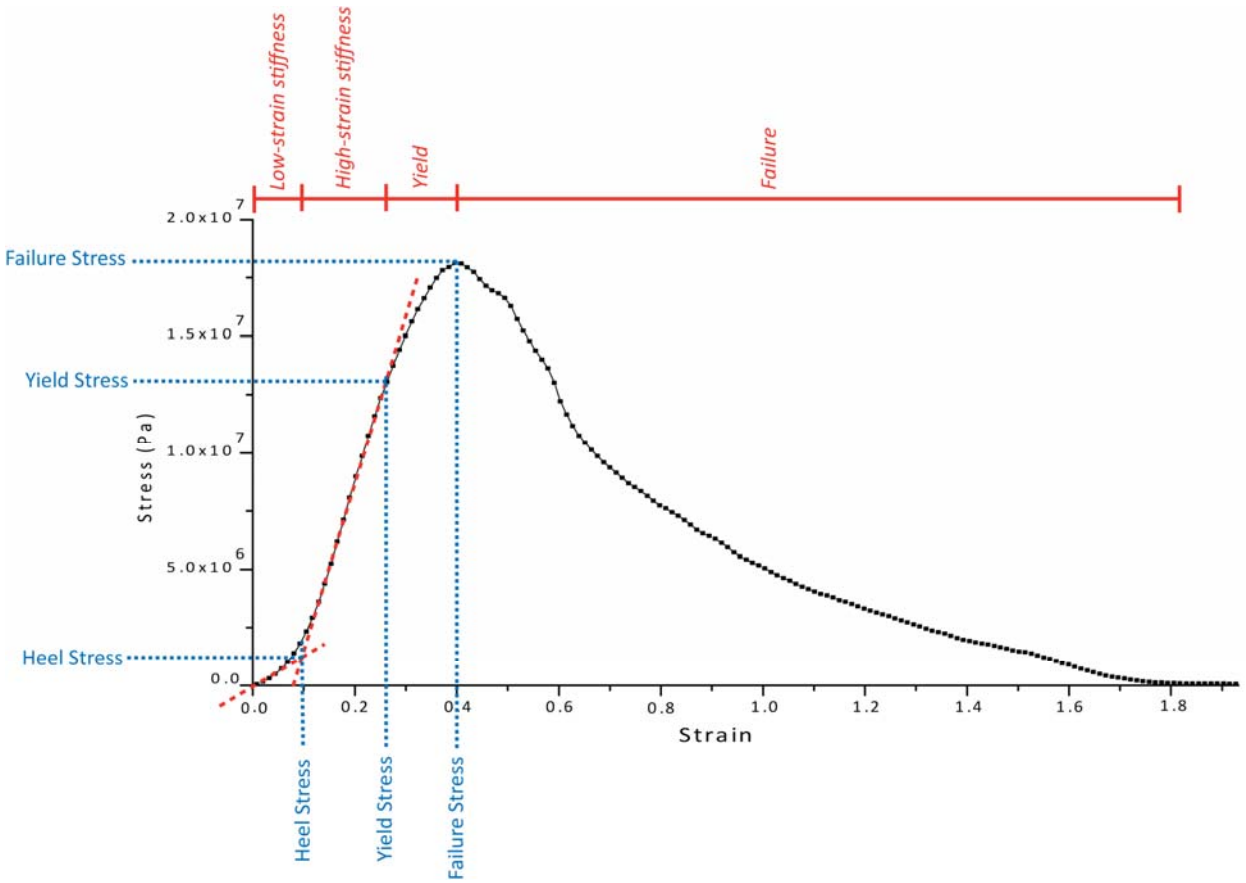

Figure 3:2 the characteristic 'S' shaped tensile stress-strain curve of tendon, annotated to show key properties and regions of behaviour. Data obtained experimentally in preliminary mechanical studies of the bovine flexor tendon performed as part of the current research project.

Table 3:1 presents the high strain Tensile modulus of a variety of tendons at different hierarchical levels. In can be seen that the value of high strain Tensile modulus for a collagen molecule, as calculated by Sasaki et al [68], is relatively high for a polymeric material, being similar to nylon and polystyrene and approximately 10x greater than natural rubber [70]. This stiffness is produced by the semi-rigid nature of the triple helix [71]. However, examination of the Tensile modulus values presented for higher levels within the structure reveals that the bulk tissue, fibres and fibrils are generally less stiff than the collagen molecule, as might be expected from the rule of mixtures for composite materials.

There is also a great deal of variability between the tensile modulus reported for different tendons at different hierarchical levels using different test methods. Whilst this variability is, in part, caused by experimental inconsistencies such as variations in test method and testing media, the more important consideration is the effect of strain rate; in general tendons are stiffer at higher strain rates, and fail increasingly by brittle fracture as strain rate increases [72, 73], indicating the importance of viscoelasticity in determining the mechanical properties of tendon. This viscoelastic behaviour gives tendon its energy absorption capabilities and is strongly associated with the second most important constituent of tendon, its ground substance.

Table 3:1 Variation in Tensile Modulus of Tendon in Different Tendons and at Different Hiearchical Levels

Hierarchical Level	Source Tendon	Tensile Modulus (GPa)	Strain Rate	Investigation Technique	Testing medium	Comments	Ref.
Bulk Tissue	Human Plantaris	1.24	not stated	Tensile	Air	• Samples were embalmed and tested in air so mechanical properties expected to be high	[74]
	Human Digitorum Profundus	0.76					
	Human Anterior Tibialis	0.45 - 1.2	N/A	Joint Flexion	*In vivo*	• Stiffness calculated using ultrasound measurement of joint displacement and tendon cross-sectional area	[75]
	Bovine Achilles	≈0.4	Rate of creep	Tensile (creep)	Saline		[67]
	Rat Tail	0.8	10% min^{-1}	Tensile	Saline		[76]
Fibres	Rat Tail	0.48	100% min^{-1}	Tensile	PBS		[77]
		0.57	10% min^{-1}				
		0.50	50% min-1	Tensile	PBS		[78]
Fibrils	Bovine Achilles	$2x10^{-3}$	600 nm s^{-1}	Indentation	PBS	• Changing buffer solution has an influence on the mechanical properties of the fibrils	[79]
		≈0.43	Rate of creep	Tensile (creep)	Saline	• 'Small-angle X-ray scattering(SAXS) methods were employed for measuring strain ε_D at the fibril level'	[67]
		0.07-0.17	<3µm at 1.3Hz	Indentation	PBS	• Stiffness dependent on fibril thickness	[80]
		0.25-0.45	not stated	Tensile (with AFM)	PBS		[81]
	Rat Tail	5 – 11.5	5Hz	Indentation	Air	• Tested in air so value is expected to be significantly higher than values for wet tissue	[82]
Collagen Molecule	Bovine Achilles	2.9	Rate of creep	Tensile (creep)	Saline	• 'molecular strain was estimated from elongation of the helix pitch of a collagen molecule'	[68]

3.3.2 Ground Substance

'Ground substance' is the material in which the cells and collagenous architecture of tendon are embedded, and is thus the matrix component of this fibre composite material [83, 84]. The ground substance is primarily composed of water and acid mucopolysaccharide (proteoglycan) complexes. Figure 3:3 illustrates how these space-occupying gel-like structures are composed of proteoglycans (PGs) (disaccharide core proteins chains with sulphated glycosaminoglycan (GAG) side chains) attached to a central strand of hyaluronic acid, a non-sulphated GAG [85]. *In vivo*, the sulphate and carboxyl groups of the PGs and sulphated GAGs are ionised, creating a fixed negative charge that attracts water molecules and cations, giving rise to the considerable swelling properties of tendon.

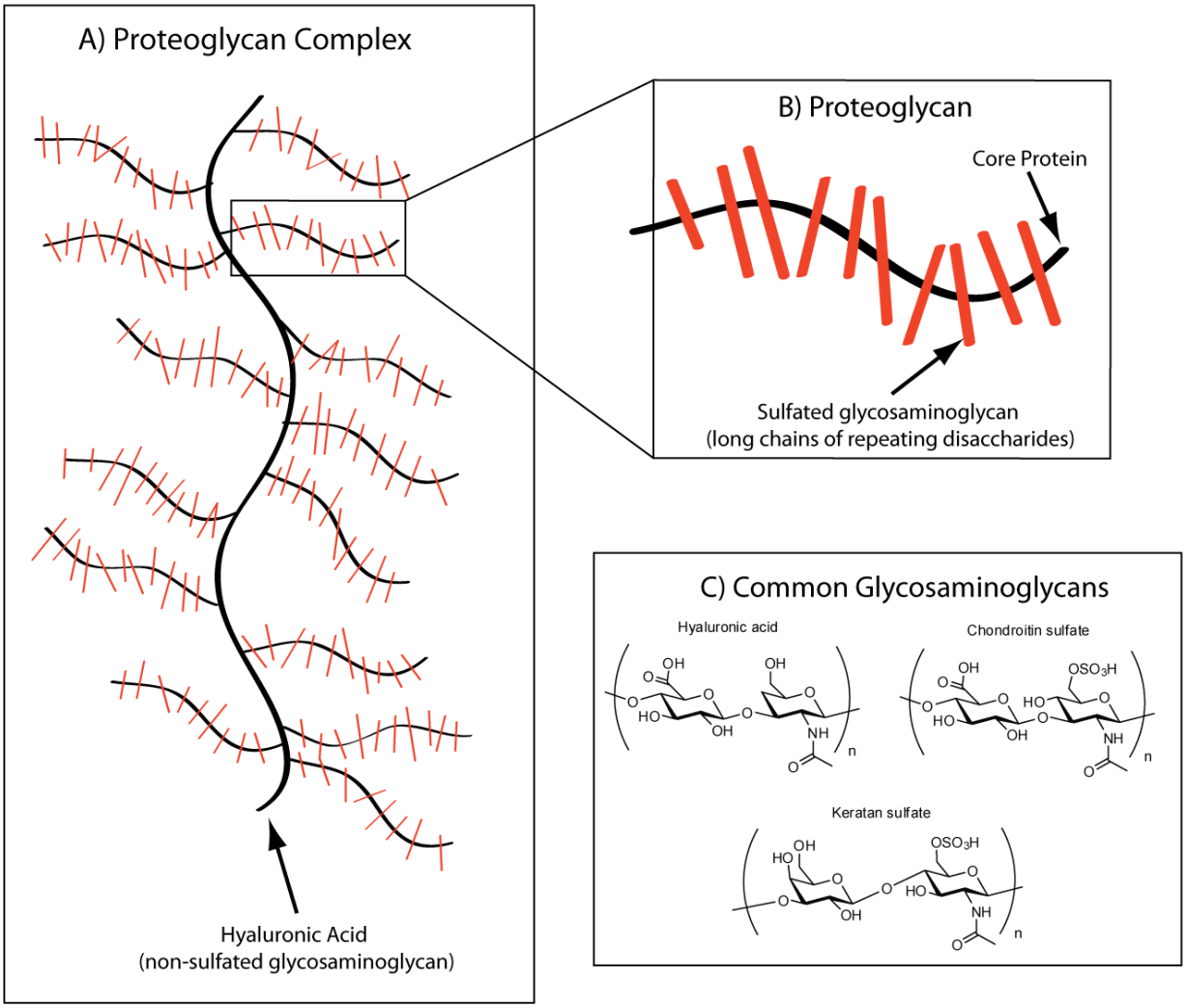

Figure 3:3 Hierarchical structure of a proteoglycan complex. A) The complex is composed of proteoglycans (PGs) attached to a central hyaluronic acid strand. B) The typical structure of a PG consists of a central disaccharide core protein to which are attached one or more sulphated glycosaminoglycans (GAGs). C) The molecular structure of some common GAGs, hyaluronic acid, chondroitin sulphate and keratin sulphate. Original Artwork.

GAGs constitute approximately 0.2% of the dry mass of tendon subjected to tension, and over half of this GAG component is dermatan sulphate [86]. PGs constitute between 1–5% of the dry weight [87, 88] and approximately 90% of these PGs are small leucine-rich proteoglycans (SLRPs), so named for the presence of the leucine-rich repeat unit within their structure [86, 89]. The primary SLRP found in tendon is decorin, an SLRP which has only one chondroitin sulphate or dermatan sulphate side-chain. As the name suggests, decorin 'decorates' the collagen fibrils [90], binding via electrostatic interactions (binding force of approximately 12.4nN [91]) between its core protein and particular locations on collagen fibrils [92-95]. The GAG side-chains of the decorin molecules stretch out across the fibrils and into the inter-fibrillar space where they interact with each other, 'forming antiparallel dimers' [96]. For a thorough review of the interactions between SLRPs and collagen fibrils, the reader is referred to Kalamajski et al [97].

The spacial arrangement of decorin and its GAG side-chains in tendon has led researchers to speculate that PGs and GAGs play an important role in the elastic properties of tendon, possibly acting as pseudo-crosslinks between the fibrils and fibres [98-100]. It has also been suggested that the ground substance plays an important role in the viscoelastic properties of tendon. For example, Shen et al reported that during creep and stress-relaxation tests the 'fibrillar relaxation time was smaller than literature values for tissue-level relaxation time' and suggested that this indicated the importance of the ground substance [101]. This work supports the findings of other studies which have shown that, although fibril arrangement does occur, fibre sliding is a more significant contributing factor in tendon deformation mechanics (i.e. elongation of fibrils is always less than elongation of bulk sample) [66, 69, 102-105]. This is further supported by the series of studies by Fung et al which have shown that fatigue damage accumulation in tendon is associated with accumulation of fibre delamination and discontinuities [106-108].

Experimental evidence for the role of ground substance in the mechanical properties of tendon is often contradictory. For example, GAG-depleted (chondroitinase-treated) tendon samples exhibit increased fibre sliding and decreased fibril sliding, with inter-fibre failure being more dominant compared with control samples, indicating that ground substance plays a role in strain transfer [109, 110]. However, GAG-depletion also increases the failure stress, possibly due to increased interaction between the collagen units. Similarly, when Fessel et al removed the GAGs from tendon, they found no change in the viscoelastic properties of rat tail tendon [111], but when Smith et al examined the strain-rate dependence of bovine

flexor tendons, they found that GAG-depleted tendons exhibited significant reductions in their viscoelastic behaviour compared with untreated samples [73].

Such discrepancies between the findings of various experiments may be explained by consideration of the fibre composite nature of tendon. The properties of fibre composites are dominated by load transfer between the different elements of the composite, and are thus controlled by parameters such as fibre length (critical length), fibre spacing, fibre cross-section etc. Consequently GAGs alone cannot account for the changes in properties, and features such as fibril and fibre spacing and length must also be considered [99, 100, 112, 113]. The viscoelastic nature of the ground substance itself must also be taken into account. As Puxkandl et al note, 'the ratio of fibril strain to tendon strain is dependent on the applied strain rate' [114], increasing as the strain rate increases. Given this observation, differences in strain rate between different experimental studies are likely to lead to very different results.

3.4 TENDON ADAPTABILITY

3.4.1 Regulation of Composition and Structure

A key advantage of biological materials compared to engineering materials is their ability to adapt their loading environment, altering their form to better suit their function. This regulation is performed by the cells within the tissue, the vast majority of which have a fibroblastic phenotype [115, 116]. These spindle-shaped cells, termed tenocytes, are aligned longitudinally along the collagen fibres, with their cell processes extending such that the cells are interconnected in 3D space; each cell is associated with up to nine collagen bundles [117-119]. Tenocytes synthesise growth factors, secrete the collagens and glycoproteins of the extracellular matrix [48, 120] and produce the matrix metalloproteinases (enzymes) that breakdown and remove old extracellular matrix and the associated tissue inhibitors of metalloproteinases [117, 121], in order to better adapt the tendon to its mechanical environment.

One key way in which cells are thought to regulate the collagen architecture of tendon is through the interaction between collagen fibrils and SLRPs. Numerous studies of collagen-based tissues in knock-out mice have shown that SLRPs play an important role in the regulation of fibril diameter, spacing and alignment during fibrillogenesis [122, 123]. For example, Danielson et al reported that the collagen fibrils in

the skin and tendons of decorin-null mice were 'coarser and irregular in size and shape. Furthermore, they were often haphazardly arranged with increased inter-fibrillar spaces' [124].

The importance of SLRPs is further highlighted by the results of studies of collagen fibril formation *in vitro* studies [125-128] and during maturation *in vivo* [129, 130], which appear to indicate that SLRPs, and particularly decorin, play a regulatory (not inhibitory) role in the lateral fusion of fibrils [131, 132], while their glycosaminoglycan side-chains may play an important role in the determination of inter-fibrillar spacing [96, 133, 134]. Since the *in vivo* proliferation capacity of tenocytes is reportedly less than 4% [135, 136], regulation of the form of tendon by proteoglycans, which have a much higher turnover rate than collagen [137], allows this relatively avascular, metabolically inactive material to adapt reasonably well to its loading environment.

3.4.2 Adaptation to Mechanical Environment

Studies of tendons from a range of species during development, maturation and aging have demonstrated differences in their material properties. For example, maturation is associated with increasing mechanical tensile stiffness and strength coupled with structural adaptations such as decreased fibril packing density, increased structural organisation and increases in collagen fibril diameter [37, 138-140], and compositional changes such as alterations in the ratios of collagen type I to type III and collagen to proteoglycans, and in the crosslinking densities [140, 141]. Post-maturity further adaptation occurs, probably as a result of senescence. According to the excellent review by Tuite et al [142], senescent tissue exhibits decreased fibril diameters, decreased GAG content, decreased collagen turnover and changes in the crosslinks compared with mature tissue, all of which lead to lower mechanical properties. Aging has also been reported to produce changes in crimp length and angle [143]. These changes associated with maturation and aging occur to different extents in tendons that perform different anatomical functions [141, 144, 145] and, given the strong correlation between structure, composition and mechanical properties [37, 146, 147], are likely to correspond to difference in the mechanical environments.

This dependence of the material properties of tendons on their mechanical environment is epitomised by the functional adaptations of wrap-around tendons such as the digital flexor tendons (DFT) and, to a lesser extent the rotator cuff tendons. Much like the superficial DFT (SDFT), the deep DFT (DDFT) contains two distinct sections, a proximal section and a distal section. The proximal section runs down the back of the limb and is thus in pure tension, while the distal section runs under the sesamoid bones, exerting forces on these bones that are similar to the contact pressures between long bones of the foot [148, 149]. Finite element analysis studies have shown that in this distal region wrap-around tendons experience hydrostatic compressive strains that decrease as they radiate away from the region of contact, in addition to a non-constant strain fields [150-153].

Several studies have reported compositional adaptations in the compressive regions of wrap-around tendons compared with purely tensile regions; higher fractions of PGs and GAGs, higher ratios of aggrecan to decorin and of dermatan sulphate to chondroitin sulphate, and higher proportions of keratin sulphate and biglycan compared with tensile tendon have all been reported [86, 154-158]. These differences are generally associated with the development of fibrocartilage, localised on the articular (bone) side of the tendon [151, 159, 160]. Such compositional adaptations, particularly increased content of aggrecan (a PG typically found in cartilage [159]), allow the tissue to better resist the compressive forces: the fixed negative charge of aggrecan creates an osmotic gradient that dramatically reduces the permeability of the tissue, and thus significantly increases the time taken for fluid to flow out of the tissue upon application of load. Therefore the presence of this fibrocartilage increase the length of time the load can be applied before it is transferred from the fluid to the surrounding tissue [115, 161].

The existence of microstructural and ultrastructural differences between the collagen architecture of tendon subjected to tension compared with tendon subjected to compression have also been demonstrated, with regions of tendon subjected to tensile forces alone exhibiting fibrils with larger diameters and 'D' spacing (also known as repeat unit) compared with regions subjected to compressive forces [151, 162-165]. Furthermore, differences in the PG and GAG distribution, collagen fibre arrangement and bulk structure within the dorso-ventral plane have been reported [38, 159, 166, 167], with the collagen fibres taking on 'basket-weave-like arrangements' [63, 163]. Whether similar variations in other structural features exist in the dorso-ventral plane is unclear [141, 151] but, given the differential

hydrostatic pressure and differential strain fields experienced by this region, and the role of proteoglycans in adaptation of tendon, such structural differences are expected [115].

3.5 OBJECTIVE AND AIMS

Later in this thesis (Chapters 6, 7 and 9), the material adaptation of healthy and degenerative human rotator cuff tendon samples will be characterised in order to gain insight into the relationship between the mechanical environment and adaptations of tendon in health and disease. To achieve this it is first necessary to establish a portfolio of techniques suitable for the characterisation of human tendon samples. These techniques must be able to extract information from samples that have been preserved and processed in the manner favoured by surgeons and pathologists. It is also necessary to establish the effect of different loading environments on the material properties of tendons, as measureable by the intended analysis techniques.

The work presented in the next chapter (Chapter 4) aims to establish a portfolio of techniques suitable for characterisation of bulk histological samples whilst gaining insight into the adaptations of tendon in response to different loading environments. To this end, a spectrum of compositional, structural and mechanical characterisation techniques will be used to assess the healthy material adaptations at different anatomical locations within the bovine deep digital flexor tendon (DDFT) and the ovine infraspinatus tendon, with the aim of testing the following hypotheses:

1. There are significant material adaptations in wrap-around tendons subjected to different loading environments.
2. In regions of compression the material adaptations of tendon vary with distance from the bony contact.
3. The material adaptations of tendon are inter-related.

Chapter Four

Material Adaptations in Response to Loading Environment

4.1 MATERIALS AND METHODS[*†]

4.1.1 Sample Collection and Pre-embedding Treatment

4.1.1.1 Bovine Deep Digital Foot Flexor Tendon

Biopsy Samples – Effect of Fixation and Location

Twelve hind feet of cattle under thirty months of age were obtained from a wholesale butcher (Mutchmeats Ltd, Witney, UK) and dissected within eight hours of slaughter. Using a handheld razor blade and a no. 10 surgical blade each hoof was dissected to expose the digital flexor tendons, remove the tendon sheath and peel back the superficial digital flexor tendon to reveal the underlying deep digital foot flexor tendon (DDFT) (Figure 4:1a). The DDFT was then released from the foot and a 2.5mm disposable biopsy punch (Kai Medical, Hawaii, USA) was used to remove two through-thickness biopsies from the region approximately 3cm distal to the point of bifurcation, and four through-thickness biopsies from the region 3cm proximal of the point of bifurcation (Figure 4:1b). The distal biopsy samples incorporated the mid-substance fibrocartilage described by Vogel and Peters [159], and for consistency, were all taken from the right-hand bifurcation of the tendon.

[*] Sections 4.1.1.1, 4.1.2.2, 4.1.4.4, 4.2.3, 4.3.1.4, and 4.3.2.1 in this chapter are adapted from **Micron 42**(5) p.531-535 Atomic Force Microscopy of Bulk Tendon Samples: Affect of Location and Fixation on Tissue Ultrastructure. Tilley, J.M.R., Carr, A.J., Czernuszka, J.T. Copyright (2011). with permission from Elsevier [DOI: 10.1016/j.micron.2011.01.001]

[†] Sections of text in this chapter are adapted from **Atomic Force Microscopy (AFM): Principles, Modes of Operation and Limitations 1(6),** H. Yang (Editor). Characterisation of Tendons at Different Length Scales Using Atomic Force Microscopy and Polarised Light Microscopy May Provide Insight into Tendon Disease, J. M. R. Tilley A. J. Carr and J. T. Czernuszka, copyright (2014), with permission from Nova Science Publishers, Inc.

Storage conditions and fixatives used for biological samples are generally believed to influence the degree of preservation of the tissues' structure [168-170]. Glutaraldehyde fixation is widely held to be the gold standard for preservation of ultrastructural features and is the preferred technique for electron microscopists [171-173]. Conversely, formalin fixation is most commonly used by pathologists as it is compatible with a wide range of histological and immunohistological stains [174-176]. Both of these fixation techniques result in dramatic alterations in the mechanical properties of tissue due to the introduction of chemical crosslinks [177, 178]. Consequently, the freeze-thaw technique is commonly used in mechanical studies of bulk tissue as it avoids the need for a chemical fixative. In the absence of a cryopreservation medium it is, however, thought to damage the structural properties of the tissue [179, 180].

The human tissue samples used later in this thesis (Chapters 6, 7 and 9) were provided in the formalin-fixed state, while chondroitinase-ABC treated samples examined in this chapter (see pg 25 below) had been frozen prior to treatment and fixation. In order to assess the effect of these different storage conditions on the ultrastructure of tendon compared to the effect of the 'Gold Standard' glutaraldehyde fixation process, the structural adaptations of comparable samples stored under different conditions were compared. Each biopsy was cut into dorsal and ventral samples using a handheld razor blade, and stored in either 4% glutaraldehyde (4% GA) (Sigma Aldrich, Dorset, UK) or 10% formaldehyde (10% FA) (Sigma Aldrich, Dorset, UK) in ambient conditions, or in 0.1M NaH_2PO_4 (PBS) (Sigma Aldrich, Dorset, UK) at -80°C, as indicated by Table 4:1 for at least one month prior to further processing.

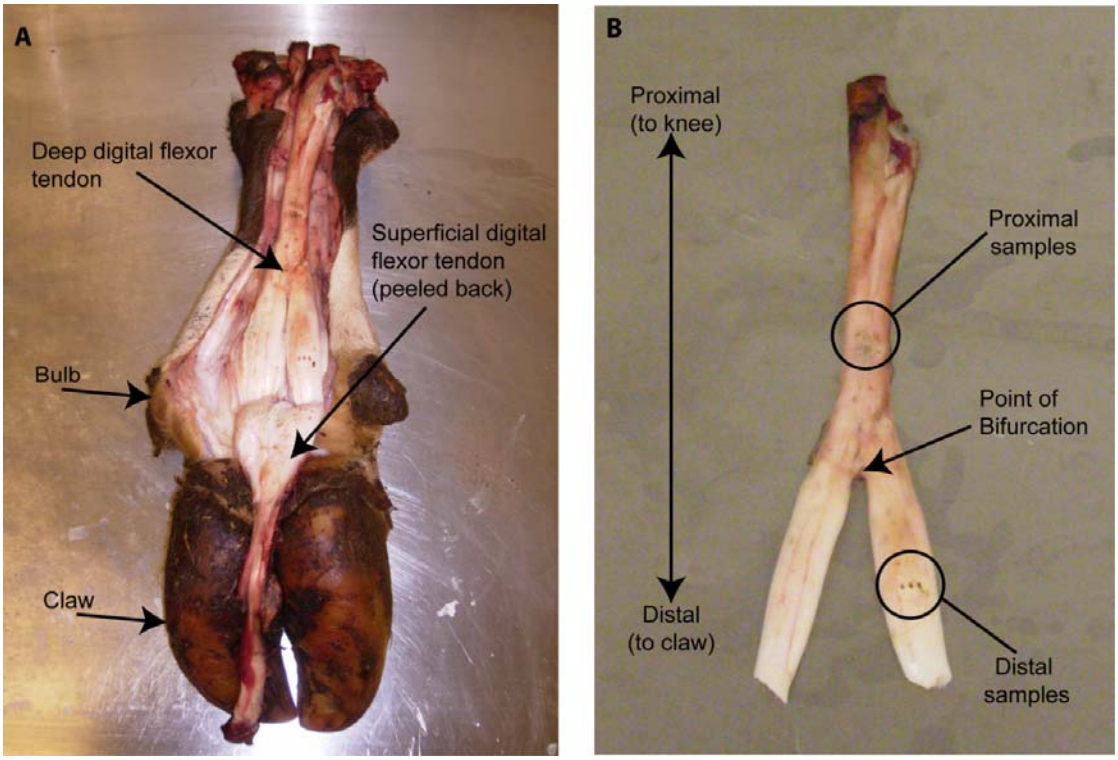

Figure 4:1 Obtaining bovine deep digital flexor tendon samples: A) Hoof dissection to reveal deep digital flexor tendon, and B) Illustration of sample origins on removed deep digital flexor tendon.

Table 4:1 Storage Conditions for Bovine Deep Digital Flexor Tendon Biopsy Samples

Anatomical Position	Sample Number	Intended Embedding Media	Preservation Medium	Preservation Temperature
Proximal Ventral	1	Resin	4% GA	Ambient
	2	Wax	10% FA	Ambient
Proximal Dorsal	1	Resin	4% GA	Ambient
	2	Wax	10% FA	Ambient
Distal Ventral	1	Resin	4% GA	Ambient
	2	Wax	10% FA	Ambient
	3	Resin	10% FA	Ambient
	4	Resin	0.1M PBS	-80°C
Distal Dorsal	1	Resin	4% GA	Ambient
	2	Wax	10% FA	Ambient
	3	Resin	10% FA	Ambient
	4	Resin	0.1M PBS	-80°C

Bulk Cross-section Samples – Effect of Enzyme Treatment

To further assess the validity and reproducibility of the characterisation techniques tested below (detailed in Section 4.1.4 below), the structural and compositional properties of as received and GAG-depleted tendons were compared. GAG-depletion was produced by treatment of tendon samples with

chondroitinase-ABC, an enzyme which attacks and degrades the GAG-side chains content within tendon [113, 137, 181]. While GAG-depletion was expected to alter the composition of the tendon samples, it was not expected to alter the ultrastructural characteristics of tendon, thus providing a method for validating the usefulness of the characterisation techniques tested below (detailed in Section 4.1.4 below).

After collection of the through-thickness biopsies, the proximal region of each DDFT was cut in half transversely and into thirds longitudinally, producing six strips of equal length. Each strip was then rinsed in 0.1M phosphate buffer, wrapped in surgical gauze, and stored at -80°C for up to three months. At an appropriate time point, these strips were allowed to defrost in ambient conditions prior to immersion in 50mM Tris-hydroxymethy-methylamine (Tris buffer) (Sigma Aldrich, Dorset, UK) at 37°C for 24 hours, at which point 0.15U ml^{-1} chondroitinase ABC (Sigma Aldrich, Dorset, UK) was added to the solution. The samples were then incubated at 37°C for a further 72 hours, before being rinsed in a 1M-phosphate buffer and re-frozen at -80°C [73]. As received (i.e. un-incubated) samples served as controls. At a suitable time point, samples were defrosted once more and mechanically tested as part of another study [73]. Post-mechanical characterization, through-thickness cross-sections were taken from six chondroitinase ABC-treated samples and from six untreated samples and immersed in 10% formalin at ambient conditions for at least 1 month.

4.1.1.2 Ovine Infraspinatus Tendon

Twelve front shoulders from six-month-old sheep were obtained from a wholesale butcher (Mutchmeats Ltd, Witney, UK) and dissected within four hours of slaughter. Using the acromion as a landmark, each shoulder was sliced along the deltoid muscle with a kitchen knife to reveal the infraspinatus muscle and tendon (Figure 4:2). A 2.5mm disposable biopsy punch (Kai Medical, Hawaii, USA) was then used to remove two through-thickness biopsies from the central region of the tendon, and each biopsy was cut in half transversely to produce a bursa-side sample and an articular-side sample. One bursa-side sample and one-articular-side sample from each tendon was stored in 4% glutaraldehyde (4% GA) prior to resin embedding. The remaining bursa-side and articular-side samples were fixed in 10% formaldehyde (10% FA) prior to wax embedding. All samples were fixed in ambient conditions for at least one month prior to further processing. One biopsy sample was also removed from the musculotendinous junction of the infraspinatus of one animal. Samples were fixed in 10% formaldehyde (10% FA) prior to wax embedding.

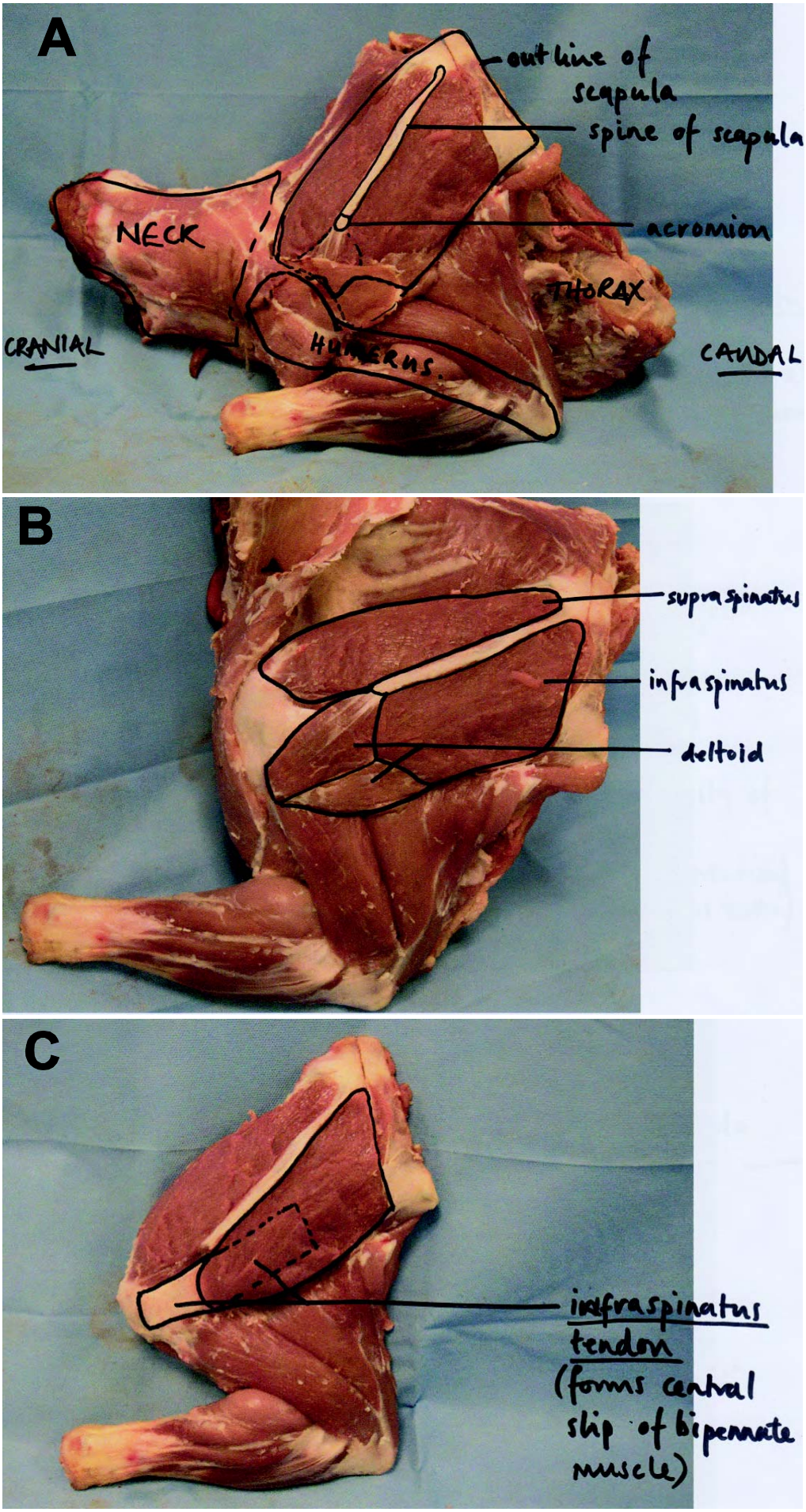

Figure 4:2 Dissection of Ovine Front Shoulder to reveal Infraspinatus tendon. Images courtesy of Dr. Richard Murphy.

4.1.2 Sample Embedding

4.1.2.1 Wax-Embedded Samples

Post-storage, formalin-fixed samples intended for wax-embedding were processed as follows: samples were removed from the storage medium and placed between two biopsy foam pads in histology embedding cassettes with detachable lids. The cassettes were then dehydrated through graded industrial Methylated spirit (IMS) (70%, 90%, 95%, 100%), immersed in xylene, and perfused with Formula R paraffin wax (Surgipath, Cambridgeshire, UK) in a Shandon Pathcentre tissue processor (Thermo Fisher Scientific, Waltham USA) over the course of 16 hours. Post-perfusion, samples were removed from the cassettes and embedded in paraffin wax blocs using an embedding centre (Leica, Wetzlar, DE). Finally, 10µm sections were cut from each embedded sample using a RM 2165microtome (Leica, Wetzlar, DE) fitted with a steel blade (Model 819), and floated off onto warm tap water. Each section was mounted on an Xtra glass slide (Sugipath, Peterborough, UK) and baked at 60°C for 24 hours before being stored in ambient conditions in standard slide boxes.

4.1.2.2 Resin-Embedded Samples

Post-storage, glutaraldehyde-fixed, formalin-fixed and frozen biopsy samples intended for resin embedding were electro-negatively stained with osmium tetroxide, dehydrated through graded alcohol and then embedded in medium low viscosity (Taab Laboratories Equipment, Aldermaston, UK) resin following the steps detailed in Table 4:2. At each stage, the samples were immersed in approximately 4ml of medium. After Step 12, samples were immersed in approximately 1ml of resin in polyethylene containers and cured at 60°C for 16 hours. They were then cut at 0.5mm s^{-1} using a PT-PC PowerTome Ultramicrotome (RMC Products, Boeckeler Instruments, Inc, Tucson, USA) fitted with a 3mm, 45° diamond ultra-microtome knife (Boeckeler Instruments Inc, Tucson, USA) to produce 500nm slices. Slices were deposited onto glass microscope slides (Thermo Fisher Scientific, Waltham USA) moistened with distilled water. The slides were then dried on a hot plate and each slice was stained with 1% Toludine blue in order to differentiate the collagen from the resin.

Table 4:2 Resin Embedding Procedure

Step	Medium	Immersion Time	No. of repeats
1	water[#]	10 minutes	x2
2	1:99 osmium: water[#]	60 minutes	x1
3	water[#]	10 minutes	x2
4	1:1 ethanol: water[#]	10 minutes	x2
5	7:3 ethanol: water[#]	10 minutes	x2
6	9:1 ethanol: water[#]	10 minutes	x2
7	95:5 ethanol: water[#]	10 minutes	x2
8	100% ethanol	15 minutes	x2
9	100% propylene oxide	15 minutes	x2
10	1:1 resin*: propylene oxide	30 minutes	x1
11	2:1 resin*: propylene oxide	30 minutes	x1
12	100% resin*	30 minutes	x1

[#] distilled water
* Taab® low viscosity (medium) resin

4.1.3 Sample Preparation

4.1.3.1 Alcian Blue Staining

In order to compare the ratio of collagen to ground substance in the samples, glass-mounted, wax embedded sections were stained with alcian blue as follows: slides were immersed twice in xylene for 7 minutes and then rehydrated in graded IMS (100% x2, 90%, 70%, 0%) followed by distilled water (dH_2O) for 5 minutes each. Slides were then immersed in alcian blue in 3% acetic acid for 30 minutes before being rinsed in running tap water for 3 minutes to remove residual stain. Slides were then counter-stained by immersion in nuclear fast red in $Al_2(SO_4)_8$, dH_20 for 10 minutes, before being rinsed in running tap water for 1 minute, and fast dehydrated in graded IMS followed by xylene for 2x5 minutes. Each sample was then mounted in DPX mounting media (Sugipath, Peterborough, UK) and covered with a cover slip.

4.1.3.2 Picrosirius Red

In order to compare the relative distribution of fibre thicknesses in different samples, glass-mounted wax embedded sections were stained with picrosirius red as follows: slides were immersed twice in xylene for 7 minutes and then rehydrated in graded IMS (100% x2, 90%, 70%, 0%) followed by dH_2O for 5 minutes each. Slides were then immersed in picrosirius red solution (0.5g Sirius red F3B in 500ml saturated aqueous picric acid) for 1 hour. Post-staining, slides were rinsed in two changes of acidified water (0.5% acetic acid),

dehydrated through graded alcohols and rinsed twice in xylene for 2x 5 minutes. Each sample was then mounted in DPX mounting media (Sugipath, Peterborough, UK) and covered with a cover slip.

4.1.3.3 De-waxing

In preparation for characterisation by atomic force microscopy, Raman spectroscopy and nanoindentation, one glass-mounted wax-embedded section from each sample was dewaxed by immersion in xylene (Thermo Fisher Scientific, Waltham USA) for up to 2 hours. Sections were then removed from the xylene and transferred to a fumehood, where they were left for up to 24 hours to allow the remaining xylene to evaporate. De-waxed slides were stored in slide boxes prior to analysis.

4.1.4 Sample Characterisation

4.1.4.1 Brightfield Light Microscopy

Alcian blue-stained samples were imaged using an Imager M1 microscope (Carl Zeiss Ltd., Welwyn Garden City, UK) fitted with an AxioCam HRc camera. Camera settings of 7.6ms exposure time, 1.0 saturation levels, 0.49 gamma levels and 1x gain factor were found to produce the best images. 8 bit, RGB images were obtained at 5x and x20 magnification were obtained. The proportion of collagen and ground substance in each 20x image was then analysed using ImageJ image analysis software together with a custom-written macro based on the colour threshold plug-in (See Appendix). To aid the analysis, the background was removed from each image using Adobe Photoshop CS3 extended digital photo editing software (Adobe, San Jose, USA), prior to threshold analysis.

4.1.4.2 Polarised Light Microscopy

Picrosirius red-stained samples were imaged with polarised light microscopy using a Polyvar Met (Reichert-Jung) fitted with a DFC 420 (Leica, Wetzlar, DE) digital camera. Samples were imaged in transmission mode, with the polarisers adjusted to the angle which produced the brightest birefringence. 8 bit, RGB images were obtained at 2.5x and x10 magnification. Using the macro based on the threshold colour plug-in for ImageJ (See Section 4.1.4.1 above, and Appendix), the percentage area of each image that contained hue values (x) $0 \leq x < 111$ and $234 < x \leq 255$, split into bins of 5 pixel hue values (i.e. $0 \leq x < 5$, $5 \leq x < 10$, $10 \leq x < 15$ etc) for each sample, was calculated. The subsequent histograms were then compared. Using ImageJ, the average crimp length of each picrosirius red-stained sample was also calculated from at least 25 crimp length measurements per image.

4.1.4.3 Raman Spectroscopy

Raman spectra were collected from dewaxed, glass-mounted sections of proximal bovine DDFT samples (untreated and enzyme-treated) using a LabRAM Aramis Raman spectrometer equipped with a confocal microscope (Horiba, Kyoto, Japan), calibrated with pure silica. Samples were excited with a diode-pumped solid-state Nd:YAG laser, frequency doubled to operate at $\lambda = 532nm$. With the confocal microscope set to 50x magnifications, the laser was focused on sections of fibrous matrix within the sample. Spectra were recorded between 300-1800cm^{-1}, with hole size of 300µm and slit size of 150µm, giving a spot size of 590nm and a special resolution of approximately 295nm. An acquisition time of 10 seconds was chosen and spectra were averaged over 6 acquisitions. To eliminate the presence of cosmic rays in the data, the software's automatic spike filter was applied. Each sample was scanned in 4 different locations. The background florescence of each spectrum was subtracted as a 4^{th} order polynomial and each spectrum was normalised to the peak at approximately 1242 cm^{-1}. To aid with peak identification spectra were collected for paraffin wax and chondroitin sulphate A from bovine trachea (Sigma Aldrich, Dorset, UK) using the same experimental conditions. Peak fitting was performed on the individual spectra using a custom code in MatLab (Mathworks, Cambridge, UK), in order to assess the effect of chondroitinase ABC treatment on peak intensities.

4.1.4.4 Atomic Force Microscopy

Non-contact Mode Imaging

Atomic force microscopy (AFM) was employed to characterise the ultrastructure of the extracellular matrix in each sample. Glass-mounted sections were imaged using an AutoProbe AFM (Veeco, Plainview, USA) in non-contact mode [182] using a scan rate of 1Hz and cantilever probes with a tip radius of curvature of ≈10nm, force constant between 4.5-14.0 Nm^{-1} (µmasch, Tallinn, EE). Six, 3x3µm images from different locations were obtained from each sample. Each image was processed using IP AutoProbe Imaging Processing and Data Analysis software (TM Microscopes, Sunnyvale, USA) prior to analysis of the diameter, 'D' spacing and average angle between 5-10 fibrils from each image using Gwyddion v2.23 SPM Data Visualisation and Analysis software (Central European Institute of Technology, Masaryk University Kamenice, Czech Republic). Imaging and analysis was performed blind.

Contact Mode Indentation

The stiffness of de-waxed, glass-mounted section was assessed using an AutoProbe AFM (Veeco, Plainview, USA) in contact mode. Cantilever probes with a tip radius of curvature of <10nm, force constant ≈7.5Nm^{-1} (µmasch, Tallinn, Estonia) were used to indent the fibrous matrix of samples to a depth of ~450nm at 1Hz. To allow for viscoelasticity effects, cyclical indentation was repeated fifteen times and a force-distance curve was recorded after the first and last cycle. Each sample was indented a total of twenty times (four indentations per location, five locations per sample) in order to produce an average stiffness value for each sample.

To calculate stiffness values, each force distance curve was compared with a standard curve produced for indentation of the glass substrate (with a new calibration curve produced for each new cantilever). Assuming that the system acts as two compliant springs and that the cantilever had a higher stiffness than the sample so that deflection of the cantilever upon indentation of the sample was due to compression of the sample only the average stiffness of the tendon sample upon the application of 1 x10^{-6} N of force was calculated using Equation 4:1 [183]. The validity of these assumptions is discussed later* (Section 4.3.1.5).

$$k = F_{overall} / (\Delta\delta_{overall} - \Delta\delta_{substrate\ only}) \qquad \text{Equation 4:1}$$

k = stiffness
$F_{overall}$ = force applied
$\Delta\delta_{overall}$ = total indentation depth
$\Delta\delta_{substrate\ only}$ = indentation depth of sample on substrate only

Each stiffness value was converted to an effective tensile modulus using the Sneddon formulation. The Sneddon exponent is the power to which indentation depth (aka tip deflection) is raised in the generalised formula governing the relation between tip indentation and applied force (Equation 4:2), and indicates the shape of the area of contact of the tip and the sample [184], where n=1 indicates a cylindrical indentation, n = 1.5 indicates a parabolic indentation and n=2 indicates a conical indentation.

* As is discussed later (Section 4.3.1.5, pg 73) this second assumption which is unlikely to be true and is likely to significantly influence the results – stiffness values reported for samples vary wildly with cantilever stiffness. To increase the accuracy of the results it would be necessary to test a wide range of cantilevers of varying stiffnesses in order to find one best suited to the samples being tested.

$F = CE^* \delta^n$ Equation 4:2

F = force applied
C = geometrical constant
E = effective Tensile modulus*
δ = indentation depth of sample
n = Sneddon exponent.

Each indentation force-distance curve was plotted as ln (force) versus ln (indentation depth) producing a straight line, the gradient of which was the Sneddon exponent, n. This value was then used to select the appropriate expression for the relationship between tip indentation and applied force as described by Sneddon [184], in order to calculate the effective tensile modulus.

4.1.4.5 Nanoindentation

Post-AFM characterization, glass-mounted de-waxed samples were mounted on Al specimen holders using paraffin wax. The fibrous matrix of each sample was then indented using a Nanoindenter XP (MTS, Eden Prairie, USA) and a diamond Bercovich indentation tip (Micro Star Technology, Huntsville, USA). Samples were indented to a depth of 500nm with a surface find stiffness of $25Nm^{-1}$, a surface approach velocity of $10nm\ s^{-1}$ and a strain rate target of $0.05s^{-1}$. Each sample was indented in ten different locations. Raw load-displacement data was converted to variation in hardness and modulus with depth using the continuous stiffness measurement method described by Oliver and Pharr [185]. To investigate the influence of the glass substrate on the results, a glass substrate and a glass-mounted tendon sample were indented to a depth of 2µm.

4.1.5 Statistical Analysis

Power analysis, assessed using the biostatistics package 'R' (R Foundation for Statistical Computing), revealed that a minimum of 5 samples were needed in order to distinguish differences of 1 standard deviation in tendon fibril diameter and 'D' spacing at $p<0.05$ statistical significance and 80% confidence level. Where data is presented as box plots, box ends and whisker ends represent 25th/75th and 5th/95th percentiles respectively, with crosses indicating outliers. In all other cases data is presented as mean values ± standard deviation unless otherwise indicated. Statistical significance was evaluated using one-way analysis of variance (ANOVA) and Tukey's multiple comparison test performed in Origin data analysis. A significance level of $p<0.05$ was considered statistically significant, and statistical significance is indicated

using the standard asterisk notation, where * indicates $p<0.05$, ** indicates $p<0.01$, and *** indicates $p<0.001$. Where appropriate, Pearson's rank correlations were calculated and are reported as a Pearson's rank coefficient (r-value) and a significance value (p-value).

4.2 RESULTS

4.2.1 Compositional Characterisation

4.2.1.1 Representative Images

Figure 4:3 shows representative images of alcian blue-stained samples from bovine DDFT and ovine infraspinatus tendon in different anatomical locations. Collagen is stained pink, ground substance is stained blue and cells are stained dark pink. The glass slide, visible as a yellow background, can also been seen between gaps in the samples. These gaps are preparation artefacts as a result of the microtomy process and would not be expected in vivo. The image of the distal ventral region of the bovine DDFT (Figure 4:3C) is visibly different when compared with the other images, containing a much higher proportion of ground substance throughout the sample (blue pixels), and a very low proportion of collagen (pink), and much less alignment of the sample in general.

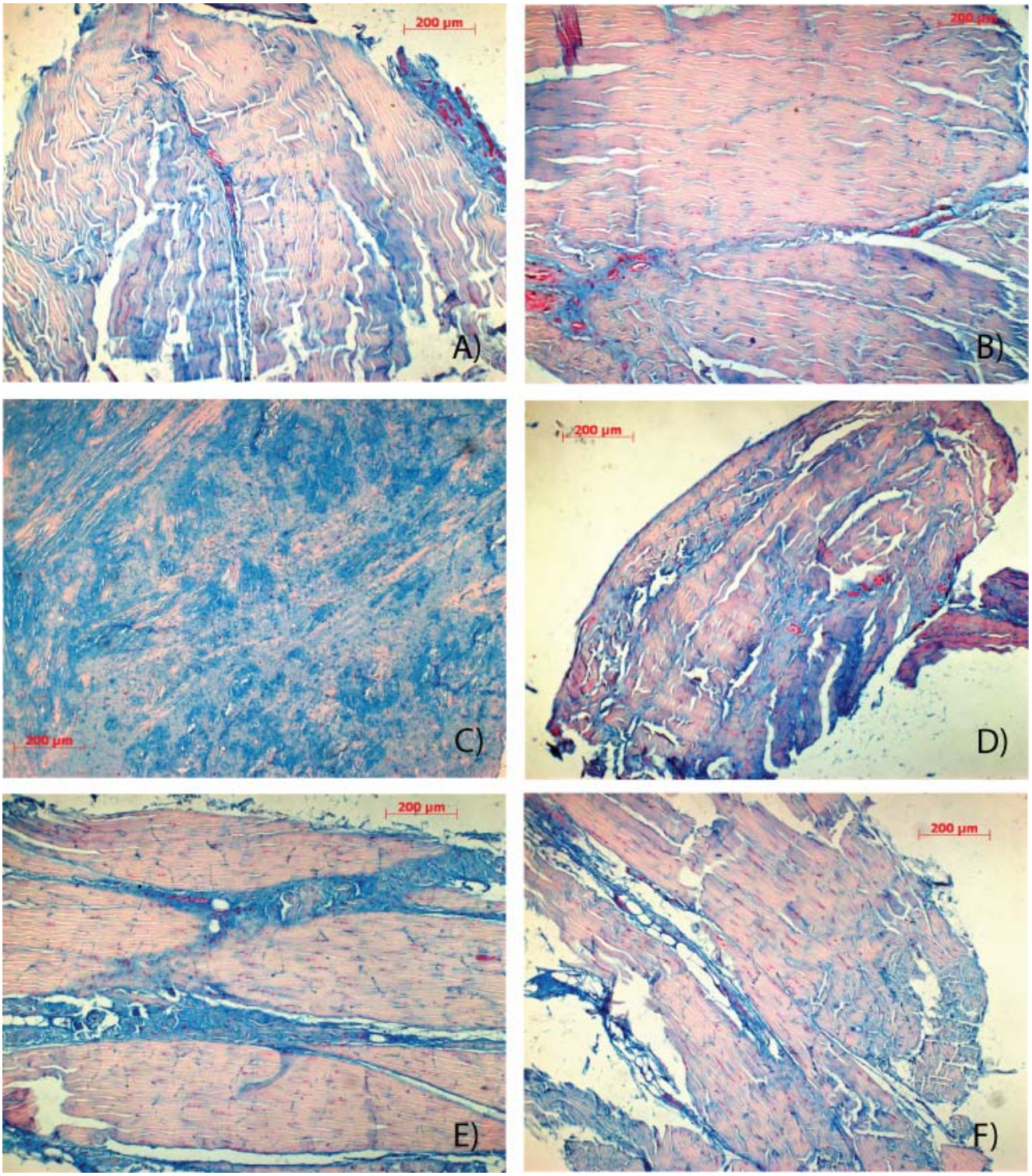

Figure 4:3 Representative images of alcian blue-stained samples from bovine DDFT (A-D) and ovine infraspinatus tendon (E,F) in different anatomical locations: A) bovine DDFT proximal ventral, B) bovine DDFT proximal dorsal, C) bovine DDFT distal ventral, D) bovine DDFT distal dorsal, E) ovine infraspinatus tendon articular-side, and F) ovine infraspinatus tendon bursa-side. The image of the bovine DDFT distal ventral sample (C) appears to contain a much higher proportion of blue-stained material when compared with the other samples. Gaps between the samples are preparation artefacts and would not be expected in vivo.

4.2.1.2 Pink to Blue Ratio

Figure 4:4 shows box plots representing measurements of the ratio of pink to blue pixels in images of alcian blue-stained bovine DDFT samples from different anatomical locations. The ratio is significantly smaller in samples from the distal ventral region compared with all other regions. Additionally, the ratio is significantly smaller in proximal ventral samples compared with proximal dorsal samples, and in distal dorsal samples compared with proximal dorsal samples. For all locations the ratio of pink to blue pixels is less than one, indicating a higher proportion of ground substance (blue) than collagen (pink).

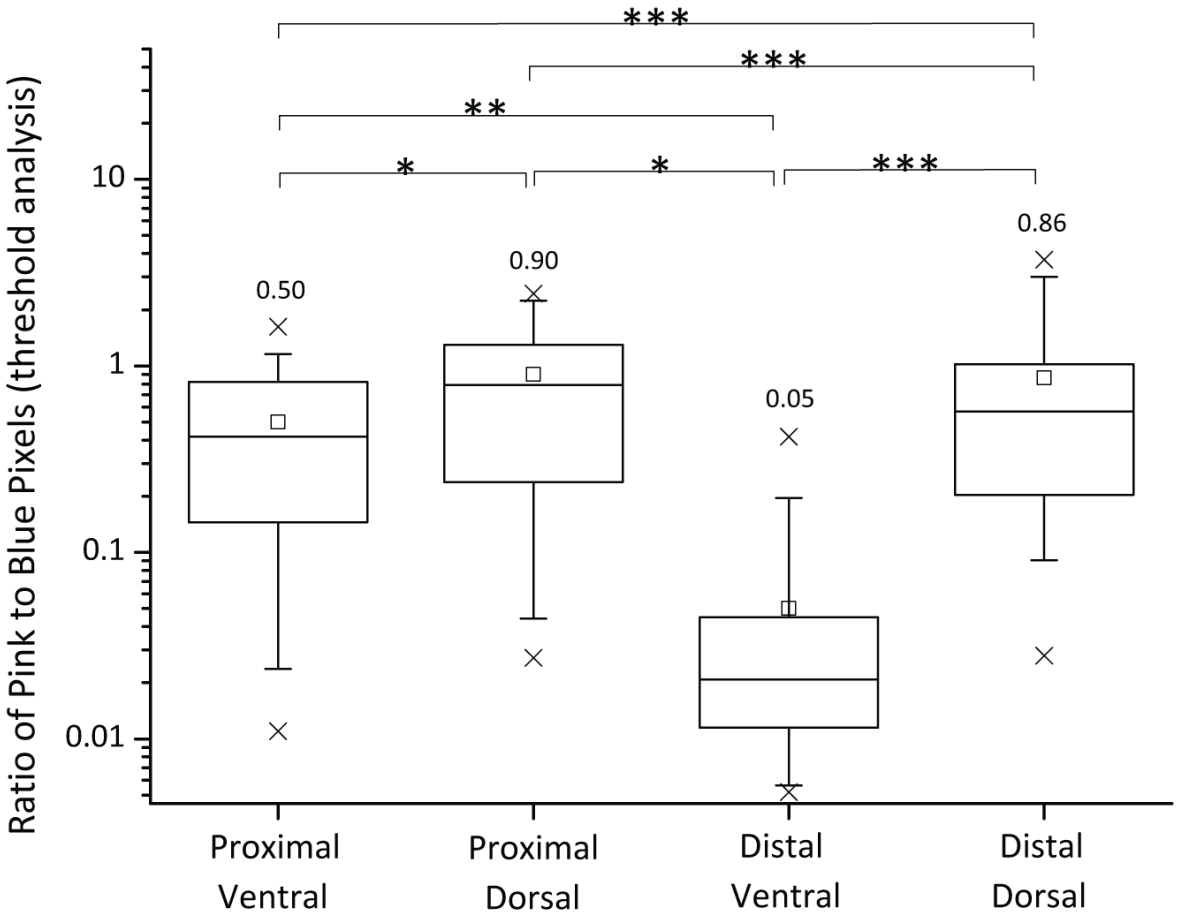

Figure 4:4 Box plots comparing the ratio of red to blue pixels in images of alcian blue-stained bovine DDFT samples. The ratio is significantly smaller in distal ventral samples when compared with all other locations. It is also significantly smaller in proximal ventral samples compared with proximal dorsal samples, and in distal dorsal samples compared with proximal dorsal samples. The ratio is less than one for all locations, indicating a higher proportion of ground substance than collagen.

Figure 4:5 shows box plots representing measurements of the ratio of red to blue pixels in images of alcian blue-stained ovine infraspinatus tendon samples from different anatomical locations. Again the ratio is less than one for both locations, indicating a higher proportion of ground substance than collagen. There are no significant differences between the different locations.

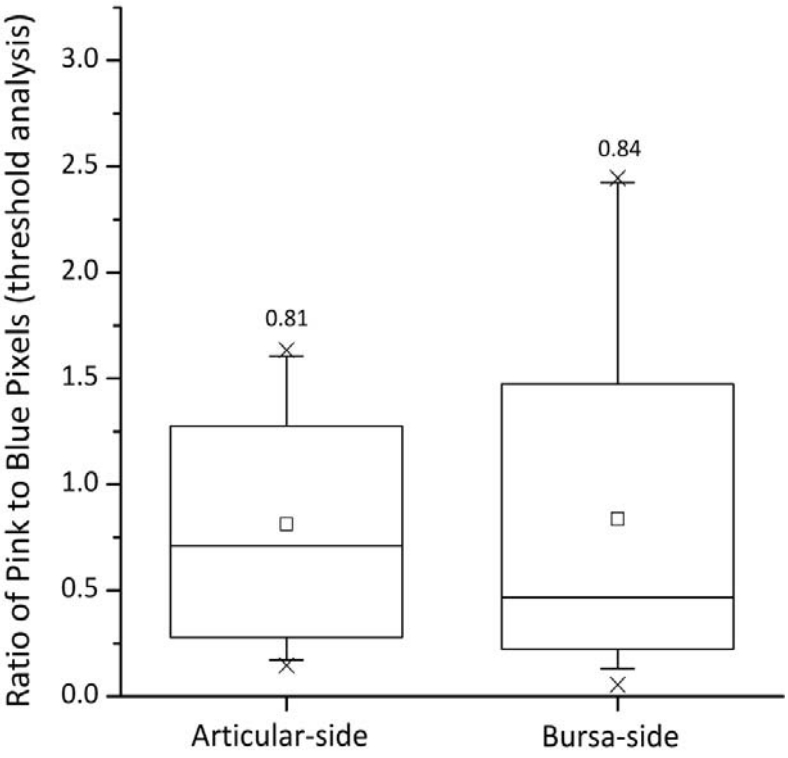

Figure 4:5 Box plots comparing the ratio of red to blue pixels in images of alcian blue-stained ovine infraspinatus tendon samples. The ratio is less than one for both locations, indicating a higher proportion of ground substance than collagen. There are no significant differences between the two locations.

4.2.1.3 Raman Spectral Analysis

Raman spectroscopy is a spectroscopic technique that measures the inelastic (Stokes and anti-Stokes) scattering of monochromatic light in order to characterise the vibrational and rotational modes within a system. Thus it reveals information concerning the structure and environment of the molecules within the system [186, 187]. It is non-invasive and offers high spatial resolution from very small (diameter less than 1μm) sample volumes, making it a widely accepted technique for the characterisation of biomolecules [188, 189]. Analysis of Raman spectra requires knowledge of the specific peak designations within the spectra, however, making Raman analysis of tissues complicated due to the overlapping spectral contributions of different biomolecules present within the tissue [190-192].

In order to identify peaks associated with inter-fibril and inter-fibre GAGs, the profiles of which are known to change as a result of disease, Raman spectra of as received and chondroitinase ABC-treated bovine tendon samples (Section 4.2.1.3) were compared with the spectrum for chondroitin sulphate A. Figure 4:6 shows average Raman spectra obtained from untreated and chondroitinase ABC-treated bovine DDFT proximal samples, and from chondroitin sulphate A and paraffin wax. Tendon samples contain sharp peaks

at 998.1cm^{-1}, 1060.1cm^{-1}, 1131.3cm^{-1}, 1293.8cm^{-1}, and 1416.1cm^{-1}. Since these peaks are also present in the wax spectrum this indicates contamination of the bovine samples with wax. There are no obvious differences between the Raman spectra obtained from the two bovine sample types. However, according to peak analysis, the intensity of the peak at 1165cm^{-1} is significantly lower for chondroitinase ABC-treated samples compared with untreated samples. As this peak is present as a broad shoulder in the chondroitin sulphate A spectrum, this suggests that the decreasing intensity of this peak in chondroitinase ABC-treated tendons is associated with decreasing concentrations of chondroitin sulphate A.

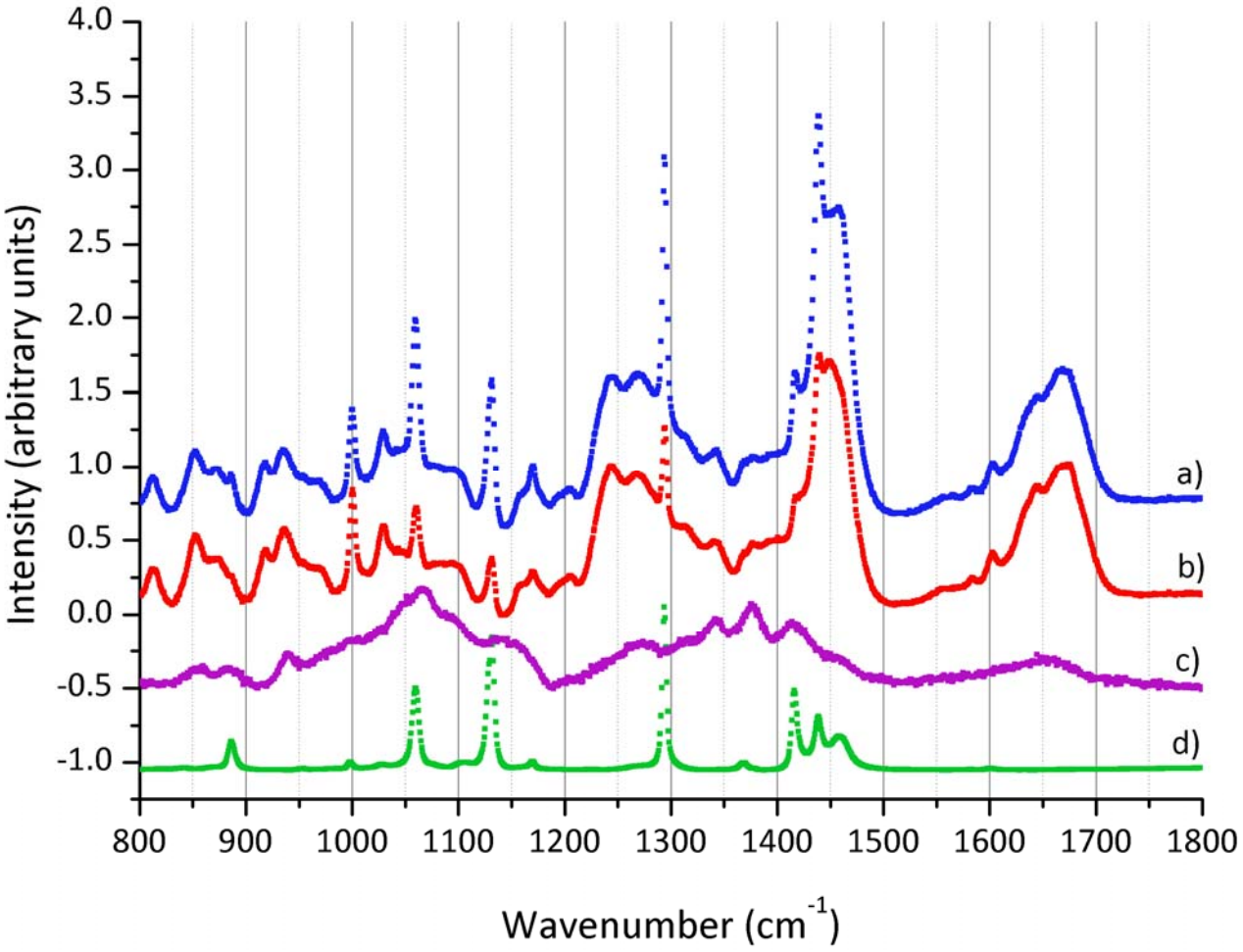

Figure 4:6 Average Raman spectra for a) untreated bovine DDFT proximal samples, b) chondroitinase ABC-treated bovine DDFT proximal samples, c) chondroitin sulphate A and d) paraffin wax. Contamination of the bovine samples with wax is evident. There are no obvious differences between the two bovine DDFT spectra.

4.2.2 Microstructural Characterisation

4.2.2.1 Representative Images

Sirius Red is a highly orientated, birefringent dye that binds to collagen in such a way that its long axis lies parallel to the long axis of the collagen molecule, thus enhancing the intrinsic positive birefringence of collagen [174, 193, 194]. The binding of Sirius red to collagen occurs via interactions between the six

sulphonic acid groups on the Sirius red molecule and the lysine and hydroxylysine residues on the collagen molecule [194]. Since the reaction between the dye and the collagen molecule occurs at low pH (≤pH2) staining is performed in the presence of picric acid. This is advantageous since picric acid is highly penetrative resulting in even very thin collagen fibres being stained, meaning that picrosirius red staining possesses far greater sensitivity than other collagen stains [194, 195].

The contrast mechanism by which picrosirius red staining of collagen produces a range of colours from green to red when viewed in polarised light, is not fully understood. Generally, colour in polarised light images arises due to birefringence retardation (a.k.a. phase difference) of the orthogonally polarized light components upon passing through the sample. For example, if the retardation corresponds to the wavelength of green light, green light would be extinguished by the analyser lens and the complementary colour (red) would be seen [196]. Considering this, it was originally suggested that contrast arose due to the presence of different types of collagen, with different retardations exhibited by different collagen types [197]. However, it is now generally accepted that contrast is strongly associated with differences in the fibre thickness, with differences in birefringence colours arising due to thicker fibres binding more dye molecules [198-200]. As such, fibres which appear red can be considered to be thicker in diameter than those which appear orange, those which appear orange are likely to be thicker in diameter than those which appear yellow, and so on.

Figure 4:7 and Figure 4:8 show representative polarised light images of picrosirius red-stained bovine DDFT and ovine infraspinatus tendon samples from different anatomical locations at x2.5 and x10 magnifications respectively. At the lower magnification (x2.5) the sample from DDFT distal ventral location is visibly different to all the other samples, seemingly containing a higher proportion of pixels with orange hues, and showing a lesser degree of organisation of the dense tissue when compared with the other samples. The crimp (Hierarchical Level 4 in Figure 3:1, pg 13) is clearly identifiable in the higher magnification images. Measurement of crimp length is demonstrated in Figure 4:9. Figure 4:10 shows representative brightfield images of the same samples at x2.5 magnification. Compared with the polarised images, these images are more uniform in colour. The sample from DDFT distal ventral location is again visibly different to the other samples, being paler in colour and again showing a lesser degree of organisation when compared with the other samples.

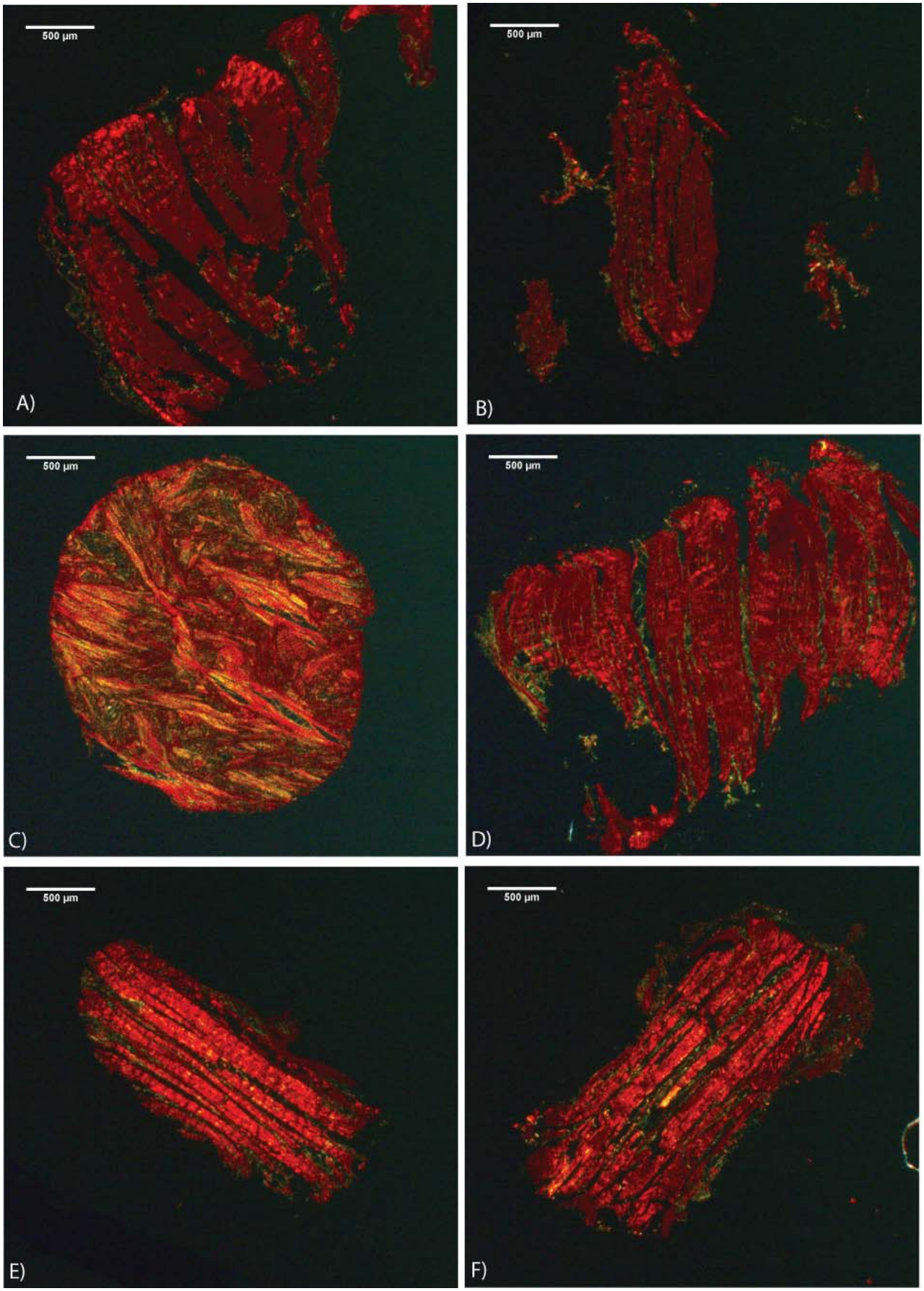

Figure 4:7 Representative polarised light images of picrosirius red-stained bovine DDFT and ovine infraspinatus tendon samples from different anatomical locations (x2.5 magnification): A) DDFT proximal ventral, B) DDFT proximal dorsal, C) DDFT distal ventral, D) DDFT distal dorsal samples, E) infraspinatus articular-side, F) infraspinatus bursa-side. The DDFT distal ventral sample (C) is visibly different to the other samples.

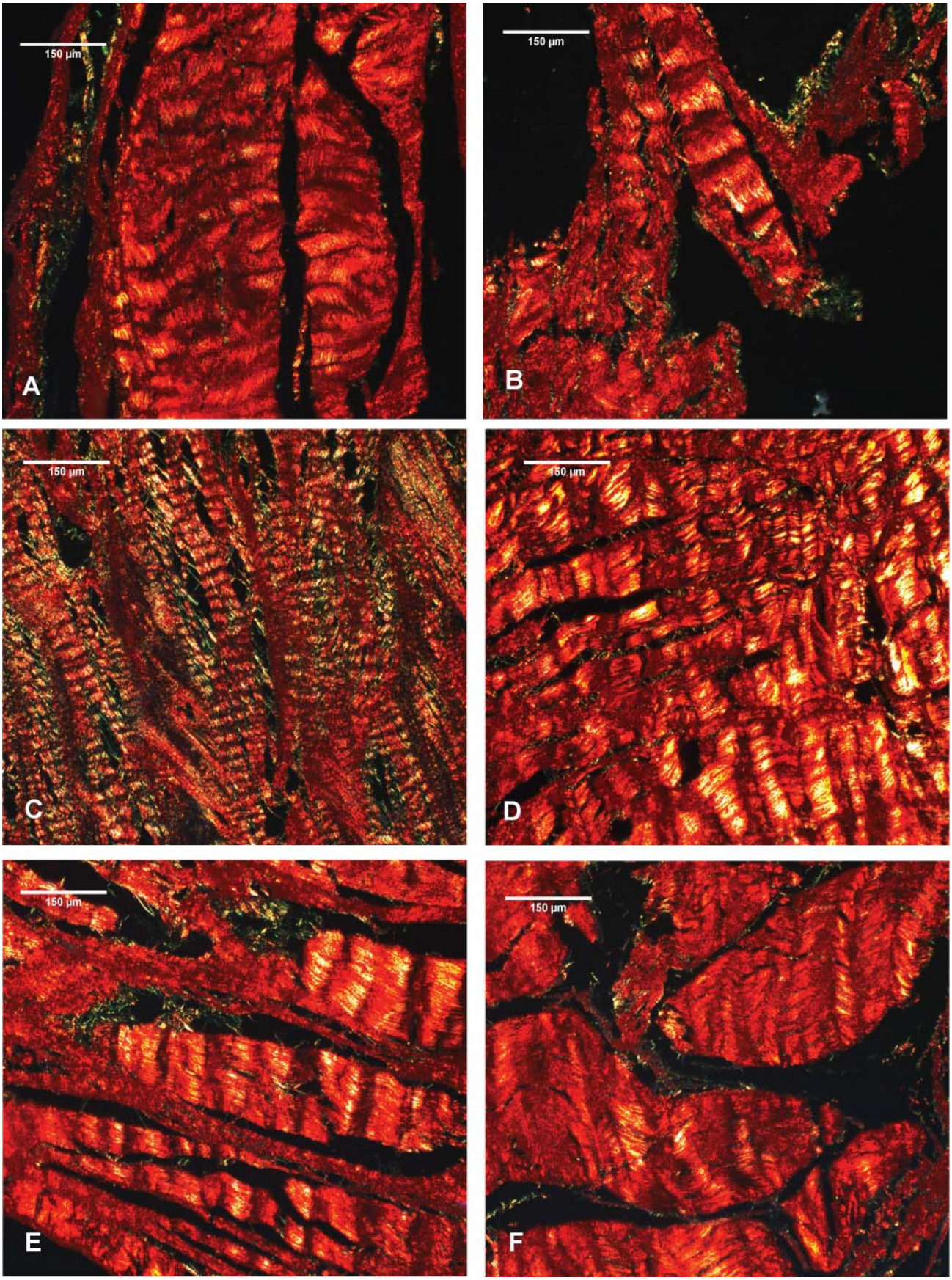

Figure 4:8 Representative polarised light images of picrosirius red-stained bovine DDFT and ovine infraspinatus tendon samples from different anatomical locations (x10 magnification): A) DDFT proximal ventral, B) DDFT proximal dorsal, C) DDFT distal ventral, D) DDFT distal dorsal samples, E) infraspinatus articular-side, F) infraspinatus bursa-side. The DDFT distal ventral sample (C) is visibly different to the other samples.

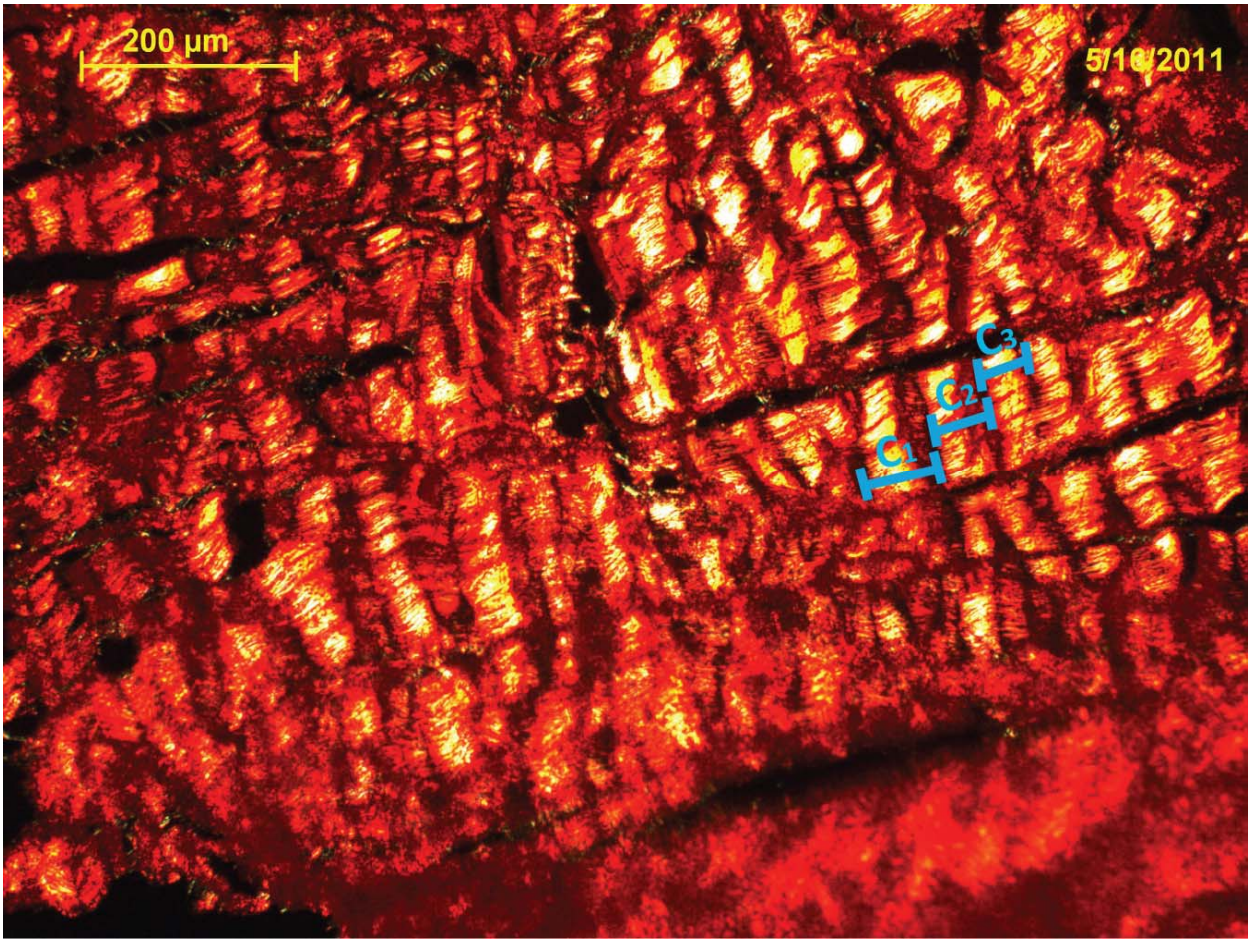

Figure 4:9 Polarised light images of picrosirius red-stained bovine deep digital flexor tendon (x10 magnification) showing measurement of the length of three crimps (C_1, C2, C_3) in blue.

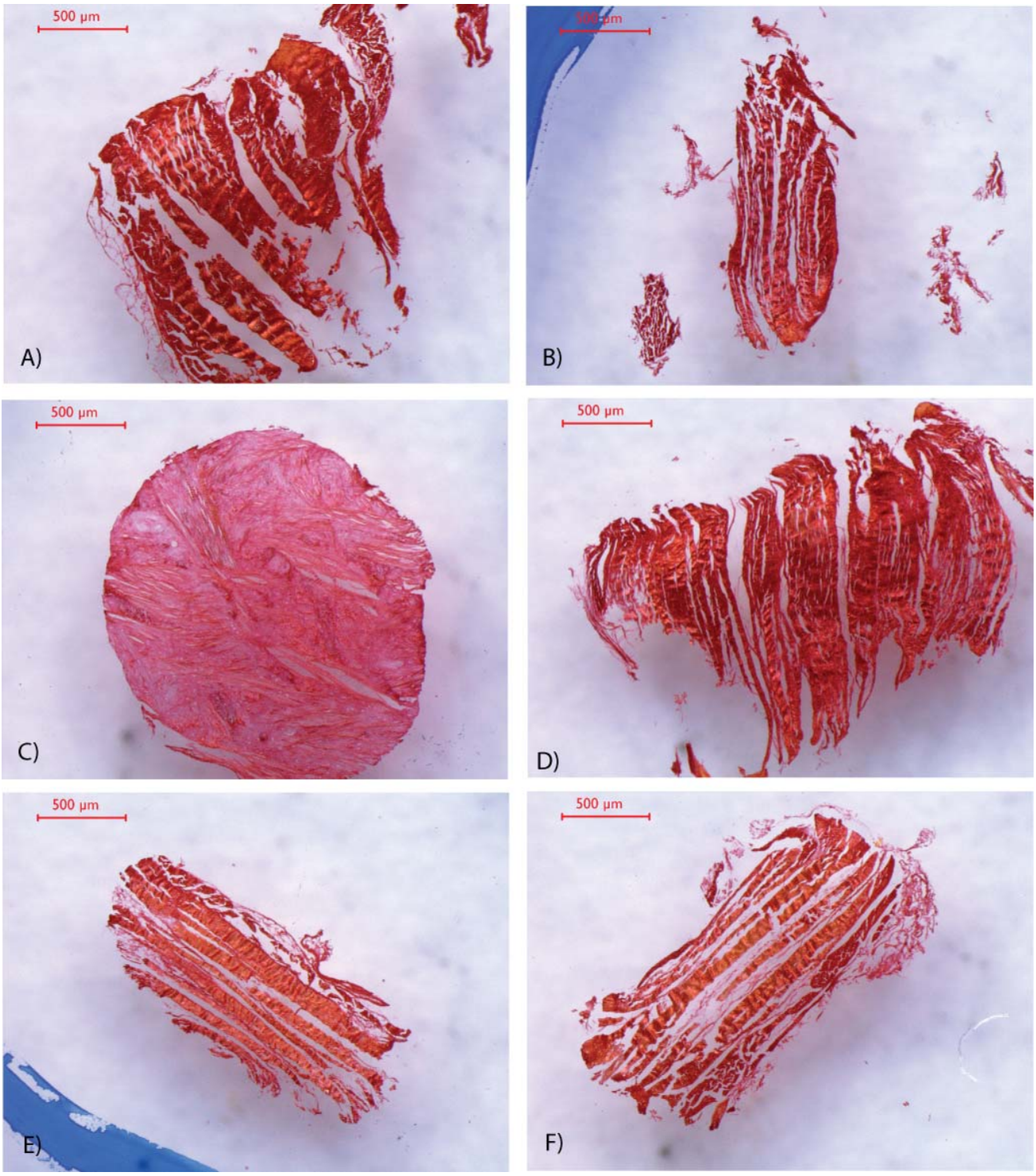

Figure 4:10 Representative brightfield images of picrosirius red-stained bovine DDFT and ovine infraspinatus tendon samples from different anatomical locations (x2.5 magnification): A) DDFT proximal ventral, B) DDFT proximal dorsal, C) DDFT distal ventral, D) DDFT distal dorsal samples, E) infraspinatus articular-side, F) infraspinatus bursa-side. The DDFT distal ventral sample (C) is visibly different to the other samples, being lighter in colour and less well aligned.

Figure 4:11 shows polarised light images of a picrosirius red-stained sample taken from the musculotendinous junction in an ovine infraspinatus at different magnifications. Muscle filaments and tendon fibres are clearly distinguishable at all three magnifications: the tendon fibres, stained red/orange/green can be seen to extend along and around the muscle filaments, which are greenish-blue and clearly striated.

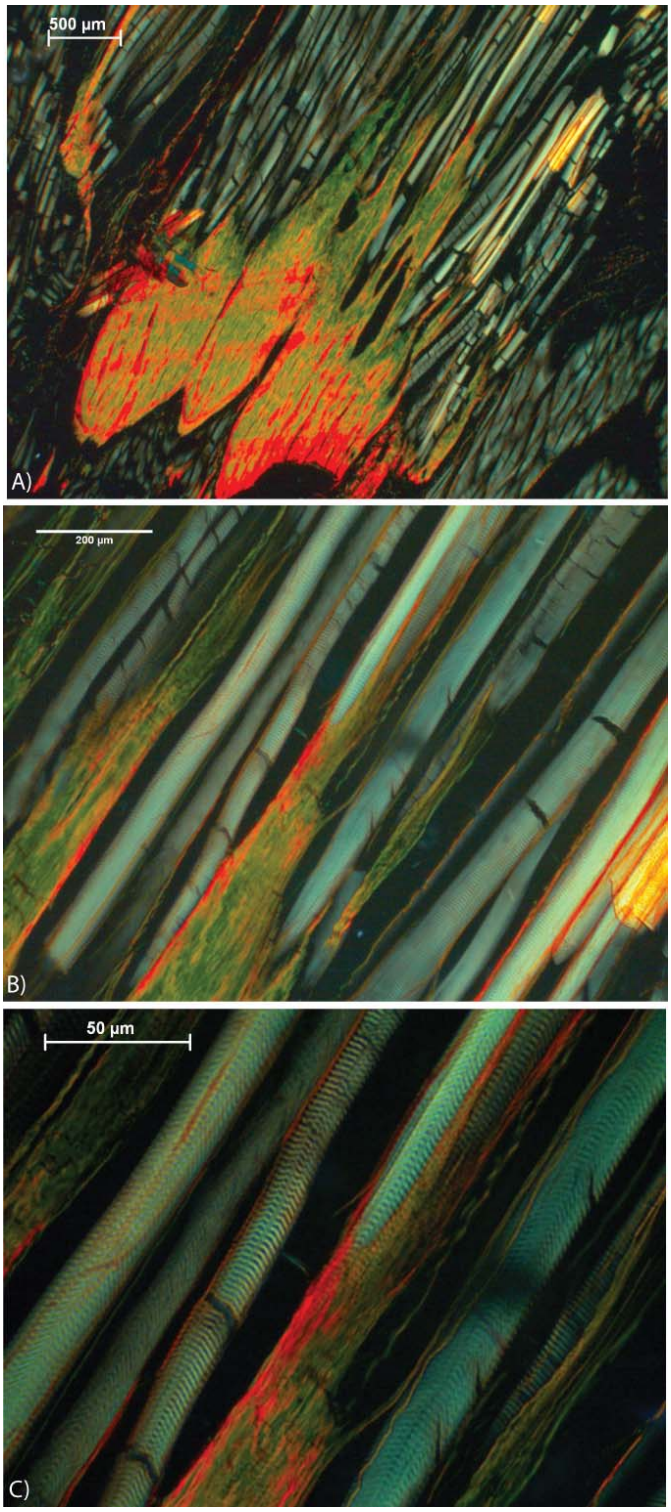

Figure 4:11 Polarised light images of a picrosirius red-stained sample taken from the musculotendinous junction in an ovine infraspinatus: A) x10 magnification, B) x 20 magnification and C) x50 magnification. The tendon fibres, stained red/orange/green by the dye can be seen to extend along and around the muscle filaments which are greenish-blue and clearly striated.

4.2.2.2 Ratio of Red to Orange Pixels

Figure 4:12 and Figure 4:13 show histograms depicting the average percentage of picrosirius red images occupied by different pixel hues (numerical value, x) from different anatomical locations in bovine DDFT and ovine infraspinatus tendon respectively. Distinct peaks representing red ($235 < x \leq 255$, $0 \leq x < 11$) and orange hues ($11 \leq x \leq 40$) are clearly visible. Statistical analysis software (OriginPro8) was used to fit curves to the peaks in the histograms for each sample in order to calculate the integral (percentage of total area) of each peak.

Figure 4:14 and Figure 4:15 present box plots representing the ratio of red to orange peak area for individual samples from different anatomical locations in bovine DDFT and ovine infraspinatus tendon respectively. In the bovine DDFT the ratio of red to orange pixels is significantly different in all anatomical locations, with the exception of proximal dorsal versus distal dorsal. The ratio is largest in the proximal ventral location and smallest in the distal ventral location, indicating that the proximal ventral contains the highest proportion of thicker fibres, while the distal dorsal region contains the lowest proportion of thicker fibres. In the ovine infraspinatus tendon there is no significant difference between the ratios of red to orange pixels between the two anatomical locations, indicating that there are no significant differences between the proportions of thicker fibres in either region.

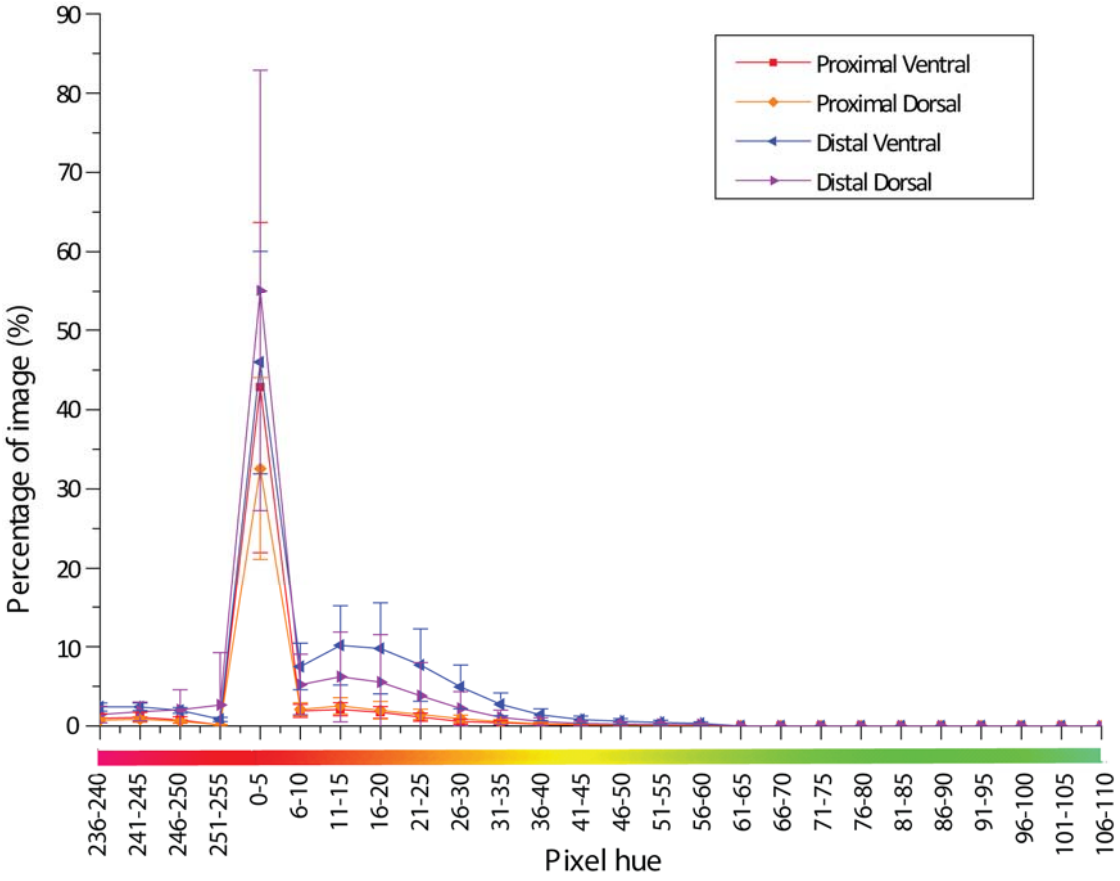

Figure 4:12 Representative histograms of percentage of image occupied by different pixel hues for bovine DDFT samples from different anatomical locations. Proportion of the image that is orange appears to be slightly higher in distal ventral and distal dorsal samples than in proximal ventral and proximal dorsal samples.

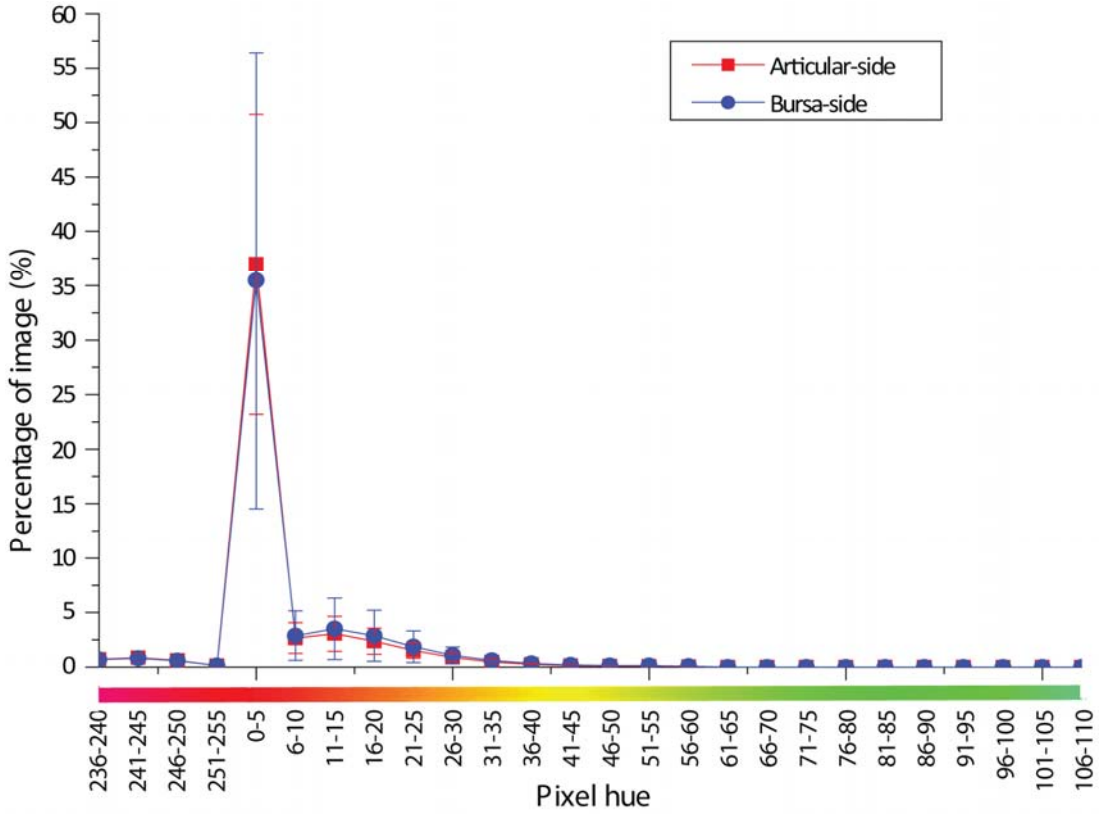

Figure 4:13 Representative histograms of percentage of image occupied by different pixel hues for ovine infraspinatus tendon samples from different anatomical locations. There do not appear to be any obvious differences between the two histograms.

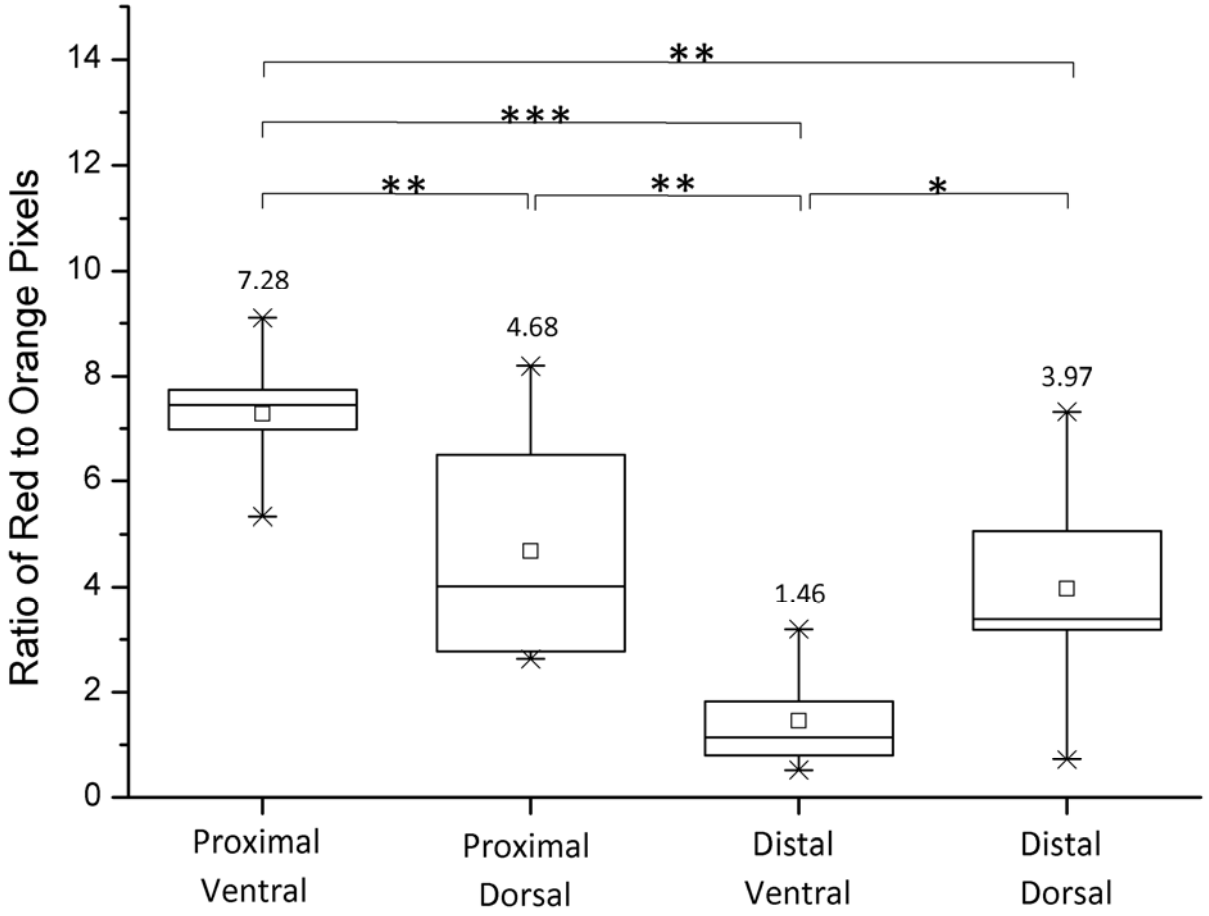

Figure 4:14 Box plots representing measurements of the ratio of red to orange pixels in bovine DDFT samples from different anatomical locations. The ratios are significantly different in all locations with the exception of proximal dorsal versus distal dorsal.

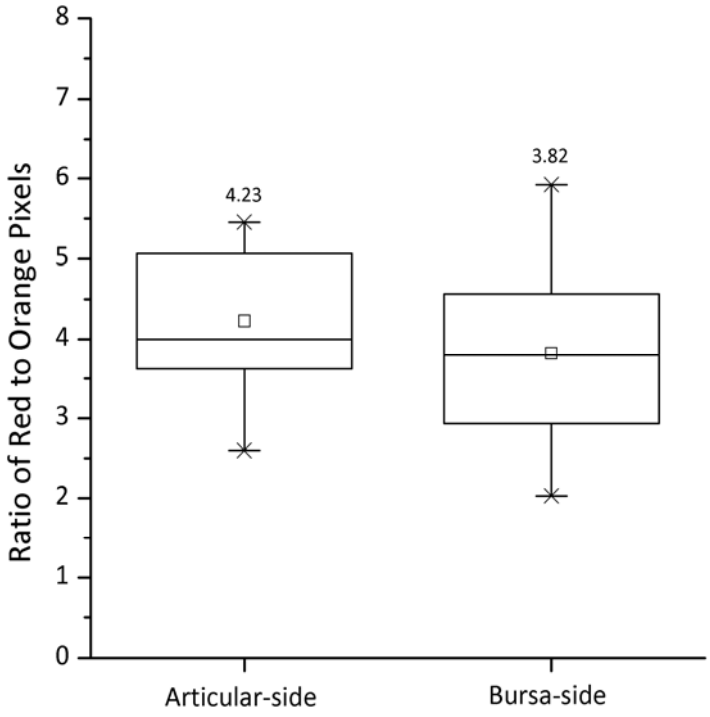

Figure 4:15 Box plots representing measurements of the ratio of red to orange pixels in ovine infraspinatus tendon samples from different anatomical locations. There is no significant difference between the ratios of red to orange pixels in the two locations.

Figure 4:16 shows histograms of the variation in pixel hue averaged over untreated and chondroitinase ABC-treated DDFT proximal samples. Figure 4:17 shows box plots depicting the variation in the ratio of red to orange fibres in bovine DDFT proximal samples that are untreated and chondroitinase ABC-treated. Although the ratio is higher for untreated samples, there are no statistical differences between the two sample types.

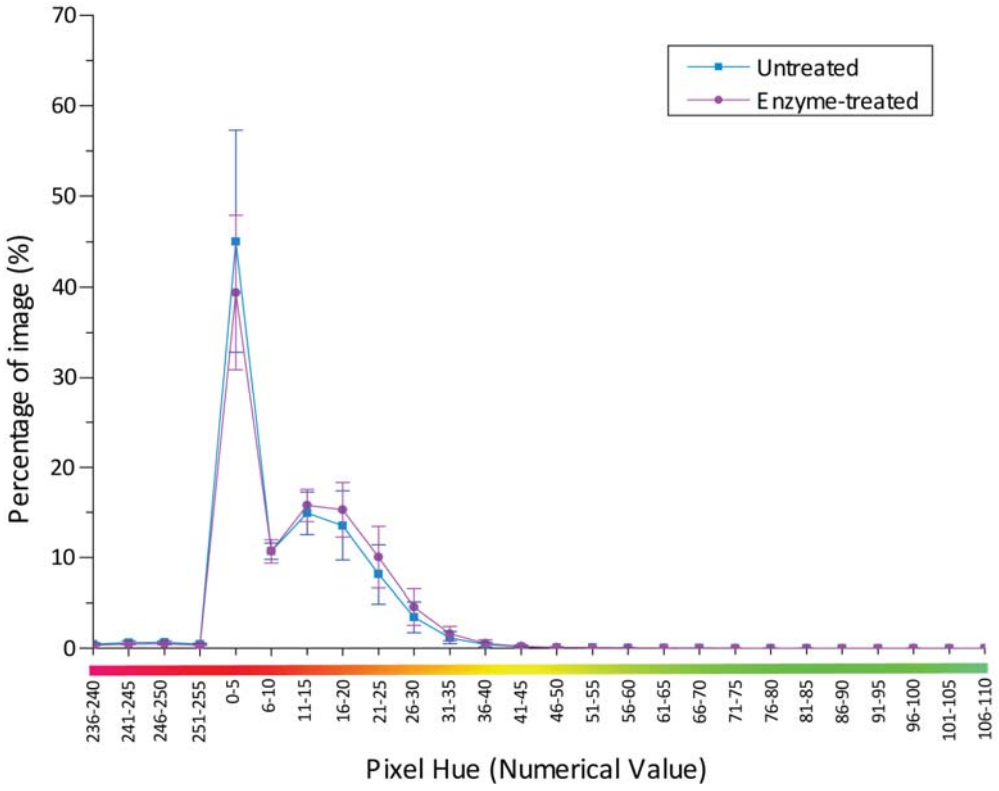

Figure 4:16 Histograms of picrosirius red-stained proximal bovine DDFT samples, for untreated and enzyme-treated samples. There are no statistical differences between the two histograms.

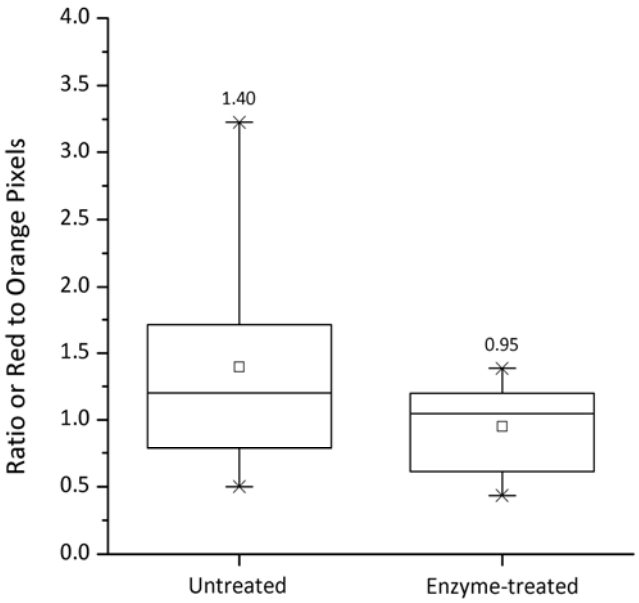

Figure 4:17 Box plots depicting the variation in ratio of red to orange fibres in picrosirius red-stained proximal DDFT untreated and enzyme-treated samples. The ratio of red to orange pixels is not statistically different between the two sample types.

4.2.2.3 Crimp Length

Figure 4:18 shows box plots representing the variation in crimp length between different anatomical locations within the bovine DDFT. Crimp length is significantly shorter in the distal portion compared with the proximal portion. It is larger in the proximal ventral samples and shortest in the distal ventral samples. Crimp length is not significantly different between the proximal ventral and proximal dorsal samples. It is significantly shorter in the distal ventral samples compared with the distal dorsal samples. Figure 4:19 shows box plots depicting the variation of crimp length with anatomical location within the ovine infraspinatus tendon. Crimp length is significantly shorter on the articular-side compared with the bursa-side. Figure 4:20 shows box plots representing measurements of crimp length in proximal bovine DDFT for untreated and chondroitinase ABC-treated samples. Crimp length is significantly longer in chondroitinase ABC-treated samples compared with untreated samples, possibly indicating that the ground substance plays an important role in the regulation of crimp length.

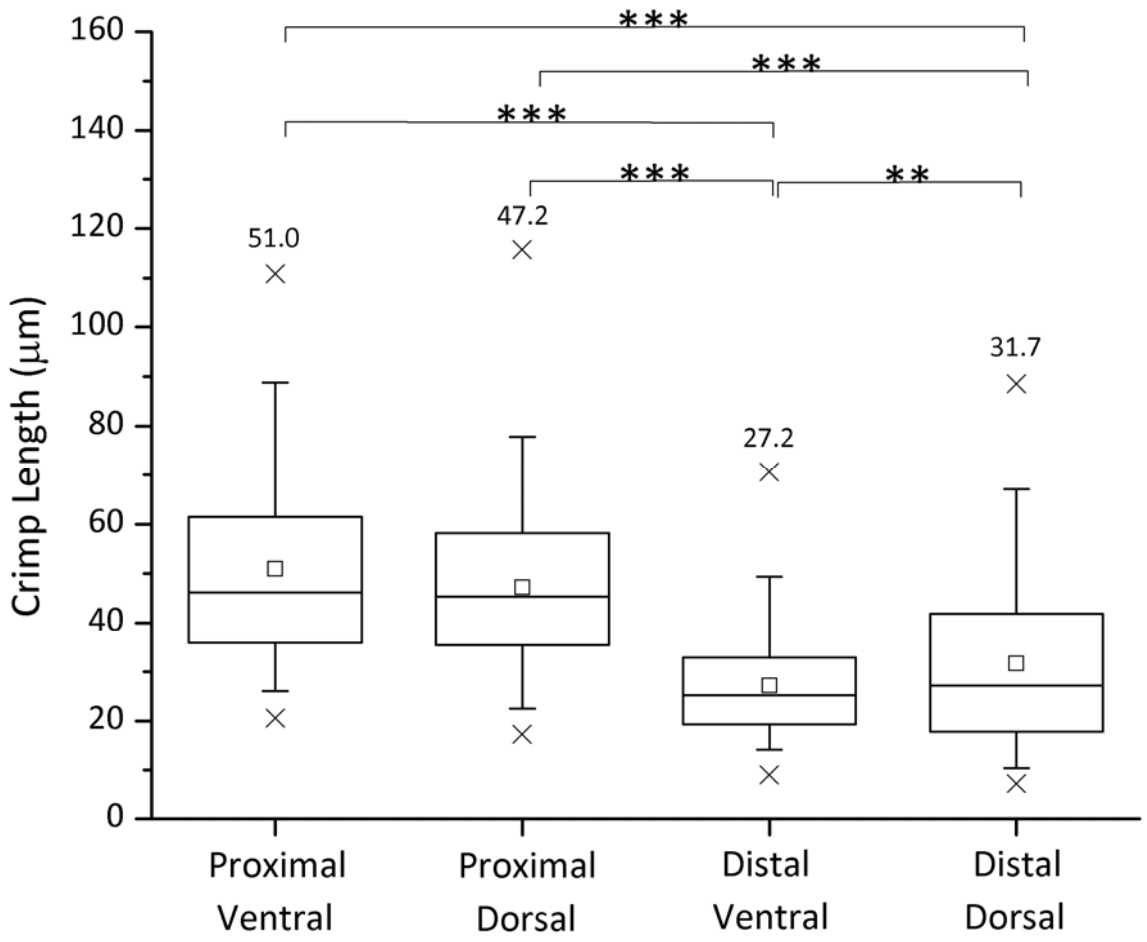

Figure 4:18 Box plots representing the variation in crimp length between different anatomical locations within the bovine DDFT. Crimp length is significantly shorter in the distal portion compared with the proximal portion. It is larger in the proximal ventral samples and shortest in the distal ventral samples. Crimp length is not significantly different between the proximal ventral and proximal dorsal samples. It is significantly shorter in the distal ventral samples compared with the distal dorsal samples.

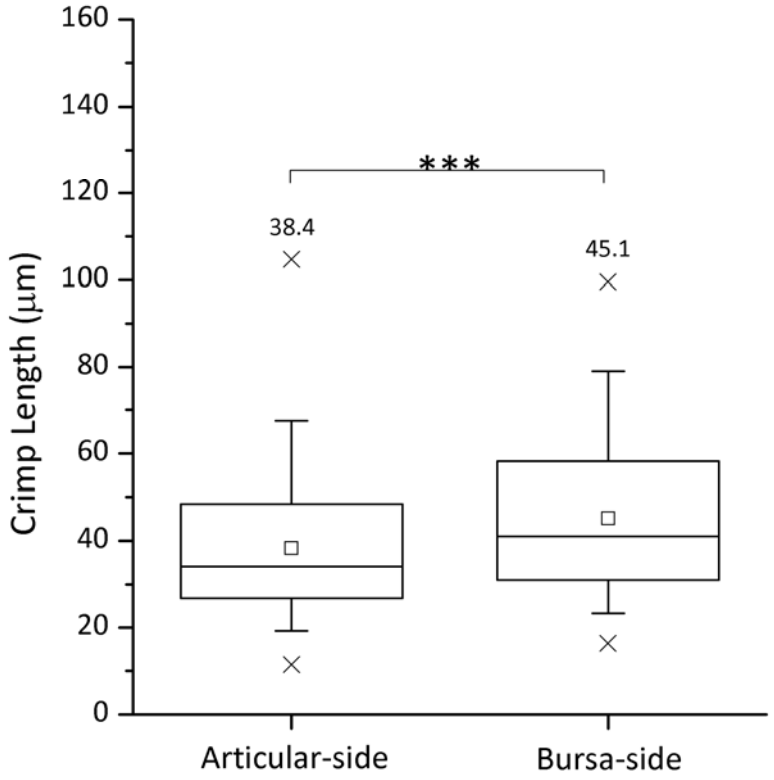

Figure 4:19 Box plots representing variation in crimp length between different anatomical locations within the ovine infraspinatus tendon. Crimp length is significantly shorter on the articular-side compared with the bursa-side.

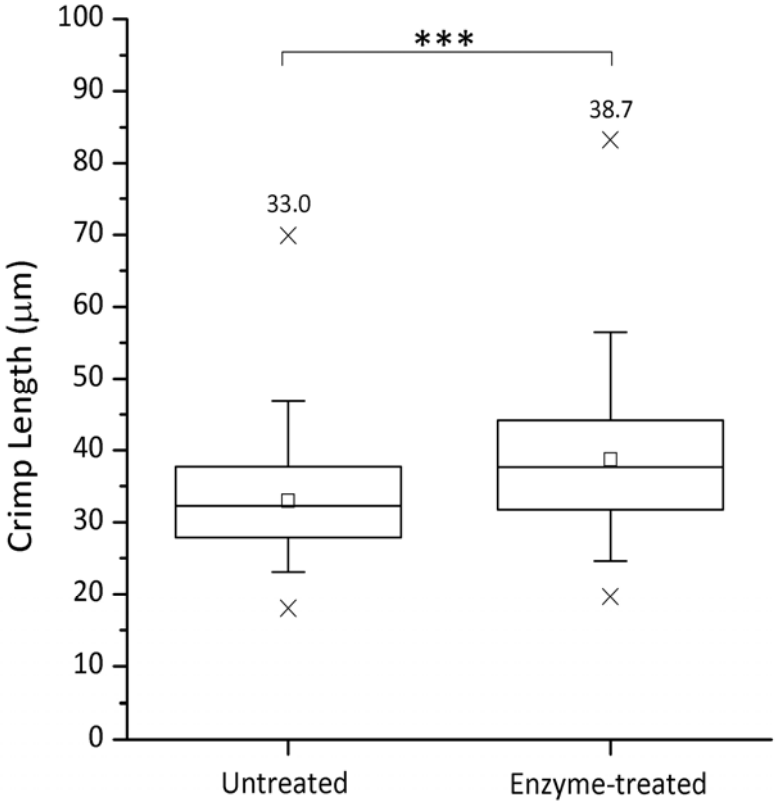

Figure 4:20 Box plots representing measurements of crimp length in proximal bovine DDFT for untreated samples and chondroitinase ABC-treated samples. Crimp length is significantly longer in enzyme-treated samples compared with untreated samples.

4.2.3 Ultrastructural Characterisation

4.2.3.1 Representative Images

Figure 4:21 shows representative AFM images of bovine DDFT samples taken from the distal region, prepared using different preservation and embedding techniques. In all images individual fibrils (Hierarchical Level 3 in Figure 3:1, pg 13) are clearly visible. However, while the 'D' spacing (regular striations perpendicular to the long axes of the fibrils) are clearly visible by eye for the aldehyde-fixed samples regardless of embedding condition, these are not as pronounced for the frozen samples. Figure 4:22 presents representative images of GA-fixed, resin-embedded bovine DDFT and ovine infraspinatus tendon from different anatomical locations. Again, individual fibrils are clearly distinguishable in each image, as is 'D' spacing.

Figure 4:23 shows representative AFM images of bovine DDFT proximal samples that are untreated and chondroitinase ABC-treated at different magnifications. There are no obvious differences between untreated and chondroitinase ABC-treated samples. 'D' spacing is clearly visible for both samples. Figure 4:24 shows how the use of Gwyydion analysis software allows information contained in these topographical AFM images to be extracted. This allows characterisation of fibril diameter and 'D' spacing, present as topographical features in the AFM images.

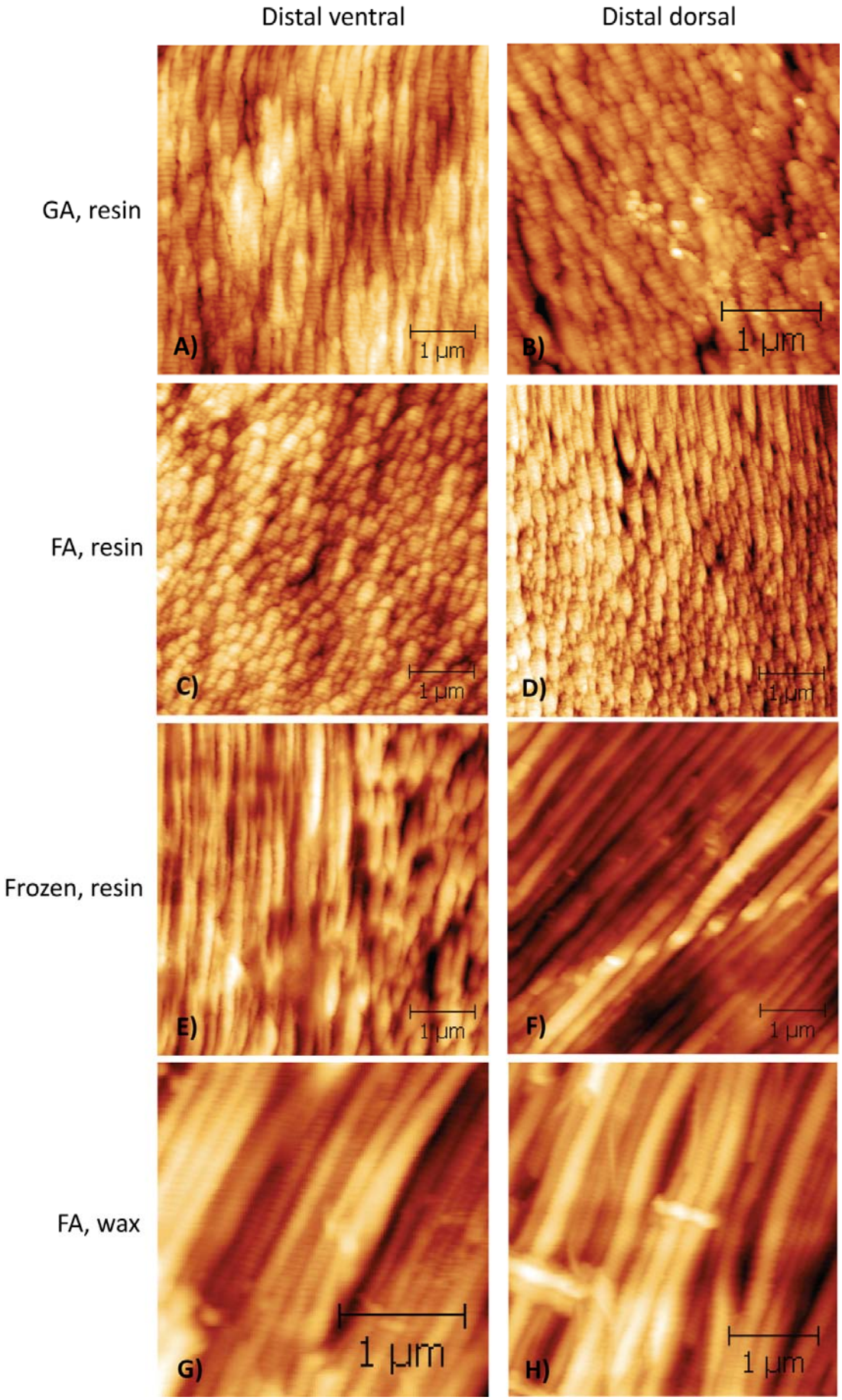

Figure 4:21 Representative AFM images of bovine DDFT distal samples prepared using different preservation techniques and embedding media: glutaraldehyde (GA) -fixed, resin embedded (A,B), formalin (FA)-fixed, resin-embedded (C,D), frozen, resin-embedded (E,F) and FA-fixed, wax-embedded (G,H). In all samples, individual fibrils are visible. 'D' spacing is not as readily distinguishable by eye in the frozen samples but is clearly visible in the aldehyde-fixed samples

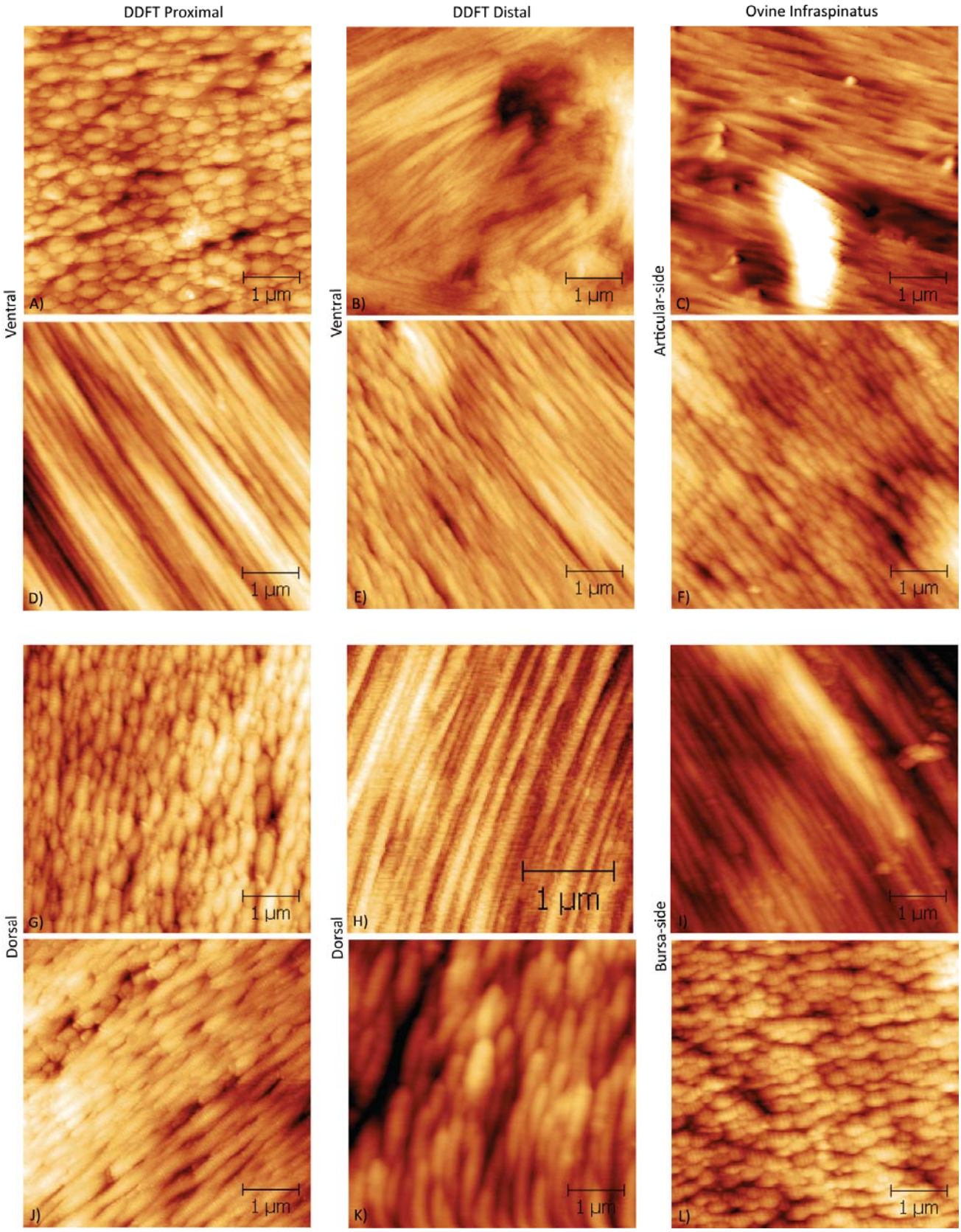

Figure 4:22 Representative AFM images of glutaraldehyde (GA)-fixed, resin-embedded bovine deep digital flexor tendon (A, B, D, E, G, H, J, K) and ovine infraspinatus tendon (C, F, I, L) from different anatomical locations.

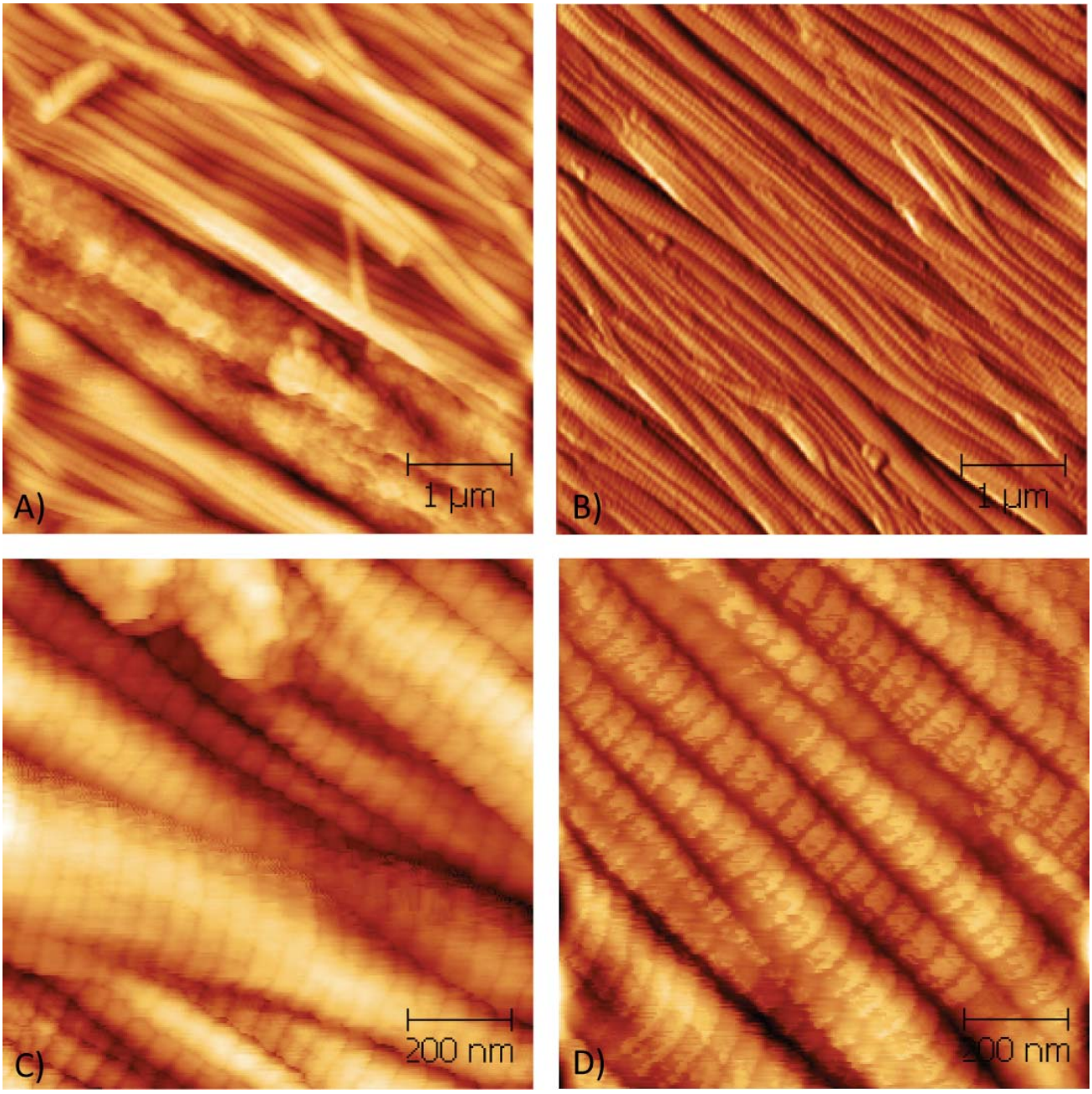

Figure 4:23 Representative AFM images of formalin (FA)-fixed, wax-embedded bovine deep digital flexor tendon proximal samples: A) 5x5µm topographical image of untreated sample, B) 5x5µm topographical image of chondroitinase ABC-treated sample, C) 1x1µm topographical image of untreated sample, D) 1x1µm topographical image of chondroitinase ABC-treated sample. There are no obvious differences between untreated and chondroitinase ABC-treated samples.

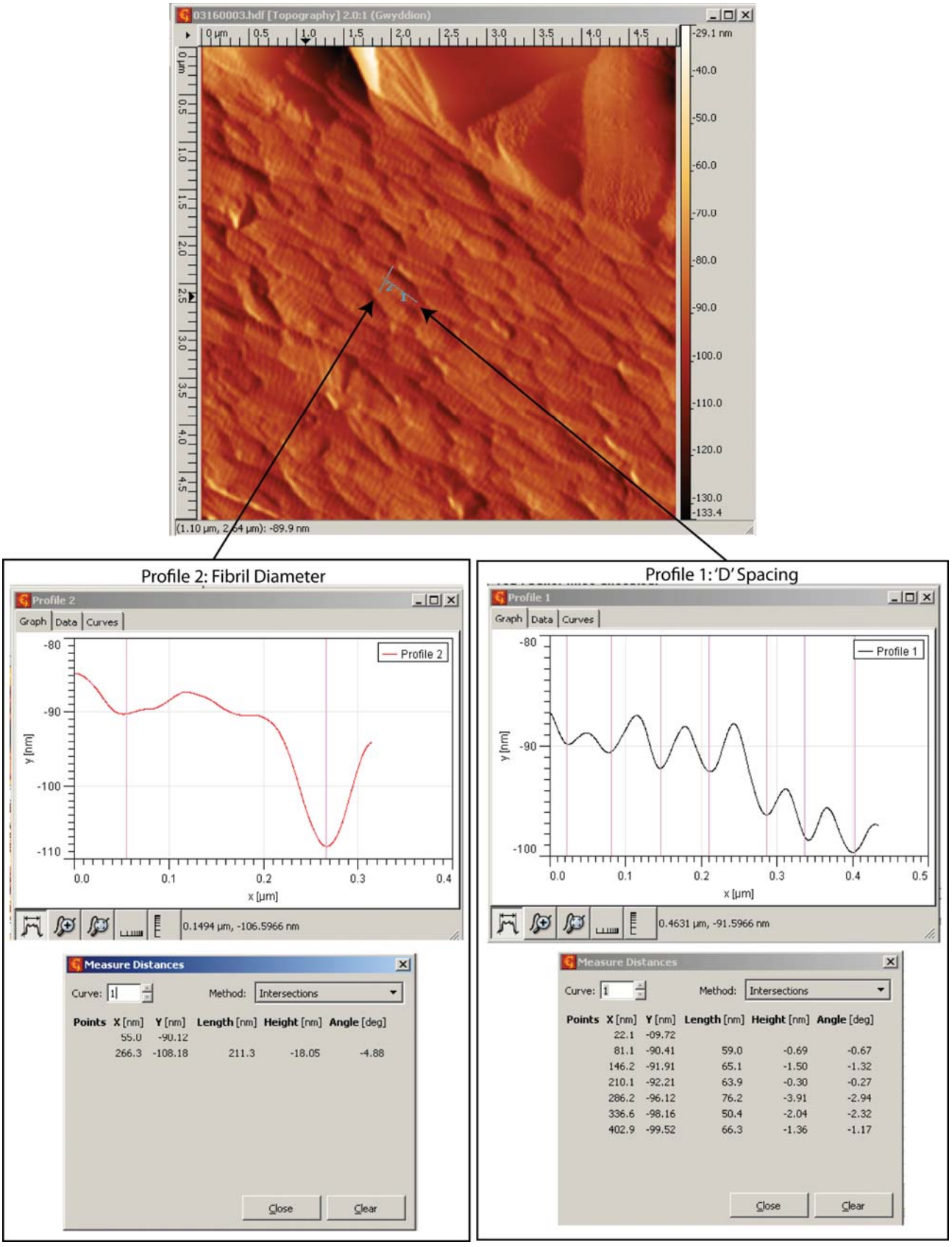

Figure 4:24 Depiction of measurement of fibril dimensions from topographical images using Gwyydion Analysis software. By analysing the clear changes in topology it is possible to measure both the fibril diameter (Profile 2) and the 'D' spacing (Profile 1).

4.2.3.2 Fibril Diameter

Figure 4:25 shows box plots of the variation of fibril diameter in bovine DDFT distal samples prepared using various preservation techniques and embedding media. For all methods fibril diameter is significantly larger in samples from the dorsal samples compared with the ventral samples. Wax-embedded samples exhibit significantly larger diameter fibrils than resin-embedded samples. Resin-embedded dorsal samples that were preserved by freezing at -80°C exhibit significantly larger diameter fibrils than samples preserved by immersion in either aldehyde solution. This difference is not seen in the ventral samples.

Figure 4:26 shows box plots of the variation of fibril diameter in GA-fixed, resin-embedded samples taken from different anatomical positions within the bovine DDFT. Fibril diameters at each anatomical location are significantly different to each other, with fibrils in the proximal region being significantly thicker than fibrils in the distal region. In the proximal portion, fibrils from the ventral region are significantly thicker than fibrils from the dorsal region. In the distal portion, fibrils from the ventral region are significantly thinner than fibrils from the dorsal region. Figure 4:27 shows box plots of the variation of fibril diameter in GA-fixed, resin-embedded samples taken from different anatomical locations within the ovine infraspinatus tendon. Fibrils from the bursa-side of the tendon are significantly thicker than fibrils from the articular-side. Figure 4:28 shows box plots depicting variation of fibril diameter for untreated and enzyme-treated bovine DDFT proximal samples. There is no significant difference between the fibril diameters for the two sample types.

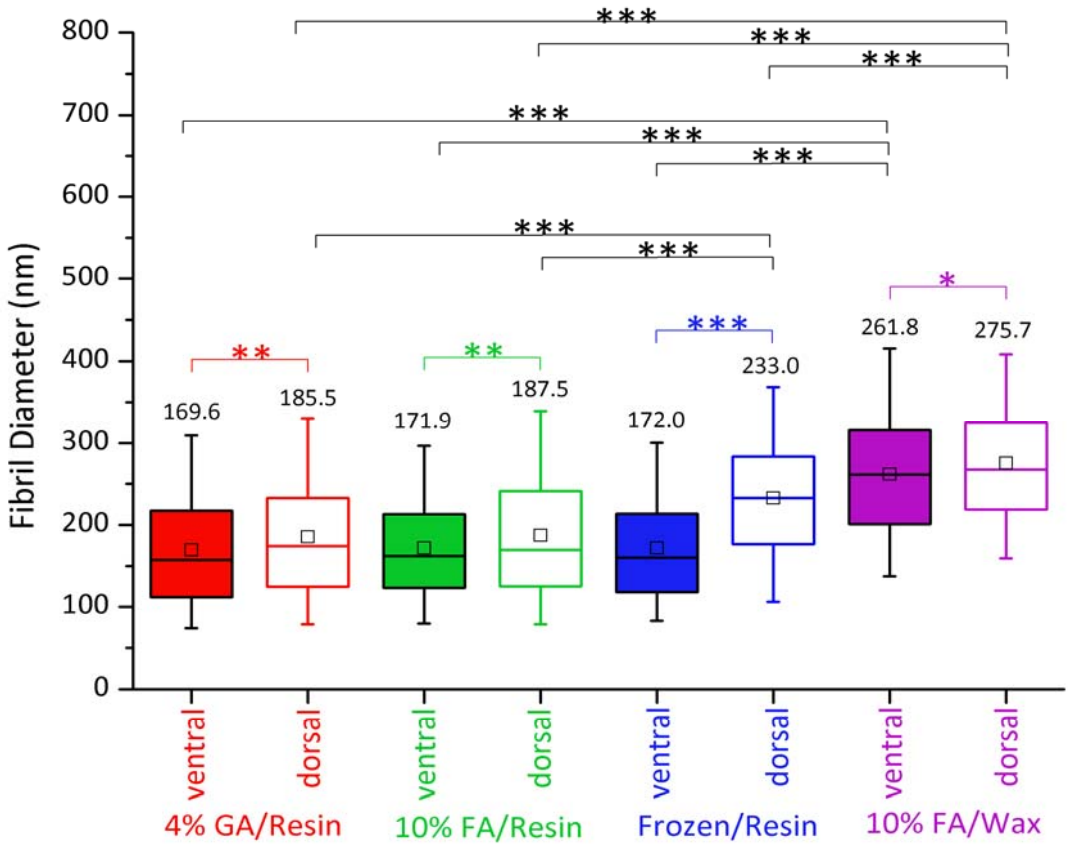

Figure 4:25 Box plots representing variation in measurements of fibril diameter in bovine distal samples prepared using different preservation techniques and embedding media. In samples that have undergone the same preservation and embedding technique dorsal samples exhibit significantly thicker fibrils than ventral samples. Wax-embedded samples exhibit significantly thicker fibrils than resin-embedded samples.

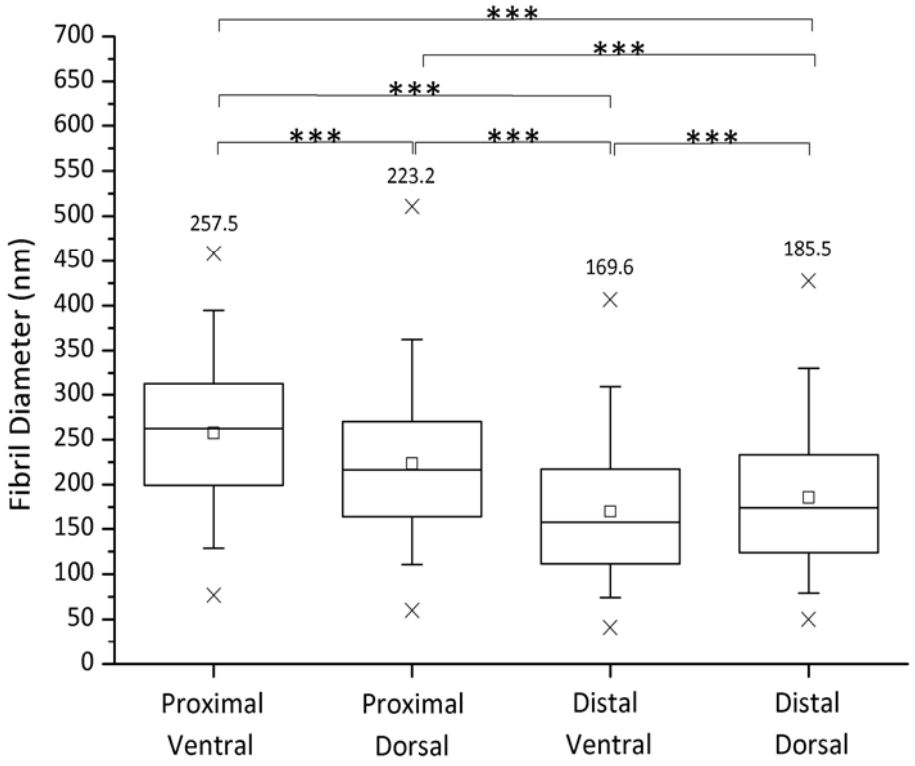

Figure 4:26 Box plots depicting the variation of fibril diameter in glutaraldehyde (GA) -fixed, resin-embedded bovine DDFT samples from different anatomical locations. Fibril diameters are significantly different at each anatomical location.

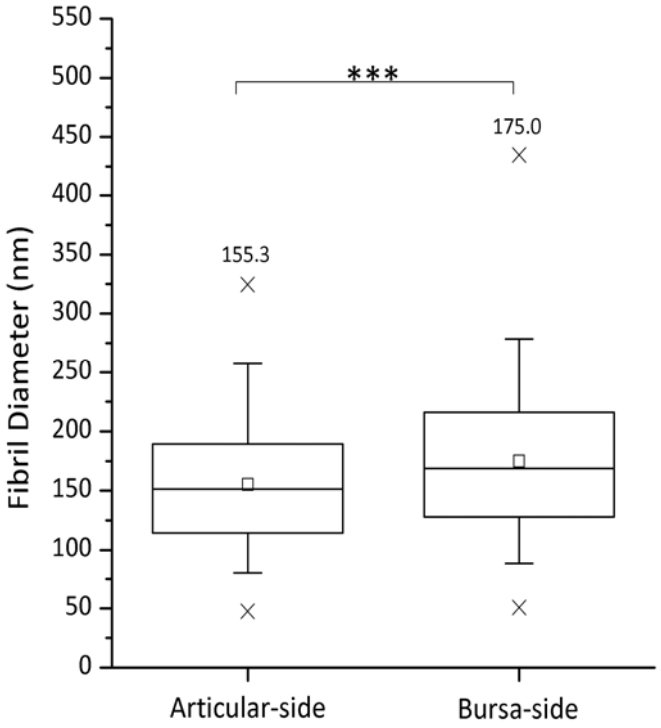

Figure 4:27 Box plots depicting the variation in fibril diameter in glutaraldehyde (GA) -fixed, resin embedded ovine infraspinatus tendon samples from different anatomical locations. Fibrils are significantly thicker on the bursa-side than on the articular-side.

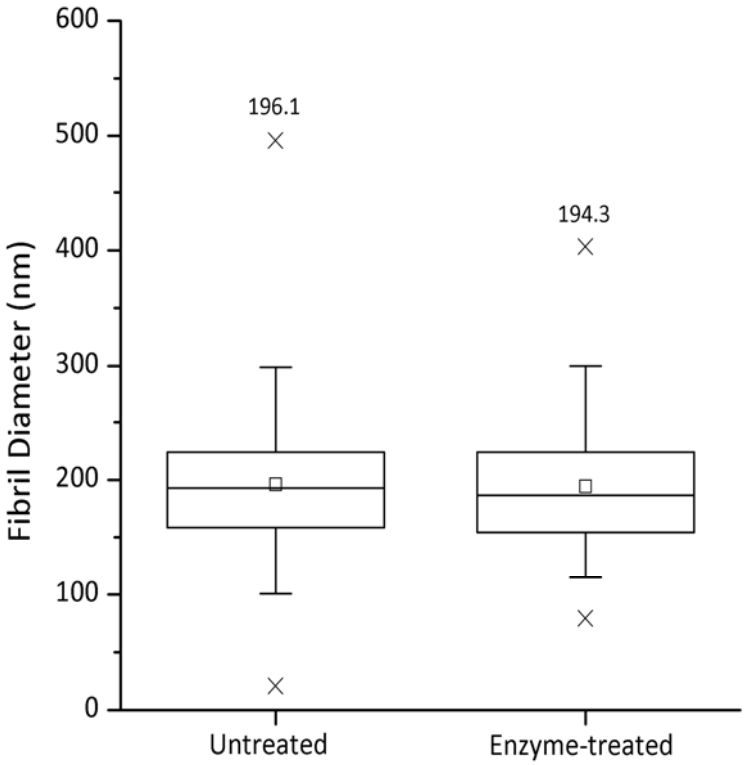

Figure 4:28 Box plots depicting variation in fibril diameter for formalin-fixed, wax-embedded untreated and enzyme-treated bovine DDFT proximal samples. Fibril diameter is not significantly different between the two sample types.

4.2.3.3 'D' Spacing

Figure 4:29 shows box plots of the variation in measurements of 'D' spacing in bovine DDFT distal samples prepared using various preservation techniques and embedding media. With the exception of GA-fixed, resin-embedded samples, there are no statistical differences between 'D' spacing in the ventral and dorsal regions within treatment conditions. In the dorsal region, 'D' spacing in GA-fixed, resin-embedded samples is significantly larger than in FA-fixed, resin-embedded samples and frozen, resin-embedded samples. In the ventral region, 'D' spacing in GA-fixed resin-embedded samples is significantly larger than in frozen, resin-embedded samples and in FA-fixed, wax embedded samples. There are no other statistical differences.

Figure 4:30 shows box plots depicting the variation of 'D' spacing in GA-fixed, resin-embedded samples taken from different anatomical positions within the bovine DDFT. With the exception of proximal ventral versus proximal dorsal, 'D' spacing is significantly different at each anatomical location, with 'D' spacing being significantly larger in the distal samples compared with the proximal samples. Figure 4:31 shows box plots depicting the variation of 'D' spacing in GA-fixed, resin-embedded samples taken from different anatomical locations within the ovine infraspinatus tendon. 'D' spacing is significantly larger on the bursa-side of the tendon compared with the articular-side. Figure 4:32 shows box plots depicting the variation of 'D' spacing between untreated and enzyme-treated bovine DDFT proximal samples. There is no significant difference between the 'D' spacing for the different sample types.

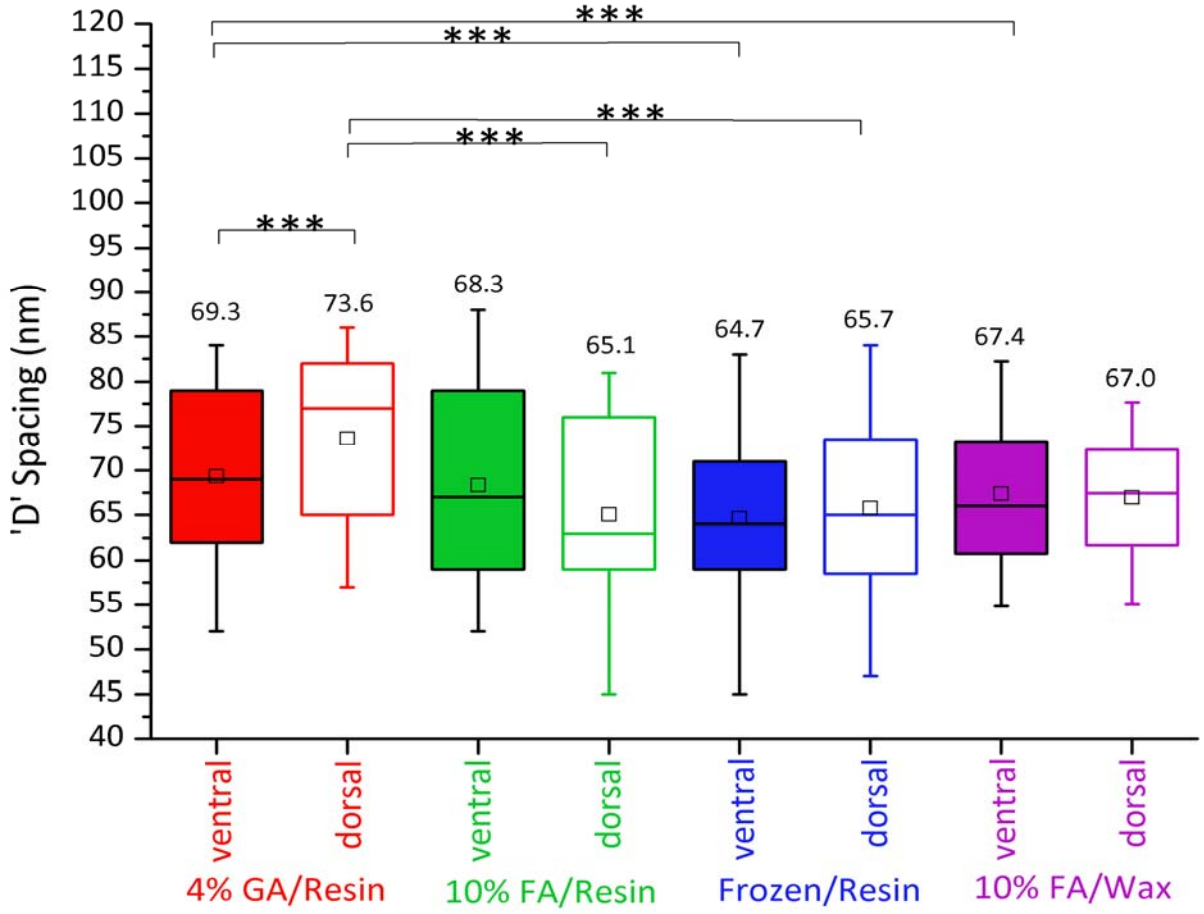

Figure 4:29 Box plots depicting the variation in measurements of 'D' spacing in bovine distal samples prepared using different preservation techniques and embedding media. With the exception of GA-fixed, resin-embedded samples, there are no statistical differences between 'D' spacing in the ventral region and the dorsal region within treatment conditions. There are no significant differences in 'D' spacing between frozen, resin-embedded samples, FA-fixed, wax-embedded samples and FA-fixed, resin embedded samples.

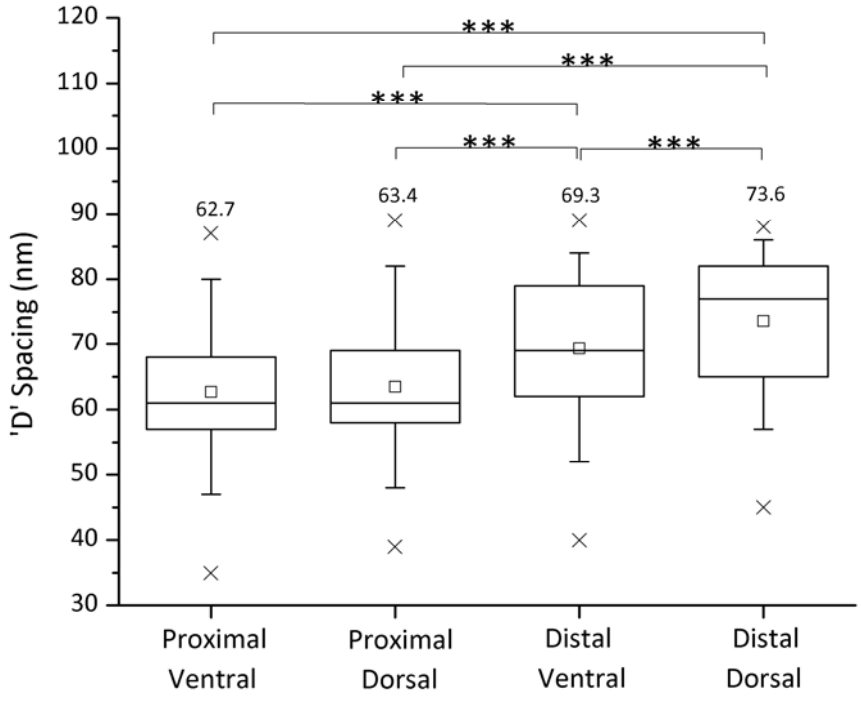

Figure 4:30 Box plots depicting variation in 'D' spacing for GA-fixed, resin-embedded bovine DDFT samples from different anatomical locations. With the exception of proximal ventral versus proximal dorsal, 'D' spacing is significantly different at each location.

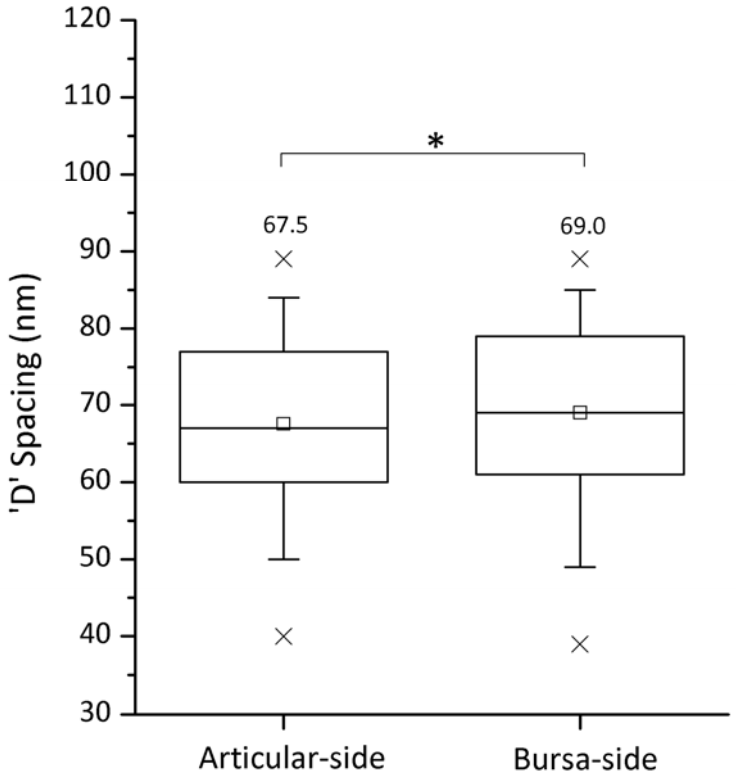

Figure 4:31 Box plots depicting variation in 'D' spacing in GA-fixed, resin embedded ovine infraspinatus tendon samples from different anatomical locations. 'D' spacing is significantly larger on the bursa-side than on the articular-side.

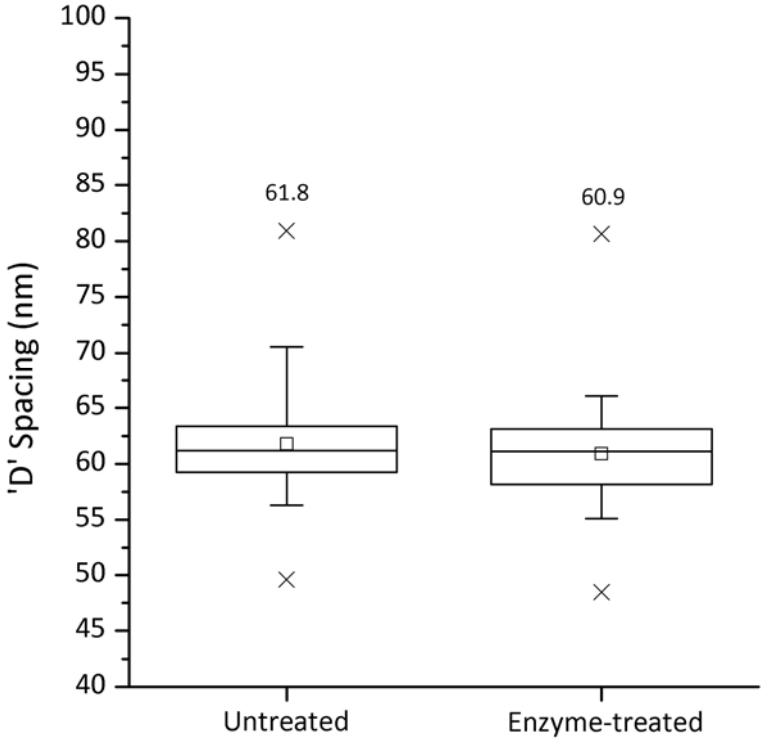

Figure 4:32 Box plots depicting variation in 'D' Spacing for untreated and enzyme-treated bovine DDFT proximal samples. 'D' Spacing is not significantly different between the two sample types.

4.2.4 Mechanical Characterisation

4.2.4.1 Indentation with AFM

Figure 4:33 shows typical force distance curves obtained for the glass substrate only (calibration curve) and a glass-mounted tendon sample, annotated to show the various parameters that can be obtained from the graph. The gradient for the glass-mounted tendon sample is less than the gradient for the glass substrate alone, giving rise to a cantilever deflection difference at any given applied force. The difference in deflection at 1 x10^{-6} N of indentation force was used to calculate stiffness values, mean values of which are presented in Table 4:3. Stiffness is lower for proximal dorsal samples than for distal ventral samples, and decreases after 15 cycles of indentation for both samples. However, the only statistical difference is between distal ventral cycle 1 and proximal dorsal cycle 15.

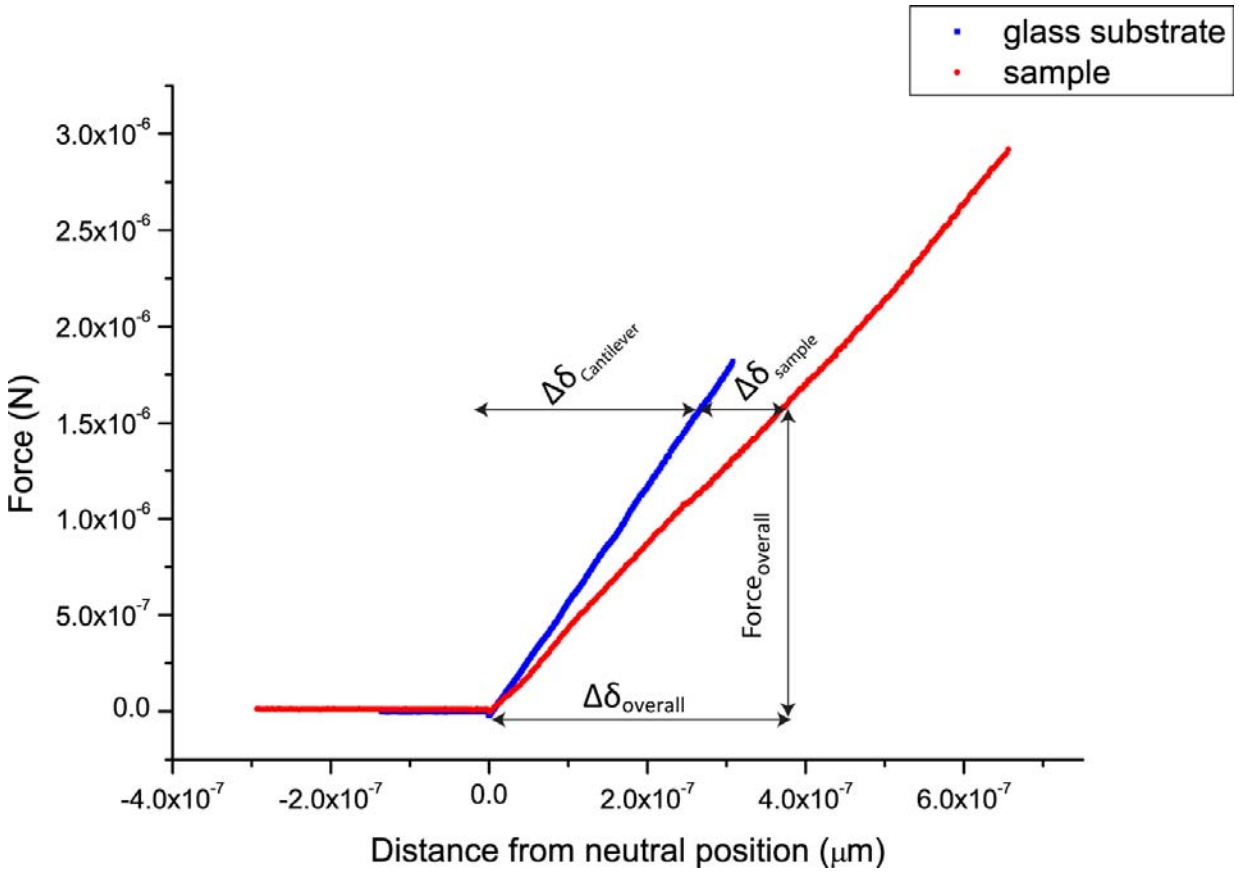

Figure 4:33 Typical Force-Distance curves of glass and tendon obtained by indentation with an atomic force microscope. The curve is annotated to illustrate how stiffness was calculated: assuming the system acts as two compliant springs, the stiffness of the sample is calculated as total force, F_t, divided by sample compression, δ_s.

Table 4:3 Values of Stiffness, Sneddon Coefficient and Tensile Modulus for Bovine Samples, as assessed using AFM-indentation

	Distal Ventral		Proximal Dorsal	
	Cycle 1	***Cycle 15***	***Cycle 1***	***Cycle 15***
Stiffness ($N\ m^{-1}$)	39.72 ± 33.04	34.51 ± 28.45	28.16 ± 24.32	23.22 ± 17.80
Sneddon Exponent	0.88 ± 0.16	0.91 ± 0.14	1.05 ± 0.13	1.08 ± 0.14
Tensile Modulus (MPa)	49.7 ± 41.4	43.1 ± 35.5	35.2 ± 30.4	29.0 ± 22.2

Mean values of the Sneddon exponent for different samples after different numbers of cycles are presented in Table 4:3. Since the average Sneddon exponent for all samples is approximately 1 for both sample types, stiffness values were converted to effective Tensile modulus values using the expression for the relation between indentation force and indentation depth when indentation area is cylindrical (Equation 4:3) [183, 184].

$$F_{cylindrical} = 2RE^{*}\delta \qquad \text{Equation 4:1}$$

where R is the characteristic radius of the tip.

Mean values of the effective tensile modulus of different samples after 1 and 15 cycles are presented in Table 4:3. As for the mean stiffness values, effective tensile modulus is lower for proximal dorsal samples than for distal ventral samples, and decreases after 15 cycles of indentation for both samples although the only statistical difference is between distal ventral cycle 1 and proximal dorsal cycle 15. The values of the tensile modulus are similar to those reported by Yang et al for indented tendon fibrils [80], but are much lower than other data listed in Table 3:1 (pg 16).

4.2.4.2 Nanoindentation

Figure 4:34 shows characteristic load-unload curves for large indentations (2µm) into a glass substrate and a glass-mounted tendon sample, and small indentations (500nm) into a distal ventral sample and a proximal dorsal sample. The load and unload curves are not linear and all samples show creep between load and unload cycles. Furthermore, glass is much stiffer than glass-mounted tendon samples. Up to

approximately 300nm, the distal ventral and proximal dorsal samples show similar load curves, but after 300nm distal ventral samples appear stiffer than proximal dorsal samples.

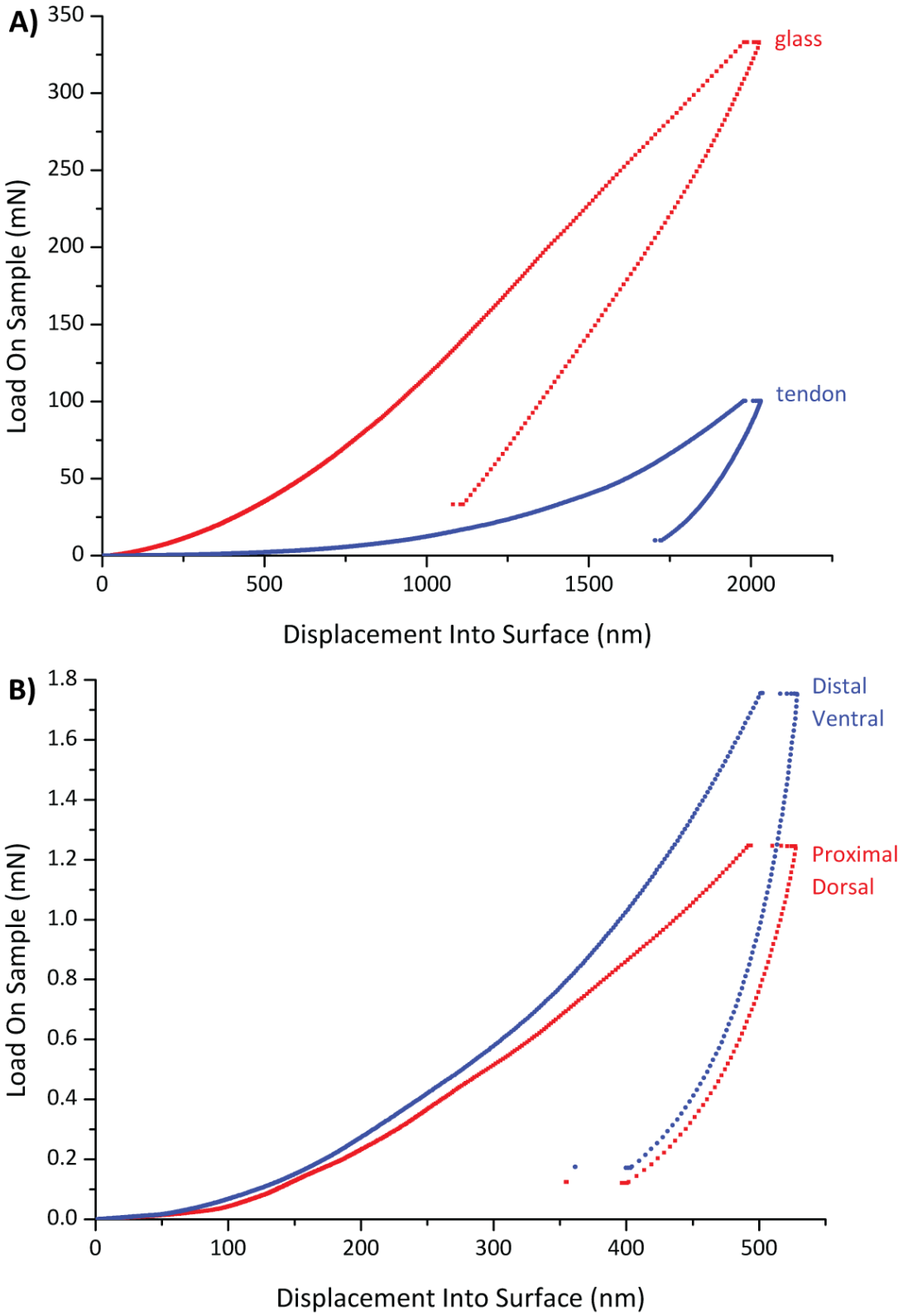

Figure 4:34 Characteristic load-unload curves: A) large indentations (x-scale = 2µm) into a glass substrate and a glass-mounted tendon sample, and B) small indentations (x-scale = 500nm) into distal ventral sample and proximal dorsal sample. The load and unload curves are not linear. All samples show significant creep between load and unload curves. For the large indentations, glass is much stiffer than glass-mounted tendon samples. For the 500nm indents, below 300nm the distal ventral and proximal dorsal samples show similar load curves. However, after 300nm distal ventral samples appear stiffer than proximal dorsal samples

Figure 4:35 and Figure 4:36 show line plots of the variation in hardness and modulus respectively with displacement into the surface for large indentations into the glass substrate only and glass-mounted tendon samples together with an apparently anomalous curve for a large indentation into a tendon sample, in which the sample appears to rapidly approach the behaviour of the glass. For the glass substrate both hardness and modulus decrease slightly over the course of the experiment. Conversely, for the glass-mounted tendon samples, hardness and modulus both increase over the course of the experiment, gradually approaching the curves for the glass substrate. This occurs far more rapidly for the anomalous curve than for the average curve, possibly indicating that at this location the sample is less thick. To exclude such anomalous results, hardness-displacement curves that appeared to rapidly approach the behaviour of glass (i.e. curves that appeared similar to the anomalous curve in Figure 4:35 and Figure 4:36) were removed from further analyses. Approximately 10% of the curves were deemed to be anomalous.

Figure 4:37 and Figure 4:38 present line plots depicting the variation of hardness and modulus respectively with displacement into the surface for small (500nm) indentations into distal ventral and proximal dorsal samples. Below 50nm, hardness decreases rapidly, becoming approximately constant from approximately 100nm indentation depth. Conversely, modulus is approximately constant between 100nm and 200nm but increases over the course of the experiment. There is no difference between the hardness and modulus of the two samples over the course of the experiment.

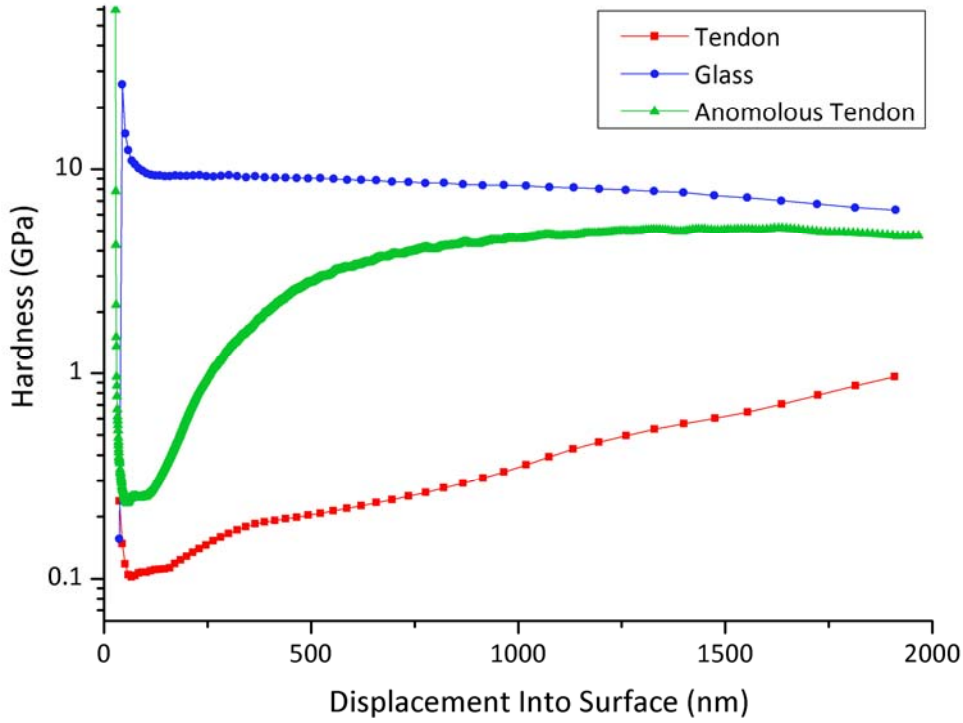

Figure 4:35 Line graphs of variation of Hardness with Displacement into surface for large indentations into tendon and glass, shown together with an anomalous curve for a large indentation into tendon. Hardness is shown on a log-scale. For the large tendon indentation, hardness increases steadily throughout the course of the indent. For the anomalous tendon indentation result, hardness rapidly approaches the hardness curve for glass.

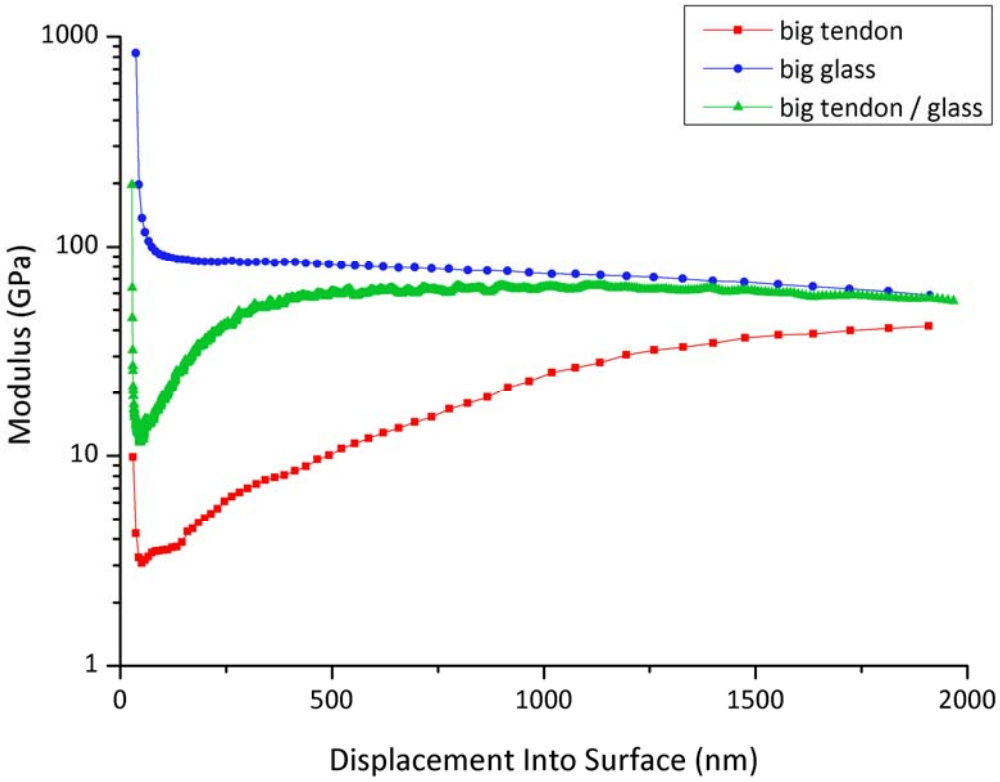

Figure 4:36 Line graphs of variation of Modulus with Displacement into surface for large indentations into tendon and glass, shown together with an anomalous curve for a large indentation into tendon. Modulus is shown on a log-scale. For the large tendon indentation, modulus increases steadily throughout the course of the indent, almost reaching the modulus curve for glass over the course of the experiment. For the anomalous tendon indentation result, modulus rapidly approaches the hardness curve for glass.

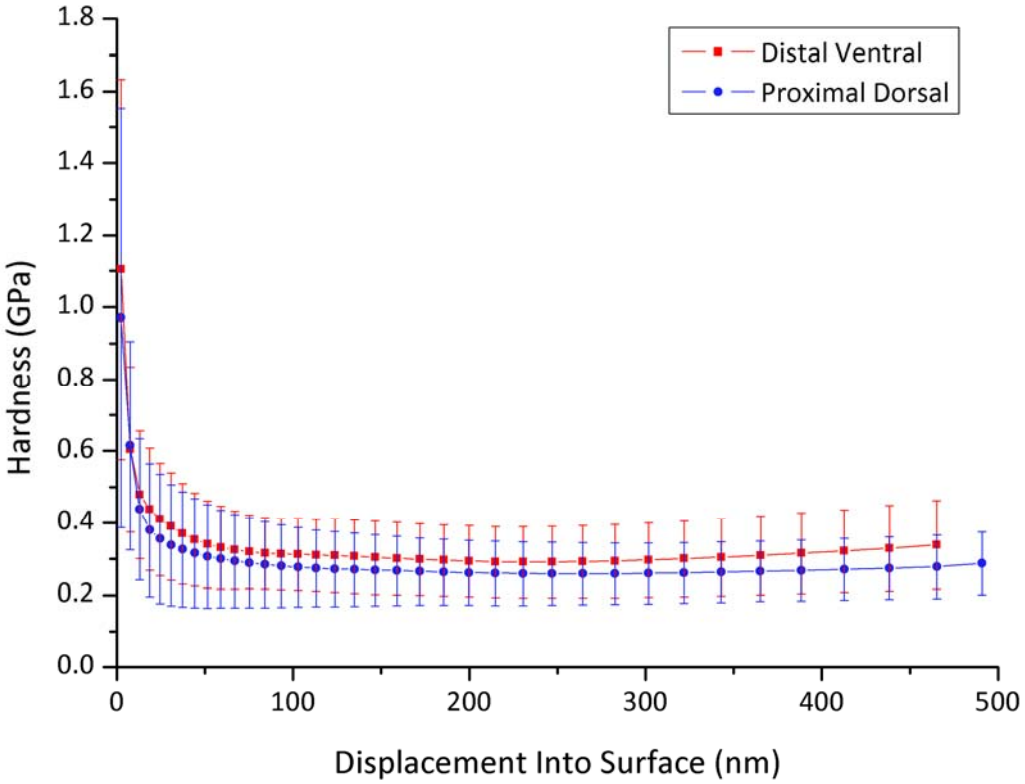

Figure 4:37 Line plots demonstrating variation of hardness with displacement into surface for distal ventral and proximal dorsal samples. There is no difference within error bars between the hardness of the two samples. Below 50nm, hardness decreases rapidly with indentation depth, before increasing gradually with increasing indentation depth through the remaining displacement.

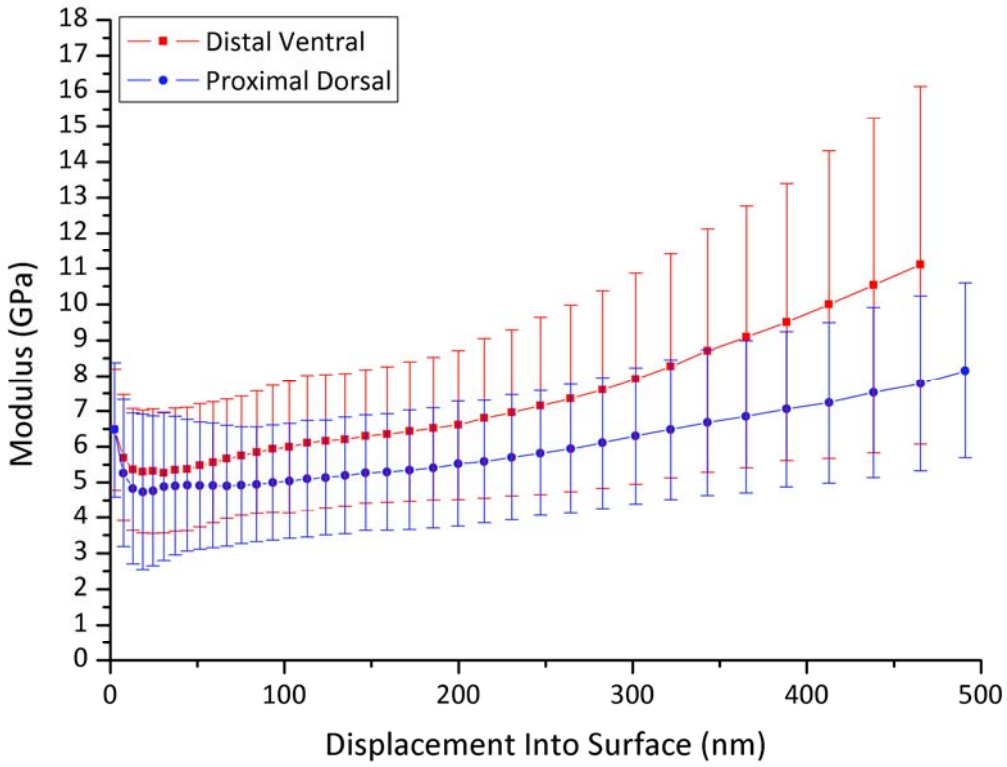

Figure 4:38 Line plots demonstrating variation of modulus with displacement into surface for distal ventral and proximal dorsal samples. Error bars are large for both samples, and overlap indicating that there is no difference between the modulus of the two samples over the displacement depth. Modulus increases throughout the course of the indentation, and appears to increase to a greater extent for the distal ventral samples

Table 4:4 presents the mean hardness and moduli for distal ventral and proximal dorsal samples averaged between 100-300nm and mean creep length at the hold point between load and unload. Mean hardness, modulus and creep length of glass samples over the same region are included for comparison. Distal ventral samples are significantly stiffer ($p = 0.016$) than proximal dorsal samples but are not significantly harder ($p = 0.215$). There is no statistical difference between the amount of creep exhibited by distal ventral samples and proximal dorsal samples between load and unload ($p = 0.121$). Values of hardness and modulus of the tendon samples are an order of magnitude smaller than the values for glass, but are two orders of magnitude greater than the stiffness values presented for AFM indentation (Section 4.2.4.1 and Table 4:3 above), and the reported stiffness of the collagen molecule [68]. Surprisingly, the amount of creep exhibited by the glass sample between load and unload is significantly larger than that exhibited by distal ventral samples ($p = 3.218 \times 10^{-4}$) and proximal dorsal samples ($p = 0.006$). This is probably due to creep of the mounting material (paraffin wax) as glass is not expected to exhibit viscoelastic behaviour.

Table 4:4 Tensile modulus and Hardness of different samples over a defined range

	Hardness averaged over defined Loading Range (GPa)	Tensile modulus averaged over defined Loading Range (GPa)	Creep between load and unload (nm)
Distal Ventral	0.29 ± 0.10	6.52 ± 2.14	27.64 ± 5.94
Proximal Dorsal	0.26 ± 0.09	5.38 ± 1.79	30.02 ± 3.08
Glass	9.31 ± 0.39	86.58 ± 2.76	37.73 ± 1.77

4.2.5 Correlations

Figure 4:39 presents scatter plots showing the correlations between different characteristics measured for the healthy animal tendons. There are significant negative correlations between fibril diameter and 'D' spacing, and red to orange ratio and 'D' spacing. There are significant positive correlations between red to orange ratio and fibril diameter, crimp length versus red to orange ratio, and crimp length versus fibril diameter. Pearson's correlation coefficient is less than 0.6 for all correlations, which is in agreement with the large degree of scatter in the data as seen on the graphs. The largest correlation coefficient and the most significant correlation is between red to orange ratio and fibril diameter ($r = 0.521$, $p = 3.82 \times 10^{-5}$).

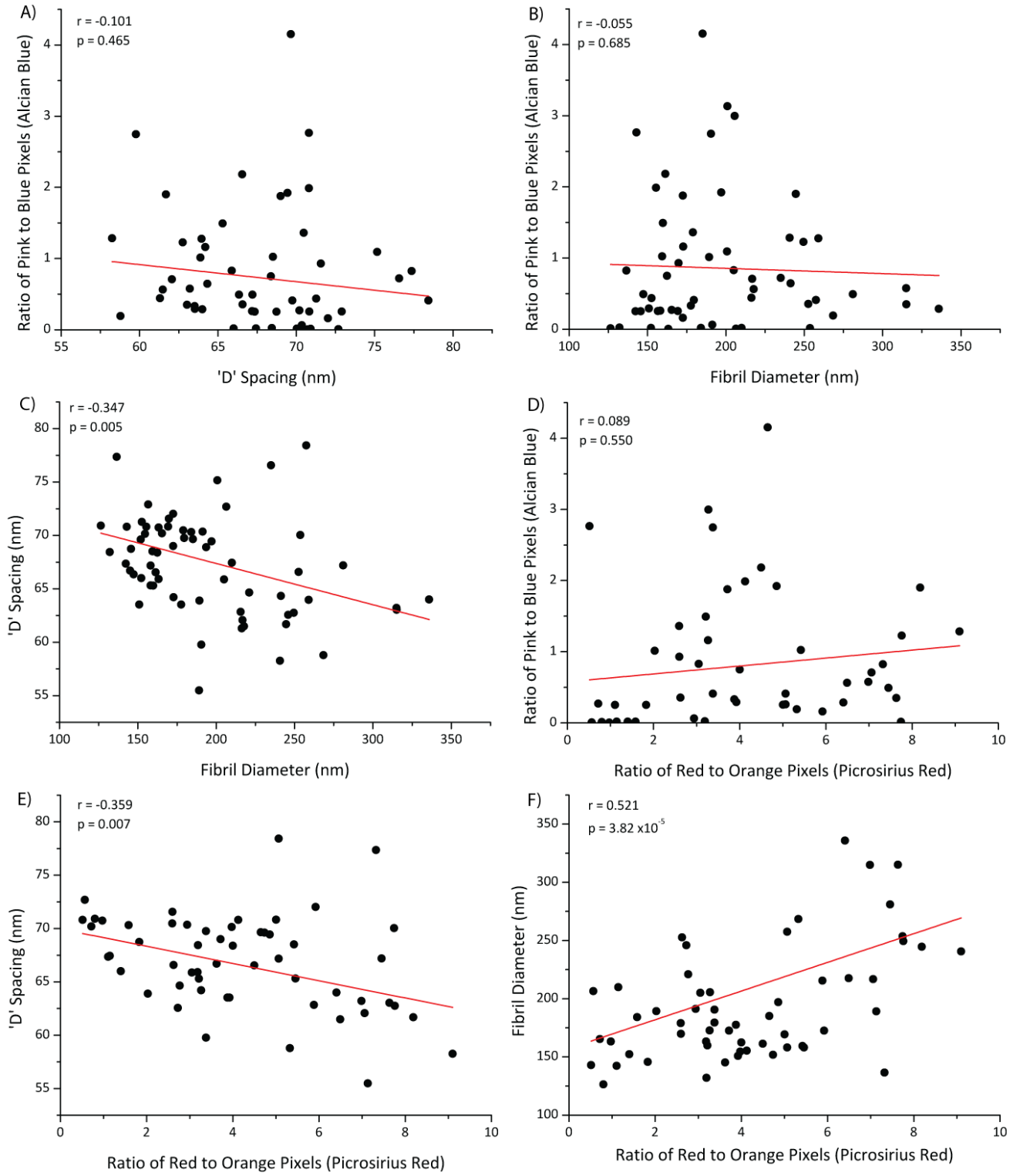
A)
r = -0.101
p = 0.465
Ratio of Pink to Blue Pixels (Alcian Blue)
'D' Spacing (nm)
B)
r = -0.055
p = 0.685
Ratio of Pink to Blue Pixels (Alcian Blue)
Fibril Diameter (nm)
C)
r = -0.347
p = 0.005
'D' Spacing (nm)
Fibril Diameter (nm)
D)
r = 0.089
p = 0.550
Ratio of Pink to Blue Pixels (Alcian Blue)
Ratio of Red to Orange Pixels (Picrosirius Red)
E)
r = -0.359
p = 0.007
'D' Spacing (nm)
Ratio of Red to Orange Pixels (Picrosirius Red)
F)
r = 0.521
p = 3.82 x10-5
Fibril Diameter (nm)
Ratio of Red to Orange Pixels (Picrosirius Red)

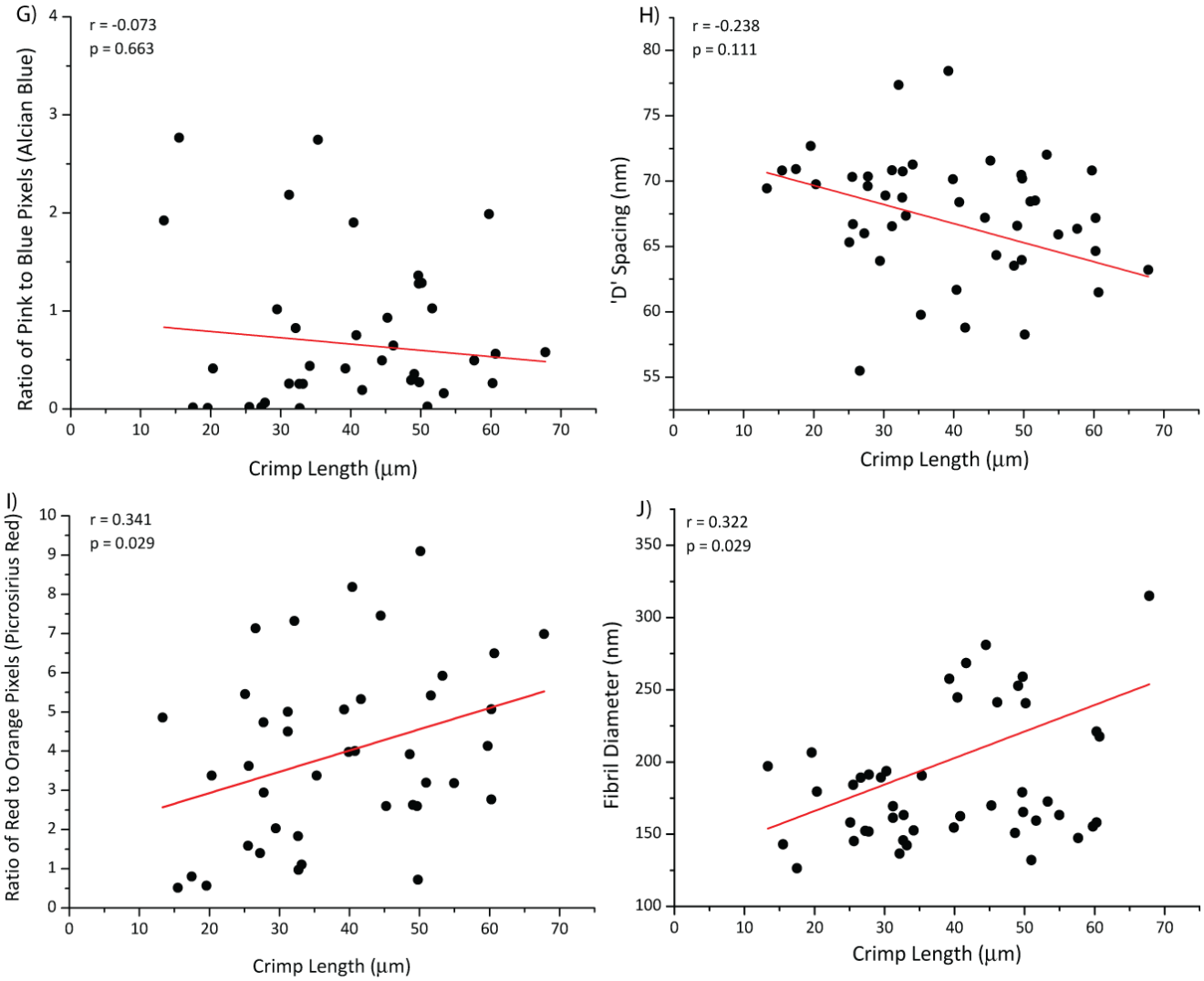

Figure 4:39 Scatter plots showing correlations between different properties measured. There are significant ($p<0.05$) trends between: fibril diameter - 'D' spacing (C), red to orange ratio - 'D' spacing (E), red to orange ratio - fibril diameter (F), crimp length - red to orange ratio (G), and crimp length - fibril diameter (J). The strongest, most significant correlation is between red to orange ration - fibril diameter. Pearson's correlation coefficient is less than 0.6 for all correlations.

4.3 DISCUSSION

4.3.1 Suitability of Techniques

4.3.1.1 Alcian Blue

Alcian blue is a copper-based dye that, when ionised, possesses up to four cationic groups depending on the strength of the acid. This cationic dye is electrostatically attracted to the fixed negative charge of the ground substance [201], staining the ground substance blue. Nuclear-fast red is a counter-stain that dyes nuclei deep red, and the surrounding connective tissue pale pink. Analysis of alcian blue-nuclear fast red-stained samples therefore gives some insight into the ratio of collagen to ground substance.

It is interesting to note that all of the pink to blue (collagen to ground substance) ratios are less than one (Figure 4:4 pg. 36, and Figure 4:5 pg. 37), indicating greater ground substance content than collagen content in all the samples, even the proximal (tensile) ones. Whilst this may be believable for the bovine DDFT distal ventral samples, in which there is expected to be a large amount of fibrocartilage [159], the typical values of PG, GAG and collagen content given by other studies suggest that this result is very improbable for the proximal samples: PG content typically makes up less than 10% of the dry weight of tendon exposed to tensile loads only, and the majority of this is the small SLRP, decorin, which is found attached to the fibrils [116, 164, 166, 202].

This discrepancy is probably caused by the alcian blue dye's large cationic charge. This makes it a very 'sticky', non-specific dye that is attracted to any chemical species within tissue that carry a negative charge. Thus while this staining technique is very simple to perform, it is unlikely to provide accurate and precise data regarding infer-fibre and inter-fascicle ground substance content, even with the use of sophisticated image analysis techniques. To facilitate specificity of staining for such a compound, highly controlled staining conditions are required. Alternatively, the results could be improved by the use of more selective histological dyes, such as Thionin and Safranin O [203], or even immunohistochemistry.

4.3.1.2 Raman Spectroscopy

As Meade et al note, 'vibrational spectroscopy (Raman and FTIR microspectroscopy) is an attractive modality for the analysis of biological samples since it provides a complete noninvasive acquisition of the biochemical fingerprint of the sample.' [204] The technique offers high spatial resolution and the ability to

probe both the molecular structure and molecular environment of different samples once the exact designations of the different peaks within the spectra are known. It has therefore become a widely accepted method for the characterisation of biomolecules [205]. Previous studies have applied vibrational spectroscopy to diseased tissues and demonstrated that significant differences compared with healthy tissue [189, 206-208], suggesting that this may be a sensitive technique for analysis of biochemical changes within degenerative tendon samples. However, detailed analysis of such spectra has in the past proved difficult, owing to the overlapping spectral contributions of different biomolecules contained in these tissues, such as lipids, carbohydrates and proteins [190, 192, 204].

In the current study, efforts have been made to identify peaks associated with inter-fibril and inter-fibre GAGs, the profiles of which are known to change as a result of disease. Raman spectra of as received and chondroitinase ABC-treated bovine tendon samples (Section 4.2.1.3) were compared with the spectrum for chondroitin sulphate A. The results identify one such peak, and suggest that Raman spectroscopy may therefore prove to be a sensitive technique for analysis of ground substance content at the fibril and fibre levels in tendon samples. Further work should now explore the application of such techniques to these samples in order establish the accuracy of the results presented here.

4.3.1.3 Picrosirius red

Picrosirius red is an anionic dye that enhances collagen's birefringence by attaching to, and aligning along, the long axis of the collagen molecule [174, 193, 194]. Variations in the wavelength of the light viewed through the analyser are strongly correlated with differences in collagen fibre thicknesses, with smaller fibres resulting in light with a shorter wavelength being seen through the analyser [199, 200]. The exact mechanism by which this contrast occurs is not fully understood, but is thought to be related to the number of dye molecules capable of attaching to different diameter fibres [198, 199]. Regardless of the exact contrast mechanism, fibres which appear red are likely to be thicker in diameter than those which appear orange, those which appear orange are likely to be thicker in diameter than those which appear yellow, and so on.

This histological stain is easy to use and produces beautiful images when viewed through cross-polars (see Figure 4:7 pg. 40, and Figure 4:11 pg. 44), with the additional benefit that the use of polarised light makes

crimp patterns easy to identify (see Figure 4:9 pg. 42). Figure 4:11 clearly demonstrates how well this stain distinguishes between tendon fibres and muscle filaments, a fact that may be useful in the topographical analysis of cadaveric tendons (see Chapter 6). When used in conjunction with digital image analysis techniques, it also provides a method for determining the ratio of fibre thicknesses, although it should be noted that there is a large amount of scatter in the data from the analysis of histograms images. This is partly due to the qualitative nature of histological analysis but is also limited by the fact that the samples were only imaged in one orientation (plane polarised light). This causes the birefringence of fibres aligned in other directions to be extinguished. The precision of these results would therefore be improved by the use of circularly polarising light. Regardless of these limitations, this technique provides a relatively simple method for characterisation of the microstructural features in tendon samples.

4.3.1.4 Non-contact Mode Atomic Force Microscopy

In Atomic Force Microscopy (AFM) a microscale cantilever with a sharp tip (<50nm radius of curvature) is scanned across a surface and cantilever tip deflection is measured. This gives insight into the interaction between the tip and the surface and allows detailed topographical images of the surface to be created. In non-contact mode, the cantilever is oscillated above its resonant frequency as it is scanned across the surface and changes in the cantilever's oscillatory behaviour are monitored as well as tip deflection. In this manner, variations in the interaction between the tip and the surface (indicative of compositional variation) and topographical information are collected concurrently. This powerful technique provides a method of non-destructive 3D surface imaging technique on the ultrastructural scale (see Figure 4:24 pg. 55). It also offers considerable advantages compared with more traditional ultrastructural characterisation techniques such as transmission electron microscopy (TEM) [155, 209-212], as there is no requirement to use electron-dense dyes for contrast-enhancement. AFM is also non-destructive and can be performed on bulk samples. Thus this technique can reveal nanoscale topographical information about fragile biomaterials and biomolecules without the need for complex sample preparation [213].

AFM has already been applied to the measurement of the 'D' spacing and diameter of individual collagen fibrils extracted from various tissues and deposited on surfaces [214-216], and in histological sections of demineralised, paraffin-embedded bone and dentin [217, 218]. Raspanti et al have also applied this technique to the study of proteoglycans and glycosaminoglycans and their interaction with collagen fibrils,

managing to image these complexes as a 'thin, transverse ridge [that] decorates the gap zone' and as other filaments running across and parallel to the fibrils [94]. These results indicate that AFM may be appropriate for characterisation of the structural adaptations in bulk tendon samples. However, for the technique to be applied to surgically-obtained human samples, it must be compatible with the preservation techniques employed by surgeons and histopathologists. To this end, samples preserved and embedded in a range of ways were characterised using AFM (see Figure 4:21 pg. 52).

The choice of tissue preservation technique is an important consideration in tissue ultrastructure studies [168]: while freezing halts temperature-dependent cell autolysis, in the absence of a cryopreservation medium ice crystals can damage the tissue, altering its structure and mechanical properties [175, 179, 219, 220]. Conversely, fixation techniques that crosslink the tissue (for example aldehyde fixation) preserve the structural and chemical integrity of the proteins [175] but may modify the mechanical properties, introduce fixation artefacts and cause specimen shrinkage [177, 221-223].

Aldehydes are a popular chemical fixative, with 10% formalin (FA) and 4% glutaraldehyde (GA) being the most commonly used [221]. Both methods cause minimal shrinkage and do not change the secondary structure of the proteins present [224, 225], although they may alter the density of the fibrils that make up their tertiary structure [222]. Despite being a standard fixative for histological investigations, FA is generally considered unsuitable for ultrastructure studies, reportedly yielding inferior results to GA [168, 169, 175, 176, 219, 225-227]. However this is disputed [228].

The results presented here (see Figure 4:21 pg. 52, Figure 4:25 pg. 57, and Figure 4:29 pg. 60) indicate that none of the preservation or embedding techniques tested affect the ultrastructure of tendon to such an extent as to eliminate detectable differences between samples from different locations: for example, samples from the ventral (compressive) portion of the DDFT exhibit significantly thinner fibrils than those in the dorsal (tensile) region, regardless of preservation and embedding technique (see Figure 4:25 pg. 57). However, differences between the results for different processing techniques emphasise the importance of consistency in the choice of preservation and embedding technique; resin-embedded samples exhibit significantly thinner fibrils than wax-embedded samples, while aldehyde-fixed samples exhibit thinner fibril diameters in the dorsal region of the tendon compared with the frozen samples (see Figure 4:25. 57).

These differences are probably caused by differences in extent of embedding media shrinkage, differences in the degree of dehydration during embedding, and the introduction of additional crosslinks during fixation in aldehyde.

4.3.1.5 Contact Mode Atomic Force Microscopy and Instrumented Indentation

Mechanical characterisation of small biological samples is notoriously complicated because small sample dimensions and unfavourable aspect ratios make traditional mechanical testing impossible due to difficulties associated with sample clamping. These difficulties have led researchers to develop different techniques for the characterisation of the mechanical properties of small samples. For example, dynamic shear analysis has been used to reveal information about the storage and loss moduli of tendons, granting insight into their elastic and viscous behaviour [229]. In recent years, indentation testing of such materials using atomic force microscopy (AFM) and instrumented indentation techniques has become increasingly popular. This allows the mechanical properties to be mapped across samples, granting insight into topographical variation in properties at different length scales [162, 230].

In AFM-indentation, the cantilever free-end is driven into the sample surface by the movement of the cantilever base, the movement of which is controlled by a piezoelectric crystal. The measured cantilever deflection is then converted to an equivalent force of indentation based on probe stiffness and dimensions. Concurrently, indentation depth is calculated as the difference between the cantilever base displacement and the cantilever free-end deflection allowing a force-distance curve for the indentation to be produced (see Figure 4:40 pg. 76).

Use of AFM-indentation is increasingly popular for the mechanical characterisation of compliant viscoelastic materials, such as polymers [183, 231-234] and has also been applied to characterisation of biological materials like cartilage, a so-called ‘soft’ biological material [235-238]. However, it has only relatively recently been applied to the study of extremely compliant biological materials, such as collagenous materials. Further complications arising from viscoelasticity and structural hierarchy, have restricted such studies to characterisation of individual collagen fibrils extracted from tissues and then either a) deposited onto surfaces and tested in bending, or else b) attached at one end to a surface and at

the other end to the AFM probe to be tested in tension [79, 239, 240]. The results of such studies were discussed above (Chapter 3, Section 3.3.1).

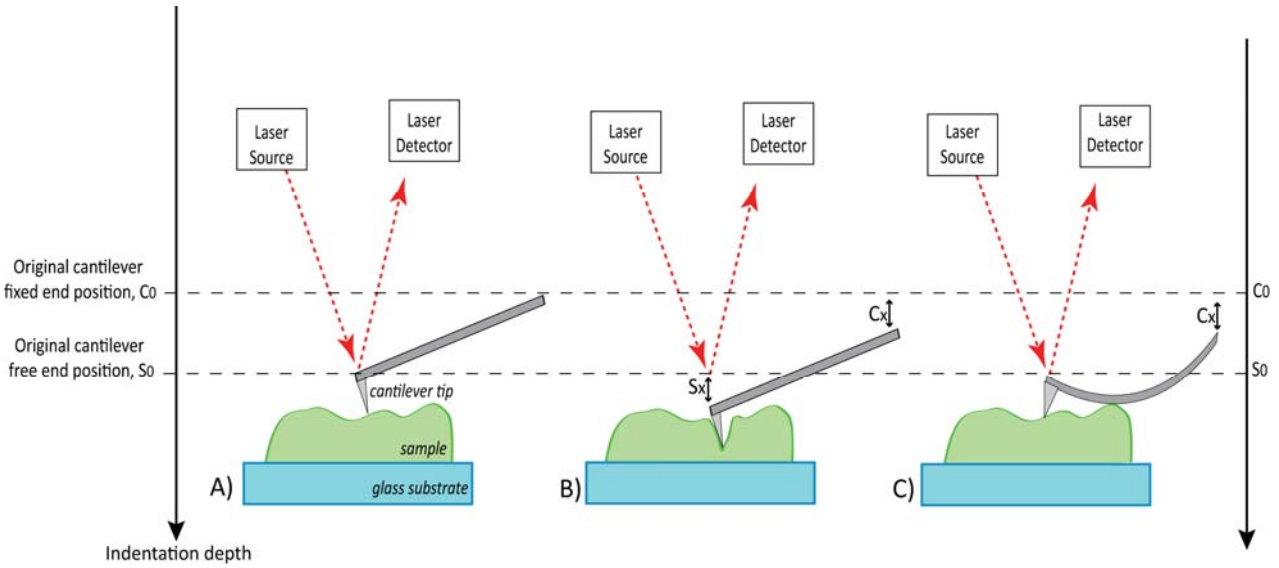

Figure 4:40 Illustration of limitations imposed by inappropriate stiffness of AFM cantilever: A) neutral position when tip is at surface of samples, B) when the lever is much stiffer than the sample, the sample is indented but there is no deflection of the cantilever, and C) when the lever is much less stiff than the sample, the cantilever is strongly deflected but there is no indentation of the sample. Original artwork.

Data produced by AFM-indentation studies must be considered cautiously. As Ebenstein notes 'characterisation of tissue-level properties using an AFM is challenging due to the very small displacements and load ranges of the probes, and the use of the cantilever to apply load...' [241]. Interpretation of the results must therefore be considered in conjunction with the relative stiffness of the probe: if the probe is much stiffer than the surface, very little probe deflection will occur (Figure 4:40B), while if the probe is much less stiff than the surface, very little surface indentation will occur (Figure 4:40C) and adhesion effects will become dominant [233, 241]. This can have important implications for the apparent stiffness of the surface; apparent stiffness varies wildly with probe stiffness and there is no way of identifying the 'correct' result without further mechanical characterisation [242].

To side-step these issues, researchers have recently begun to apply instrumented indentation techniques (nanoindentation) to bulk histological samples [243]. In this technique, perfectly normal loads are applied to the sample by indentation with a tip that is much stiffer than the sample itself. The design of the system is such that rather than measuring the deflection of a cantilever in order to infer force, a spring-mounted indenter column on which is mounted a sharp tip is driven into the surface at a constant velocity, and the change in displacement and load measured using signal transducers are recorded. Load-unload data is then

converted to elastic modulus and hardness (mean supported contact stress), typically via an elastic-plastic half-space algorithm based on that detailed by Oliver and Pharr [185].

Nanoindentation has been successfully employed to characterise the micromechanical properties of 'hard' biological materials such as bone and tooth [230, 244]. However, while it is also being increasingly used for mechanical characterisation of more compliant materials such as cartilage and polymeric materials [234, 237, 245], interpretation of the results is not straightforward. A particular complication is that the Oliver and Pharr method for calculation of indentation contact area during indentation loading for bulk samples [185, 246] - so commonplace that it is often directly incorporated into the instrumentation software - is invalid for viscoelastic materials because these materials do not adhere to the assumption of an elastic-plastic half space. Adhesion between the sample and the tip, common for biological materials further invalidates the assumptions of this model.

To our knowledge, the work presented here is the first reported attempt to probe the micromechanical properties of sections of bulk tendon samples using nanoindentation techniques. Comparison of the results for AFM indentation (Section 4.2.4.1) and nanoindentation (Section 4.2.4.2) highlights the complicated nature of such mechanical characterisation studies discussed above. Specifically, although both sets of results suggest that distal ventral samples are stiffer than proximal dorsal samples (see Table 4:3 pg. 63 and Table 4:4 pg. 68), the Tensile modulus values calculated using the different techniques differ by two orders of magnitude; the AFM indentation results lie between 35-50MPa while the nanoindentation results lie between 5.3-6.5GPa. Thus the AFM indentation results are similar to the values of Tensile modulus for indentation of individual fibrils from bovine Achilles tendon reported by Yang et al [80], and for indentation of bulk samples of ferret aorta and vena cava by Akhtar et al [243], while the nanoindentation results are similar to those for indentation of fibrils from rat tail tendon reported by Wenger et al [82], and for the collagen molecule calculated by Sasaki et al [68].

With such disparity between the results produced by the different techniques it is unclear which values more accurately represent the 'real' values. For both methods, the effective modulus values produced are expected to be much higher than values that would have been produced by identical tests on fresh, hydrated tissue because the samples tested here were fixed (crosslinked) in 10% formalin and tested in a

dry state. However, since identical samples were used for both AFM indentation and nanoindentation this limitation is unable to account for the considerable discrepancy between the results of the two characterisation techniques.

A more probable explanation is that the discrepancies arise due to the methodology limitations discussed above. For example, for the AFM-indentation results comparison of the calculated stiffness values (Table 4:3) with the stiffness values for the cantilevers (indicated in the manufacturer's specifications, Section 4.1.4.4) reveals that the cantilevers are less stiff than the samples. The assumption that deflection of the cantilever upon indentation of the sample is due to compression of the sample alone is therefore invalid. Additionally, the shape of the area of contact of the tip and the sample was only estimated, using the Sneddon approximation for the deformation of a sample around an indenting tip (see Section 4.1.4.4 above). Thus the numerical values of sample deformation are likely to be greatly overestimated, meaning that the calculated values of sample stiffness (and modulus) as assessed using AFM-indentation are likely to be considerable underestimates of the actual values.

Conversely, the nanoindentation results are probably overestimated. Both the AFM-indentation and nanoindentation results indicate that the samples are behaving viscoelastically during indentation; while the cyclic AFM-indentation demonstrate a degree of softening over the course of 15 indentation cycles (Table 4:3 pg. 63), the nanoindentation results reveal considerable creep between the loading and unloading cycles, causing a 'nose' [247] in the load-unload curves, even at relatively small indentation depths (Figure 4:34 pg. 64). Thus, as discussed above, the use of Oliver and Pharr's method for conversion of load-unload curves to modulus and hardness values is invalid for these samples. The use of this method is further invalidated by the glass-mounted nature of the samples: Oliver and Pharr's method is not appropriate for thin layers of material mounted on stiffer substrates [248, 249]. Furthermore, the results are likely to be heavily influenced by 'pile-up' of the deformed sample around the tip [250], leading to significant under-estimations of the contact area between the tip and the sample.

Due to these limitations associated with the two techniques, meaningful interpretation of these results in not possible in the absence of further exploratory work. Further studies should now explore the effect of stiffer AFM cantilevers on the tensile modulus values produced by this technique. Additionally, a method

for determination of indentation contact area with applied force that is more appropriate for glass-mounted viscoelastic samples should be applied to the nanoindentation technique [243, 249]. Improved methods for determining the depths at which sample deformation is uninfluenced by the underlying substrate, such as differentiation of the load-unload curves, should also be explored [251]. Finally, the use of more different tip geometries and fresh, hydrated samples should be explored before these techniques are applied to human samples.

4.3.2 Adaptations with Loading Environment

4.3.2.1 Bovine Deep Digital Flexor Tendon

The alcian blue images and analyses (Figure 4:3 pg. 35, Figure 4:4 pg. 36, and Figure 4:5 pg. 37) demonstrate significant compositional adaptations with loading environment. There is a significantly higher proportion of ground substance (smaller red to blue ratio) in the distal ventral samples than in the other bovine samples (Figure 4:4 pg. 36). Examination of the representative image of the alcian blue-stained distal ventral sample (Figure 4:3C pg. 35) also suggests the presence of fibrocartilage in these samples, as the collagen material is much less aligned than in the other samples [159, 160]. Furthermore, there is a higher proportion of ground substance (smaller red to blue ratio) in the distal sections compared with the proximal sections and in the ventral samples compared with the dorsal samples in each location. These results indicate that ground substance content is increased in response to compressive and shear loads, and are in agreement with previous studies [86, 154-158].

The results of the micro- and ultrastructural characterisation indicate that the DDFT also exhibits significant structural adaptation with different loading environment (Sections 4.2.2 and 4.2.3). In agreement with other work [38, 163, 252], the bovine DDFT exhibits significantly thinner fibrils (Figure 4:26 pg. 57) and a significantly higher proportion of thinner fibres (Figure 4:14 pg. 47) in the distal (compressive) section compared with the proximal (tensile) section. The distal sections also exhibit significantly shorter crimp length (Figure 4:18 pg. 49) and significantly longer 'D' spacing (Figure 4:30 pg. 60) compared with the proximal sections. Additionally, the results of this study reveal significant structural adaptations in the dorso-ventral plane: in the proximal region, ventral samples exhibit a lower proportion of thinner fibres, longer crimp length and thicker fibrils compared with dorsal samples, while for samples from the distal region ventral samples exhibit a higher proportion of thinner fibres, shorter crimp length and thinner fibrils

compared with the dorsal section (Figure 4:14 pg. 47, Figure 4:18 pg. 49, and Figure 4:26 pg. 57) . Thus the results for the DDFT support the hypotheses that there are significant structural and compositional adaptations in wrap-around tendons subjected to different loading environments and that these adaptations vary with distance from the bony contact.

4.3.2.2 Ovine Infraspinatus Tendon

The alcian blue images and analyses for the ovine infraspinatus tendon (Figure 4:3 pg. 35 and Figure 4:5 pg. 37 above) do not demonstrate significant compositional adaptations with loading environment; no significant differences were detected between the bursa-side and articular-side ovine samples, and there was no evidence of fibrocartilaginous material. This may be because the loading environment in the infraspinatus tendon is not extreme enough to produce compositional adaptations such as those seen for the bovine DDFT.

It is also possible that the loading environment of the rotator cuff tendons results an adaptation not detected by this study. Studies of the human supraspinatus tendon, which has a similar anatomy to the ovine infraspinatus tendon, have revealed that the main adaptation of this tendon is an increase in ground substance content between the individual fascicles, which are arranged in a lamellar structure in this tendon (Chapter 5, Section 5.3.2) [153, 253, 254]. A similar feature has also been shown to exist in the distal section of foot flexor tendons and is thought to be an adaptation to differential strain distribution experienced by the outer sections of the tendons [159]. Assuming this adaptation is present in the ovine infraspinatus tendon, it would be necessary to examine cross-sections transverse to the loading direction to witness this adaptation.

While the compositional results for the ovine infraspinatus do not support the hypotheses that there are significant adaptations in wrap-around tendons subjected to different loading environments, the results of the structural adaptations do. Similar to the distal section of the DDFT, ovine infraspinatus exhibits shorter crimp length (Figure 4:19 pg. 50) and thinner fibrils (Figure 4:27 pg. 58) on the articular-side (compressive) compared with the bursa-side (tensile).

Comparing the compositional and structural adaptations presented here, the results suggest that micro- and ultrastructural characterisation may be a more sensitive method of determining adaptations of tendon to different loading conditions than compositional analysis techniques.

4.3.3 Inter-dependence of structural and compositional adaptations

In order to examine the dynamic relationship between these properties, the strength and significance of correlations between the different structural and compositional adaptations of individual samples (see Figure 4:39 pg. 69) were compared. These results reveal significant positive correlations between i) fibril diameter and red to orange ratio, ii) crimp length and red to orange ratio, and iii) crimp length and fibril diameter, possibly indicating that these features are inter-related. However, there are no significant correlations between the structural and compositional adaptations, again suggesting that ground substance content does not have a significant influence on the dimensions of the collagen architecture. This result is surprising given the wealth of studies that have indicated that ground substance, particularly proteoglycans, play a strong role in determining the ultrastructural dimensions of tendon.

This discrepancy between previous studies which indicated the importance of small proteoglycans in determining the dimensions of the collagen architecture and the results of the current study probably arises due to the nature of the alcian blue stain. Alcian blue is a non-specific cationic stain (Section 4.3.1.1) that that is unable to distinguish between large and small proteoglycans, the alcian blue results presented here are therefore likely to be dominated by the massive increase in large proteoglycans situated between the collagen fibre and fibrils in compressive tendon, and are thus unlikely to reveal any insightful information regarding the changing concentrations of small proteoglycans located intra- and inter-fibrillarly. To gain any useful information regarding changes in the intra- and inter-fibrillar concentrations of SLRPs in response to the changing loading environment it would be necessary to use a different technique, such as the Raman spectroscopy.

Chondroitinase ABC is an enzyme that degrades chondroitin sulphate A (a.k.a. chondroitin-4-sulphate), chondroitin sulphate B (a.k.a. dermatan sulfate), and chondroitin sulphate C (a.k.a. chondroitin-6-sulphate) [255, 256]. Chondroitinase ABC-treated tendon is therefore be expected to exhibit decreased amounts of all three of these glycosaminoglycans, which can be found between the fibrils, fibres and fascicles of the

tendon. Previous studies have shown that chondroitinase ABC treatment reduces the amount of inter-fibre and inter-fascicle GAG [73]. In the present study, Raman spectroscopy combined with a confocal microscope has been used to assess whether chondroitinase ABC-treatment also decreases the amount of inter-fibrillar GAG. To do this, the Raman spectra from untreated and chondroitinase ABC-treated bovine DDFT proximal samples were compared with the Raman spectrum from chondroitin sulphate A (Figure 4:6 pg. 38).

Comparison of the spectra reveals that chondroitinase ABC-treatment produces a significant decrease in the intensity of the Raman peak at 1165cm^{-1} (Figure 4:6 pg. 38). Since a peak centred at this wavenumber is seen in the Raman spectra from chondroitin sulphate A, B and C, it is unclear which of these GAGs is represented by the decreasing intensity of this peak in the chondroitinase ABC-treated bovine samples. However, examination of the *shape* of this peak may offer some insight; while the Raman peak centred at 1165cm^{-1} is seen as a broad shoulder in the chondroitin sulphate A spectrum (Figure 4:6 pg. 38) and chondroitin sulphate C [231], it presents as a much sharper peak in chondroitin sulphate B. The sharpness of the Raman peak centred at 1165cm^{-1} in the Raman spectra from bovine proximal samples therefore suggests that its presence in these samples is associated with chondroitin sulphate B. Thus the results suggest that chondroitinase ABC-treatment of bovine tendon depletes the inter-fibrillar chondroitin sulfate B (a.k.a. decorin sulphate) content of this tendon. The results also indicate that Raman spectroscopy is an appropriate technique for characterisation of inter-fibrillar ground substance content.

As-received and GAG-depleted samples were also characterised structurally in order to assess the sensitivity and reproducibility of the structural analysis techniques used in the present study (Figure 4:6 pg. 38, Figure 4:17 pg. 48, Figure 4:20 pg. 50, Figure 4:28 pg. 58, and Figure 4:32 pg. 61). GAG-depletion does not affect the proportion of thinner fibres (Figure 4:17 pg. 48), the fibril diameter (Figure 4:28 pg. 58) or the 'D' spacing (Figure 4:32 pg. 61) in the samples compared with untreated samples. This is unsurprising; while previous studies have indicated that GAG-content and fibre / fibril dimensions are inter-related, it is thought to take the form of GAGs influencing the arrangement of the fibrils and / or fibres during fibrillogenesis and maturation, a characteristic not investigated here. Surprisingly, the results here do demonstrate that GAG-depletion by chondroitinase ABC treatment results in a significantly longer crimp length compared with untreated samples (Figure 4:20 pg. 50). This suggests that, in addition to playing a

role in compressive properties of tendon, inter-fibre ground substance influences the crimp length (and thus built in safety factor, see Section 3.3.1 above) of tendon samples.

4.4 SUMMARY AND FURTHER WORK

The work in this chapter has investigated the material adaptations of tendon in response to different loading environments using a range of different techniques. The results reveal that while some of the techniques used are highly suited to characterisation of the material properties of tendon, others are of limited usefulness. In particular, alcian blue staining for characterisation of the ground substance content of tendon is not specific enough to provide meaningful information regarding compositional adaptations, although the presence of such adaptations could provide valuable insight into the loading environment of the tissue. Furthermore, a great deal of additional work is required in order to establish appropriate methodologies and data analysis algorithms before AFM-indentation and nanoindentation can be reliably used to characterise the micro-mechanical properties of tendon.

AFM is highly appropriate, however, as a technique for characterisation of the ultrastructural adaptations of tendon, being able to extract reproducible information regarding fibril diameters and 'D' spacing from samples preserved and embedded in a variety of manners, including those typically used by surgeons and pathologists (formalin-fixation, wax-embedding). Additionally, the picrosirius red histological stain provides a useful methodology for characterisation of the microstructural features of tendon, granting insight into the ratio of different thickness fibres and crimp length, whilst providing a method for distinguishing tendon fibres and muscle filaments. The results also indicate that Raman spectroscopy may provide a method for examining changes in the inter-fibrillar concentrations and profiles of ground substance, although the analyses required are not straightforward.

Using these techniques, it is possible to demonstrate that there are significant structural adaptations in the two different wrap-around tendons investigated. The results provide evidence to support the hypotheses that there are significant structural and compositional adaptations in wrap-around tendons subjected to different loading environments, and that in regions of compression the material adaptations of tendon vary with distance from the bony contact. Specifically, it appears that regions of tendons exposed to compression and/or shear exhibit a higher proportion of thinner fibres, shorter crimp lengths, and thinner

fibrils compared with regions of tendon exposed to tension. However, the results have provided no strong evidence to support or disprove the hypothesis that the material adaptations of tendon are inter-related.

PART III

MATERIAL ADAPTATIONS OF ROTATOR CUFF TENDONS

Chapter Five

Background Literature: The Rotator Cuff

5.1 FUNCTION AND ANATOMY

The shoulder consists of three bones and more than twenty muscles, and is by far the most mobile joint in the body [257]. Consequently it is an 'indeterminate mechanical system... [in which the] number of unknown forces far exceeds the number of force and moment equilibrium equations available for the three shoulder bones' [258]. The rotator cuff is one of two dynamic stabilisers within this joint [48, 259], providing 'an integral force in elevation of the arm... in all phases of elevation' [45] and acting as a fulcrum [260].

The cuff is composed of four musculotendinous units, the subscapularis, supraspinatus, infraspinatus and the teres minor, all of which insert on the humeral head (Figure 5:1). Approximately 1.5cm from their enthesis point, the tendons interdigitate [259], and are thus considered to form a continuous 'cuff' which covers all sides of the joint 'except the lower quadrant' (Figure 5:1-F) [261]. Owing to the mobility of the shoulder joint, the cuff tendons are 'subject to non- uniform loading during normal shoulder activity' [253]. Additionally, while the cuff tendons function as a unit rather than individually, the individual muscles do exhibit different force-generating capacities: 53% of the cuff moment is provided by the subscapularis muscle, compared with 20% by the infraspinatus, 14% by the supraspinatus and 10% by the teres minor [262]. Thus the rotator cuff experiences a complicated mechanical environment.

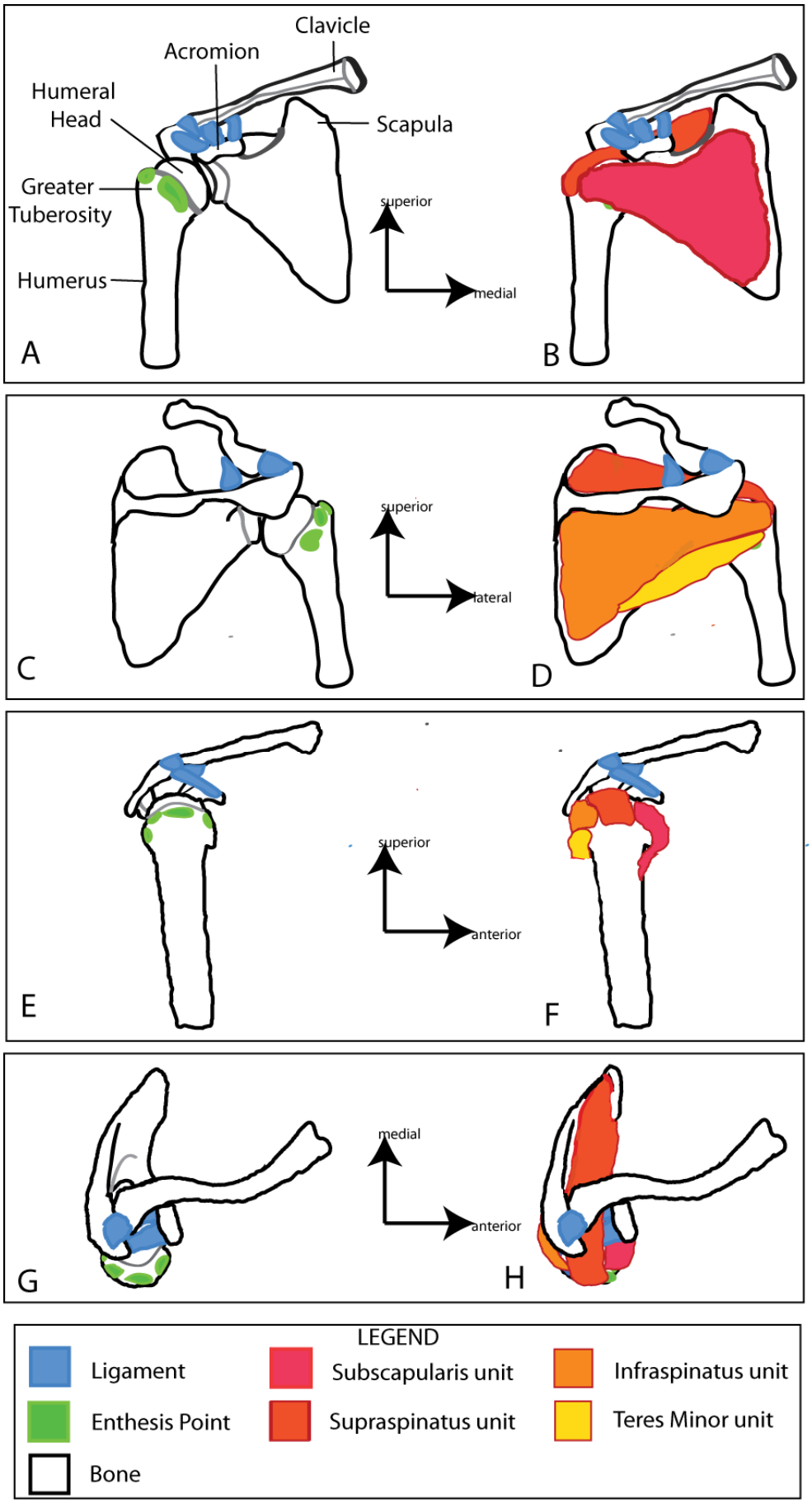

Figure 5:1 Anatomy of the Rotator Cuff of the right shoulder as viewed from the front (5:1-A, 5:1-B), back (5.1-C, 5:1-D), side (5:1-E, 5:1-F) and top (5:1-G, 5:1-H). In images 5:1-A, 5.1-C, 5:1-E, and 5:1-G only the bones and ligaments are visible. In images 5:1-B, 5:1-D, 5:1-F and 5:1-H, the rotator cuff musculotendinous units have been included. Original artwork based on a 3D model of the rotator cuff (3B Scientific® Products, Hamberg)

5.2 ROTATOR CUFF TEARS

5.2.1 Prevalence and Impact

Considering the complicated nature of the shoulder joint, and the importance of the rotator cuff, it is perhaps unsurprising that the shoulder represents the third most common musculoskeletal complaint [263], with disorders of the rotator cuff representing up to 75% of all shoulder morbidity [19, 264]. Inflammation and swelling of the cuff tendons (a.k.a. tendinitis) associated with overuse is common. Disorders relating to impingement, chronic degeneration (a.k.a. tendinosis) and tears of the cuff tendons are also widespread; while impingement is reported to be the 'most frequent cause of shoulder pain in the general population' [265], incidence of rotator cuff tears is also reportedly in excess of 20% in the general population [20-23]. This is thought to be higher in older sub-populations [24, 25], and participants in manual labour, particularly those who work at, or above, shoulder height [26].

In many cases rotator cuff tears are asymptomatic. Tempelhof et al [23] and Schibany et al [266] investigated the existence of asymptomatic tears and found tears in 23% (all tears) and 90% (full-thickness tears) of patients respectively. Consequently, clinical tests which assess strength and function are often more sensitive than those which assess pain [267]. This is because cuff tears lead to retraction and underuse of the muscle [268], which over time, results in atrophy, degeneration, and fatty degeneration of the muscle [269-272], and a subsequent reduction in the contraction force of the muscle [25, 35, 273].

To compensate for the lost moment arms associated with rotator cuff muscle deficiency [35], the joint and muscle forces in the remaining intact tissues must increase [273, 274]. This gives rise to joint instability and differences in muscle activation patterns, altering the dynamics of the joint. For many patients, these modifications ultimately result in pain, weakness and disability [275-279], and have 'a profound effect on a person's activity level': patients with a tear can perform significantly fewer activities than those without. 'Specific problems listed as reasons for surgery include inability to hang washing, drive a car, comb hair, or shake hands.' [276]

5.2.2 Tear Patterns and Aetiology

The supraspinatus tendon is the most commonly torn cuff tendon [34, 280-282]. Tears of this tendon predominantly initiate as partial tears on the articular (aka articular-side) surface [280], although initiation on the bursal surface, or within the tendon mid-substance has also been reported. Once formed, tears are thought to progress from partial to full thickness tears and then increase in size, generally growing in the lateral direction. Commonly, tears are classified as small if their largest diameter is less than 1cm, medium if it is between 1cm and 3cm, large if it is between 3cm and 5cm, and massive if the largest diameter is greater than 5cm [283]. There is evidence that rate of size increase accelerates as tear size increases [281], while the incidence of concurrent tears in the supraspinatus and infraspinatus suggests that tears grow posteriorly as well as laterally [284, 285].

The exact aetiology of rotator cuff tears is disputed. Biologically, the presence of tears is associated with genetic factors [286, 287] and age [24, 29, 288]; incidence of rotator cuff tears are significantly higher in patients whose siblings also have a rotator cuff tear [286, 287], and in older patients [24, 29, 281]; Fehringer et al find a 2.69-fold increase in chance of finding a tear with a 10-year increase in patient age [288]. Moreover, the likelihood of successful repair surgery decreases with age [25, 289]. However, genetics and age are unlikely to account for all incidences of rotator cuff degeneration: as Longo et al note **'**nonruptured supraspinatus tendons, even at an advanced age, and ruptured supraspinatus tendons are clearly part of two distinct populations' [290]. The increased occurrence of rotator cuff tears in manual labourers, particularly those working at or above shoulder height [26], and the prevalence of tears in the supraspinatus tendon (discussed below, Section 5.3.2), has led many researchers to postulate that the function adaptation of the supraspinatus tendon to its mechanical environment may play an important role in its susceptibility to degeneration and tearing.

5.3 SUPRASPINATUS TENDON

5.3.1 Loading Environment

5.3.1.1 Tensile and Compressive Loading

The supraspinatus musculotendinous unit (see Figure 5:1) passes under the acromion and the subacromial bursa* before running over the humeral head and attaching at the greater tubercle. Although it plays an important role in the elevation of the arm, the force generating capacity of the supraspinatus muscle is small compared with the subscapularis [262]. Consequently, the supraspinatus tendon is halfway between a positional tendon and an energy storage tendon. Owing to its anatomy, it experiences complicated loading patterns, and must be functionally adapted to a range of non-constant strain profiles.

Figure 5:2 shows the minimum principal stress value in the humeral head and supraspinatus tendon at different arm abduction angles†. It can be seen than when the arm is at an angle of less than 60° abduction, the articular-side of the supraspinatus tendon is in contact with the humeral head [34]. At this range of angles the supraspinatus tendon is a typical wrap-around tendon, passing over the geometrical restraint of the humeral head before inserting at its enthesis point on the greater tubercle. In this position the articular-side of the tendon therefore experiences compressive strains at the centre of the curve imposed by the humeral head, while the bursa-side experiences large tensile strains in the same location [33, 34]. In this range of abduction angles the muscle contraction forces and the mass of the hanging arm further complicate the strain field experienced by the supraspinatus tendon, causing the bursa-side of the tendon to experience large positive (tensile) principal stresses in the region of the enthesis and large negative (compressive) principal stresses in the region of the muscle insertion. Concurrently the articular-side of the tendon experiences large positive (tensile) principal stresses in the region of the muscle insertion and large principal stresses in the region of the enthesis.

* The subacromial bursa is the sac of fluid that sits between the acromion and the supraspinatus tendon. Its function is to facilitate movement and prevent damage of the rotator cuff tendons as the move under the acromion.

† Abduction of the arm: The process of moving the arm away from the midline of the body i.e. from beside the body (0° abduction) to above shoulder height (increasing abduction angle)

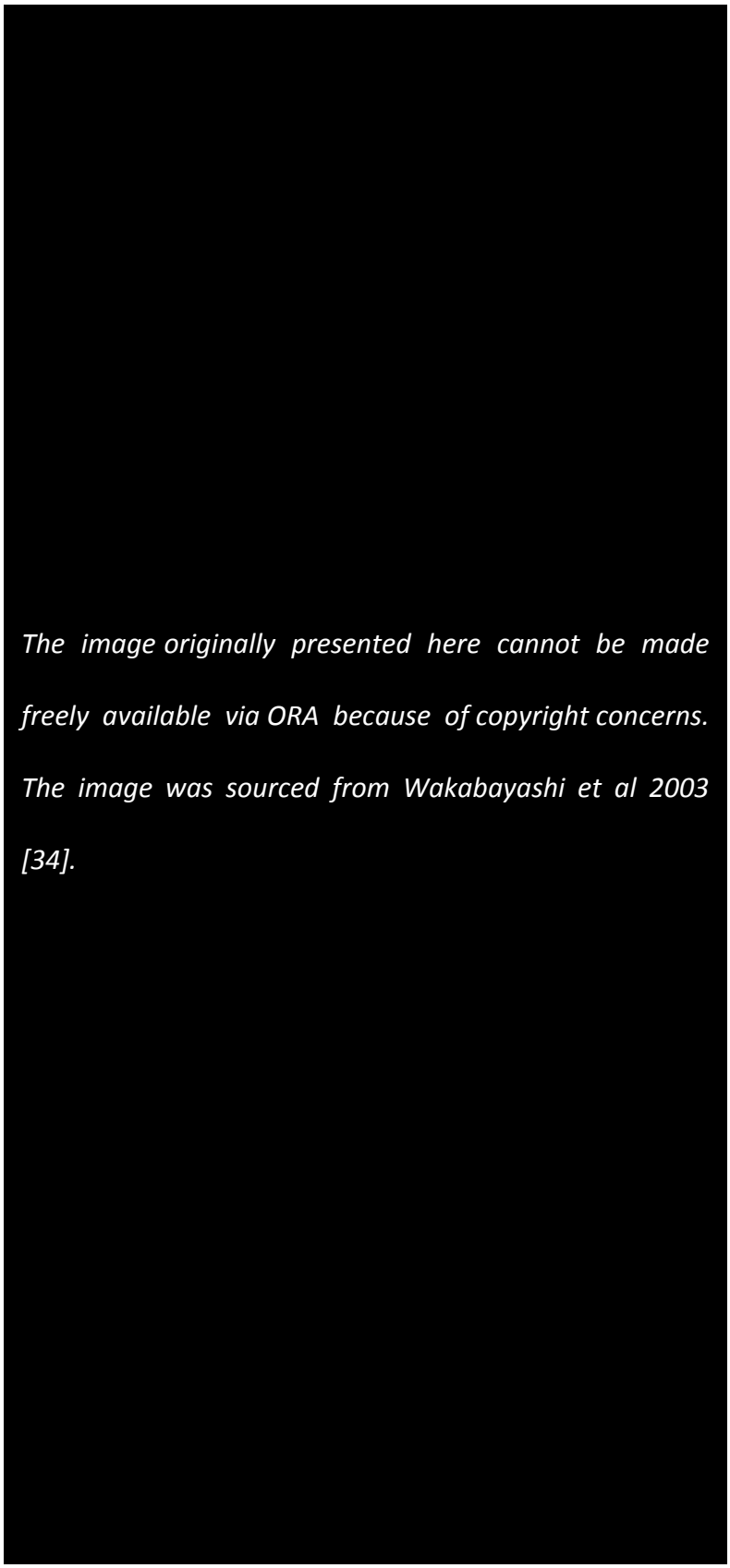

Figure 5:2 Minimum Principle Stress Value (i.e. compressive stress) in the supraspinatus tendon and humeral head at different abduction angles: A) 0°, B) 30° and C) 60°. There is significant compressive stress present in the supraspinatus tendon at 0° and 30° abduction angle, but this disappears at 60° abduction, at which point the articular-side of the tendon is no longer in contact with the humeral head. Taken from Wakabayashi et al 2003 [34].

Whether the large principal stress at the articular-side enthesis is tensile or compressive is unclear; while multiple 2D modelling studies have suggested that it is compressive [33, 34, 291], Seki et al refer to it as tensile [292]. This may be a consequence of experimental details of the finite element models. Alternatively, it may simply be a terminology issue: Seki et al confusingly state that 'the positive value of the principal stress represents tensile stress, and the negative value reflects compressive stress. Hereafter, the term "tensile stress" is used instead of "principal stress" because the former term is more familiar to clinicians' [292]. Regardless of these differences, all the studies provide evidence that within this range of abduction angles, the tendon experiences non-constant stress distributions.

Were this the sole position the shoulder joint could take, the supraspinatus tendon would be expected to exhibit structural and compositional adaptations typical of a wrap-around tendon, such as smaller collagen fibrils and increased proteoglycan (PG) and glycosaminoglycan (GAG) contents in the compressive regions compared with the tensile regions (Chapter 3, Section 3.4.2 and Chapter 4, Section 4.2). However, these features are unlikely to be pronounced in the supraspinatus tendon due to the extreme mobility of the shoulder joint: as can be seen in Figure 5:2 above, when the arm abduction angle increases above 60°, the tendon loses contact with the humeral head [291] and, in the absence of other constraining factors, becomes a purely tensional tendon. As a result, compositional and structural adaptations caused by the presence of compressive stresses in the hanging arm position are unlikely to be pronounced.

A geometrical constraint that may, for many patients, significantly influence the stress distributions within the supraspinatus tendon is impingement by the acromion. The acromion is a bony process that extends laterally from the scapula and overhangs the glenoid cavity. At the point where is passes laterally over the supraspinatus tendon it may take either a flat (class I), curved (class II) or hooked (class III) morphology, as illustrated in Figure 5:3. Many researchers have reported a strong correlation between the morphology of the acromion process and the prevalence of rotator cuff tears [293-296], although it is unclear whether acromial morphology is an innate anatomical feature or a dynamic characteristic that can change with age [297]. Regardless of its origin however, subacromial impingement has been shown to alter the mechanical environment of the supraspinatus tendon, introducing large compressive strains in the region inferior to the acromion and increasing the strain levels at the articular-side of the enthesis [291]. Such alterations of

the mechanical environment can be expected to further complicate the material adaptations of the cuff tendons.

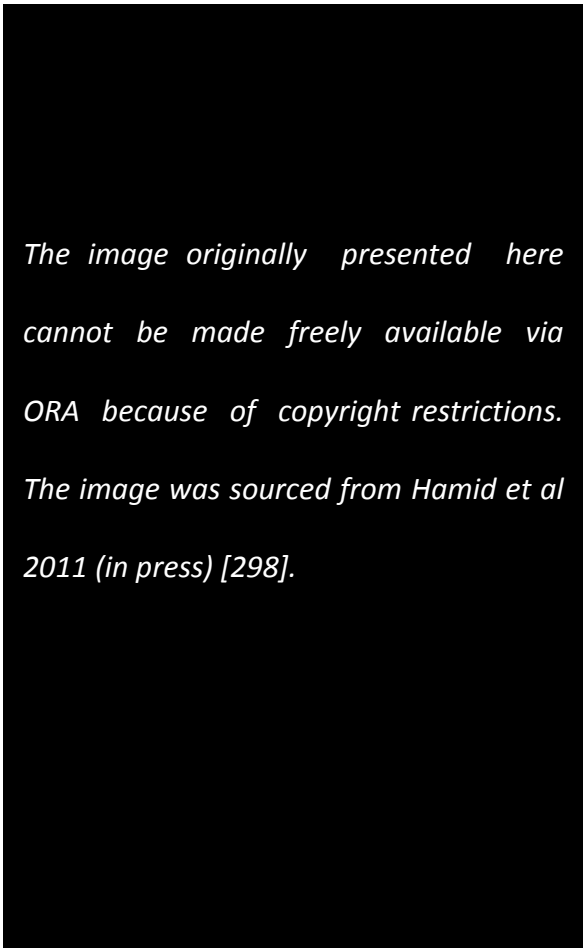

Figure 5:3 Pictorial representations of the categories of acromion morphology: A) Type I - Flat, B) Type II – curved, and C) Type III – hooked. Figure taken from Hamid et al 2011(in press) [298].

5.3.1.2 Shear Loading

In addition to producing a non-constant tensile and compressive strain fields in the supraspinatus tendon, the large mobility range of the shoulder joint also produces non-constant shear strains [299]. As demonstrated in Figure 5:4, strain levels are generally greater at the insertion point than at the tendon mid-substance [153], and on the bursa-side compared with the articular-side [300]. Moreover, while the strain on the articular-side increases continuously during abduction from 0° to 120°, the strain on the bursa-side initially increases and then decreases, becoming negative (compressive) at around 50° abduction.

Figure 5:4 Depiction of the maximum Principle Strain profile in the supraspinatus tendon, as assessed using MRI, at different arm abduction angles. Strain is inhomogeneous across the tendon, and varies significantly with joint position. Taken from Bey et al 2002 [299]

The extent of this non-constant strain profile is clearly seen upon examination of the shape of the supraspinatus tendon at different abduction angles; radiography images have shown that external and internal rotations of the arm at a range of abduction angles alter the shape of the tendon, even introducing 'twisting' of the tendon in certain configurations, as demonstrated in Figure 5:5 [301]. Thus in addition to adapting to differential, non-constant tensile and compressive strain distributions, the supraspinatus tendon must adapt to significant levels of shear strain between the articular-side and bursa-side of the tendon.

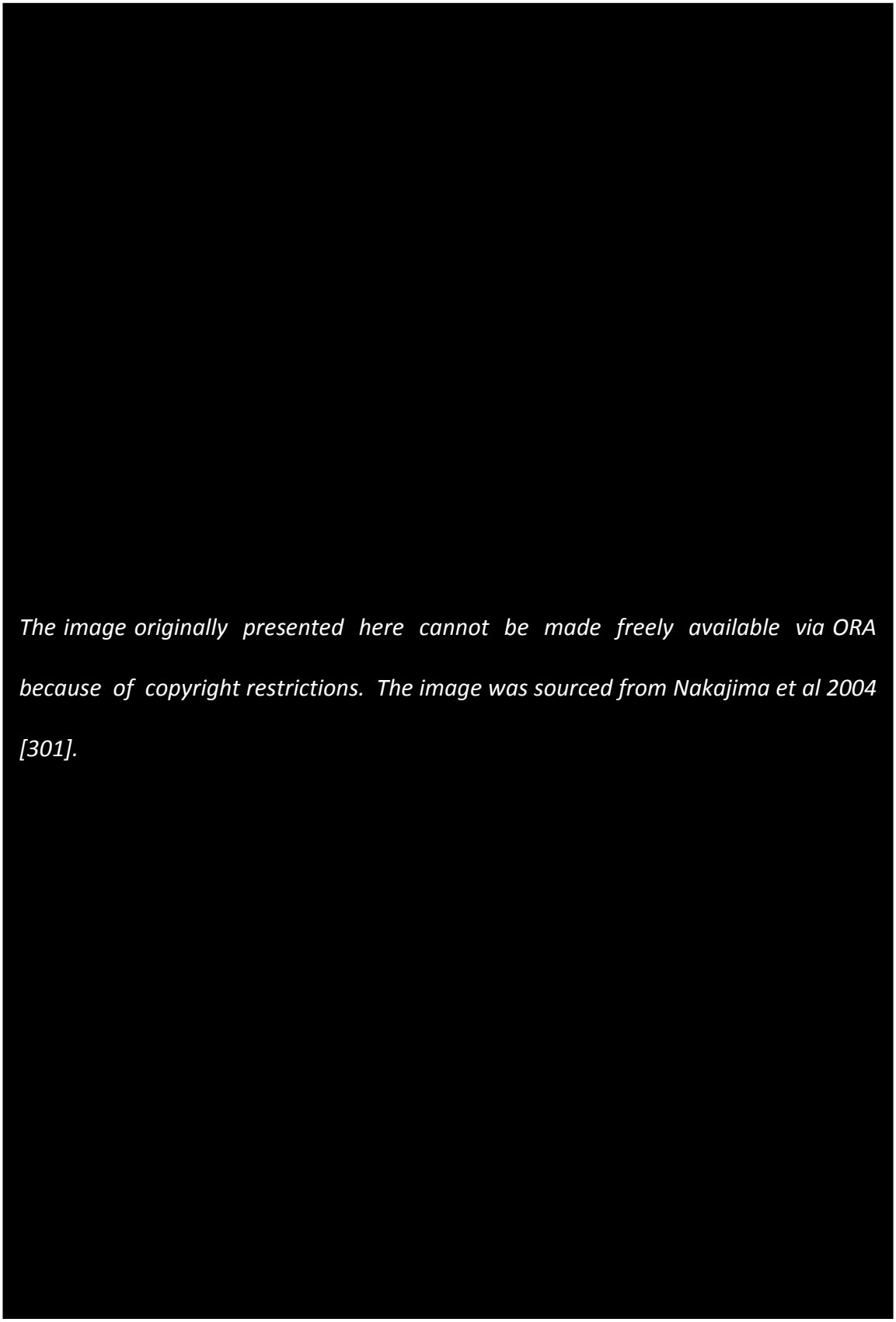

Figure 5:5 Top down MRI view of supraspinatus tendon (shown in white), and its attachment to the humerus (shown in grey) and supraspinatus muscle (shown in dark grey) when the arm is in various positions: Internal Rotation (IR), no rotation (Neutral) and External Rotation (ER), at 0, 30 and 60 degrees of abduction (ABD). The position of the arm can be seen to have a significant influence on the shape of the supraspinatus tendon. Taken from Nakajima et al 2004 [301].

5.3.2 Functional Adaptations

5.3.2.1 Structural and Compositional Adaptations

Surprisingly, the effects of the non-constant tensile, compressive and shear loading profiles on the structural adaptation of the supraspinatus tendon have not been fully investigated. In particular, the adaptations of this tendon to the principal stress distributions in the hanging arm position are largely unknown. Two associated studies [302] [303] have, however, demonstrated topographical variations in the fibre alignment; the lateral portion of the supraspinatus exhibits a higher degree of fibre alignment in the articular-side compared with the bursa-side, an adaptation which appears to be reversed in the medial portion. In contradiction of the mechanical results (Section 5.3.2.2), fibre alignment is also reported to be much greater in the medial portion compared with the lateral portion of the tendon. These differences are also present in the infraspinatus tendon, but are far less pronounced. The fibres are also much more aligned in the infraspinatus compared with the supraspinatus.

> *The adaptations of the bulk structure of the supraspinatus tendon to the non-constant strain field it experiences have been well characterised. Unlike most tendons, which show a significant degree of interconnectivity between their constituent fascicles, the fascicles of the supraspinatus tendon are comparatively non-interdigitated, exhibiting less than 20% fascicle convergence along the length of the endon [234]. Furthermore, as can be seen in*

Figure 5:6, the supraspinatus tendon is composed of 5 distinct layers that lie perpendicular to the superior-inferior plane of the tendon [261]. The fascicles and the lamellae are separated by 'loosely organized,

alcian blue-stained material running between the longitudinal collagen fiber bundles' [253]. This compositional adaptation is hypothesised to facilitate sliding between the lamellae and thus reduce the build up of shear stresses associated with changing joint angle within the structure.

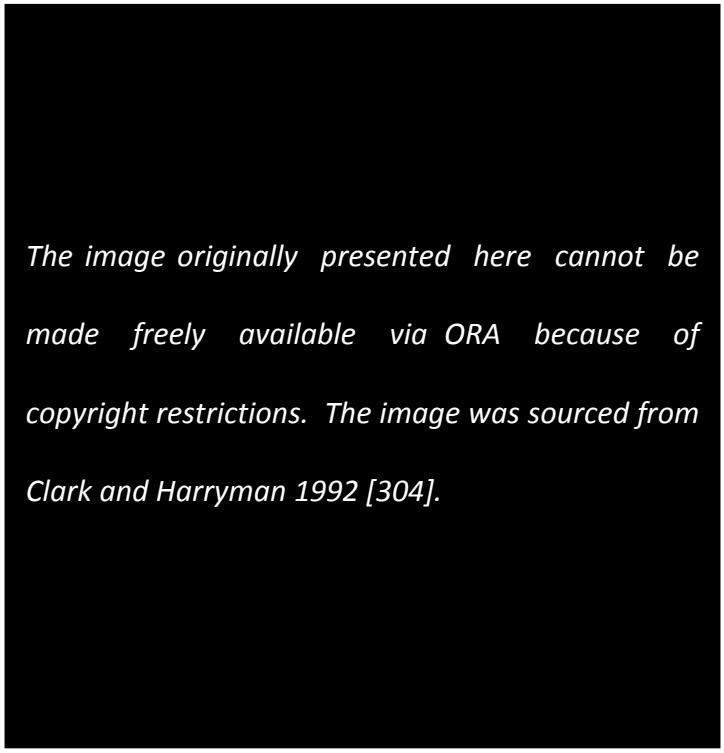

Figure 5:6 Illustration of the lamellar structure of the supraspinatus (SP) and infraspinatus (IS) tendons. Layer 1: Superficial fibres that extend from the corocohumeral ligament (chl). Layer 2: Tendon fibres that lie parallel to long axes of the tendons. Layer 3: Smaller tendon fibres arranged at an angle to the fibres in Layer 2. Layer 4: Deep fibres that extend from the corocohumeral ligament. Layer 5: Shoulder joint capsule. Taken from Clark and Harryman 1992 [304].

Compositionally, the healthy supraspinatus tendon exhibits increased levels of high molecular weight proteoglycans, such as aggrecan, compared with the common biceps tendon [36, 253] with up to 2.5 times more glycosaminoglycans and a high chondroitin sulphate to dermatan sulphate ratio. As was discussed in Chapter 3, Section 3.4.2, increased aggrecan and chondroitin sulphate content is typically associated with compressive stresses [86, 161, 163, 166], such as those that result in the presence of fibrocartilage in wrap-around tendons. However, excluding the enthesis, there is no histological evidence of fibrocartilage in the supraspinatus tendon. Furthermore, since the healthy supraspinatus tendon only experiences significant compressive stresses at small abduction angles, the high concentrations of aggrecan, chondroitin sulphate and dermatan sulphate found in this tendon are unlikely to be an adaptation to compressive stresses.

They may be an adaptation to the significant shear strains experienced by this tendon; a similar lamellar structure in which longitudinal collagen fibres are separated by regions of aggrecan and GAGs has been reported in the region opposite the compressed surface of wrap-around tendons [83, 159, 305]. It has been suggested that this adaptation facilitates sliding between the fascicles, reducing the build up of shear stress within the tendon [159]. However, this is not supported by experimental evidence; enzymatic removal of chondroitin sulphate increases the degree of sliding between fibres [110, 306], suggesting that at this hierarchical level chondroitin sulphate is important for resistance of shear strain. Increased resistance to shear deformation may appear counterintuitive in wrap-around tendons as it would increase levels of shear stress within the tendon. However, such an adaptation may be beneficial for the resistance of delamination caused by inter-fascicle and inter-laminar sliding.

5.3.2.2 Mechanical Adaptations

Regardless of the reasons governing the presence of the structural and compositional adaptations discussed above (Section 5.3.2.1), their presence has important implications for the mechanical integrity of the tissue. In particular, since PGs and GAGs exhibit lower tensile stiffness and strength than collagen, their presence is likely to compromise the tensile properties of the tendon, possibly influencing its susceptibility to damage and tearing.

Table 5:1 compares the mechanical properties of the long head of biceps tendon and the supraspinatus tendon from cadaveric specimens. Despite the efforts taken to ensure that the samples tested were macroscopically normal, the presence of microscopic degenerative changes associated with either aging or pathological tendon disorders (see below) can be expected because the mean age of the samples used was greater than 50 years old. The mechanical values reported are therefore expected to be lower than those for younger patients. Furthermore, the range of strain rates used across the studies makes direct comparison difficult. Even so, comparison of the data reveals interesting similarities and differences.

First it is obvious that the long head of biceps tendon exhibits a higher tensile modulus and ultimate tensile strength and a smaller strain at failure compared with the supraspinatus tendon. This is expected as the long head of biceps tendon is a purely tensional, energy storage tendon and thus possesses lower PG and GAG concentrations compared with the supraspinatus tendon. While interesting, this difference in the

mechanical properties of the bulk tissues is unlikely to play a role in rotator cuff tears; the supraspinatus muscle only contributes approximately 14% of the muscle contraction force generated by the cuff muscles (Section 5.1). However, the topographical variations in mechanical properties of the supraspinatus tendon may play an integral role in rotator cuff tears.

Direct comparisons of the supraspinatus studies detailed in Table 5:1 are not possible due to variability in testing conditions. However, examination of the individual studies reveals the mechanical properties of the supraspinatus tendon are not topographically homogeneous: in agreement with the patterns of non-constant strain fields discussed above (Section 5.3.1), the bursa-side of the tendon exhibits higher indentation stiffness [162], higher stiffness transverse to the long axis of the tendon [302], higher ultimate tensile stress [307], and higher strain to failure [153] compared with the articular-side. This may explain why the majority of rotator cuff tears initiate on the articular-side of the supraspinatus tendon. It can also be seen from Table 5:1 that the anterior portion of the supraspinatus tendon exhibits higher stiffness and ultimate tensile strength compared with the posterior portion [308], an observation that may explain why full-thickness tears tend to progress from the supraspinatus into the infraspinatus tendon.

Table 5:1 Mechanical Properties of Long head of biceps tendon and supraspinatus tendon

Tendon	Tensile Modulus	Ultimate Tensile Stress	Ultimate Tensile Strain	Strain rate	Testing Mode	Mean Age	Comments	Ref.
Long head of biceps	412 MPa	32.5 MPa	10.1 %	100 mm min^{-1}	Tensile (to failure)	67 years	• Tendon samples underwent a freeze-thaw cycle prior to testing	[309]
Supraspinatus	3.28 g mm^{-1} (bursa-side) 2.19 g mm^{-1} (articular-side)	---	---	0.1 mm s^{-1}	Indentation (Indentation force 250g)	63 years	• Bursa-side significantly stiffer than articular-side • 3mm ø flat indentation tip	[162]
	---	6.3 MPa (bursa-side) 2.8 MPa (articular-side)	---	0.17 mm s^{-1}	Tensile (to failure)	59 years	• Tendon samples underwent a freeze-thaw cycle prior to testing	[307]
	---	11.5 MPa	18.5% (bursa-side) 14.4% (articular-side)	1 % s^{-1}	Tensile (to failure)	55 years	• Significant difference between ultimate tensile strain in bursa and articular-sides • No significant differences in ultimate tensile strain within mediolateral plane or anterior-posterior plane	[153]
	≈35MPa (anterior bursa-side) ≈1MPa (anterior articular-side) ≈30MPa (posterior bursa-side) ≈2MPa (posterior articular-side)	---	---	0.1 % s^{-1}	Tensile (to failure)	63 years	• Samples loaded transverse to the long axis of the tendon • Bursa-side much stiffer than articular-side, and lateral portion much stiffer than medial portion • Toe stiffness much greater on bursa-side than articular-side, and in lateral portion than in medial portion	[302]
	≈165 MPa (anterior) ≈ 75 MPa (middle) ≈45 MPa (posterior)	16.5 MPa (anterior) 6.0 MPa (middle) 4.1 MPa (posterior)	---	10 % s^{-1}	Tensile (to failure)	64 years	• Anterior portion significantly stiffer and stronger	[308]

5.3.2.3 Vascular Adaptations

Studies of the vasculature of the supraspinatus tendon in cadaveric subjects have indicated the presence of a critical zone within the articular portion of the tendon, in which the vasculature is greatly reduced [310]. The size of this critical zone is greatly increased in older subjects [311]. More recently, studies of the vasculature in healthy volunteers using contrast-enhanced ultrasound have shown that blood flow in this area is further reduced after forward elevation exercises [312].

The critical zone is probably an adaptation to the compressive stresses experienced in this region when the arm is at 0° abduction. As was previously discussed (Chapter 3, Section 3.4) 'when load is applied to a porous, wet material, the load is initially born by the fluid and is gradually transferred to the material as the fluid flows out of the material, dissipating the fluid pressure.' In the case of blood vessels however, dissipation of fluid pressure by the fluid flowing out of the material is not possible without rupture of the blood vessel walls. Thus the presence of blood vessels in this region of the tendon would require that the blood vessel walls possessed much higher radial stiffness and strength in order to resist the increased fluid pressure associated with compressive loading. A greater restriction on the presence of blood vessels within this region of the tendon, however, is the fact that during development and maturity of the tendon it would be necessary for the blood vessels to grow into this region of compressive stress. This is very unlikely as indicated by the avascularity of cartilage, a material which is subjected to both compressive and shear loading. Whatever the reason for the presence of this avascular region in the supraspinatus tendon, it has been postulated that the resulting decreased blood supply may increase the susceptibility of this region of the tendon to degeneration and tearing.

5.3.3 Degenerative Adaptations

Examination of the pathological adaptations of torn rotator cuff tendons indicates that rotator cuff tendon pathology is potentially:

A. Multifactoral, involving biological, biochemical, and histological changes, and

B. Progressive.

For example, torn tissue appears to show a higher turnover rate compared with healthy tissue. Ruptured (partial and full thickness) supraspinatus tendons also exhibit increased concentrations and mRNA expression of metalloproteinase (MMP) 1 and MMP13, and decreased expression of MMP2, MMP3 and tissue inhibitors of metalloproteinases (TIMP) 2, TIMP3, and TIMP4 [40, 313]. Torn tendons also exhibit increased levels of collagen type III and decreased levels of collagen type I compared with macroscopically normal cadaveric supraspinatus tendons [61, 314, 315]. Vascular markers are also increased in samples taken from the edge of small tendon tears [316], while increased levels of fibronectin have been found in rupture tendons [317].

These results indicate that the extent of tissue turnover and remodelling is increased in ruptured rotator cuff tendons, possibly indicating that the tissue is responding to tissue damage by laying down scar tissue (collagen type III) and removing the damaged tissue (collagen type I) [36, 61]. The results may also indicate that the tissue is undergoing a remodelling process in response to the changing mechanical environment. Interestingly, the reduced vascularity of the critical zone of the supraspinatus tendon would restrict this repair mechanism. This may explain why tears initiating on the articular-side of the supraspinatus tendon are likely to progress to full thickness tears.

Torn cuff tendons have been shown to contain high levels of apoptotic cells [32, 318]. Significant numbers of cells with a rounded profile have also been found, with higher numbers in samples taken from large and massively torn tendons [316, 319]. These rounded cells are similar in profile to the cells seen in the released rotator cuff tendons in the initial stages of repair, possibly indicating that these cells are active tenoblast-like cells [320]. However, most researchers believe that the rounded cells in degenerate rotator cuff tendons share more in common with the rounded profile chondrocytes found in cartilage, and are thus likely to be tenocytes that have undergone chondroid metaplasia [315]. If this is the case, it indicates that the cells are responding to different mechanical stimuli, specifically the presence of compressive stresses.

Further evidence for the presence of compressive and shear strains in torn tendons is provided by finite element models of torn cuff tendons [33, 321, 322], and also by differences in PG and GAG profiles of torn rotator cuff tendons compared with macroscopically normal cadaveric tendons [36]. For example, torn

cuff tendons contain elevated levels of inter-fascicle and inter-fibre PGs, a characteristic commonly referred to as mucoid degeneration [36]. Specifically, levels of aggrecan are significantly increased compared with intact tendons. The profile of the inter-fibrillar PGs and GAGs is also altered in torn tendons; levels of decorin are significantly decreased [323] and the ratio of chondroitin sulphate to dermatan sulphate is increased, although the total GAG content of torn rotator cuff tendons does not change [36]. These adaptations may indicate attempts to adapt to the increased amounts of increased shear strain within the tendon.

In addition to these biochemical adaptations, torn rotator cuff tendons have been shown to be structurally different to healthy tendons. For example, ruptured tendons possess thinner fascicles [317] and thinner, less-organised collagen fibres compared with normal tendons, particularly in the deeper layers of the tendon, and at the enthesis [30, 43, 324-326]. This decrease in alignment of the fibres is similar to that seen prior to healing in released cuff tendons [320], and may be associated with the increased concentrations of collagen type III in torn samples. Increased concentrations of inter-fascicle and inter-fibre aggrecan may also play a role in the decreased fibre and fascicle thicknesses due to simple space-saving considerations. Concurrently, as an important regulator of fibril thickness and alignment during fibrillogenesis, decreasing concentrations of decorin may lead to decreased fibril thickness and alignment in torn samples. To date, however, the structural and compositional adaptations of torn rotator cuff tendons on an ultrastructural level have not been reported.

5.4 OBJECTIVES AND AIMS

This review has highlighted that whilst the bulk adaptations of the rotator cuff tendons as a result of their loading environment is fairly well known, the micro- and ultra-structural adaptations in healthy and torn tendons are less well understood. Characterisation of the architecture of healthy and degenerative rotator cuff samples could reveal important information regarding the role of the mechanical environment in the aetiology and pathology of rotator cuff tendinosis. Such information could significantly influence clinical decision-making, and could potentially highlight key markers that could be used for detection and diagnosis of tendon degeneration. It may also give some insight into pre-rupture degenerative changes.

In Chapter 4, Sections 4.2.2 and 4.2.3 it was shown that the collagenous architecture of tendon exhibits significant structural adaptations according to its the loading environment, and that non-contact AFM and picrosirius red-staining are sensitive methods with which to detect these adaptations. The objective of the work presented in Chapters 6, 7 and 9 is therefore to characterise the structural adaptations of the supraspinatus tendons in health and disease. The dimensions of the collagen architecture of normal and torn tendons will be assessed in order to elucidate information regarding the role of mechanical environment in tear aetiology and progression. Specifically, the following hypotheses will be tested:

1. Healthy rotator cuff tendons exhibit structural adaptations, associated with the topographical variation in loading environment, that increase the susceptibility of tendons to tearing.
2. Age has a significant influence on the structural adaptations of the rotator cuff tendons.
3. Chronically torn rotator cuff tendons exhibit different structural adaptations compared with healthy tendons.
4. The extent of the structural differences introduced by chronic rotator cuff tears increasing with tear size.

Chapter Six

Topographical Adaptations in Health and Disease

6.1 MATERIALS AND METHODS

6.1.1 Sample Collection

To assess the topographical variation of the material properties in rotator cuff tendons, bilateral shoulders from two formalin-perfused cadavers were obtained. These samples were provided by Professor John Morris (Medical Sciences Teaching Centre, Medical Sciences Division, University of Oxford. HTA Licensing Number: 12178). Using number 10 surgical blades, the supraspinatus and infraspinatus musculotendinous units were removed intact from the humeral head (Figure 6:1). A 2.5mm biopsy punch (Kai Medical, Hawaii, USA) was then used to remove through thickness biopsies from the anterior and posterior portions of each tendon, at four locations radiating medially, beginning at the enthesis and ending at the muscle insertion point. Each biopsy was split into inferior (articular-side) and superior (bursa-side) halves, producing 32 individual samples per shoulder. Each sample was stored separately in 4% formalin (Sigma Aldrich, Dorset, UK) in appropriately labelled 2ml eppendorf tubes (Thermo Fisher Scientific, Waltham USA). Clinical data for these cadavers is detailed in Table 6:1.

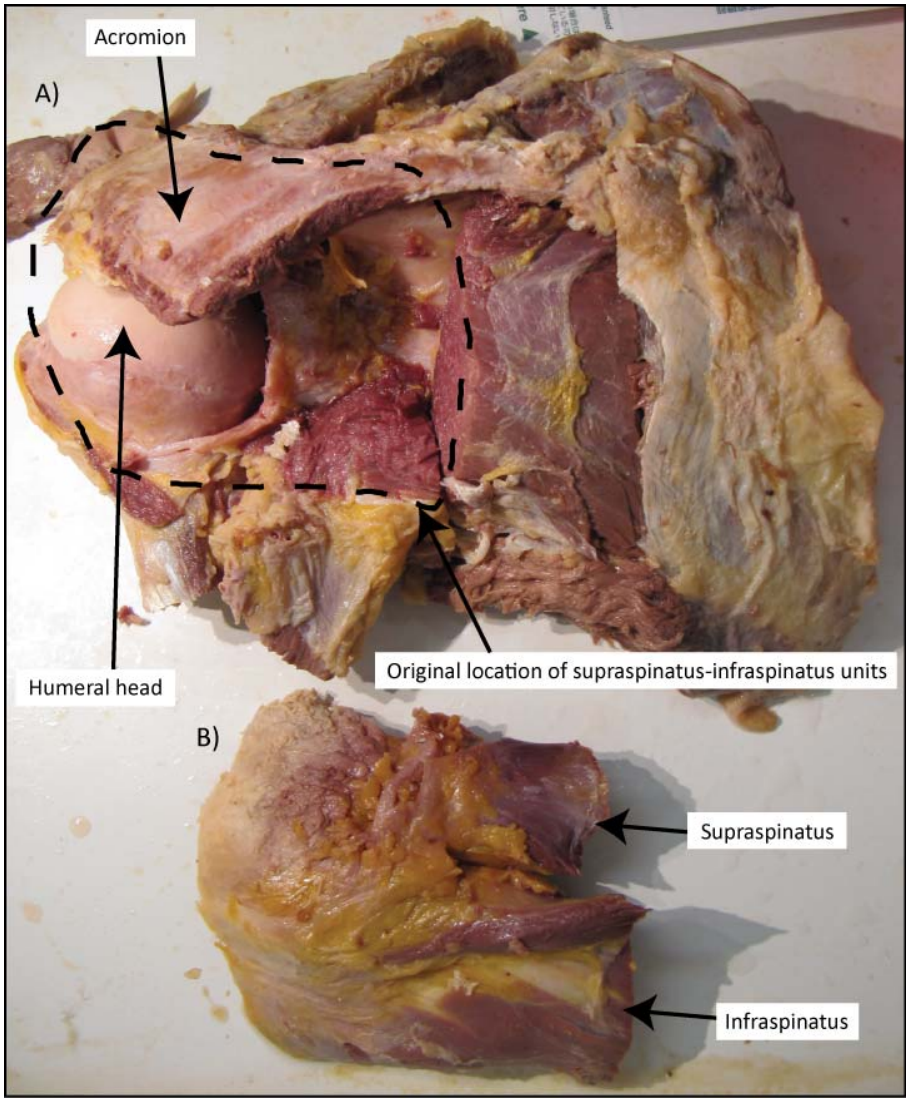

Figure 6:1 Image of a cadaveric shoulder with the supraspinatus and infraspinatus units removed (A). The isolated supraspinatus and infraspinatus musculotendinous units are shown below (B).

Table 6:1 Clinical data describing cadaveric specimens

Patient	Gender	Age at death	Cause of death	Condition of tissue	
				Left Shoulder	***Right Shoulder***
1	Male	91	Bronchial Pneumonia	Macroscopically normal	Macroscopically normal
2	Female	82	Congestive Cardiac Failure	Delaminated supraspinatus	Macroscopically normal

6.1.2 Sample Preparation

6.1.2.1 Tissue Processing and sectioning

Post-collection, specimens were fixed in 10% formalin for at least 1 month prior to being placed between biopsy foam pads and transferred to histology embedding cassettes with detachable lids. The cassettes were placed in a Shandon Pathcentre tissue processor (Thermo Fisher Scientific, Waltham USA) and the fixed specimens were dehydrated through graded IMS (70%, 90%, 95%, 100%), rinsed in xylene, and perfused with Formula R paraffin wax (Sugipath, Peterborough, UK) over the course of 16 hours. Post-perfusion, samples were removed from the cassettes and embedded in paraffin wax blocs using an embedding centre (Leica, Wetzlar, DE). Finally, two 10µm sections were cut from each sample using a RM 2165 microtome (Leica, Wetzlar, DE) fitted with a steel blade (Model 819), and floated off onto warm tap water. Each section was mounted on an Xtra glass slide (Sugipath, Peterborough, UK) and baked at 60°C for 24 hours.

6.1.3 Sample Characterisation

6.1.3.1 Atomic Force Microscopy

In preparation for ultrastructural analysis by atomic force microscopy, one glass-mounted 10µm section from each sample was dewaxed following the procedure detailed in Chapter 4, Section 4.1.3.3. Atomic force microscopy (AFM) was employed to characterise the ultrastructure of the extracellular matrix in each sample. Dewaxed sections were imaged using an AFM in non-contact mode [182] following the experimental and analysis procedures detailed in Chapter 4, Section 4.1.4.4. In addition, the average angle between fibrils was calculated as follows:

1. For each fibril being analysed, record the average angle the fibril makes to the x-axis (see Figure 6:2), when the fibril is considered to run in the positive x-direction (i.e. angle must lie between -90° and +90°).

2. Calculate angle between Fibril 1 and Fibril 2. If the angle between them is greater than 90°, subtract the angle from 180°, producing an angle between 0° and 90°.

   Microsoft Excel formula: $= IF(ABS (Fibril1_{angle\ to\ x\text{-}axis} - Fibril2_{angle\ to\ x\text{-}axis})>90, (180-(ABS(Fibril1_{angle\ to\ x\text{-}axis} - Fibril2_{angle\ to\ x\text{-}axis}))),(ABS(Fibril1_{angle\ to\ x\text{-}axis} - Fibril2_{angle\ to\ x\text{-}axis})))]$

3. Repeat Step 2 until angle calculated between Fibril 1 and all other fibrils.

4. Repeat Steps 3 and 4 for Fibril 2 etc. until the angle between all fibrils has been calculated.

5. Calculate average angle between fibrils

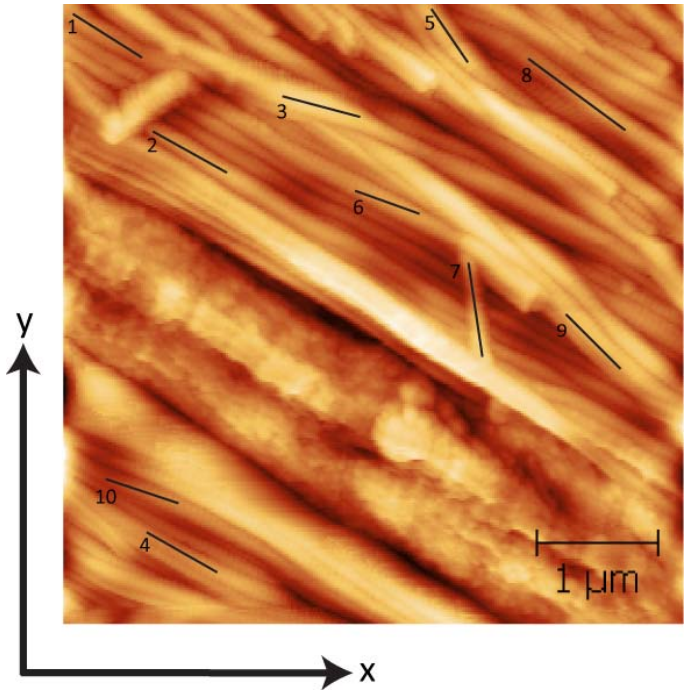

Figure 6:2 Illustration of Step 1 in the calculation of average angle between fibrils

6.1.4 Statistical Analysis

Data is presented as mean values ± standard deviation unless otherwise indicated. In all cases, mean values represent the mean value of the individual sample means to avoid giving undue weight to samples for which more measurements were possible [327]. Where relevant, linear regression analysis was performed on the data using 'R' Biostats with and without the inclusion of confounding factors.

6.2 RESULTS

6.2.1 Fibril Diameter

6.2.1.1 Macroscopically Normal Cuff

Figure 6:3 is a pictorial representation of the topographical variation of the fibril diameter in the cuff tendons, averaged over the three macroscopically normal cuffs. Table 6:2 presents statistical data for the fibril measurements averaged over the bursa-side and articular-side of the tendons for different shoulders. Fibril diameter varies heterogeneously throughout the supraspinatus and infraspinatus tendons, as indicated by the large standard deviations and inter-quartile ranges (Table 6:2). Fibrils are generally thinner on the articular-side than on the bursa-side, although this difference is only significant in the right shoulder of Patient 1. In the medial-lateral plane, fibril diameter generally increases from the enthesis to the muscle insertion on the articular-side, and decreases in the same direction on the bursa-side. In the anterior-posterior plane, fibril diameter is generally larger in the centre of the cuff unit (posterior portion of the supraspinatus and anterior portion of the infraspinatus) on the bursa-side but this trend is less pronounced on the joint side.

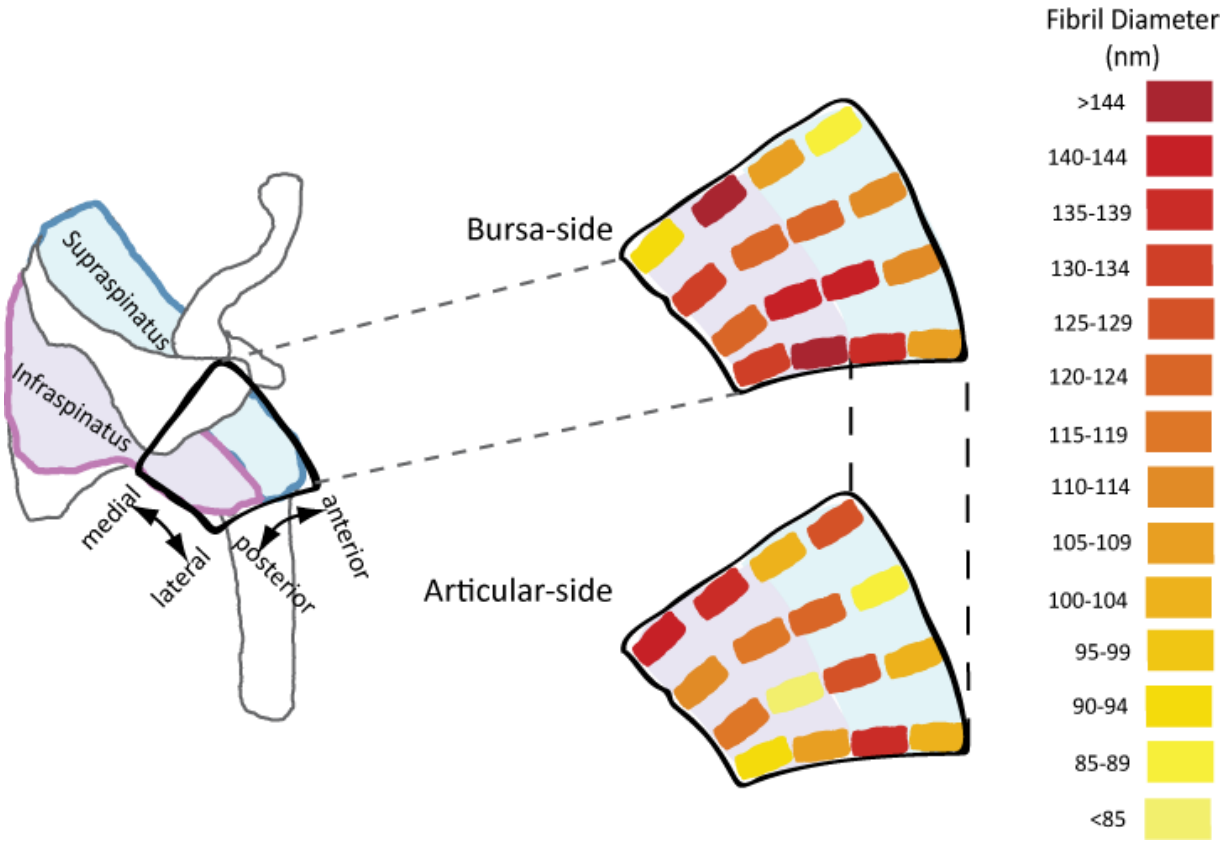

Figure 6:3 Pictorial depiction of topographical variation in fibril diameter across the supraspinatus and infraspinatus tendons averaged over macroscopically normal cadaveric rotator cuff samples. An annotated schematic of the rotator cuff is included for reference.

Table 6:2 Statistical Data for Fibril Measurements, averaged over bursa-side and articular-side in different shoulders

			Mean (nm)	Standard deviation	1st Quartile – 3rd Quartile (Inter-quartile range)
Patient 1	**Left**	**Bursa-side**	118.4	47.0	85.4 - 136.3 (50.9)
		Articular-side	117.7	51.6	80.8 - 142.4 (61.6)
	Right	**Bursa-side**	138.7	59.7	94.8 - 172.2 (77.4)
		Articular-side	116.0	49.0	80.7 - 142.7 (62.0)
Patient 2	**Right**	**Bursa-side**	124.0	42.0	95.3 - 143.5 (48.2)
		Articular-side	122.1	43.3	90.8 - 148.6 (57.8)

6.2.1.2 Delaminated Cuff

Figure 6:4 presents a pictorial representation the topographical variation in fibril diameter in the cuff tendons affected by delamination of the supraspinatus tendon (Patient 2, left shoulder). Table 6:3 presents the descriptive statistics for this data. Compared with the macroscopically normal tendons (Figure 6:3, Table 6:2), the delaminated cuff exhibits thinner fibrils in both the bursa-side and the articular-side. Standard deviation and inter-quartile range are also smaller for these samples, and the 1st and 3rd quartiles are lower. Furthermore, and unlike the macroscopically normal tendons, the fibrils in the delaminated cuff tendons are significantly smaller in the bursa-side compared with the articular-side.

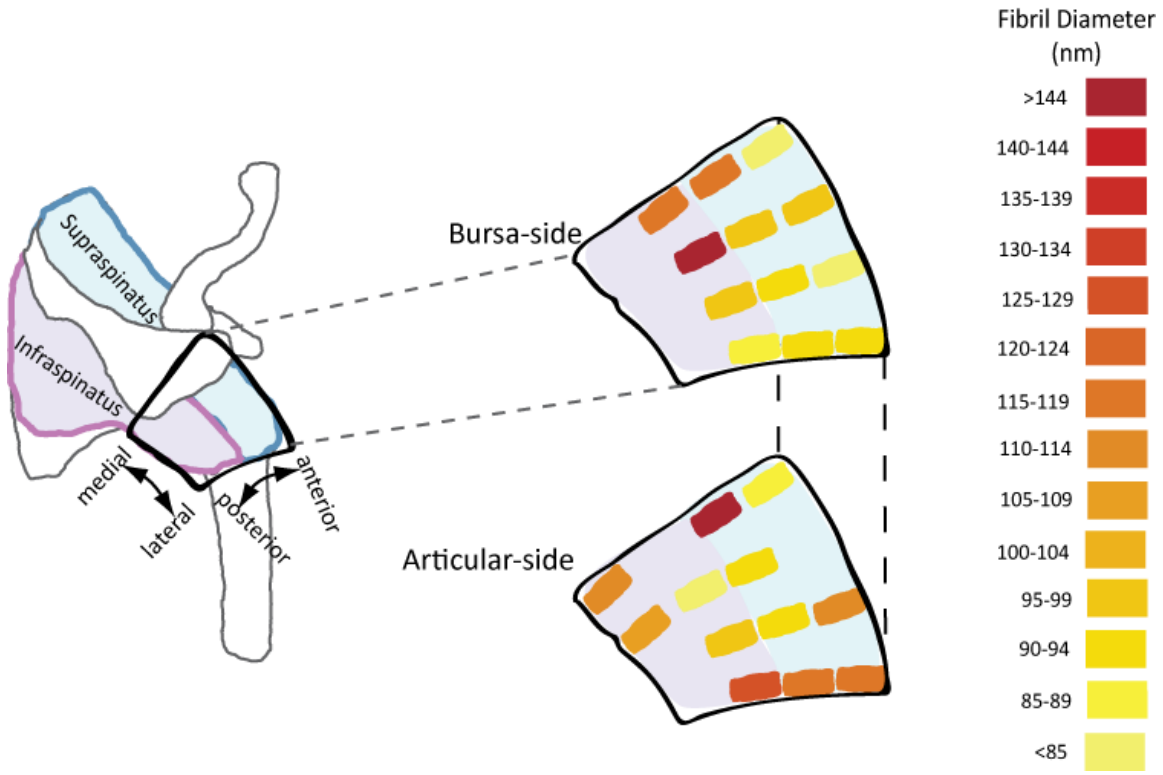

Figure 6:4 Pictorial depiction of topographical variation in fibril diameter across the supraspinatus and infraspinatus tendons, for cadaveric rotator cuff sample affected by delamination of the supraspinatus tendon. An annotated schematic of the rotator cuff is included for reference.

Table 6:3 Descriptive statistics for cuff tendon affected by delamination of supraspinatus tendon

	Mean (nm)	Standard deviation	1st – 3rd Quartile (Inter-quartile range)
Bursa-side	103.6	40.6	76.7 - 119.8 (43.1)
Articular-side	113.3	38.5	85.3 – 133.0 (47.7)

6.2.2 'D' Spacing

6.2.2.1 Macroscopically Normal Cuff

Table 6:4 presents statistical data for the 'D' spacing in the in macroscopically normal cadaveric samples averaged over the bursa-side and articular-side of the tendons for different shoulders. Figure 6:5 illustrates the variation of 'D' spacing with fibril diameter. There is no significant topographical variation in 'D' spacing and no significant correlation between 'D' spacing and fibril diameter ($\beta = 0.007$, $R = 0.098$, $p = 0.418$).

Table 6:4 Statistical Data for 'D' Spacing, averaged over bursa-side and acrticular-side for all macroscopically normal cadaveric shoulders

			Mean (nm)	Standard deviation	1st – 3rd Quartile (Inter-quartile range)
Patient 1	**Left**	**Bursa-side**	60.97	7.08	56.34 - 65.15 (8.81)
		Articular-side	60.40	7.06	55.54 - 64.66 (9.12)
	Right	**Bursa-side**	60.08	6.90	55.77 - 63.9 (8.13)
		Articular-side	59.16	7.26	54.195 - 63.625 (9.43)
Patient 2	**Right**	**Bursa-side**	60.31	7.05	55.03 - 64.46 (9.43)
		Articular-side	60.69	7.48	55.44 - 66.03 (10.59)

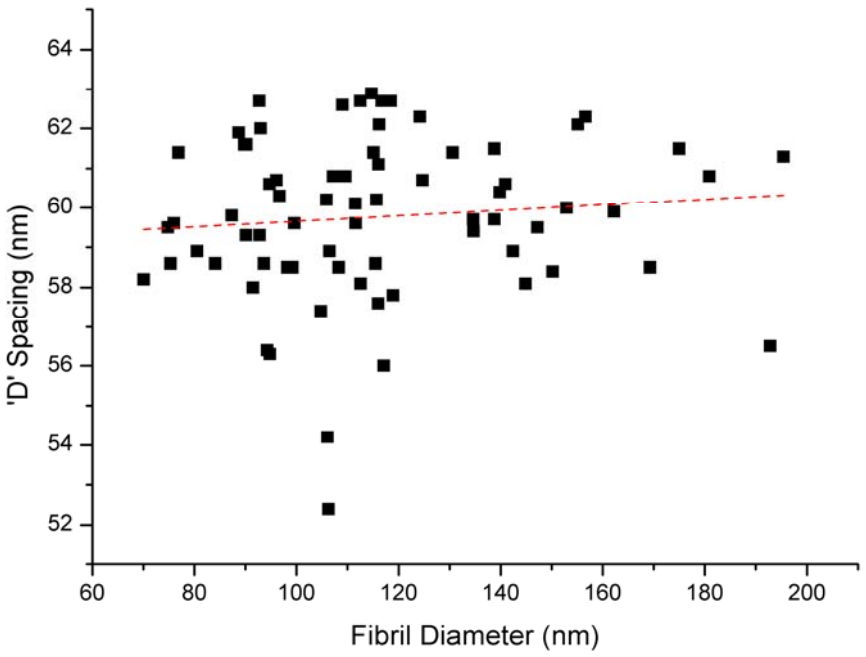

Figure 6:5 Correlation between 'D' spacing and fibril diameter for macroscopically normal cadaveric samples.

6.2.2.2 Delaminated Cuff

Table 6:5 shows the descriptive statistics for 'D' spacing measurements in cuff tendons affected by delamination of the supraspinatus tendon. There is no significant topographical variation. Furthermore, the 'D' spacing is not significantly different compared to macroscopically normal cadaveric cuff tendons (see Table 6:4).

Table 6:5 Topographical variation in 'D' spacing in cadaveric rotator cuff affected by delamination of the supraspinatus tendon

	Mean (nm)	Standard deviation	1st – 3rd Quartile (Inter-quartile range)
Bursa-side	59.71	7.19	54.25 - 64.21 (9.97)
Articular-side	59.44	6.80	54.69 - 64.33 (9.64)

6.2.3 Fibril Alignment

6.2.3.1 Macroscopically Normal Cuff

Figure 6:6 shows a pictorial representation of mean angle between fibrils in macroscopically normal cadaveric samples, averaged over the three samples. Table 6:6 presents descriptive statistics of this data averaged over the bursa-side and articular-side of the tendons for different shoulders. Mean angle between fibrils varies topographically, with the supraspinatus tendon generally exhibiting a higher angle between fibrils compared with the infraspinatus tendon on the bursa-side. On the articular-side the mean angle between fibrils is generally smaller in the middle portion (posterior supraspinatus and anterior infraspinatus) compared with the edges, although this trend is less pronounced towards the muscle insertion.

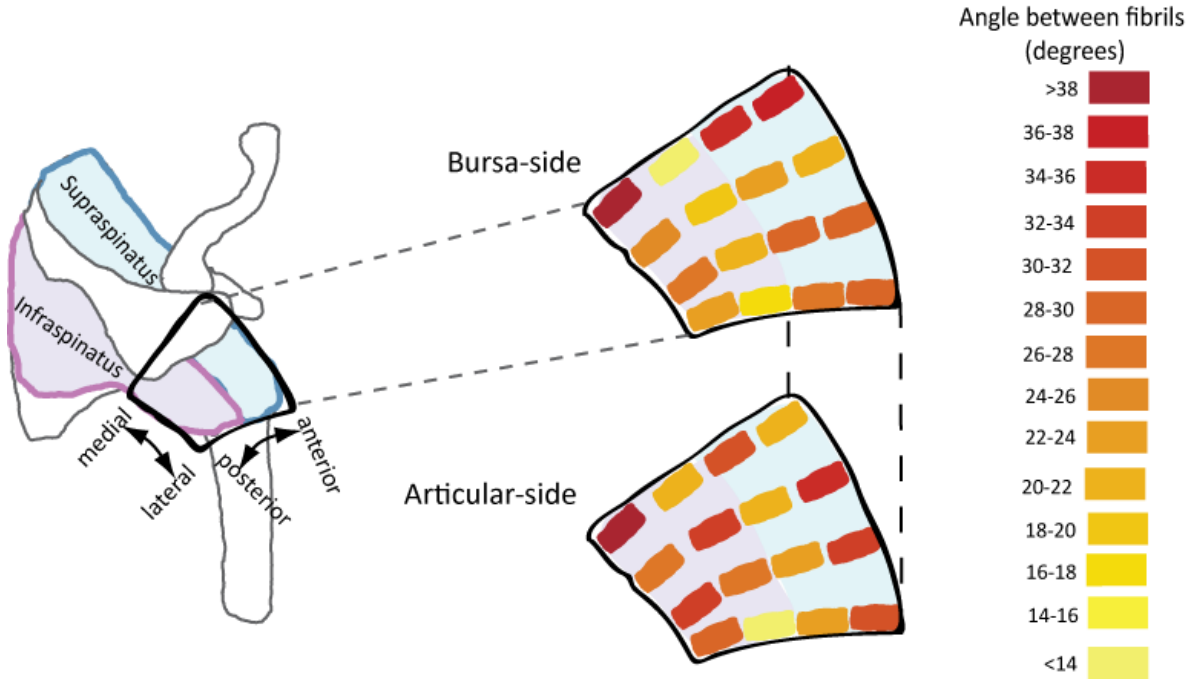

Figure 6:6 Pictorial depiction of topographical variation in mean angle between fibrils, averaged over macroscopically normal cadaveric rotator cuff samples. An annotated schematic of the rotator cuff is included for reference.

Table 6:6 Statistical Data for Average angle between fibrils, averaged over bursa-side and articular-side in different shoulders

			Mean (nm)	Standard deviation	1st – 3rd Quartile (Inter-quartile range)
Patient 1	**Left**	**Bursa-side**	24.4	14.2	11.95 - 36.95 (25.0)
		Articular-side	24.9	12.0	13.8 - 33.3 (19.5)
	Right	**Bursa-side**	26.7	12.6	17.2 - 35.9 (18.7)
		Articular-side	25.3	11.9	16.1 - 33.4 (17.3)
Patient 2	**Right**	**Bursa-side**	23.3	15.0	9.3 - 38.4 (29.1)
		Articular-side	28.3	14.7	14.7 - 40.2 (25.5)

Figure 6:7 displays the correlation between the mean angle between fibrils and fibril diameter in macroscopically normal cuff tendons. There is a strong trend for smaller mean angles between fibrils with smaller fibril diameter ($\beta = -0.161$, $R = 0.505$, $p = 3.217 \times 10^{-7}$).

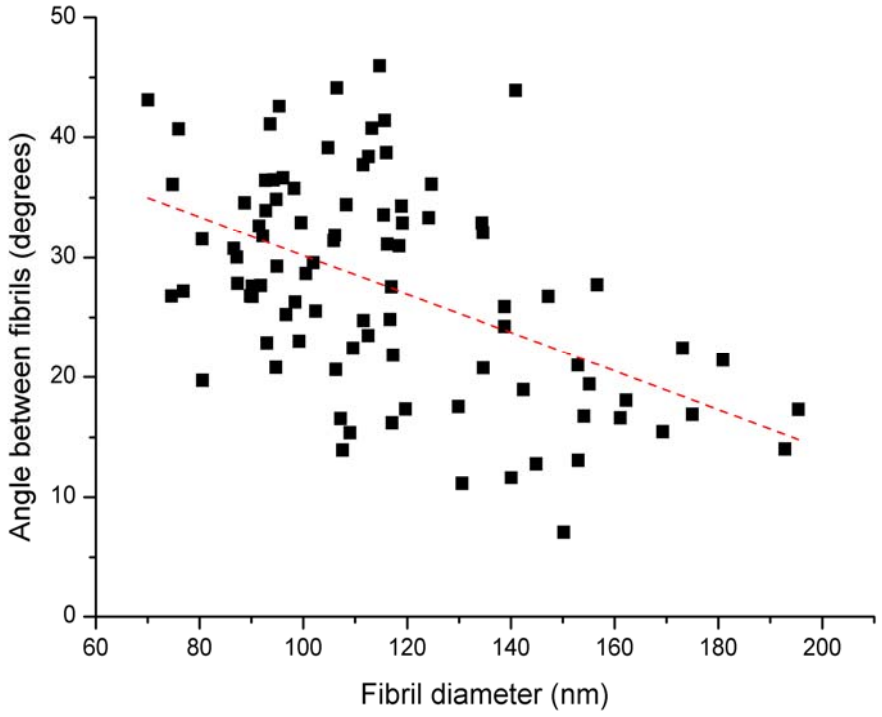

Figure 6:7 Variation of mean angle between fibrils with fibril diameter for macroscopically normal cadaveric samples.

6.2.3.2 Delaminated Cuff

Figure 6:8 shows a pictorial representation of the topographical variation of mean angle between fibrils in the cuff tendons affected by delamination of the supraspinatus tendon. Table 6:7 shows descriptive statistics of this data. Compared with macroscopically normal samples (Figure 6:6, Table 6.6), the mean angles are higher in the delaminated cuff. However, the size of the distribution is not significantly different between the macroscopically normal and delaminated cuffs.

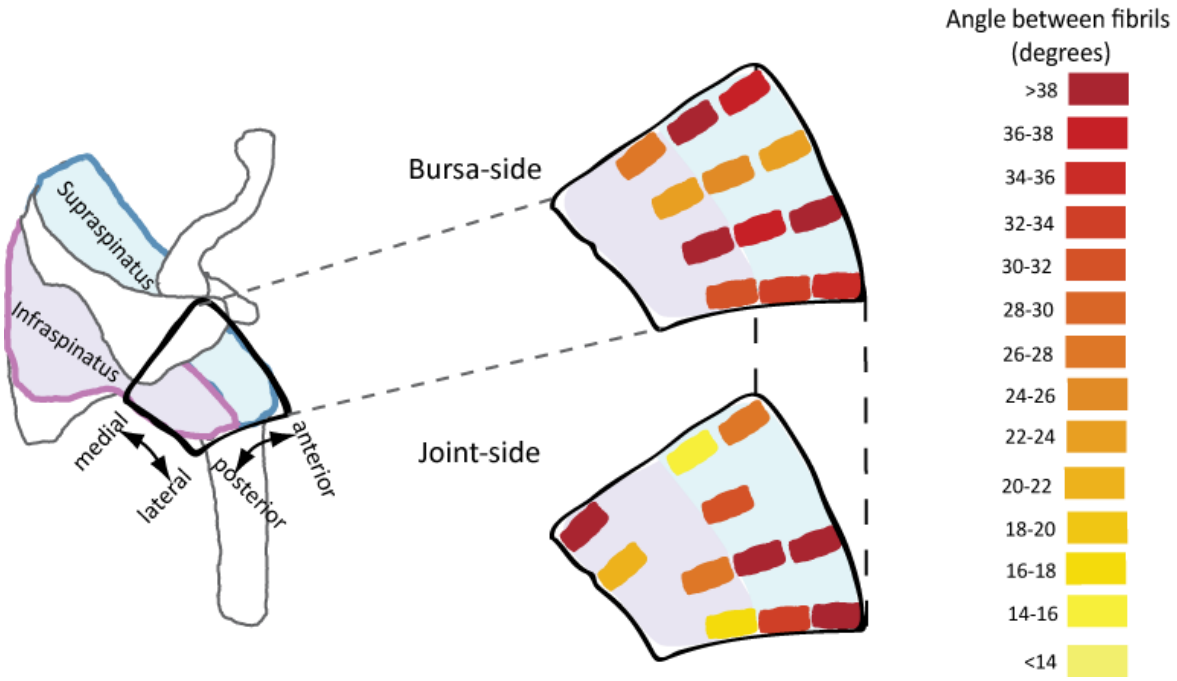

Figure 6:8 Pictorial depiction of topographical variation in mean angle between fibrils across the supraspinatus and infraspinatus tendons, for cadaveric rotator cuff sample affected by delamination of the supraspinatus tendon. An annotated schematic of the rotator cuff is included for reference.

Table 6:7 Topographical variation in average angle between fibrils for cadaveric rotator cuff sample affected by delamination of the supraspinatus

	Mean (nm)	Standard deviation	1st – 3rd Quartile (Inter-quartile range)
Bursa-side	31.72	12.84	22.85 - 43.2 (20.35)
Articular-side	28.58	13.69	20.40 - 41.9 (21.5)

6.3 DISCUSSION

6.3.1 Structural Adaptations of the Healthy Supraspinatus Tendon

As was previously discussed (Section 5.2.2), the observation that the supraspinatus tendon is the most commonly torn rotator cuff tendon, and that these tears commonly initiate on the articular-side before growing in both medial and posterior directions has led many researchers to postulate that the function adaptation of the supraspinatus tendon to its mechanical environment may play an important role in its susceptibility to degeneration and tearing. However, while the adaptations of the bulk structure of the supraspinatus tendon to the non-constant strain fields it experiences are well established, the structural adaptations are largely unreported. Therefore, this is the first study to investigate the topographical variation in ultrastructure in the supraspinatus and infraspinatus tendons.

The results clearly demonstrate that both supraspinatus and the infraspinatus tendons exhibit a heterogeneous distribution of fibril diameters (Figure 6:3 pg. 112), and that there are trends within this heterogeneity:

a) Fibrils are generally thicker on the bursa-side compared with the articular-side,

b) Fibrils diameter decreases from the enthesis to the muscle insertion on the bursa-side, and increases from the enthesis to the muscle insertion on the articular-side.

c) Fibrils are thicker in the centre of the supraspinatus-infraspinatus unit (posterior region of the supraspinatus /anterior region of the infraspinatus) on the bursa-side of both tendons.

These results are in direct agreement with previous studies that have demonstrated heterogeneity in the mechanical properties of the healthy supraspinatus tendon [302, 303, 328]. For example, assuming that thicker fibrils are an adaptation for stiffness and strength in tension, the increased fibril thickness on the bursa-side compared with the articular-side is consistent with the previously reported higher indentation stiffness and uniaxial stiffness of the bursa-side compared with the articular-side [162, 302, 307].

Given the numerous experimental limitations associated with mechanical characterisation of rotator cuff tendons, it is perhaps of more relevance to compare the results of this study with the stress and strain

fields within the cuff tendons previously predicted by finite element studies [34, 292]. According to these models, the bursa-side of the supraspinatus experiences large positive (tensile) principal stresses in the region of the enthesis and large negative (compressive) principal stresses in the region of the muscle insertion. Concurrently, the articular-side the tendon experiences large compressive principal stresses in the region of the enthesis and large positive (tensile) principal stresses in the region of the muscle insertion. Given the trend for smaller fibril diameters in regions of compressive and shear stresses and larger fibril diameters in tensile regions previously reported (Chapter 4, Sections 4.2.2 and 4.2.3), the results reported here are consistent with these finite element models.

The results of this study therefore provide evidence that the cuff tendons are structurally adapted to their mechanical environment. However, the extent of this adaptation appears to be restricted; compared with the large differences in diameter between the articular-side and the bursa-side of the ovine infraspinatus (Chapter 4, Section 4.2.3), the differences in fibril diameter reported here are relatively small (Table 6:2 pg. 113). This suggests that the non-constant strain fields within the cuff tendons (see Section 5.3.2) result in structural adaptations that are a compromise between the adaptations best suited to compressive and shear strains experienced in hanging arm position, and those best suited to the purely tensile strains experienced at greater than 60° arm abduction. As a result, the cuff tendons are unlikely to be ideally adapted to *any* of the strain fields they experience.

The restricted adaptation of the cuff tendons may limit their ability to perform under different loading conditions, increasing their susceptibility to damage. For example, the thinner, less aligned fibrils on the articular-side compared with the bursa-side - caused by the presence of compressive strains when the shoulder is in the hanging arm position - are likely to reduce the ability of the articular-side to resist the tensile strains experienced at abduction angles of greater than 60°. This would increase the likelihood of the articular-side tearing at these large abduction angles would be greatly increased.

Thus, the topographical variation in the structural adaptations of macroscopically normal cadaveric rotator cuff tendons presented here (Figure 6:3 pg 112, Figure 6:6 pg 116) support the hypothesis that the extreme mobility of the human shoulder joint and associated non-constant strain fields limit the ability of the cuff tendons to fully adapt to their mechanical environment and increases their susceptibility to

degeneration and tearing. Assuming this damage is cumulative and that the body's ability to repair decreases with aging, particularly post-maturity, increasing age is likely to have an important influence on the structural adaptations of the cuff tendons. Further work is now needed to characterise the effect of structural adaptations of the mechanical integrity of the tissue. The effect of age on the ability of the rotator cuff tendons to repair mechanical damage should also be investigated.

6.3.2 Effect of Delamination on the topographical variation

In the cadaveric rotator cuff specimen affected by delamination of the supraspinatus the topographical variation of fibril diameter is greatly reduced, with the fibrils being thinner (Figure 6:4 pg. 113) and less aligned (larger angle between fibrils) (Figure 6:8 pg. 118) compared with fibrils in the macroscopically normal cadaveric specimens (Figure 6:3 pg. 112, Figure 6:6 pg. 116). This result is in agreement with work by Magnesson et al which demonstrated reduced concentrations of larger diameter fibrils in ruptured Achilles tendons [329]. The results presented here also appear to support the suggestion of other studies that partial tears affect the loading environment of the rotator cuff [321, 322]. Specifically, the reduced fibril diameter and alignment indicate that the damaged tendons are adapting to compressive and/or shear loading (see Chapter 4, Sections 4.2.2 and 4.2.3). These adaptations are likely to have important implications for the mechanical integrity of the damaged tissue, especially if they accompanied by the compositional adaptations typically associated with the compressive loading in tendon [154, 156, 164]. Further work should now investigate the adaptations of torn rotator cuff tendons in response to tear progression to establish whether the adaptations indicated in this study are progressive with tear size.

6.4 Summary, Limitations and Further Work

The work in this chapter set out to determine the topographical variation in the structural adaptations of rotator cuff tendons in health and disease. The results demonstrate that healthy rotator cuff tendons exhibit a heterogeneous distribution of fibril diameters and fibrillar alignment with topology. Trends in this heterogeneity appear to reflect adaptations to the differential stress fields predicted by finite element models. However, comparison of these results with those for ovine rotator cuff tendons (see Chapter 4, Sections 4.2.2 and 4.2.3) provide evidence that the structural adaptations are limited due to the non-constant nature of the stress fields. Thus the work is this chapter has provided evidence to

support the hypothesis that healthy rotator cuff tendons exhibit structural adaptations, associated with the topographical variation in loading environment, that increase the susceptibility of the cuff tendons to tearing.

The results presented here also provide evidence that delamination of the supraspinatus tendon alters the topographical variation of structural adaptations of the tendon. Specifically, the cuff affected by delamination shows decreased fibril diameters and decreased fibril alignment compared with the macroscopically normal cuff tendons. These structural adaptations may be indicative of increased compressive stresses and shear loading and provide evidence to support the hypothesis that chronically torn rotator cuff tendons exhibit different structural adaptations compared with healthy tendons.

Two important limitations of this study must be acknowledged; sample number and sample age. Regarding sample number, power analysis based on previous studies indicated that at least five independent samples were required to distinguish differences of 1 standard deviation in tendon fibril diameter and 'D' spacing at $p<0.05$ statistical significance and 80% confidence level. However, the results presented in this chapter are based on only three macroscopically normal specimens - two of which were dependent samples - and one delaminated specimen. The mean values reported for these samples are therefore unlikely to represent statistical differences and only grant insight into trends in the data. A future study investigating whether the trends reported here hold true in a larger patient cohort would therefore be very interesting. Secondly, since the tissues used in this study came from patients over the age of 80, the material is likely to have reached senescence. This is likely to have significantly influenced the properties of the tissue, although it is not known to what extent. Further work is now needed to establish the effect of maturation and biological aging on the structural adaptations of tendon tissues, specifically rotator cuff tendons.

Regardless of these limitations, the findings of this study have important implications for future practice. Firstly, since the cuff tendons are not homogeneous, they should not be treated as such during surgical repair. Secondly, since delamination of the cuff tendons reduces the heterogeneity of the structure, treatments and repairs should aim to re-establish heterogeneity within the tissue. This is likely to be especially important for the design of tissue engineering scaffolds; a tissue engineering scaffold that is

designed to resist shear and compressive stresses on the articular-side and significant differential strain profiles between the articular-side and bursa-side may well prove more successful than a scaffold that is designed purely for tensile strains. Finally, while animal studies have demonstrated that adaptations of tendon to different loading environments are reversible (Section 3.4.2) [158, 252, 330], this has only been shown in healthy tendon; the reversibility of adaptations associated with disease and tearing is not known. Future work should therefore investigate whether the reduced topographical heterogeneity of torn cuff tendons is reversible since, if it is not, this has serious implications for the time scale of surgical interventions.

Chapter Seven

Effect of Age and Tear Progression on Cuff Properties

7.1 MATERIALS AND METHODS

7.1.1 Sample Collection

To assess the effect of tear propagation on the material properties of rotator cuff tendons, biopsies were collected from the anterior edge of torn rotator cuff tendons during open surgical repairs. These samples were provided by the Oxford Musculoskeletal BioBank (Oxford Musculoskeletal Biomedical Research Unit, University of Oxford) and were collected as part of the UK Rotator Cuff Surgery Trial (UKUFF), a randomised trial in which patients with full thickness rotator cuff tears were randomly allocated to arthroscopic or open surgical repair over an 18 month period. The inclusion and exclusion criteria for this study are detailed in Table 7:1. Ethical approval for the use of this tissue as part of this research project was obtained from the Oxfordshire Research Ethics Committee C (Project number: 09/H0606/11, Project name: 'Changing mechanical properties of rotator cuff tears and their repairs').

Patients with rotator cuff tears were identified preoperatively using ultrasound. Intra-operatively, the size of the rotator cuff tear was measured as the widest diameter of the tear and classified as small (<1 cm), medium (1-3 cm), large (3-5 cm) or massive (>5cm), according to the commonly accepted classification by Post et al [283]. Five control biopsies were obtained from the subscapularis tendon of patients undergoing hemiarthroplasty of the shoulder when the tendons appeared macroscopically normal.

Table 7:1 Inclusion and Exclusion Criteria for UKUFF trial

Inclusion Criteria **ALL of the following must apply**
• Male or female • Over 50 years old • Degenerative rotator cuff tear • Full thickness rotator cuff tear • Diagnosed using MRI or ultrasound • Able to consent
Exclusion Criteria **NONE of the following may apply:**
• Previous surgery on affected shoulder • Dual shoulder pathology • History of rheumatoid arthritis / systemic disease • Significant osteoarthritis problems • Significant neck problems • Cognitive impairment / language issues

Table 7:2 Clinical Data For Samples Obtained from UKUFF Trial

Cohort	**Number of Patients**	**Mean Age (range)**	**Number of patients having had 1 or more previous steroid injections (%)**	**Gender (M:F)**
Control	5	74.6 (64 to 83)	Unknown	2:3
Small Tear	9	66.1 (58 to 78)	4, 1 unknown (≥44%)	6:3
Medium Tear	7	57.4 (51 to 67)	5, 1 unknown (≥71%)	3:4
Large Tear	6	63.7 (60 to 73)	3, 2 unknown (≥50%)	4:2
Massive Tear	11	69.0 (61 to 80)	5, 2 unknown (≥45%)	10 male 1 unknown

Samples collected as part of a serial biopsy study designed to assess the effects of common clinical treatment for rotator cuff disorders on tendon properties were collected from partially torn tendons pre-subacromial corticosteroid injection, and pre- subacromial decompression (SAD) surgery. These samples were provided by Dr. R. Murphy (Lord Nuffield Scholar in Orthopaedic Surgery, Nuffield Department of Orthopaedics, Rheumatology and Musculoskeletal Sciences, University of Oxford), and were collected as

part of an observational cohort study of participants undergoing treatment for rotator cuff pathology (See Chapter 9, Section 9.1.1), ethical approval for which was obtained from the Oxfordshire Research Ethics Committee B (Project Number: 09/H0605/111, Project title: 'Evaluation of the tissue effects of current therapies used in the treatment of rotator cuff pathology'). The inclusion and exclusion criteria for this study are detailed in Table 7:3. Using a core biopsy needle under ultrasound guidance, biopsies were collected from the mid portion of tendons containing partial tears. Control rotator cuff tendon biopsies were obtained from patients without a history of rotator cuff problems or subacromial corticosteroid injections, during anterior stabilisations of the shoulder where the tendons appeared macroscopically normal appearance.

Table 7:3 Inclusion and Exclusion Criteria for Patients recruited to Serial Biopsy Study

Inclusion Criteria **ALL of the following must apply:**
• Male or female • Between 35-65 years old • Diagnosed with subacromial impingement OR partial thickness rotator cuff tear • Referred to secondary care for management of rotator cuff pathology • Symptom duration greater than 3 months • Planning to have glucocorticoid injection or subacromial decompression surgery as a treatment intervention • Able to consent
Exclusion Criteria **NONE of the following may apply:**
• More than 3 previous glucocorticoid injections to the affected shoulder • Glucocorticoid injection to the affected shoulder within 6 weeks prior to intervention • History of significant trauma, surgery, osteoarthritis or other pathology of the affected shoulder unrelated to the rotator cuff • Allergy / hypersensitivity to lidocaine local anaesthetic • Meet the exclusion criteria for administration of SonoVue™ contrast agent • Any other factor that, could jeopardize the safe and ethical conduct of participant care, study operations or other research projects

Table 7:4 Clinical Data For Samples Obtained from Serial Biopsy Study

Cohort	Number of Participants	Mean Age (range)	Number of patients having had 1 or more previous Injections	Gender (M:F)
Control	16	23.3 (17 to 29)	0 (0%)	14:2
Glucocorticoid injection	11	51.5 (35 to 64)	6 (55%)	4:7
Subacromial decompression	14	49.1 (36 to 61)	9 (64%)	10:4

7.1.2 Sample Preparation

Post-collection, specimens were fixed in 10% formalin for at least 1 month prior being embedded in wax and cut into 10µm glass-mounted sections and either de-waxed or stained with picrosirius red following the procedures detailed in Chapter 4, Section 4.1.3.

7.1.3 Sample Characterisation

7.1.3.1 Atomic Force Microscopy

Atomic force microscopy (AFM) was employed to characterise the ultrastructure of the extracellular matrix in each sample. Dewaxed sections were imaged using an AFM in non-contact mode following the experimental and analysis procedures detailed in Chapter 4, Section 4.1.4.4. In addition to characterising the diameter and 'D' spacing of up to ten fibrils in each image, the mean angle between each fibril was characterised as detailed previously (Chapter 6, Section 6.1.3.1 above)

7.1.3.2 Polarised Light Microscopy

Picrosirius red-stained samples were imaged and analysed for red to orange pixel ratio and crimp length using polarised light microscopy as detailed in Chapter 4, Section 4.1.4.2.

7.1.3.3 Raman Spectroscopy

Post-AFM analysis, Raman spectra were collected from dewaxed sections using a LabRAM Aramis Raman spectrometer equipped with a confocal microscope (Horiba, Kyoto, Japan) following the experimental procedure outlined in Chapter 4, Section 4.1.4.3. To aid with peak identification spectra were collected for paraffin wax, chondroitin sulphate A from bovine trachea (Sigma Aldrich, Dorset, UK), and type I

collagen from bovine Achilles tendon (Sigma Aldrich, Dorset, UK) using the same experimental conditions. Where necessary, samples were photobleached* for up to 2 hours prior to spectrum collection [331, 332].

7.1.4 Statistical Analysis

Where data is presented as box plots the box ends represent 25th and 75th percentiles, while the whisker ends represent the 5th and 95th percentiles respectively, with crosses indicating outliers. In cases were data is tabulated, it is presented as mean values ± standard deviation unless otherwise indicated. In all cases, mean values represent the mean value of the individual sample means to avoid giving undue weight to samples for which more measurements were possible [327]. Statistical significance was evaluated using one-way analysis of variance (ANOVA) and Tukey's multiple comparison test performed in Origin data analysis. A significance level of $p<0.05$ was considered statistically significant, and statistical significance is indicated using the standard asterisk notation, where * indicates $p<0.05$, ** indicates $p<0.01$, and *** indicates p: 0.001. Where relevant, linear regression analysis was performed on the data using 'R' Biostats with and without the inclusion of confounding factors.

7.2 RESULTS

7.2.1 Fibril Diameter

Figure 7:1 presents box plots of the distribution of fibril diameters for control samples from different aged normal populations. Fibril diameter is significantly larger in normal samples from older patients (>63 years) compared with younger patients (<30 years). Figure 7:2 presents box plots of the mean fibril diameter for samples obtained from the edge of different sized tears. Despite samples from small, large and massive tears exhibiting a significantly smaller fibril diameter compared with both normal (>63 years) samples and partial torn samples pre-injection (Figure 7:2), the trend for decreasing fibril diameter with increasing tear size is not significant (β= -0.317, R=-0.017, p=0.86). However, when age is included as a confounding variable, a significant model emerges in which fibril diameter decreases with tear size and increases with age ($\beta_{tear\ size}$ = -3.328, β_{age} = 1.0861, $p=2.87\times10^{-4}$, R=0.23). Tear size and age are both significant predictors in this model ($p_{tear\ size}$ = 0.006, $p_{age} = 5.89\times10^{-5}$).

* In some cases it is necessary to 'photobleach' samples by exposing them to the laser for a period of time prior to signal acquisition in order to remove effects of sample fluorescence

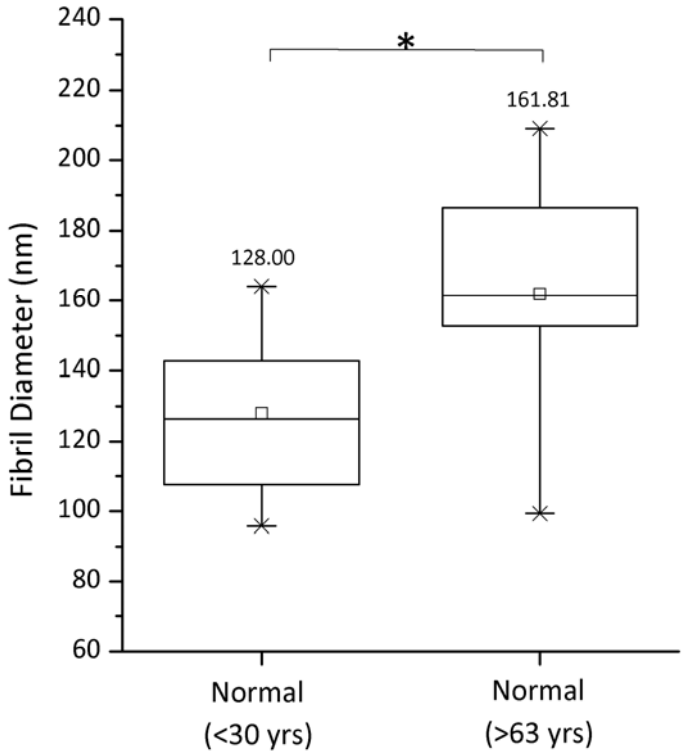

Figure 7:1 Box plots representing distribution of fibril diameter measurements for control samples from different aged normal populations. Fibrils are significantly thicker in older patients.

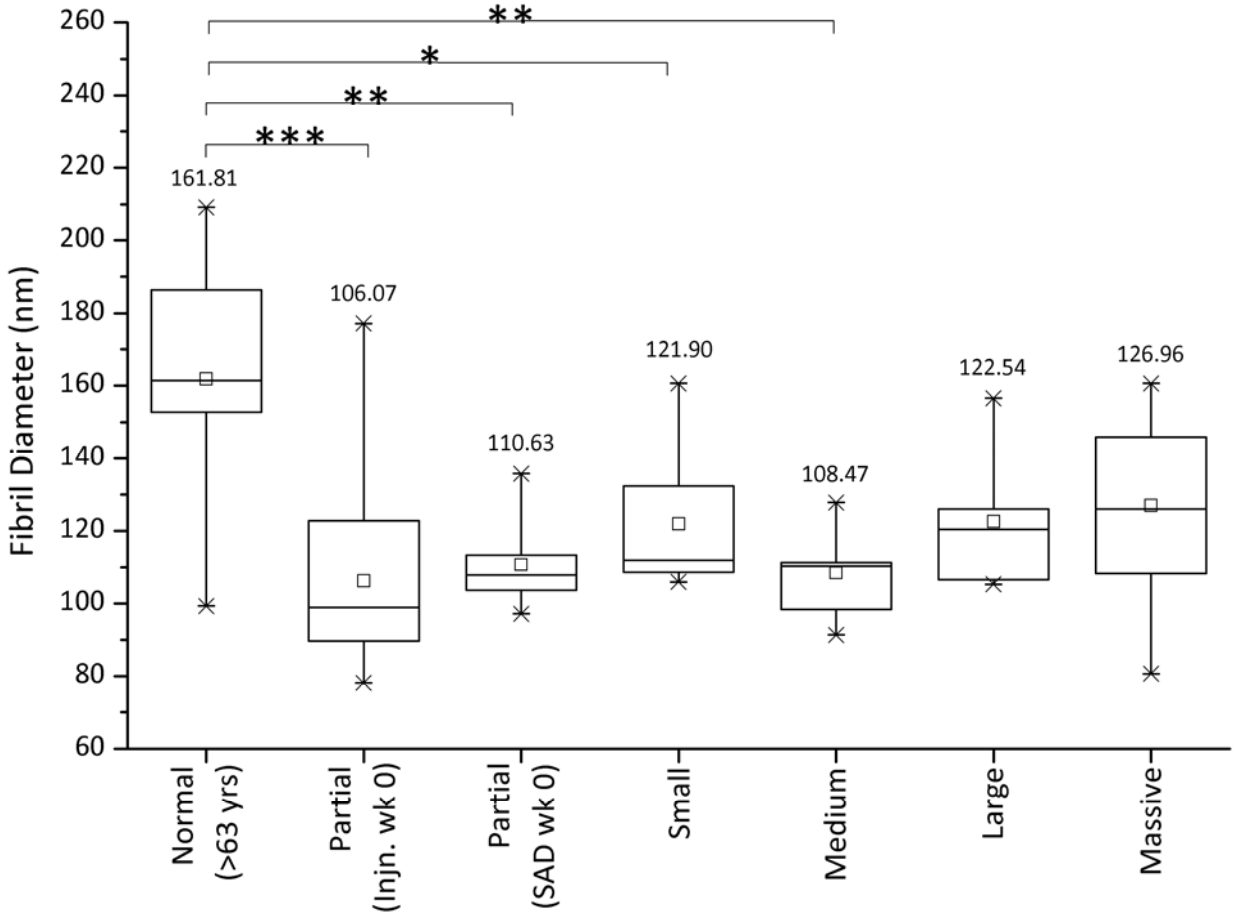

Figure 7:2 Box plots representing the distribution of collagen fibril diameter measurements for samples containing different tear sizes. Fibrils found in samples from small tears are and medium tears are significantly smaller than fibrils found in control subscapularis. Fibrils found in tendon containing large and massive tears are not significantly different to those found in control subscapularis tendon.

7.2.2 'D' Spacing

Figure 7:3 presents box plots of the distribution of 'D' spacing for control samples from different aged normal populations. There is no statistical difference between the 'D' spacing in control samples taken from older patients compared with younger patients (Figure 7:3). Figure 7:4 present box plots of 'D' spacing in samples taken from the edge of different sized tears. There is no significant trend for decreased 'D' spacing in torn samples (β= -0.125, R=-0.003, p=0.38) (Figure 7:4). When age is included as a confounding factor in this model, 'D' spacing decreases with tear size and increases with age although the model is not significant ($\beta_{tear\ size}$ = -0,230, β_{age} = 0.036, p=0.166, R=0.030). Neither tear size nor age are significant predictors in this model ($p_{tear\ size}$ = 0.135, p_{age} = 0.095).

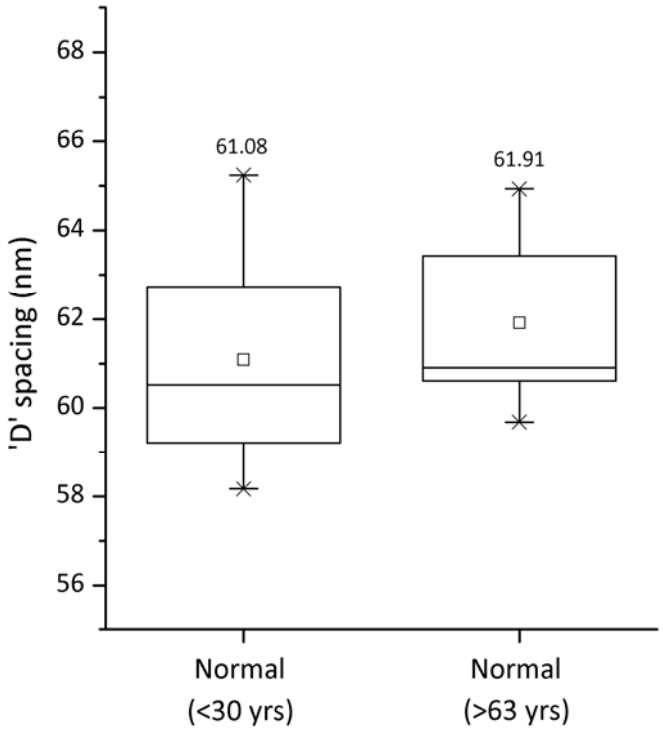

Figure 7:3 Box plots representing measurements of 'D' spacing for control samples from different aged normal populations. 'D' spacing is significantly larger in older patients.

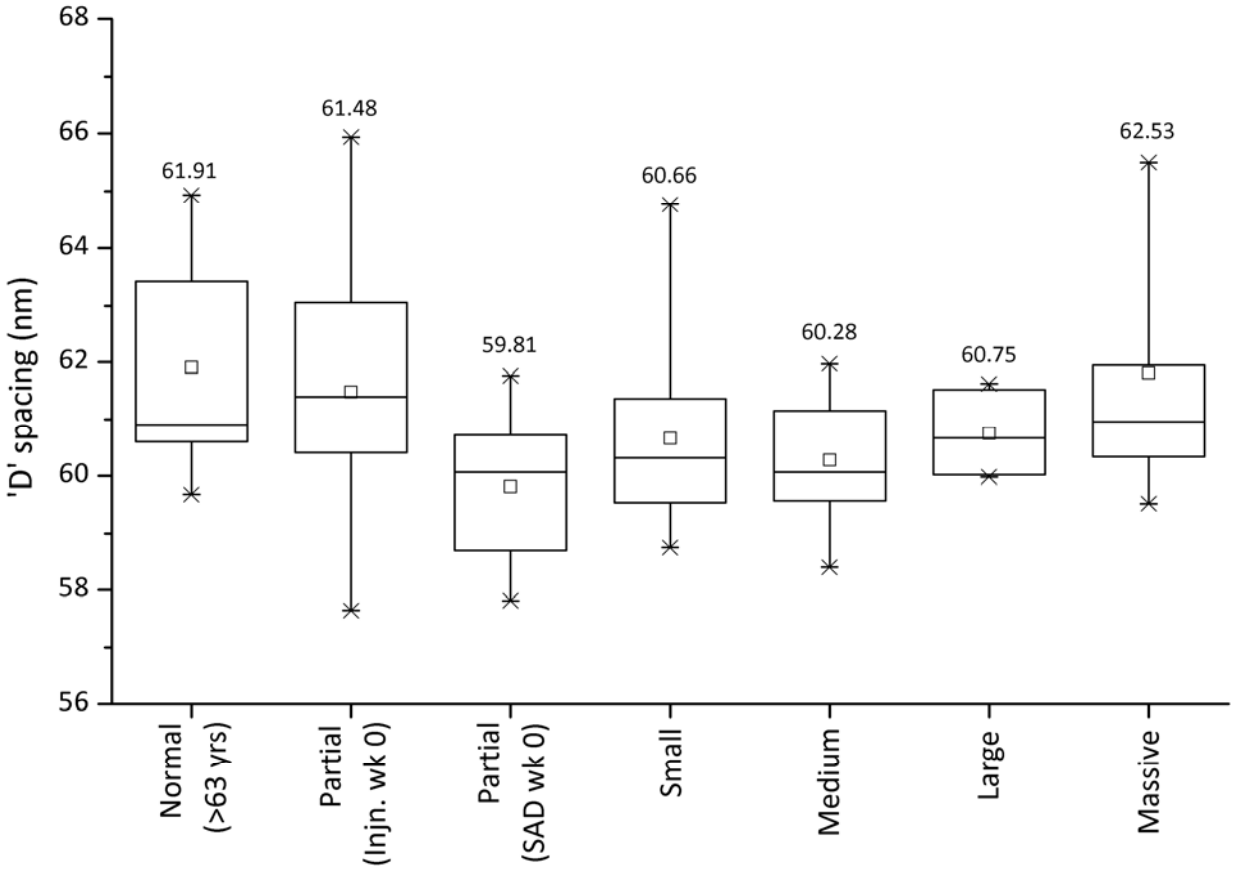

Figure 7:4 Box plots representing measurement of 'D' spacing for samples containing different tear sizes compared with normal (>63 years) samples. There is no statistical difference in 'D' spacing between the different tear sizes.

7.2.3 Fibril Alignment

Figure 7:5 presents box plots of the distribution of mean angle between fibrils for control samples taken from different aged populations. Mean angle between fibrils is higher with a narrower distribution in normal samples taken from older patients (>63 years) compared with younger patients (<30 years), although this difference is not significant. Figure 7:6 presents box plots of the average angle between the collagen fibrils for samples taken from the edge of different sized tears, and in partially torn samples pre- and post-treatment respectively. There are no significant differences in average angle between samples taken from different tear sizes (Figure 7:6), and no significant model for increasing inter-fibrillar angles as tear size increases (β= 0.629, R=0.03, p=0.089). The model remains insignificant when age is included as a confounding factor, ($\beta_{tear\ size}$ = 0.817, β_{age} = -0.074, p=0.108, R=0.04), although tear size is a significant predictor in the model ($p_{tear\ size}$ = 0.041, p_{age} = 0.211).

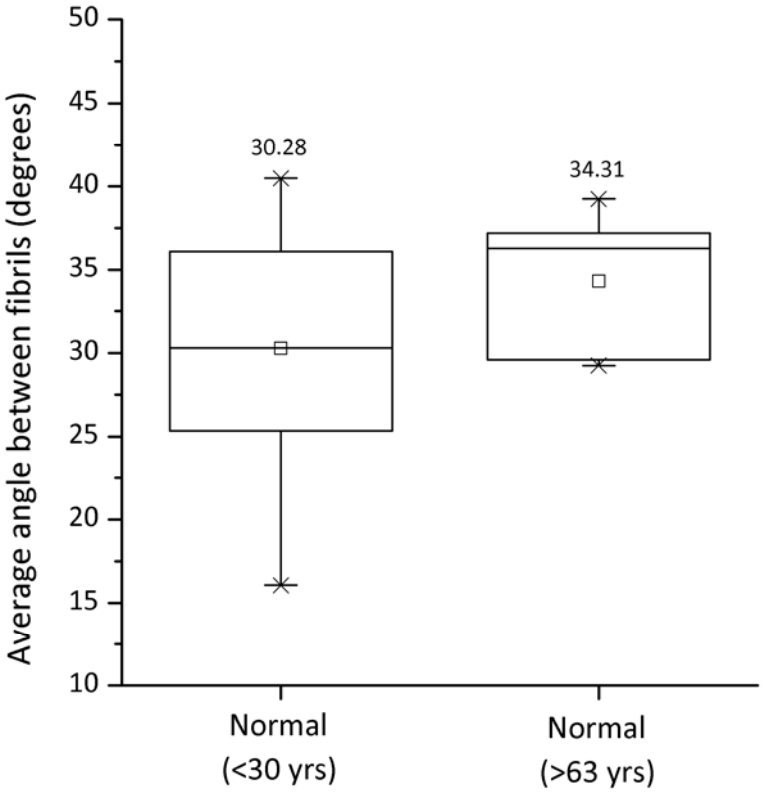

Figure 7:5 Box plots representing measurements of average angle between fibrils for control samples from different aged normal populations. The distribution of angles is narrower and the mean angle is higher for older samples, although there are no significant differences.

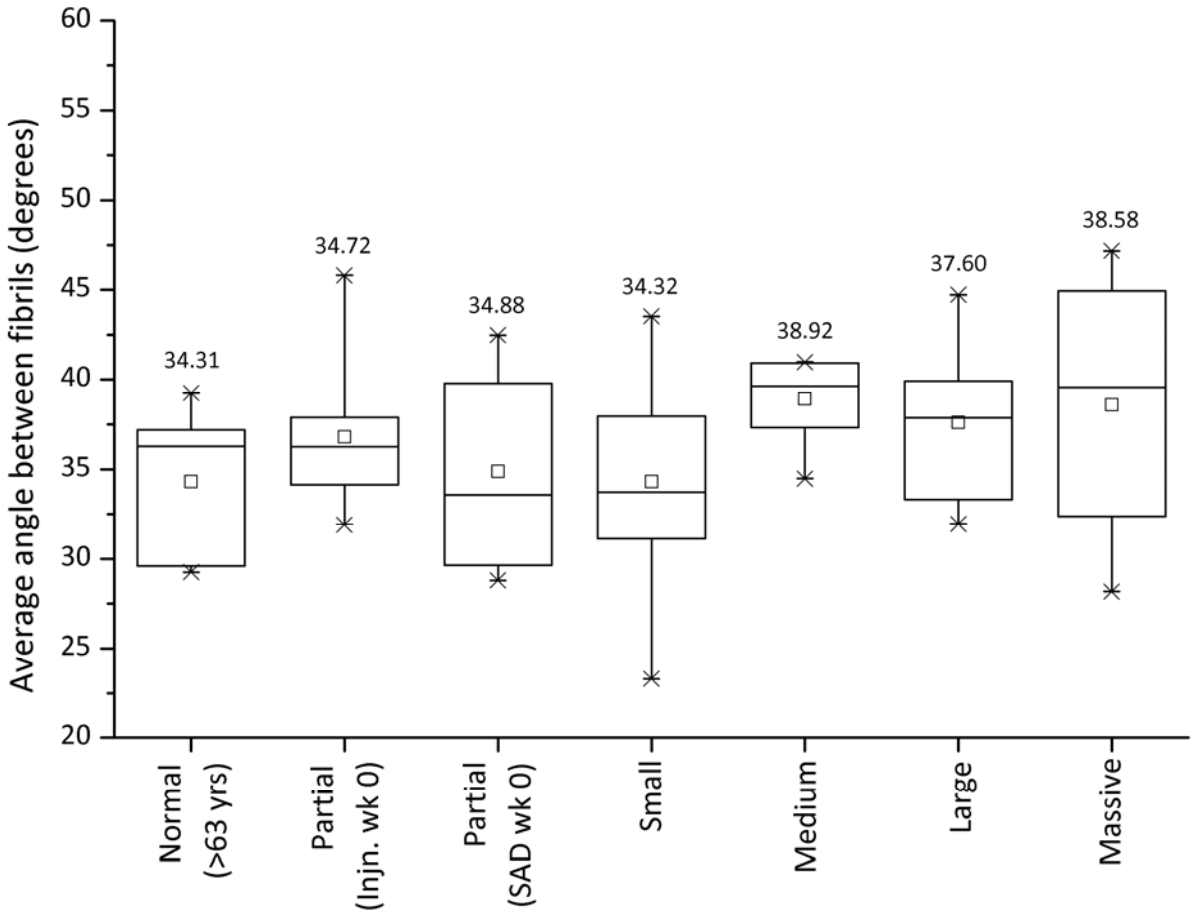

Figure 7:6 Box plots presenting measurements of average angle between fibrils in samples containing different tear sizes compared with normal (>63 years) samples. There is a trend for increased angle between fibrils as tear size increases although this is not significant.

7.2.4 Ratio of Red to orange fibres

Figure 7:7 present box plots of the mean ratio of red to orange fibres for picrosirius red-stained control samples from different aged normal populations. The ratio of red to orange fibres is significantly larger in normal samples taken from older patients compared with younger patients (Figure 7:7) Figure 7:8 present box plots of the mean ratio of red to orange fibres taken from the edge of different sized tears. The ratio of red to orange fibres does not change significantly as tear size increases (β= -0.147, R=0.01, p=0.255), although samples from small and massive tears exhibit a significantly smaller ratio compared with normal (>63 years) samples (Figure 7:8). When age is included as a confounding factor in this model, the ratio of red to orange fibres decreases with tear size and age although the model is not significant ($\beta_{tear\ size}$ = -0.087, β_{age} = -0.021, p=0.294, R=0.01). Neither tear size nor age are significant predictors in this model ($p_{tear\ size}$ = 0.534, p_{age} = 0.284).

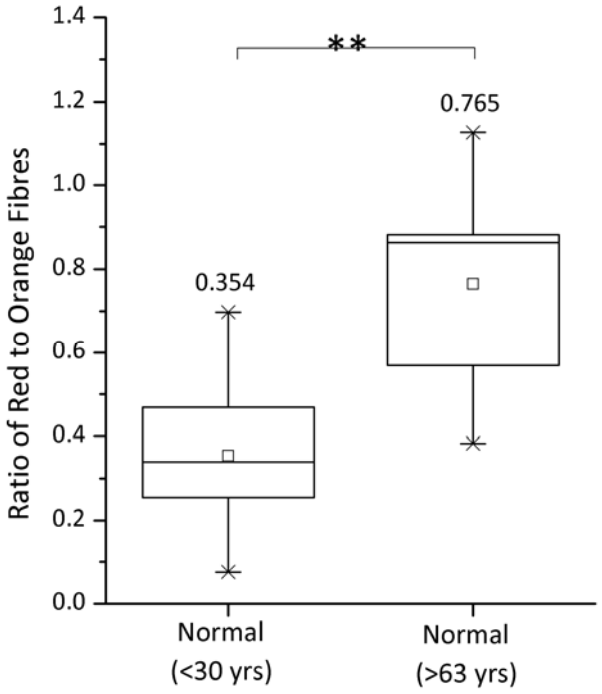

Figure 7:7 Box plots representing the ratio of red to orange fibres for picrosirius red-stained control samples from different aged normal populations. The ratio is significantly larger in sample taken from older patients.

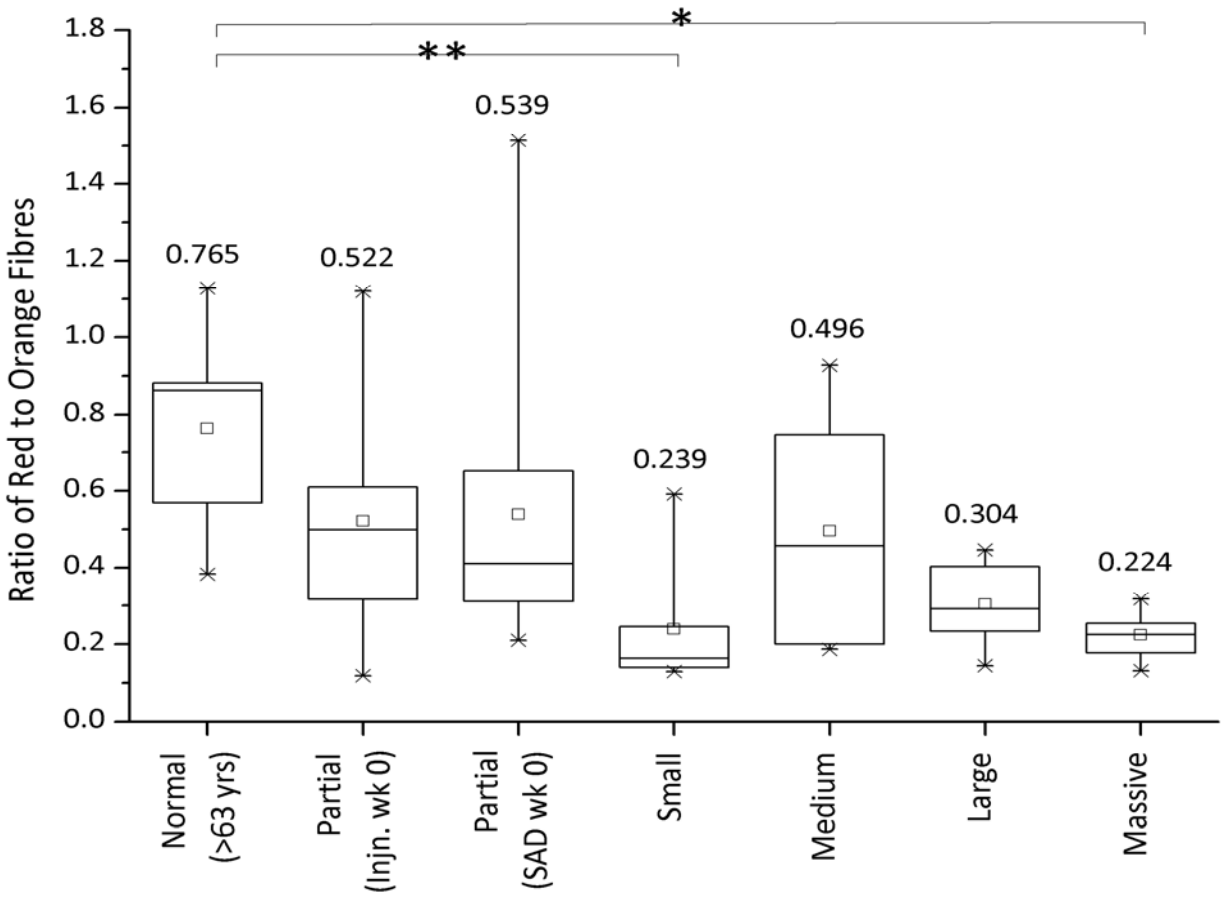

Figure 7:8 Box plots representing the ratio of red to orange fibres in picrosirius red-stained samples containing different tear sizes. The ratio is significantly smaller in sample taken from small tears and massive tears. Ratio decreases as tear size increases.

7.2.5 Crimp Length

Figure 7:9 present box plots of the mean crimp length in control samples from different aged normal populations. There is no significant different in the crimp length in older patients compared to younger patients. Figure 7:10 presents box plots of the crimp length measurements taken from the edge of different sized tears. Crimp length decreases significantly as tear size increases (β= -1.412, R=0.2566, $p=6.78\times10^{-5}$), with samples from small, large and massive tears exhibiting a significantly smaller crimp length than from normal (>63 years) samples, and partially torn samples pre-steroid injection (Figure 7:10). There is also a significant linear trend when age is included as a confounding variable ($\beta_{tear\ size}$ = -1.329, β_{age} = -0.028, $p=3.38\times10^{4}$, R=0.23), although age is not itself a significant predictor in the model ($p_{tear\ size} = 8.55\times10^{4}$, p_{age} = 0.61).

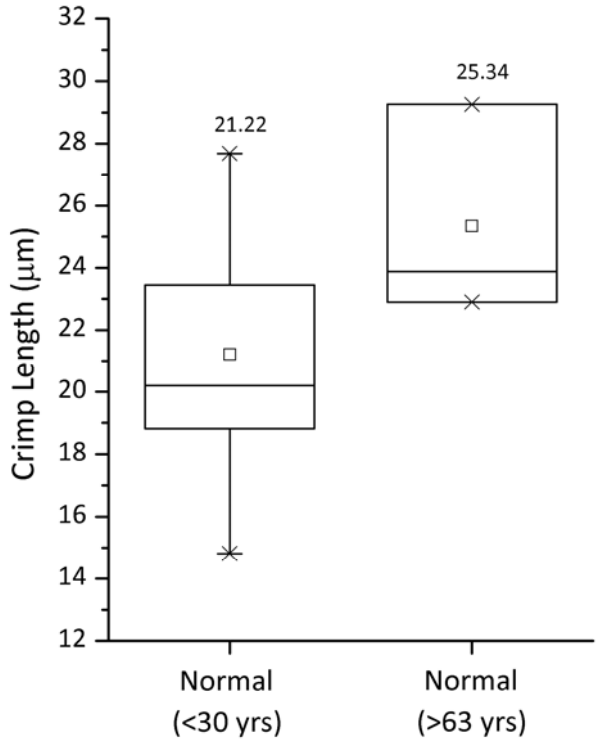

Figure 7:9 Box plots representing the distribution of crimp length measurements for different aged normal samples. Crimp length increases insignificantly with age.

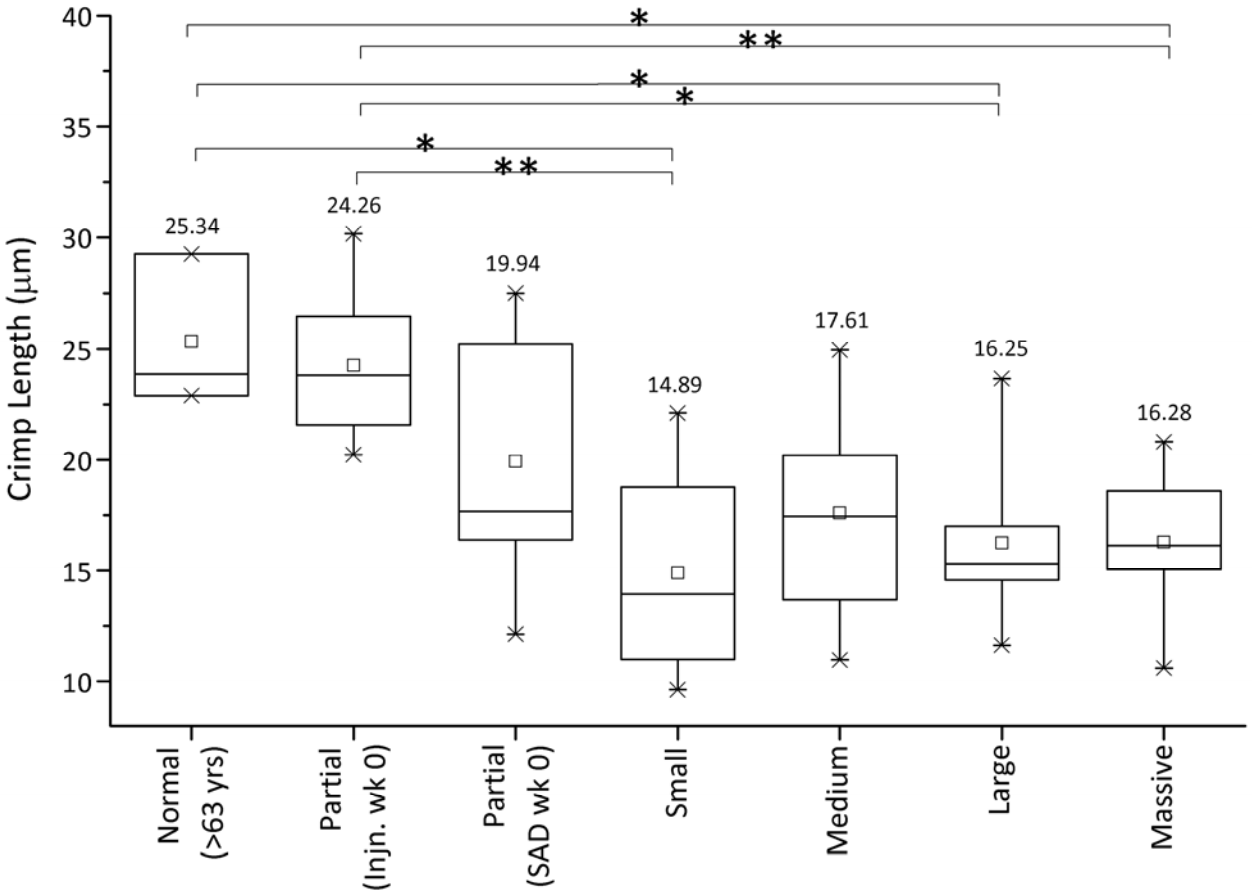

Figure 7:10 Box plots representing the distribution of crimp length measurements for samples containing different tear sizes compared with normal (>63 years) samples. Crimp length decreases as tear size increases, although there is no difference between partially torn samples and normal samples. With the exception of medium tears, full thickness tears exhibit a significantly smaller crimp length than control samples and week 0 Injection samples.

7.2.6 Compositional Characterisation

Figure 7:11 shows the average Raman spectra of the extracellular matrix for samples taken from the edge of different sized tears compared with normal (>63 years) samples. The Raman spectra of paraffin wax, chondroitin sulphate A from bovine trachea and type I collagen from bovine Achilles tendon are also shown. The Raman spectra from tendon samples contain sharp peaks at 998.1cm^{-1}, 1060.1cm^{-1}, 1131.3cm^{-1}, 1293.8cm^{-1}, and 1416.1cm^{-1} indicating the presence of wax contamination.

Peak fitting was performed on the individual spectra using a custom code in MatLab (Mathworks, Cambridge, UK), in order to assess the effect of tear size on their intensities. Peaks for analysis were chosen by examination of the spectra for type I collagen and chondroitin sulphate A characteristic Raman peaks. Peaks that decreased significantly when tendon was treated with chondroitinase ABC were also characterised (Chapter 4, Section 4.2.1.3). The peaks that were analysed are labelled in Figure 7:11.

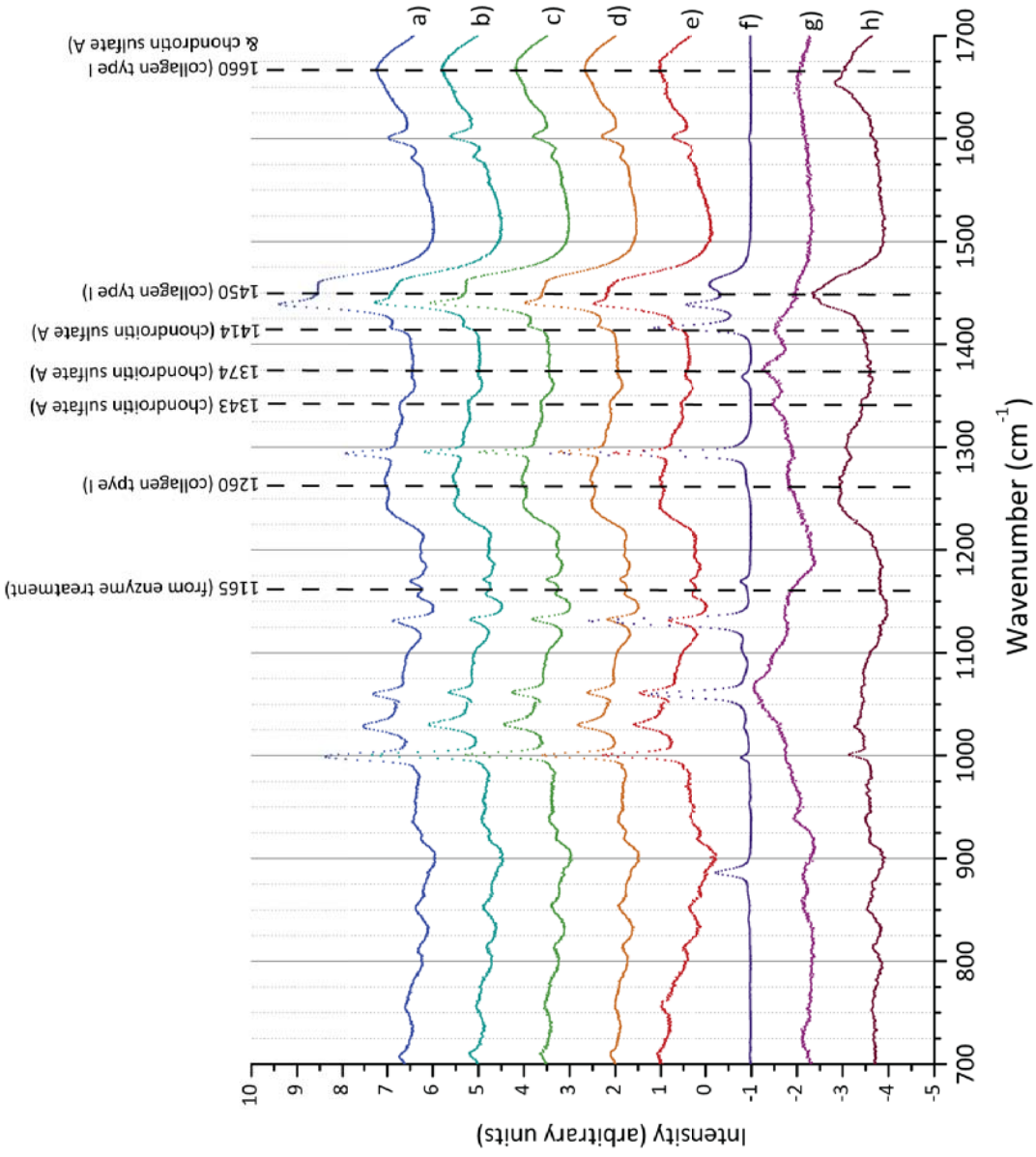

Figure 7:11 Average Raman spectra for biopsies taken from a) massive tears, b) large tears, c) medium tears, d) small tears, and e) normal (>63 years) samples, and representative Raman spectra of f) paraffin wax, g) chondroitin sulphate A, and h) collagen type I. The positions of the peaks selected for analysis are indicated by black dashed lines. There are no visible differences between the tendon samples by eye, although wax contamination of the tendon spectra is clearly visible.

Box plots representing the results of the peak analyses for different tear sizes are presented in Figure 7:12 and Figure 7:13. Descriptive statistics for the linear regression models fitted to the data presented are presented in Table 7:5. The intensities of the amide peaks associated with collagen type I (Amide III: 1260 cm^{-1}, Amide II: 1450 cm^{-1}, Amide I: 1660 cm^{-1} [190, 192]) increase significantly with tear size (Figure 7:12, Table 7:5). Additionally, the amide I peak intensity (1660 cm^{-1}) is significantly higher in massive tears compared with small tears, the Amide II peak intensity (1450 cm^{-1}) is significantly higher in large and massive tears compared with normal samples, and the Amide III peak intensity (1260 cm^{-1}) is significantly higher in medium tears compared with normal samples. The intensities of the peaks at 1374cm^{-1}, 1414cm^{-1} and 1660cm^{-1} associated with chondroitin sulphate, and at 1165cm^{-1} reduced by treatment with chondroitinase ABC (Chapter 4, Section 4.2.1.3), also increase significantly with tear size. The intensity of the chondroitin sulphate peak at 1343 cm^{-1} does not increase significantly with tear size, but is significantly higher for the large and massive samples compared with the normal and small samples.

Table 7:5 Statistics Describing Linear Regression Models of Changing Peak Intensity With Tear Size

Peak Position (cm^{-1})	β	R	p	Significant?	Identified from
1165	0.021	0.112	$4.56x10^{5}$	Yes, increases	Enzyme treatment
1260	0.046	0.133	$8.85x10^{6}$	Yes, increases	Collagen type I
1343	0.013	0.021	0.051	No	Chondroitin sulphate
1374	0.046	0.130	$1.09x10^{-5}$	Yes, increases	Chondroitin sulphate
1414	0.048	0.082	$4.61x10^{-4}$	Yes, increases	Chondroitin sulphate
1450	0.011	0.026	0.035	Yes, increases	Collagen type I
1660	0.121	0.073	$9.58x10^{-4}$	Yes, increases	Collagen type I AND Chondroitin sulphate

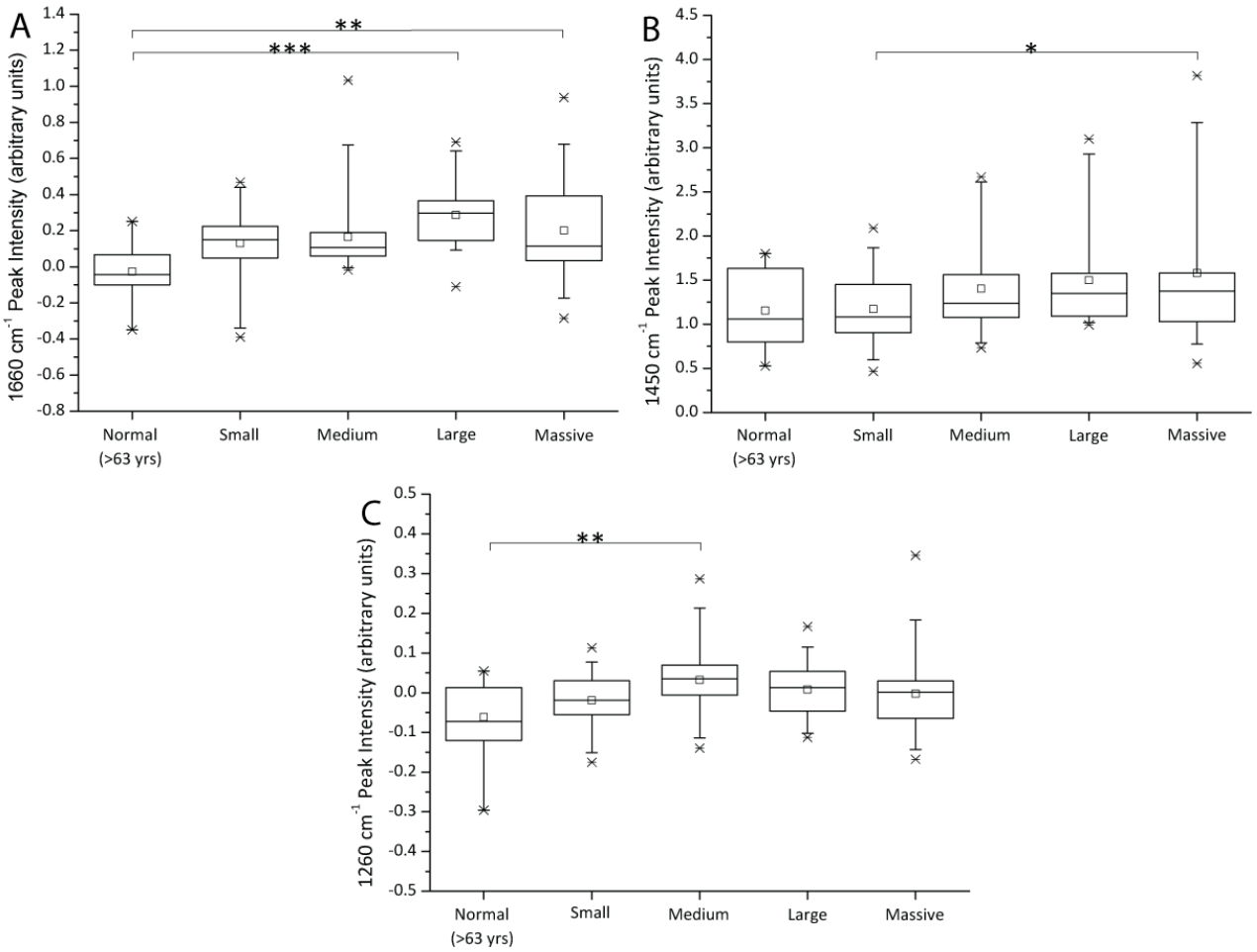

Figure 7:12 Box plots representing changing intensity of Raman peaks at 1160cm^{-1} (A), 1450cm^{-1} (B) and 1260cm^{-1} (C) associated with collagen's Amide I, II and III peaks respectively, in samples containing different tear sizes. Amide I peak intensity is significantly higher in massive tears compared with small tears, Amide II peak intensity if significantly higher in large and massive tears compared with normal samples, and Amide III peak intensity is significantly higher in medium tears compared with normal samples.

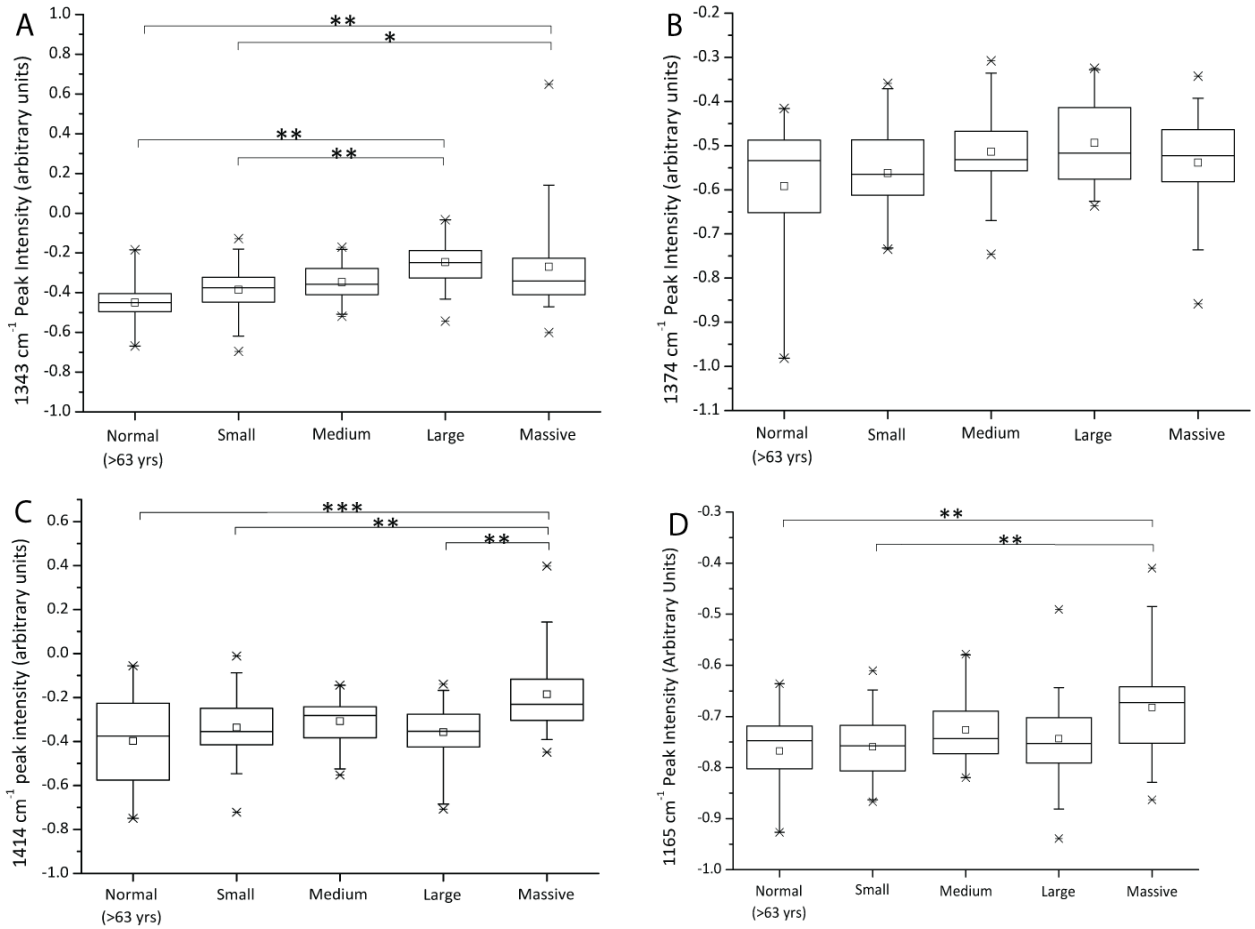

Figure 7:13 Box plots representing changing intensity of Raman peaks at 1343cm^{-1} (A), 1374cm^{-1} (B) and 1414cm^{-1} (C), associated with chondroitin sulphate, and 1165cm^{-1} (D), associated with chondroitinase ABC treatment, in samples containing different tear sizes. There is no significant change in the intensity of the peak at 1374cm^{-1}. The intensity of the 1343cm^{-1} is significantly higher in the large and massive samples compared with the normal and small samples. The intensity of the peak at 1414cm^{-1} is significantly higher in massive samples compared with normal, small and large samples. The intensity of the peak at 1165cm^{-1} is significantly higher in samples from massive tears compared with normal samples and samples from small tears.

Table 7:6 shows statistical data describing the changing Raman peak intensity ratios, for peaks whose intensities were found to change with tear size. The 1260:1450 peak intensity ratio increases significantly as tear size increases. Additionally, the 1260:1165, 1450:1165 and 1660:1165 peak intensity ratios decrease significantly as tear size increases. None of the other peak intensity ratios change significantly with tear size.

Table 7:6 Peak Intensity Ratios For Different Tear Sizes

	Normal (>63 yrs)	Small	Medium	Large	Massive	Linear Regression Equation	Significant?
1260:1450	-0.067 ±0.087	-0.022 ±0.056	0.005** ±0.058	0.008** ±0.047	-0.004** ±0.062	β = 0.011 R = 0.042 p = 0.010	Yes, decreases
1260:1660	0.046 ±0.710	-0.037 ±0.742	0.234 ±0.619	-0.047 ±0.313	0.091 ±0.790	β = -0.077 R = -0.001 p = 0.369	No
1450:1660	-2.832 ±14.966	4.556 ±9.168	10.159** ±5.329	6.258 ±3.337	6.346* ±13.749	β = -1.522 R = -0.004 p = 0.488	No
1260:1165	0.076 ±0.109	0.023 ±0.084	-0.046* ±0.126	-0.018 ±0.110	-0.001 ±0.145	β = -0.015 R = 0.024 p = 0.042	Yes, decreases
1260:1343	0.130 ±0.202	0.023 ±0.171	-0.119 ±0.259	0.028 ±0.562	0.037 ±0.303	β = 0.088 R = -0.003 p = 0.421	No
1260:1414	0.103 ±0.191	0.023 ±0.206	-0.071 ±0.237	-0.020 ±0.196	0.028 ±0.962	β = 0.003 R = -0.008 p = 0.950	No
1450:1165	-1.526 ±0.631	-1.572 ±0.587	-1.847 ±0.645	-1.889 ±0.641	-2.262* ±1.327	β = -0.257 R = 0.098 p = 1.40×10^{-4}	Yes, decreases
1450:1343	-2.510 ±1.032	-3.400 ±2.027	-4.158 ±1.929	-5.964* ±3.885	-2.971 ±4.773	β = 3.682 R = 0.002 p = 0.265	No
1450:1414	-2.571 ±1.815	-3.996 ±2.704	-4.874 ±2.567	-4.191 ±2.320	-4.870 ±11.979	β = -0.504 R = -0.006 p = 0.663	No
1660:1165	0.030 ±0.186	-0.182 ±0.254	-0.169 ±0.131	-0.391*** ±0.266	-0.326** ±0.462	β = -0.078 R = 0.096 p = 1.59×10^{-4}	Yes, decreases
1660:1343	0.047 ±0.320	-0.411 ±0.520	-0.394 ±0.336	-1.659*** ±2.247	-0.265 ±1.557	β = -0.111 R = 0.003 p = 0.427	No
1660:1414	-0.069 ±0.587	-0.571 ±0.739	-0.470 ±0.451	-0.735 ±0.541	-0.671 ±2.310	β = -0.227 R = 0.002 p = 0.275	No

7.3 DISCUSSION

7.3.1 Effect of Age

Aging has a significant influence on the structure and composition of tendon; as Silver et al note, 'in general, the type I collagen content of ECMs increases with age, whereas the type III collagen content is decreased. The PG content also appears to decrease with age.' [333]. The tensile stiffness and strength of mature tendon are also reportedly much greater than those of younger tissues [231]. The increased fibril diameter (indicative of greater tensile loading) (Figure 7:1 pg. 130) and increased crimp length (indicative of decreased GAG content) (Figure 7:9 pg. 136) reported for samples from older patients are therefore in agreement with previous studies. Additionally, the decreased proportion of thinner fibres (indicated by the larger red to orange fibre ratio found for picrosirius red-stained samples) (Figure 7:7 pg. 134) in older patients may indicate a lower proportion of collagen type III content [197], and is thus also in agreement with the statement by Silver et al above.

These adaptations with age are likely to be beneficial in purely tensile tendons, with increased fibril diameter and decreased PG and collagen type III content with age giving beneficial increases in tensile stiffness and strength. However, in tendons like the supraspinatus tendon that also experience significant compressive and shear loading, increased fibril diameter and decreased proteoglycan concentration with age may be deleterious, decreasing the suitability of the tendon to its mechanical environment, and thus increasing its susceptibility to damage.

Changes in the collagen profile may have even more significant implications. Decreased collagen type III content in aging supraspinatus tendons may be indicative of decreased capacity for remodelling of the tendon with increased patient age and may be associated with a post-maturation senescence point. Whilst this would contradict the findings of a study by Bank et al [334] which estimated that more than 50% of the total collagen in macroscopically normal supraspinatus tendons from older patients had been newly synthesised, such a decrease in capacity for healing in a tendon which experiences a complicated loading environment could explain the increased prevalence of tears and poorer surgical results in older patients. Since the work presented here has only inferred a change in collagen type III content with age using structural methods (Figure 7:7 pg. 134), further work is now needed to establish the effect of age on

the collagen profile (ratio of collagen type I to type III) of the supraspinatus tendon in a more accurate manner, for example through consideration of gene expression.

7.3.2 Torn Rotator Cuff Tendons

Finite element analyses have indicated that partially torn rotator cuff tendons are subjected to increased levels of compressive stresses [33], while biomechanical studies have shown that partially- and fully- torn tendons experience high levels of strain in the remaining, intact tissue [299, 335]. Furthermore, biological studies have demonstrated that torn rotator cuff tendons exhibit biochemical and cellular changes, such as altered concentrations of PGs and GAGs (mucoid degeneration) and increasing concentrations of rounded profile cells (thought to be chondrocytes), both of which could be indicative of adaptations to compressive and/or shear loading.

In Chapter 4 it was shown that the collagenous architecture of tendon is highly sensitive to the strain fields it experiences (Chapter 4, Sections 4.2.2 and 4.2.3). Specifically, compressive and shear strains were shown to produce a collagen architecture with thinner fibres (Figure 4:14 pg. 47, and Figure 4:15 pg. 47), a shorter crimp length (Figure 4:18 pg. 49, and Figure 4:19 pg. 50), thinner fibrils (Figure 4:26 pg. 57, and Figure 4:27 pg. 58), and less fibrillar alignment (Figure 4:18 pg. 49, and Figure 4:19 pg. 50) compared with tensile strains alone. The presence of compressive and shear strains in torn cuff tendons might therefore be expected to produce similar adaptations. However, the structural adaptations of partially and fully torn rotator cuff tendons have not previously been characterised. This is therefore the first study to evaluate the structural dimensions of the collagen architecture of torn cuff tendons in order to gain insight into the mechanical environment experienced by these tendons.

The results of this study provide evidence that torn rotator cuff tendons show significant structural adaptations that are indicative of the presence of compressive and shear strains, and that these adaptations are evident early in the tear progression; in agreement with the cadaveric rotator cuff results presented earlier in this thesis (Chapter 6, Section 6.3.2), the samples obtained from partially torn tendons pre-steroid injection and pre-SAD surgery and from small tears exhibit significantly thinner fibrils compared with control tendons (Figure 7:2 pg. 130). These samples also exhibit a higher proportion of thinner fibres (Figure 7:8 pg. 135) and shorter crimp length (Figure 7:10 pg. 136) compared with control

samples. Although the changes in fibre diameter and crimp length are not significant, such findings are in agreement with studies of other ruptured tendons [212, 329, 336-339].

The results indicate that not all of the structural adaptations seen in torn tendons are progressive with tear size. While there is a significant trend for decreasing crimp length with increasing tear size (Figure 7:10 pg. 136), there are no significant trends between tear size and the proportion of thinner fibres (indicated by smaller ratio of red to orange fibres) (Figure 7:8 pg. 135), fibril alignment (indicated by larger angle between fibrils) (Figure 7:6 pg. 133) or fibril diameter (Figure 7:2 pg. 130) when a single variable linear regression model is considered. However, when patient age is included as a confounding factor in the linear regression model, a significant trend for decreasing fibril diameter with increasing tear size is revealed. The importance of age as a cofounding variable in fibril diameter further emphasises the importance of age in structural adaptation of tendon, as revealed by comparison of control samples from different aged patient cohorts (Section 7.3.1).

7.3.3 Compositional Changes

Considering the inter-dependence of structure and composition in biological materials, the presence (or absence) of progressive changes in the structural features with tear size discussed above (Section 7.3.2) has important implications for the compositional adaptations of torn tendons. For example, given that crimp length is significantly longer in chondroitinase ABC-treated samples compared with untreated samples (see Section 4.3.3), the trend for decreasing crimp length with increasing tear size reported here (Figure 7:10 pg. 136) also suggest a progressive increase in inter-fibre and inter-fascicle GAG content with tear size, a finding supported by previous histological studies in other ruptured tendons [28, 340]. Conversely, the lack of a significant trend between proportion of thinner fibres and tear size (Figure 7:8 pg. 135) suggests that any potential increase in collagen type III in torn samples is not progressive with tear size. Again, this is in agreement with other studies [316, 336].

The progressive decrease in fibril diameter with tear size (when age is included as a confounding factor) (Figure 7:2 pg. 130) may also have important compositional implications. As has already been discussed (Chapter 3, Section 3.4), the small leucine-rich proteoglycans (SLRPs) decorin and biglycan play a key role in regulating the ultrastructural organisation of tendon during fibrillogenesis, regulating fibril thickness and alignment. The progressive decrease in fibril diameter with increasing tear size may therefore indicate progressive changes in the intra- and inter-fibrillar concentrations of these PGs. However, while previous histological, immunohistochemical and biochemical studies of bulk tendon samples have demonstrated that torn cuff tendons exhibit decreased concentrations of decorin and higher chondroitin sulphate A to dermatan sulphate ratios [36, 323], the effect of tears on the intra- and inter-fibrillar concentrations of PGs and GAGs has not specifically been reported.

Decorin and biglycan consist of a protein core to which is attached either one or two chondroitin sulphate A / dermatan sulphate (aka chondroitin sulphate B) chains respectively. Consequently, changes in the concentrations of the SLRPS can be inferred from changes in the concentration of chondroitin sulphate. However, since chondroitin sulphate is also a major component of aggrecan, a large proteoglycan present between the fibres and fascicles of the tendon, it is necessary to use a characterisation technique capable of excluding the aggrecan signal from the analyses. In the present study, a Raman spectrometer with an inbuilt confocal microscope was used. This allowed the laser to focussed to a to a spot size of 590nm which, in contrast to previous studies, allowed spectral analysis of the remaining intact collagenous matrix only, thus excluding any changes in chondroitin sulphate peak intensities due to aggrecan content or any other inter-fibre or inter-fascicle PG or GAG.

The increasing intensities of the Raman peaks associated with chondroitin sulphate A ($1343cm^{-1}$, $1374cm^{-1}$, $1414cm^{-1}$) and the Raman peak decreased by chondroitinase ABC treatment ($1165cm^{-1}$) in torn supraspinatus tendons (Figure 7:13 pg. 141) suggest that the amount of chondroitin sulphate is increasing in torn samples. However, because the intensities of the peaks associated with collagen also increase with tear size (Figure 7:12 pg. 140) it is necessary to compare the ratio of the collagen to chondroitin sulphate peaks (peak intensity ratios) in order to assess changes in the composition ratios. In agreement with the study by Chaudhury et al [341], comparison of the peak intensity ratios (Table 7:6 pg. 142)

suggests that the amount of collagen to chondroitin sulphate A does not change as tear size increases. On the other hand, the significant decrease in the ratio of the amide peaks to the peak at 1165cm^{-1} (the peak which may indicate the presence of dermatan sulphate (Chapter 4, Section 4.3.3)) might indicate that, in agreement with previous studies [36, 323], tearing of the supraspinatus tendon is associated with a change in the ratio of intra- and inter-fibrillar chondroitin sulphate A to dermatan sulphate. Further analysis is now required to assess whether this change does indeed imply a decrease in the amount of dermatan sulphate, and whether this is related to changes in the intra- and inter-fibrillar PG profile. Such analyses could shed light on the mechanisms governing the ultrastructural adaptations on torn rotator cuff tendons.

7.3.4 Implications for Mechanical Integrity of Torn Tendons

The structural and compositional changes reported here for torn rotator cuff tendons (Section 7.3) are expected to have important implications for the mechanical integrity of the tissue. For instance, decreased crimp length may correspond to an increase the heel strain (the point that defines the end of the toe region on the stress-strain curve of the torn tendon (Section 3.3.1, and Figure 3:2 pg. 14)), thus increasing the in-built safety factor of the tendon. Such a structural adaptation in torn tendons could be highly beneficial, given the increased strain experienced by the remaining intact tissue surrounding the tear.

However, given the association between decreased crimp length and increased levels of ground substance (Figure 4:20 pg. 50, and Figure 4:39 pg. 70), known to be weak in tension, decreased crimp lengths may also be associated with deleterious decreases in the tensile strength and stiffness of the remaining tendon. Concurrently, if the reduction in fibril diameter is not counteracted by an increase in fibril density, the reduced fibrous content of the remaining tissue would give rise to further decreases in the tissue's stiffness and strength, while the changing intra-fibrillar GAG content indicated by the Raman results (Section 7.3.3) could lead to increased intra-fibrillar sliding, reducing the viscoelastic properties of the tendon. Since only one study has reported the changing mechanical properties of torn rotator cuff tendons [229], further work is now needed to establish the changing stiffness, strength and viscoelastic properties of torn rotator cuff tendons.

7.4 SUMMARY, LIMITATIONS AND FURTHER WORK

The work presented in this chapter has investigated the influence of age and tear progression on the material adaptations of rotator cuff tendons. The results suggest that aging is associated with significant structural adaptations of the rotator cuff tendons, in particular increased fibril diameter and increased proportion of thinner fibres. This provides evidence to support the hypothesis that age has a significant influence on the structural adaptations of the rotator cuff tendons.

The results also provide evidence to support the hypothesis that chronically torn rotator cuff tendons exhibit different structural adaptations compared with healthy tendons. Specifically, partial and small tendons tears exhibit structural adaptations indicative of increased compressive and shear loading, specifically decreased fibril diameter and alignment, decreased crimp length, and a higher proportion of thinner fibres compared with control samples. Importantly, these pathological adaptations appear to occur early in the disease progression and appear to be progressive with tear size; linear regression models indicate that fibril diameter and crimp length decrease significantly with tear size when age is included as a confounding factor, further highlighting the importance of age in determining the structural adaptations of tendons. Such decreasing dimensions with increasing tear size are likely to have significant implications for the mechanical integrity of the torn tissue. Further work should now aim to characterise the mechanical integrity of torn cuff tendons, as this will have important implications for the repair of rotator cuff tears.

These results have significant implications for the development of future diagnostic and treatment modalities. Specifically, they highlight the urgent clinical need for new pre-rupture diagnostic techniques for the detection of early pathological changes in the rotator cuff. They also emphasize the requirement for new early interventions strategies that restore the healthy mechanical environment of the cuff tendons and reverse early pathological adaptations in order to prevent catastrophic failure of the cuff tendons.

Several limitations to this study need to be acknowledged. Firstly, while at least five surgical samples were used per tear size, only one 10µm slice per sample was analysed using each technique. Furthermore, while the samples obtained as part of the UKUFF study were collected from the edge of the tear, the

samples obtained as part of the serial biopsy study were collected from the intact portion of the tendon. Given the importance of topology indicated by the cadaveric results (Chapter 6), this is likely to give rise to considerable variability within the data. Future studies should aim to analyse a greater number of histological sections from different locations within the biopsy sample to reduce the associated errors. Additionally, the design future studies should try to incorporate sophisticated sampling techniques, such as those used in the serial biopsy study, in order to more tightly control the topographical origin of the samples.

A further limitation that must be considered is the anatomical origin of the control samples. The normal samples obtained from the younger (<30 years) patient cohort were collected during shoulder stabilisations and are therefore supraspinatus in origin. However, the normal samples collected from the older (>63 years) patient cohort were collected during hemiarthroplasties and are thus subscapularis in origin. It is not uncommon for studies of torn supraspinatus tendons to use subscapularis as control material, as macroscopically normal supraspinatus tendons from older patients are largely unavailable. However, the lack of age-matched controls from the relevant tendon could have serious implications for the trends reported in this, and other, studies. Further work is now urgently needed to establish the relevance of using age-matched subscapularis tendons as control material.

Regardless of these limitations, the findings of this study have important implications for future practice. Firstly, as aging is associated with significant changes in the structural adaptations of the tendons, future studies must endeavour to use age-matched controls. Secondly, as a number of the pathological adaptations of torn tendons are progressive and seen early in the disease progression it may be advisable to reconsider intervention timescales and the affect any delays in treatment may have on the, possibly irreversible, condition of the torn tissue.

PART IV

TREATMENT OF ROTATOR CUFF TEARS

Chapter Eight

Background Literature: Current and Future Treatments

8.1 CURRENT TREATMENTS FOR ROTATOR CUFF DISEASE*

8.1.1 Conservative Treatment - Corticosteroid Injection

Initial treatment for rotator cuff tears usually consists of conservative management, such as subacromial corticosteroid injections. Corticosteroid treatment is a common treatment for musculoskeletal pain due to its efficacy for inflammation reduction and thus function improvement. However, since chronic degeneration of the rotator cuff is not strongly associated with inflammation, the rationale behind steroid treatment is unclear. It may be influenced by the fact that ibuprofen (a non-steroidal anti-inflammatory drug) has been shown to be beneficial for tendinopathies, probably due to its inhibition of aggrecan expression. However, of six non-steroidal anti-inflammatory drugs tested in a study by Fallon et al [342], ibuprofen was the only one which was not detrimental to tendon properties.

The effect of steroid treatment on tendon properties and rupture rates is unclear. A single steroid injection does not alter production ratio of collagen type I to type III of tendon tissue [343]. However, repeated use of steroidal injections is associated with tissue degeneration, necrosis and decreased cellular proliferation, decreased collagen output, and decreased mechanical properties [344-349]. Repeated pre-operative steroid injections are also reportedly associated with poor post-operative repair results [289]. While the effects of steroid injections on the structural properties of tendon are not known, these are also likely to be detrimentally affected.

* Sections 8.2 and 8.3 of this chapter are adapted for use from **Journal of Materials Science: Materials in Medicine 23**(3) p823-33 Tenocyte proliferation on collagen scaffolds protects against degradation and improves scaffold properties. Tilley, J.M.R., Chaudhury, S., Hakimi, O., Carr, A.J., Czernuszka, C.T. Copyright (2011). with kind permission from Springer Science and Business Media [DOI: 10.1007/s10856-011-4537-7]

8.1.2 Surgical Interventions

8.1.2.1 Subacromial Decompression Surgery

Should conservative measures fail, patients may be given subacromial decompression (SAD) surgery in order to reduce the impingement of the acromion on the supraspinatus tendon. SAD surgery has been reported to reduce pain and improved function [350-352], although one systematic review found no difference in pain and function over a 2.5 year period between patients who had undergone SAD surgery and those who had received physiotherapy [353]. As Dines et al note 'The best results [for SAD surgery] are in patients who have active elevation and control of the descent of the shoulder as well as gleno-humeral stability' [354]. To date, the effect of SAD surgery on the structural adaptations of torn rotator cuff tendons has not been investigated. However, considering its effectiveness in improving pain scores and function, it might be expected to reverse any structural adaptations associated with impingement, degeneration and tearing.

8.1.2.2 Rotator Cuff Repair Surgery

Rotator cuff repair surgery is the last resort for clinicians; while it has been shown to reduce pain and increase function, success rates varies widely, and are heavily dependent on the condition of the tissue being repaired [355]; symptom duration, tear size and patient age are all important determining factors [277, 295, 356-358]. The choice of repair method and material also play an important role.

Suturing (stitching back together) is possibly the commonest, simplest rotator cuff repair technique [359]. This technique involves looping stitches through the remaining tendon stump and then reattaching it to the bone. There are many variations of stitch and attachment method, with different surgeons having different preferred stitches and suture material based on experience and tear size [360-364]. However, suture pull-through and strangulation can present significant issues [29, 363, 365].

The use of a repair augmentation device has been found to significantly reduce the re-tear rate compared with sutures alone [282] because it fills the gap left by large tears, allowing improved transmission of the physiological loads [366]. Augmentation devices may also encourage faster tissue repair/regeneration, acting as a template for the deposition of new extracellular matrix (ECM). Various devices are available,

and fall into three main categories based on their constituent material: biomaterial patches, transplants (either cellular or decellularised) and tissue engineering scaffolds.

Biomaterial patches are generally biocompatible, *synthetic* materials, such as Gortex, Teflon or polyethylene [117, 361, 367-369], which seek to replace damaged or lost tissue with a permanent replacement material. Some success has been had in achieving tissue in-growth [370] with aligned fibrils [77, 371] and even a tissue crimp using this approach [347]. Nonetheless, synthetic materials present significant biocompatibility issues [372, 373] and often exhibit inadequate long-term mechanical performance [368, 369, 374-376].

Conversely, transplants offer a good match of mechanical, biomechanical and biological properties between replacement and original materials [377-379]. Donor material may come from the patient (commonly Latissimus dorsi or teres major in the case of rotator cuff repair [377, 380]) but in recent years de-cellularised ECM xenografts such as small intestinal sub mucosa (SIS) [381-386] and dermal matrix have become increasingly popular. These commercially available patches side-step tissue rejection issues and are thought to prevent scarring whilst reducing pain and improving function [384, 385, 387]. However, these patches do not appear to have reduced re-tear/graft detachment rates [384, 385, 388, 389], do not always offer improvement compared to non-augmented repairs [390], and do not solve donor availability issues. Patches are also costly. Tissue engineering is believed by many to offer the ultimate solution to these issues.

8.2 FUTURE TREATMENTS: TISSUE ENGINEERING SCAFFOLDS

In 1997, $450 million was spent on tissue engineering research [367]. This technique, which originated in the 1980s [391], aims to restore physical and physiological function, by implanting externally fabricated scaffolds in the place of damaged tissue. Upon implantation, these scaffolds are designed to degrade, releasing material components that 'contribute to the recruitment of host cells, and ultimately to site-specific tissue remodelling' [392] whilst concurrently acting as templates for the deposition of new ECM, thereby encouraging natural tissue regeneration in their place [393]. By guiding the natural repair process in this way, tissue engineering scaffolds reduce levels of scar tissue and improve a mechanical integrity of the repair [362, 365, 366].

Scaffold degradation and tissue deposition have a significant influence on the mechanical properties of the scaffold. As a scaffold degrades, its mechanical integrity decreases, reducing its stress-bearing capacity. Concurrently, as the cells penetrate the scaffold and lay down new tissue, the stress-bearing capacity of the repair is increased. To be successful, a tissue engineering repair must maintain sufficient mechanical integrity throughout scaffold degradation and ECM deposition. Knowledge of the effects of degradation and cellular proliferation on the mechanical response of the overall repair is of vital importance and must be well characterised prior to use [394-397].

The changing mechanical properties of scaffolds incubated in a variety of *in vivo* and *in vitro* environments have been well documented for a wide variety of scaffolds. In general, degradation and cellular in-growth are controlled by material and environmental parameters such as chemical composition, degree of crosslinking, porosity, culture medium composition and pH, and incubation temperature and atmosphere [396, 398-401]. The effect of cellular proliferation of scaffold properties has also been well documented. The decreasing mechanical properties of scaffolds incubated with scaffold-degrading cells, such as macrophages, *in vitro* is commonly reported, particularly as a means of comparing the degradation resistance of different scaffolds [402]. Studies have also demonstrated that ECM-depositing cells, such as fibroblasts, proliferate on scaffolds, adapting their structure and composition [403, 404]. However, despite mechanical characterisation being a standard technique for comparing the efficacy of various processing and crosslinking techniques [405-407], the mechanical behaviour of scaffolds in response to the proliferation of ECM-depositing cells is mostly unreported [408].

8.3 COLLAGEN SCAFFOLDS

Tissue engineering scaffolds have been fabricated from many materials. While degradable synthetic polymers like PGA/PLA offer improved mechanical properties compared with collagen scaffolds, such materials present biocompatibility issues and do not always provide an appropriate match of mechanical properties between the scaffold and the tissue [361, 367]. Conversely, accounting for over a third of all protein found in the mammalian body, collagen possesses appropriate biology and biochemistry for use *in vivo*. Although batch variation, disease transmission, and fast degradation rates are all potential issues [117], collagen's tailorability makes it a promising material for use in tissue engineering scaffolds [409-

411]. In particular, collagen shows great promise as a biocompatible coating and delivery agent on synthetic scaffold materials [368, 412, 413].

The changing mechanical properties of collagen scaffold as a result of *in vitro* incubation with matrix-degrading cells and enzymes have been well characterised [181, 414-418], primarily as a means of characterising the degradation resistance of scaffolds [402]. Studies have also demonstrated an improvement in the stiffness and strength of collagen scaffolds as a result *in vivo* incubation [419-421] while *in vitro* studies have shown that the proliferation of tissue-depositing cells, such as tenocytes, on collagen scaffolds leads to a reorganisation of the scaffold material [422-425]. To date, however, far too little attention has been paid to the changing mechanical properties of collagen scaffolds in response to the proliferation of ECM-depositing cells *in vitro*.

8.4 OBJECTIVES AND AIMS

In previous chapters (Chapter 6 and Chapter 7), it was demonstrated that in the initial stages of degeneration and tearing rotator cuff tendons show structural adaptations typical of tendon subjected to compressive and shear strains. These adaptations are likely to have significant implications for the mechanical properties of the tissue. Conservative and surgical interventions for rotator cuff degeneration and tears aim to reinstate function and reduce pain. However, their effects on the structural adaptations of the tissue are largely unknown. Furthermore, the effect of tendon cell proliferation on the degradation behaviour and mechanical properties of collagen tissue engineering scaffolds is largely untested.

The work presented in the following chapters (Chapters 9 and 10) aims to improve current knowledge of treated tissue and tendon cell-seeded scaffolds. In Chapter 9, the structural adaptations of torn rotator cuff tendons seven weeks post intervention are compared with the tissue properties pre- intervention in order to assess the effect of treatment on the structural adaptations of torn tendons. In Chapter 10, the changing mechanical, structural and compositional properties of the scaffolds incubated in different conditions are compared in order to assess the effect of tenocyte proliferation on the degradation behaviour and mechanical properties of collagen scaffolds. Specifically, the following hypotheses are tested:

1. Corticosteroid injection has a detrimental effect on the structural adaptations of torn tendons
2. Subacromial decompression surgery reverses the structural adaptations associated with impingement, degeneration and tearing
3. Tenocyte proliferation on collagen scaffolds alters the degradation characteristics of the scaffolds, specifically degradation rate and mechanism
4. Tenocyte proliferation on collagen scaffolds produces scaffolds with increased mechanical properties, particularly Tensile modulus and failure stress, compared with acellular scaffolds.

Chapter Nine

Effect of Current Treatments Torn Cuff Tendons

9.1 MATERIALS AND METHODS

9.1.1 Sample Collection

To assess the effects of common clinical treatment for rotator cuff disorders on tendon properties, the adaptations of rotator cuff samples collected pre- and 7 weeks post-treatment were provided by Dr. R. Murphy (Lord Nuffield Scholar in Orthopaedic Surgery, Nuffield Department of Orthopaedics, Rheumatology and Musculoskeletal Sciences, University of Oxford). These samples were collected as part of the same observational cohort study of participants undergoing treatment for rotator cuff pathology as that detailed in Chapter 7, Section 7.1.1 (Project Number: 09/H0605/111, Project title: 'Evaluation of the tissue effects of current therapies used in the treatment of rotator cuff pathology'). Using a core biopsy needle under ultrasound guidance, biopsies were collected from the mid portion of tendons containing partial tears, 7 weeks post-subacromial corticosteroid injections and SAD surgery. These samples were collected from the same tendons from the patients recruited to the serial biopsy study detailed in Chapter 7 Section 7.1.1, allowing direct comparison of pre- and post-treatment properties. Patients from whom no sample was collected at the 7-week time point were excluded from further analysis.

9.1.2 Sample Preparation

9.1.2.1 Tissue Processing and sectioning

Post-collection, specimens were fixed in 10% formalin for at least 1 month prior to being embedded in wax and cut into 10µm glass-mounted sections and either de-waxed or stained with picrosirius red following the procedures detailed in Chapter 4, Section 4.1.3.

9.1.3 Sample Characterisation

9.1.3.1 Atomic Force Microscopy

Atomic force microscopy (AFM) was employed to characterise the ultrastructure of the extracellular matrix in each sample. Dewaxed sections were imaged using an AFM in non-contact mode following the experimental and analysis procedures detailed in Chapter 4, Section 4.1.4.4.

9.1.3.2 Polarised Light Microscopy

Picrosirius red-stained samples were imaged and analysed for red to orange pixel ratio and crimp length using polarised light microscopy as detailed in Chapter 4, Section 4.1.4.2.

9.1.4 Statistical Analysis

Where data is presented as box plots, box ends and whisker ends represent 25th / 75th and 5th / 95th percentiles respectively, with crosses indicating outliers. In cases were data is tabulated, it is presented as mean values ± standard deviation unless otherwise indicated. In all cases, mean values represent the mean value of the individual sample means to avoid giving undue weight to samples for which more measurements were possible [327]. Statistical significance was evaluated using one-way analysis of variance (ANOVA) and Tukey's multiple comparison test performed in Origin data analysis. A significance level of $p<0.05$ was considered statistically significant, and statistical significance is indicated using the standard asterisk notation, where * indicates $p<0.05$, ** indicates $p<0.01$, and *** indicates $p<0.001$. Where relevant, linear regression analysis was performed on the data using 'R' Biostats with and without the inclusion of confounding factors.

9.2 RESULTS

9.2.1 Microstructural Evaluation

Figure 9:1 present box plots of the mean ratio of red to orange fibres obtained from partially torn samples pre- and post-treatment. The ratio of red to orange fibres is not significantly affected by steroid injection or SAD surgery. Figure 9:2 present box plots of the crimp length measurements for samples obtained partially torn samples pre- and post-treatment. Crimp length is not significantly affected by steroid treatment of SAD-surgery.

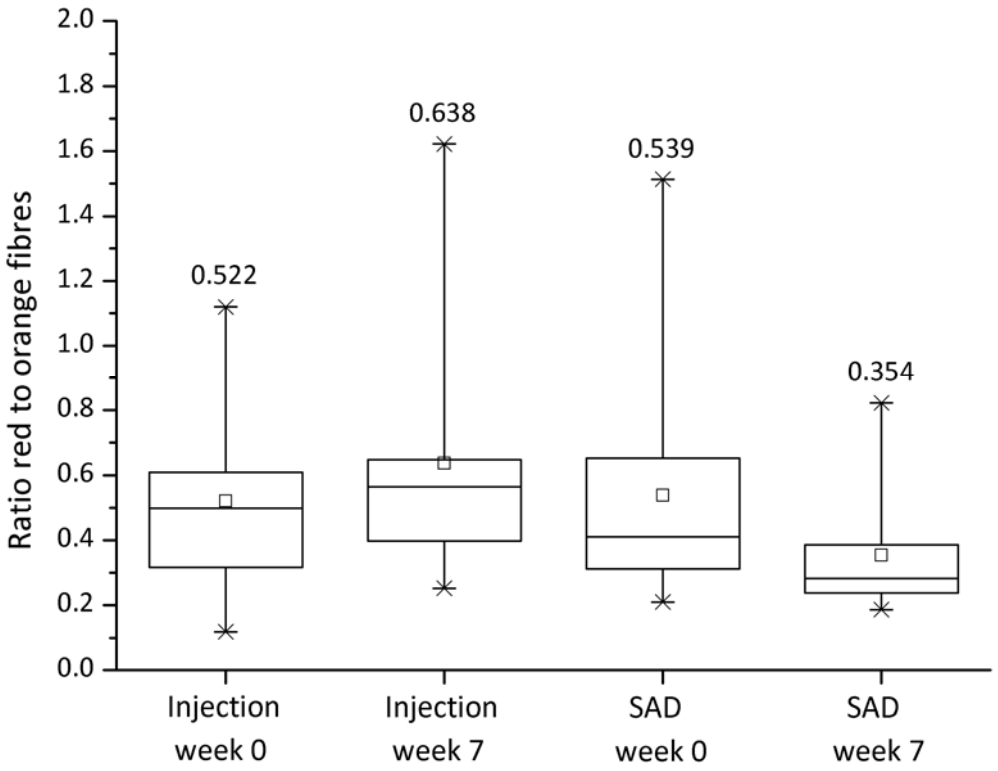

Figure 9:1 Box plots representing the ratio of red to orange fibres in picrosirius red-stained samples pre- and post- steroid injection and subacromial decompression surgery. The ratio increases insignificantly 7 weeks post-steroid injection and decreases insignificantly 7 weeks post-subacromial decompression surgery.

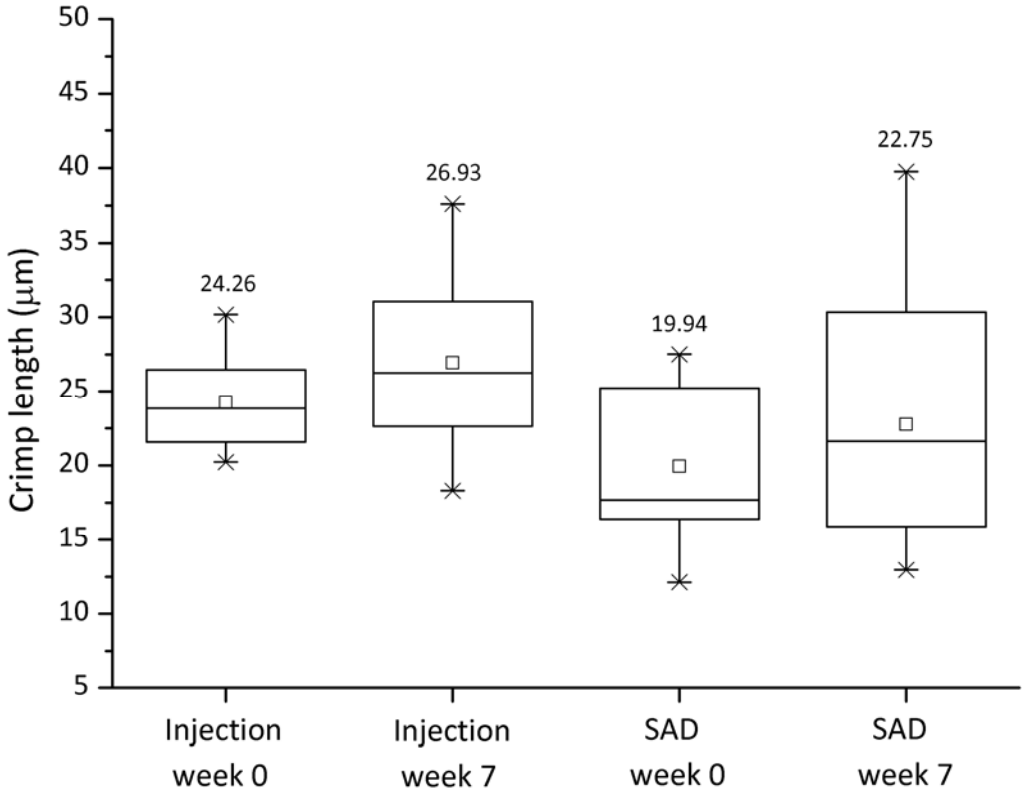

Figure 9:2 Box plots representing the distribution of crimp length measurements for samples from partially torn tendon, pre- and post- steroid injection and subacromial decompression surgery (SAD). Crimp length increases slightly after both treatments, although this is not statistically significant.

9.2.2 Ultrastructural Characterisation

Figure 9:3 present box plots of the mean fibril diameter for samples obtained from partially torn samples pre- and post-treatment. There is no significant change in the fibril diameter of samples 7 weeks post-steroid injection or 7 weeks post-SAD surgery (Figure 9:3). Figure 9:4 present box plots of 'D' spacing in samples obtained from partially torn samples pre- and post-treatment. Neither steroid injection nor SAD surgery significantly affect the 'D' spacing of these samples. Figure 9:5 present box plots of the average angle between the collagen fibrils for samples obtained from partially torn samples pre- and post-treatment. There is no difference in the average angle between fibrils in samples pre- and post- steroid injection. However, the average angle is significantly decreased in samples post-SAD surgery compared with pre-SAD surgery.

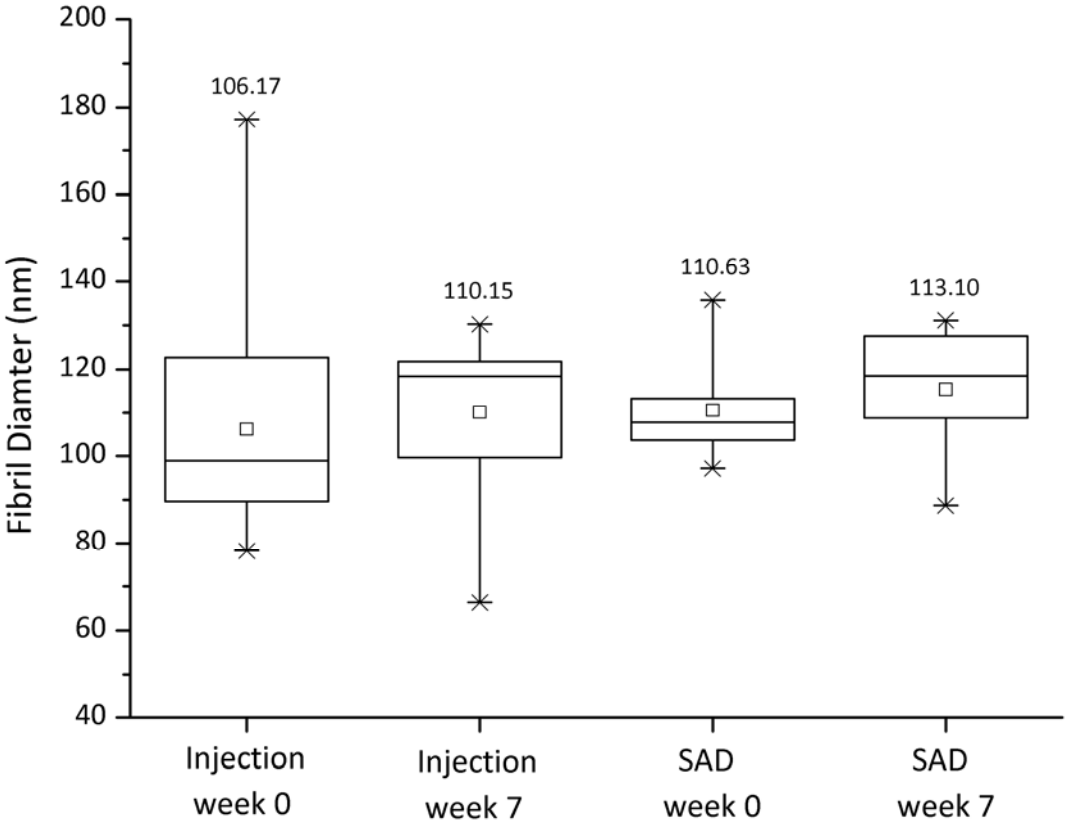

Figure 9:3 Box plots representing measurements of fibril diameter in partially torn samples pre- and post- steroid injection and subacromial decompression surgery (SAD). Fibril diameter increases slightly after treatment but this is not statistical.

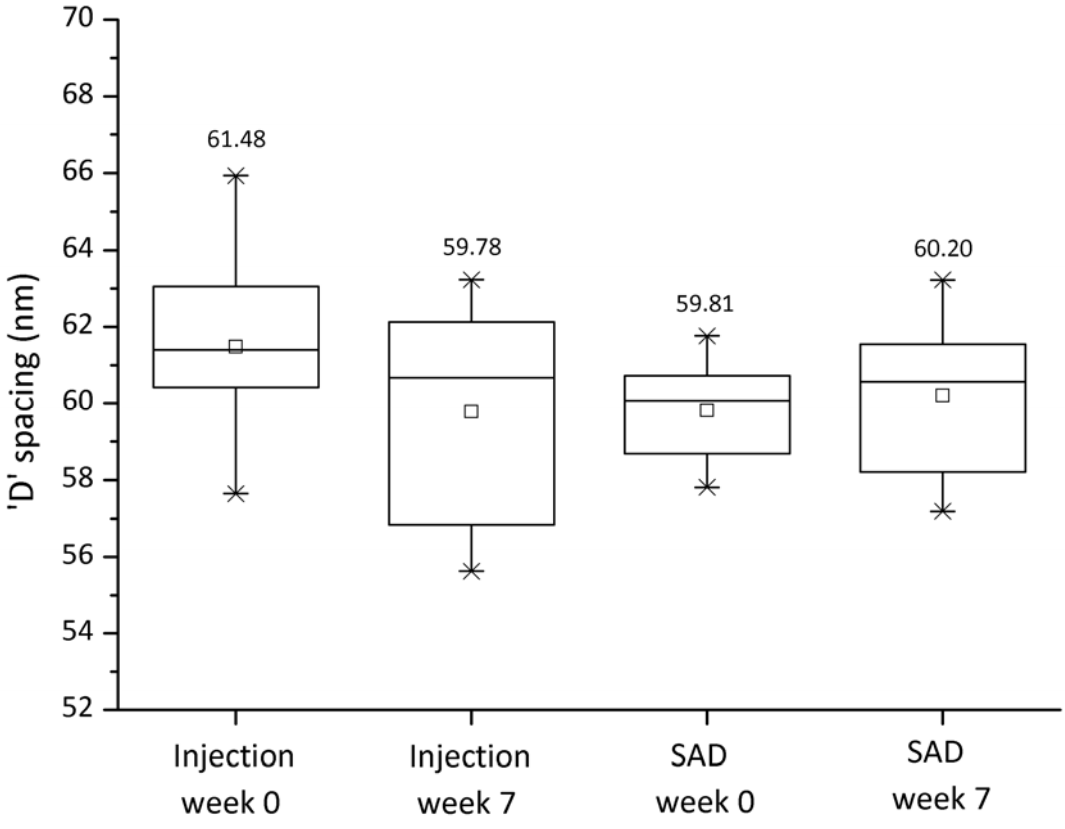

Figure 9:4 Box plots representing measurements of 'D' spacing in partially torn samples pre- and post- steroid injection and subacromial decompression surgery (SAD). 'D' spacing is not significantly different post-treatment.

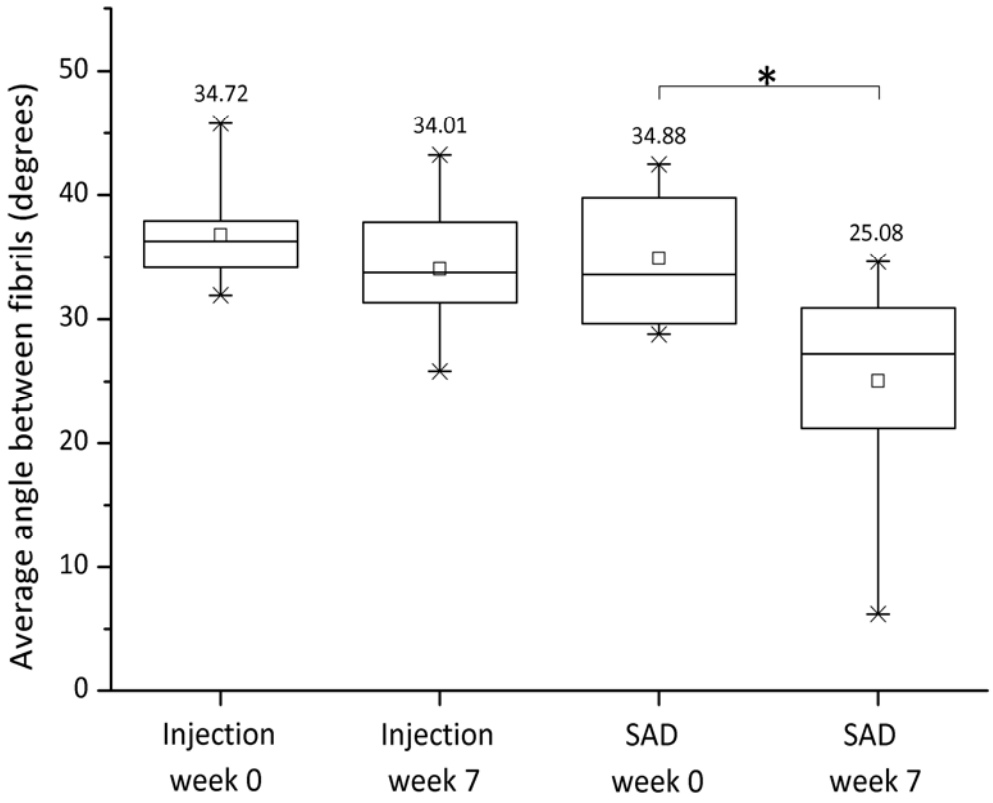

Figure 9:5 Box plots representing measurements of average angle between fibrils for partially torn samples pre- and post- steroid injection and subacromial decompression surgery (SAD). Post-SAD, average angle decreases significantly compared with pre-SAD. Steroid injection does not have any effect.

9.3 DISCUSSION

While corticosteroids are a popular conservative treatment for rotator cuff disorders, the rationale behind their use is not clear – rotator cuff degeneration is not an inflammatory disorder. Furthermore, repeated use of steroid injections have been shown to cause necrosis and decreased mechanical properties and is therefore expected to be associated with structural modifications. SAD surgery is another popular treatment option, typically offered if steroid treatment proves unsuccessful. This procedure has been reported to reduce pain and improved function [350-352], although whether it offers any significant benefit compared to physiotherapy alone is disputed [353]. The influence of SAD surgery on the structural adaptation of rotator cuff tendons is not known. However, since it is designed to remove compressive and shear strains associated with impingement of the supraspinatus tendon by the acromion, it might be expected that post-surgery the tendon would exhibit a higher proportion of structural features typical of tensile strains compared with pre-surgery.

In agreement with other studies [343], the results presented here indicate that a one-off dose of steroid does not significantly influence the structural integrity of partially torn tendons: 7 weeks post-injection there were no significant differences in the proportion of thinner fibres (Figure 9:1 pg. 161), crimp length (Figure 9:2 pg. 162), fibril diameter (Figure 9:3 pg. 163) or fibril alignment (Figure 9:5 pg. 164). SAD-surgery does not appear to significantly alter the structural adaptation of partially torn tendons either: 7 weeks post-surgery, the only statistical difference is an increase in fibrillar alignment (Figure 9:5 pg. 164). Thus the results presented here provide no evidence to support the hypotheses that corticosteroid injection has a detrimental effect on the structural adaptations of torn tendons nor that subacromial decompression surgery reverses the structural adaptations associated with impingement, degeneration and tearing.

9.4 SUMMARY, LIMITATIONS AND FURTHER WORK

The results presented in this chapter appear to indicate that neither steroid injection nor subacromial decompression surgery significantly advance or reverse the structural adaptations on torn rotator cuff tendons. However, it is highly likely that these results are impacted by the significant time limitation imposed by clinical restrictions. Specifically, it is possible that 7 weeks is not a sufficient time scale for the investigation of structural adaptations as a result of intervention. Accuracy of the sampling method should also be considered.

While the results of the work presented in this chapter are unlikely to influence future practice, due care and consideration should be given the results of biological characterisation already present in the literature before deciding on future treatment interventions. Since both treatments can bring about a short-term reduction in pain and improvement in function, the results indicate that there is no need to discontinue either treatment modality. However, the results do emphasise the need to develop new and/or improved early intervention strategies capable of restoring the healthy mechanical environment of the cuff tendons and reversing early pathological changes. Further work is now needed to assess whether there are any biological adaptations at the time point assessed here, and whether either treatment condition is associated with significant structural adaptations over much longer time scales.

Chapter Ten

Tenocyte Proliferation on Collagen Scaffolds

10.1 MATERIALS AND METHODS*

10.1.1 Chemical Procurement

All reagents were purchased from Sigma Aldrich, Dorset, UK unless otherwise stated.

10.1.2 Cell Culture

10.1.2.1 Tenocyte Origin

Foot flexor tendon-derived cells, referred to as foot flexor tenocytes (FFTs) from this point forward, were explanted from human foot flexor tendon specimens obtained from a below-knee amputation, from a 75 year old male with critical limb ischemia secondary to smoking but no other co-morbidities. Specimens were obtained intraoperatively, immediately following the amputation and transported in sterile conditions in Dubecho's minimal essential medium (DMEM) (Invitrogen Life Technologies, Grand Island, USA). Informed consent was obtained, and our institutional research committee approved use of these specimens. The tendon sample was sectioned into pieces approximately $1mm^2$ in size and cultured in DMEM containing 50% foetal calf serum (FCS) (Invitrogen Life Technologies, Grand Island, USA) with 1% penicillin/streptomycin (Pen-Strep) (Invitrogen Life Technologies, Grand Island, USA) until the cells began to migrate into the culture medium (approximately 1 week). At this point, the tendon pieces were discarded and the cells were expanded as detailed below (see Section 1.1.1.1).

* This chapter is adapted for use from **Journal of Materials Science: Materials in Medicine 23**(3) p823-33 Tenocyte proliferation on collagen scaffolds protects against degradation and improves scaffold properties. Tilley, J.M.R., Chaudhury, S., Hakimi, O., Carr, A.J., Czernuszka, C.T. Copyright (2011), with kind permission from Springer Science and Business Media [DOI: 10.1007/s10856-011-4537-7]

10.1.2.2 Tenocyte Expansion and subculture

FFTs were expanded on 10cm petri dishes (Corning, Corning, USA) in 10ml culture medium (MEM supplemented with 10% heat inactivated foetal calf serum (FCS), 1% Pen-Strep) and maintained at 37 °C and 5% CO_2 in a controlled atmosphere incubator. The culture medium was replaced every 6 days. Once the cells reached approximately 90% confluence, they were either suspended in FCS containing 10% dimethylsulfoxide and frozen in liquid nitrogen in cryovials for later use, or were passaged as follows: In a cell culture hood, 5ml of the culture medium was removed from the petri dish and discarded. A cell scraper was used to remove the cells from the base of the petri dish and suspend them in the remaining 5ml culture medium. This suspension was then split between 5 petri dishes, and 9ml fresh culture medium was added to each dish before each dish was labelled and placed in the incubator. This procedure was repeated as necessary until the 4th passage, at which point unused cells were discarded as it has been shown that 'cell phenotype is stable up until passage 5 in tenocytes isolated from tendon explants when passaged subconfluence' [346, 426].

10.1.3 Scaffold Preparation and Storage

1 w/v% collagen suspension was produced by dispersing type I tropocollagen from bovine Achilles tendon in distilled water adjusted to pH 3.3 with glacial acetic acid. The solution was then blended using a hand blender (Phillips) and degassed in a dedicator before being cast in 3x2x40mm Teflon moulds and frozen at -20°C. Frozen scaffolds were defrosted in 100% ethanol prior to immersion in 50:17:50mM EDC:NHS:MES (N- Ethyl- N'- (3-dimethylaminopropyl) carbodiimide:N-hydroxy-succinimide:2-(*N*-morpholino) ethanesulfonic acid) crosslinking solution at room temperature for 4 hours. Post-crosslinking, scaffolds were rinsed twice in 0.1 M Na_2HPO_4 for 1 hour, washed four times in distilled water for 30 minutes, and then stored in 100% ethanol at room temperature for up to 24 hours prior to use [427]. On Day -1, scaffolds were sterilised in fresh 100% ethanol for 30 minutes, rinsed three times in DPBS (Lonza, Basel, CH) for 30 minutes and then stored in minimal essential medium (MEM) (Invitrogen Life Technologies, Grand Island, USA) at 5°C overnight. Enough scaffolds were prepared to provide 16 scaffolds per time point for the mechanical study, and a further six scaffolds for cell penetration and morphology experiments on days 1 and 26.

10.1.4 Cell Seeding

On Day 0 scaffolds were cut in half laterally using a handheld razor blade. The halves were then placed in 24-well Costar® cell culture clusters (Corning, Corning, USA) with four halves in each well, and the cell clusters were placed in an incubator at 37 °C, 5% CO_2 at 100% humidity for 30 minutes. Each well was then seeded with either: a) 1ml DMEM, 10% FCS, 1% Pen-Strep or b) 1ml DMEM, 10% FCS, 1% Pen-Strep containing $5x10^5$ FFTs (Passage 3). The seeded scaffolds were cultured in an incubator at 37 °C, 5% CO_2 at 100% humidity and the medium was replaced every six days.

10.1.5 Histology and Biochemical Assays

10.1.5.1 Cell Viability

The Alamar blue™ assay was used to assess the amount of viable biomass on Days 1, 5, 13 and 26 [428]. For consistency, the 12 scaffolds intended for Day 26 mechanical characterisation were used for all readings. On the appropriate day, the culture medium surrounding the scaffolds was discarded and the scaffolds were transferred to fresh well plates (four scaffolds per well). They were then incubated in 5% Alamar blue (Lonza, Basel, CH) in MEM at 37°C for 2 hours. The supernatant was then transferred to 48-well cell culture clusters and emission at 590nm was measured following excitation at 530–570 nm using a MRX spectrophotometer (Dynex Technologies, Chantilly, USA). Using the same method, the amount of viable biomass on the original well plates on Day 1 was assessed for control purposes.

10.1.5.2 Cell Penetration and Morphology

On Day 1 and Day 26 six scaffolds were removed from the culture medium, rinsed twice in 1xPBS (Lonza, Basel, CH) for 15 minutes, and fixed in 10% formalin neutral buffered with 0.1M PBS (Lonza, Basel, CH) at room temperature for at least 24 hours. Fixed scaffolds were then cut in half transversely, dehydrated through graded IMS (70%, 90%, 95%, 100%), perfused in paraffin wax using a tissue processor and embedded in a Formula R paraffin wax bloc (Surgipath, Cambridgeshire, UK). One 10µm cross-sectional slice was then cut from each embedded sample using a microtome (Leica Microsystems, Milton Keynes, UK), mounted on a microscope slide (Leica Microsystems, Milton Keynes, UK) and baked at 60°C for at least 24 hours before being stored in ambient conditions in standard slide boxes.

The cell penetration profile and cell morphology of each cross-sectional slice was assessed by staining the slides with Nuclear Fast Red as follows; each slide was twice cleared in a clearing agent (Thermo Fisher Scientific, Waltham USA) for 7 minutes, rehydrated in graded IMS (100%, 100%, 90%, 75%, 5 minutes each), stained with 0.1% Nuclear Fast Red in 5% aluminium sulphate (Thermo Fisher Scientific, Waltham USA) for 10 minutes, rinsed in running water for 1 minute, dehydrated in graded alcohol (100%, 100%, 90%, 75%, 5 minutes each) , cleared in a clearing agent, mounted with DXP mountant (Sugipath, Peterborough, UK) and covered with a cover slip.

Using an Axio Imager M microscope (Carl Zeiss Ltd., Welwyn Garden City, UK), each slice was imaged sequentially (20x magnification). After the images had been stitched together using Adobe Illustrator CS3 extended image processing software (Adobe, San Jose, USA), image analysis software (Image J, Wayne Rasband) was used to count the number of cells in each sequential image and to calculate the minimum distance from the centre of each sequential image to the cross-section edge. Analysis was performed in this order as it allowed more accurate calculation of the closest distance of each cell from the cross section edge compared with counting the cells directly under the microscope.

10.1.6 Culture Medium Content

Culture medium was aspirated from the incubated scaffolds on Days 0, 5, 12 and 26 and assayed using a SensoLyte generic 'colorimetric' assay kit (AnaSpec, Fremont, USA) [429] to detect sulfhydryl group (-SH) concentrations from which cysteine concentration (and thus extent of scaffold degradation) can be inferred. The following were added to labelled 96-well plates: either i) 30µl aspirated culture medium and 30µl MMP substrate, ii) 30µl fresh culture medium and 30µl MMP substrate (vehicle control), iii) 60 µl Glutathione reference standards (200µM, 100µM, 50µM,25µM, 12.5µM), or iv) 60µl of MMP substrate (substrate control). 40 µl of assay buffer was then added to each well and the well plate was gently shaken for 30 seconds. The well plate was then incubated for 120 minutes at 37°C. The absorbance of each well was assessed at 412nm using a Spectra Max Plus microplate reader (Molecular Devices, Sunnyvale, USA). Data was calibrated using the appropriate control as provided with the assay kit.

10.1.7 Mechanical Characterisation

The tensile mechanical properties of scaffolds were assessed on Days 0, 1, 5, 12 and 26 using a Dynamic mechanical Analyser DMA 7e (PerkinElmer, Waltham, USA) (Figure 10:1). 16 scaffolds were removed from the culture medium, washed twice in DPBS for 5 minutes and stored in DPBS for up to 4 hours prior to testing. The initial cross-sectional area of the scaffolds was measured using digital callipers (RS). Scaffolds were then carefully loaded in the DMA clamps (Figure 10:1), immersed in tap water at ambient temperature and tested in tension using a force rate of 20mN min^{-1}. Scaffolds which failed at the clamps, or slipped from the clamps during testing, were discarded from further mechanical analyses. The force-extension curves produced were converted to stress-strain curves which were analysed for high-strain tensile modulus and failure stress of the scaffolds as defined in Figure 10:2.

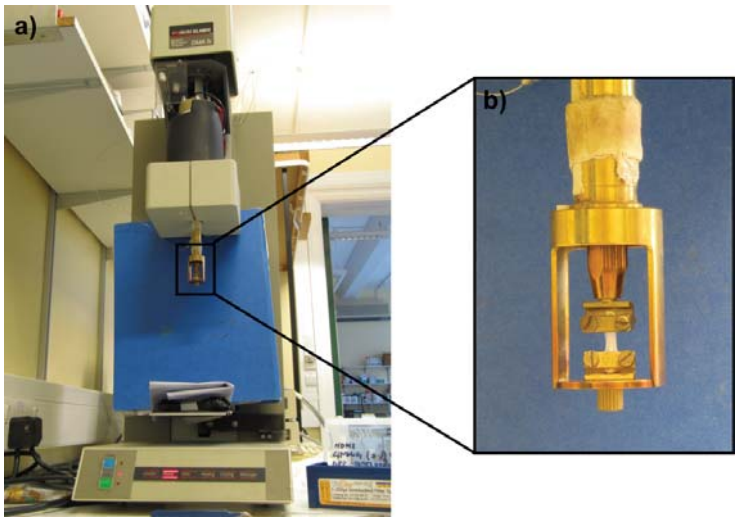

Figure 10:1 Dynamic Mechanical Analyser with a loaded collagen scaffold shown in an expanded view

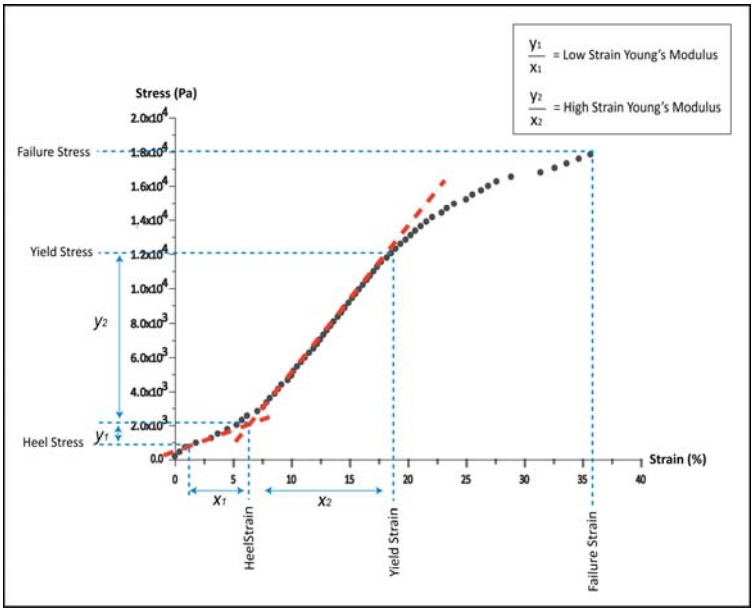

Figure 10:2 Typical stress-strain curve for collagen scaffolds used in this Chapter, annotated to illustrate the definitions of mechanical properties measured as part of this work.

10.1.8 Differential Scanning Calorimetry

Differential Scanning Calorimetry (DSC) was used to assess the effects of incubation on the denaturation temperature of the scaffold material. Post-mechanical testing, six scaffolds from Days 0, 1, 5, 12 and 26 were rinsed in 100% ethanol, air dried in ambient conditions overnight and then stored in 2ml microcentrifuge tubes (Thermo Fisher Scientific, Waltham USA). 6 ± 0.6 mg dry weight of each sample was then placed in a 40µl aluminium DSC pan (PerkinElmer, Waltham, USA) and heated to 105°C at 15°C min^{-1} using a DSC821^{e} (Mattler Toledo, Beaumont Leys, UK). The denaturation temperature (T_d) of each sample was taken as the peak in the power-temperature graph produced.

10.1.9 Infra-red Spectroscopy

Fourier Transform Infra-red Spectroscopy (FTIR) was used to assess the effects of processing and incubation on the scaffold material. FTIR spectra were collected for i) as purchased tropocollagen, ii) pre-crosslinked collagen scaffolds frozen in moulds for 24 hours and then defrosted in ethanol, and iii) crosslinked collagen scaffolds rinsed in ethanol. Spectra were also collected for six medium-only and six FFT-seeded scaffolds incubated on Days 1 and 26.

On the appropriate day, scaffolds were removed from culture medium and rinsed in PBS buffer. They were then stored in 100% ethanol for a minimum of 24 hours, rinsed in 100% HDMS for 24 hours and then left to air dry in ambient conditions for up to 1 week. Using an Excalibur FTIR spectroscope (Agilent, Stockport, UK) in attenuated total reflectance mode, scaffolds were scanned from 4000 cm^{-1} to 400 cm^{-1} 64 times with the background scan subtracted. Using Varian Resolutions Pro 4.0 software (Agilent, Stockport, UK) each spectrum was baseline corrected and normalised to the intensity of the CH_2 peak found at 1452cm^{-1}. To assess the nature of material changes resulting from incubation, the collagen fingerprint region of the average spectrum for each time point was compared.

10.1.10 Statistical Analysis

Power analysis, assessed using the biostatistics package 'R' (R Foundation for Statistical Computing) and based on preliminary experiments [402], revealed that a minimum of 14 samples were needed in order to distinguish differences of 1 standard deviation in mechanical data at $p<0.05$ statistical significance and 80% confidence level. Mechanical data points were therefore calculated as the mean of at least 14

replicates. All other experiments data was calculated as a mean of at least 6 replicates unless otherwise stated and error bars represent standard deviations. Where data is presented as a percentage difference, data points represent percentage difference in the means and error bars were calculated by converting standard deviations to relative errors based on mean values. Statistical significance was evaluated using one-way analysis of variance (ANOVA) and Tukey's multiple comparison test on raw data sets using Origin data analysis software. In this chapter statistical significance is indicated as follows: *indicates a value significantly different ($p<0.05$) to the Day 0 value, while $^{\#}$ indicates a statistically significant difference ($p<0.05$) between results at a particular time point.

10.2 RESULTS

10.2.1 Scaffold Suitability

10.2.1.1 Material Properties of Collagen

Figure 10:3 compares Fourier Transform infrared (FTIR) spectra of collagen at various stages during scaffold processing while Table 10:1 shows how the processing steps affect the intensity and position of characteristic peaks in the collagen infrared spectrum. It is clear from Figure 10:3 and the data in Table 10:1 that there are significant reductions in the height of the peaks at 2853-2937cm^{-1} and 1742-1744cm^{-1} upon dissolution of as-purchased collagen in pH 3.3 aqueous solution indicating hydrolysation of the CH_2 (methylene) and C=O (carbonyl) groups respectively. However, there are no significant differences in the positions or heights of the Amide peaks at any stage indicating that processing does not significantly affect the collagenous nature of the scaffolds.

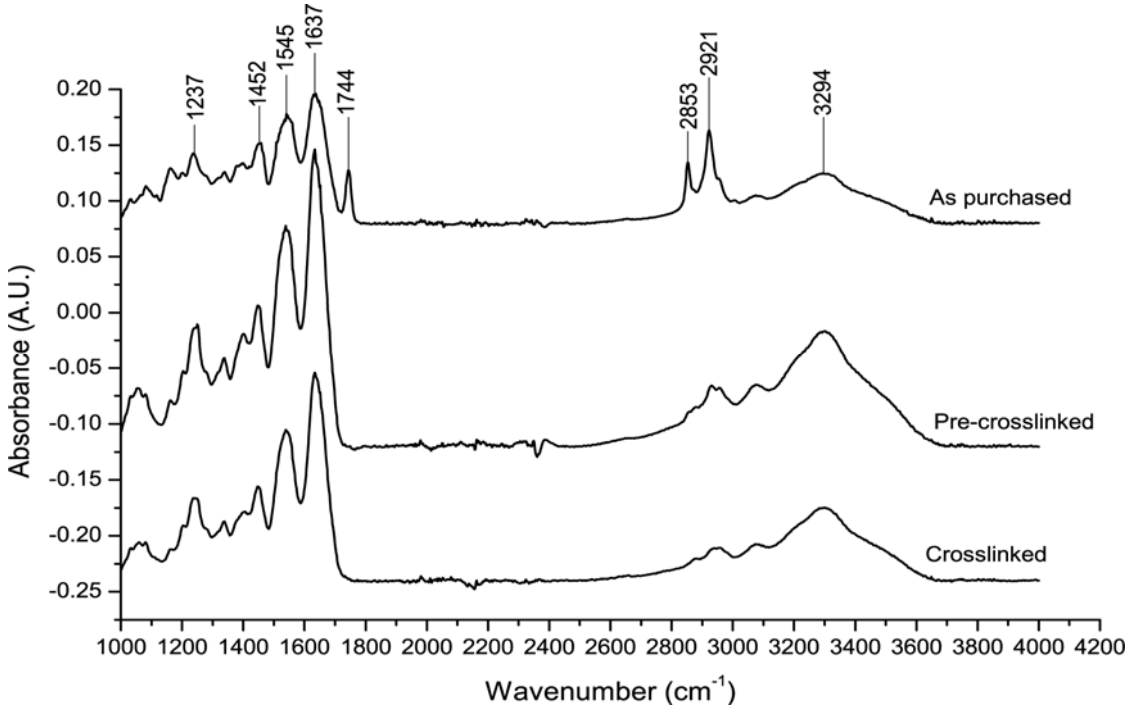

Figure 10:3 FTIR spectra of collagen at various stages during scaffold processing. Peak intensities for each spectrum are normalised relatively to the CH2 reference peak at 1453cm^{-1}. Initial dissolution in acid reduces absorbance at 2853-2937cm^{-1} and 1742-1744cm^{-1}

Table 10:1 Experimental Data showing the Affect of Scaffold Processing on Collagen Infrared Spectrum

		As- purchased	Pre-crosslinked	Crosslinked
Amide A	Peak Centre (cm^{-1})	3302 ±6.4	3300 ±2.5	3301 ±6.2
	Normalised Peak Height	0.38 ±0.22	0.41 ±0.25	0.47 ±0.26
Amide I	Peak Centre (cm^{-1})	1636 ±1.6	1637 ±1.9	1637 ±4.1
	Normalised Peak Height	3.04 ±1.78	3.35 ±1.81	3.56 ±1.94
Amide II	Peak Centre (cm^{-1})	1542 ±1.5	1541 ±1.2	1542 ±2.1
	Normalised Peak Height	1.78 ±1.31	1.92 ±1.04	2.03 ±1.09
Amide III	Peak Centre (cm^{-1})	1237 ±0.4	1246 ±6.5	1239 ±2.7
	Normalised Peak Height	0.82 ±0.41	0.97 ±0.58	0.88 ±0.47
CH_2 Asymmetric	Peak Centre (cm^{-1})	2923 ±1.5	2931 ±11.8	2938 ±11.1
	Normalised Peak Height	2.39 ±0.66	0.4 ±0.30 a	0.36 ±0.12 [a]
CH_2 Symmetric	Peak Centre (cm^{-1})	2854 ±0.5	2863 ±10.9	2877 ±11.3 [a]
	Normalised Peak Height	1.29 ±0.40	0.13 ±0.12 [a]	0.1 ±0.10 [a]
Carbonyl	Peak Centre (cm^{-1})	1744 ±0.5	1743 ±2.5	n/a
	Normalised Peak Height	1.9 ±0.68	0.14 ±0.12 a	n/a

[a] indicates significantly different to as-purchased value at 0.01 level

Table 10:2 presents the Day 0 (i.e. pre-incubation) properties of the crosslinked collagen scaffolds used in this study. These properties define the baseline values to which all subsequent measurements of scaffold properties were compared.

Table 10:2 Day 0 (i.e. Baseline) Scaffold Properties

	Mean	**Standard deviation**
Cross-sectional Area, A_X	6.5 mm^2	0.7
Low Strain Tensile Modulus, E_L	38.1 kPa	17.0
Heel Strain, ε_H	10.8 %	7.2
Heel Stress, σ_H	3.7 kPa	1.7
High Strain Tensile Modulus, E_H	70.9 kPa	20.9
Yield Strain, ε_Y	31.6 %	21.8
Yield Stress, σ_Y	14.7 kPa	3.3
Failure Strain, ε_F	51.9 %	26.0
Failure Stress, σ_F	21.7 kPa	8.9
Denaturation Temperature, D_T	82.3 °C	1.3

10.2.1.2 Cell Behaviour

Figure 10:4 compares the amount of viable biomass on collagen scaffolds relative to the Day 1 control value (i.e. cells grown on tissue culture plastic) at various time points, as assessed using the Alamar blue assay. Although there is initially less viable biomass in the scaffolds compared with the control material (33%), the amount in the collagen scaffolds increases rapidly, reaching a plateau after Day 13.

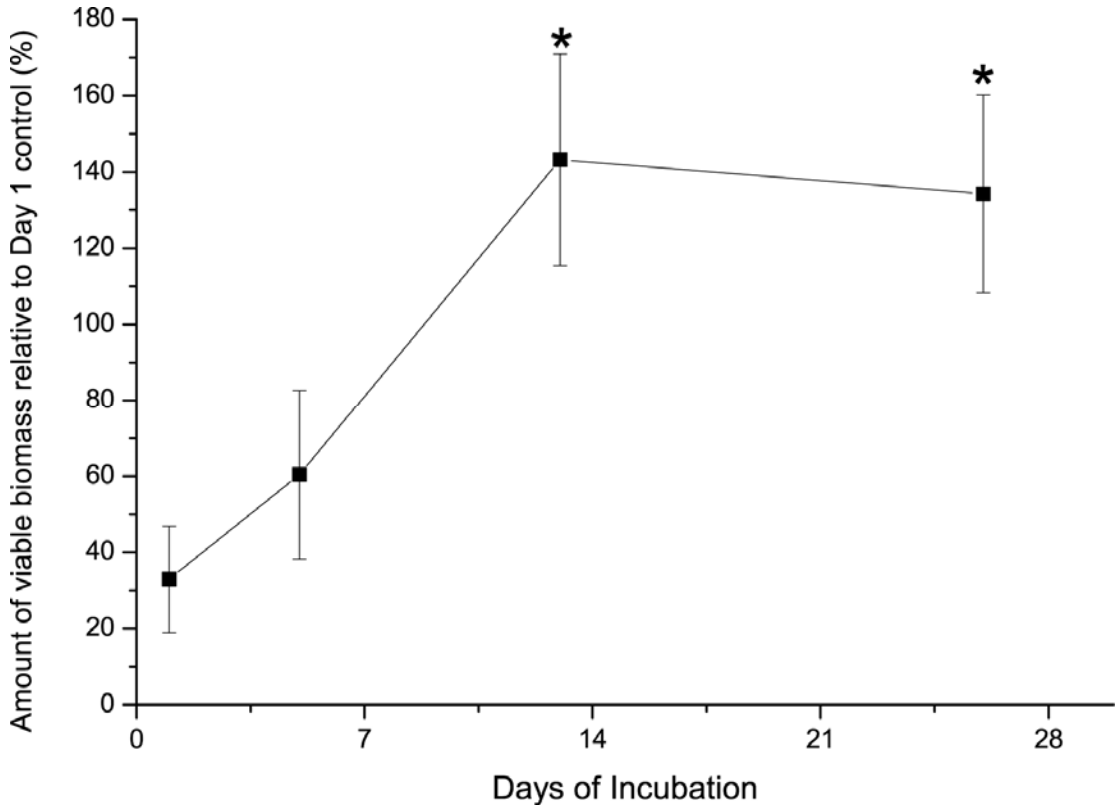

*Figure 10:4 Amount of viable biomass on collagen scaffolds relative to Day 1 control value (culture well) at different time points. *indicates significantly different ($p<0.05$) to Day 1 value. Although there is less viable biomass on the scaffolds than on the control material on Day 1, the amount increase steadily until Day 12, at which point it plateaus.*

Figure 10:5 shows the cell penetration profiles on Day 1 and day 26, as assessed using nuclear fast red-staining. On Day 1 the there are, on average, 34 FFTs per 10µm slice while on Day 26 there are, on average 132 FFTs per 10µm slice, a statistically significant increase ($p<0.05$). At both time points there are no cells further than 1.5mm from a scaffold edge, with the majority concentrating 250- 500µm from the scaffold edges. By Day 26 there are more cells and the distribution profile is visibly broader compared with Day 1. Figure 10:6 shows a complete cross-section together with images from the outer edge of the scaffold and the centre of the scaffold in order to illustrate differences in cell penetration. In agreement with the cell penetration data more cells are visible at the edge (Figure 10:6B) than in the centre (Figure 10:6C).

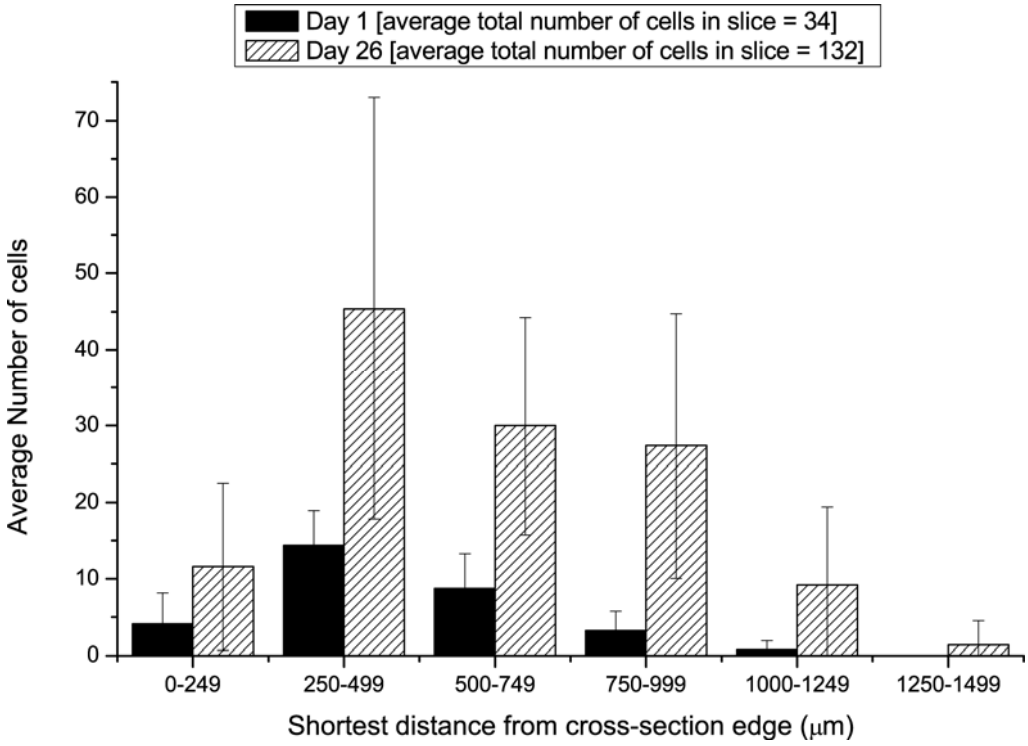

Figure 10:5 Penetration of FFT cells into collagen scaffolds. There are no cells further than 1.5mm from a scaffold edge, with the majority concentrating 250- 1000μm from the scaffold edges. By Day 26 there are more cells and the distribution profile is visibly broader compared with Day 1

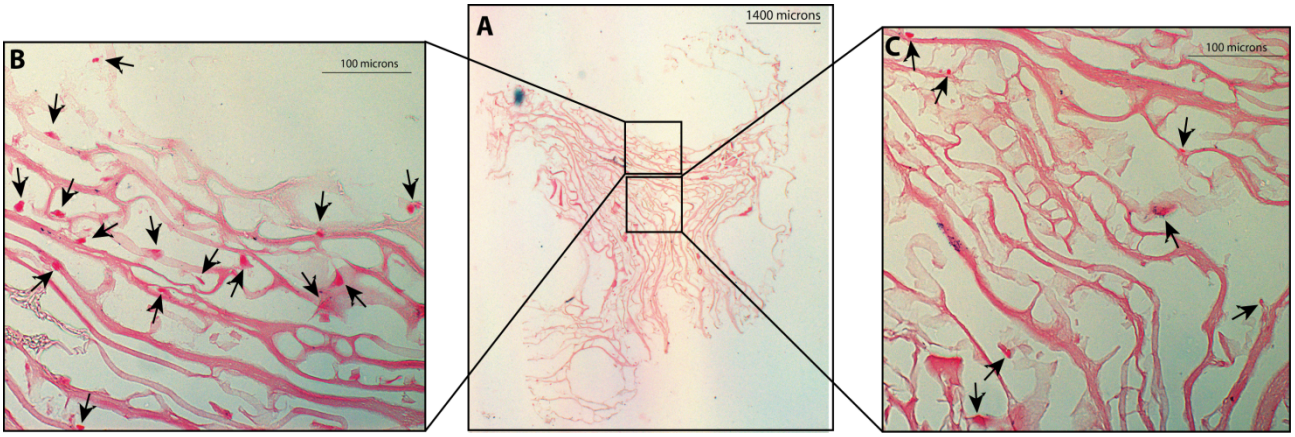

Figure 10:6 Nuclear fast red-stained FFT cells on collagen scaffold after 26 days of incubation; A) low magnification image (x2.5) of a complete cross-section, B) high magnification image (x20) of the edge of the cross-section, and C) high magnification image (x20) of the centre of the cross-section. Cells that are attached to the scaffold are indicated by arrow heads. In agreement with the cell penetration data more cells are visible at the edge (B) than in the centre (C).

10.2.2 Scaffold Changes Resulting from Incubation

10.2.2.1 Mechanical Scaffold Changes

Figure 10:7 shows the cross-sectional area (relative to Day 0 values) of scaffolds incubated in medium-only and with FFTs as a function of time. For both conditions cross-sectional area (A_X) decreases with time; by Day 13 medium-only scaffolds show a significantly greater reduction in A_X compared with FFT-seeded scaffolds, decreasing to 40% of the Day 0 value. By Day 26, scaffolds incubated in medium-only are too disintegrated to characterise.

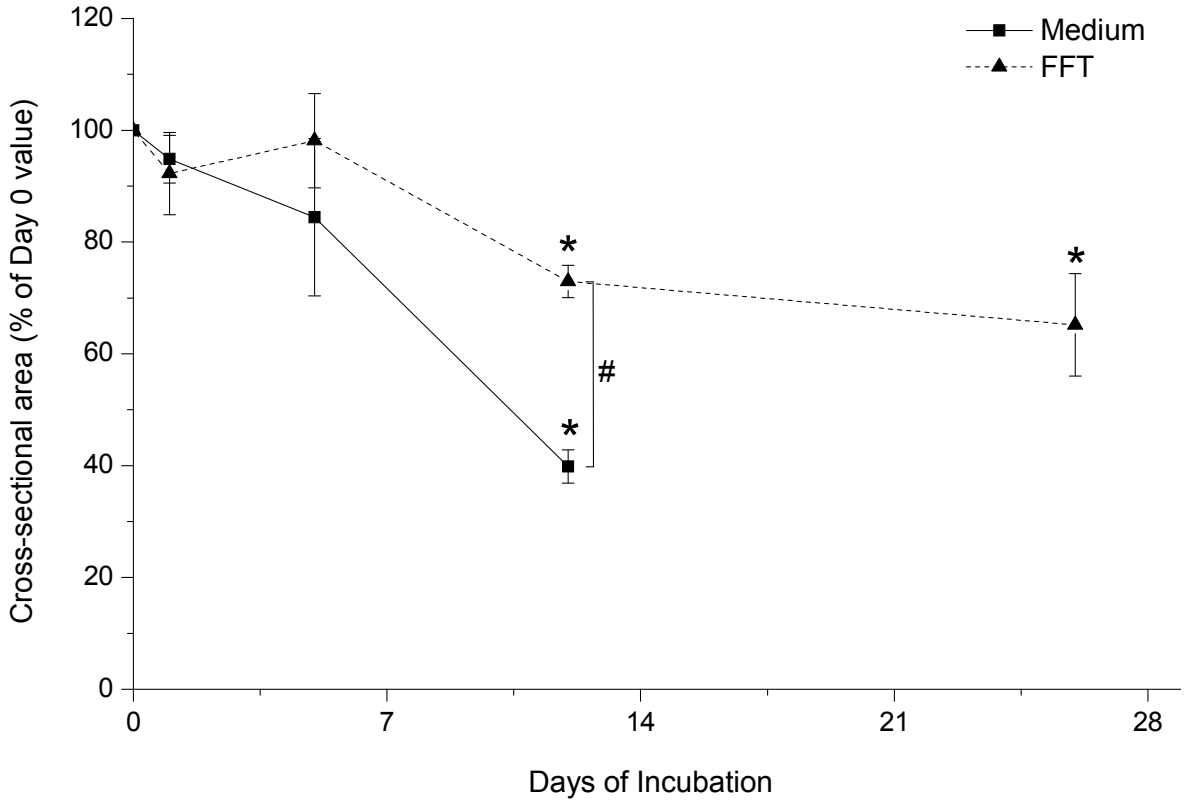

*Figure 10:7 Changing scaffold cross-sectional area (Ax), compared with Day 0, as a result of incubation in medium-only, or with FFT cells. *indicates significantly different ($p<0.05$) to Day 0 value, #indicates a statistically significant difference ($p<0.05$) between results at a particular time point. A_x of all scaffolds decreases significantly over the course of the experiment, decreasing to a greater extent in medium-only scaffolds: by Day 12 A_x of medium-only scaffolds is significantly smaller than FFT seeded scaffolds. By Day 26, medium-only scaffolds were too disintegrated to enable measurement of A_x.*

Figure 10:8 to Figure 10:15 show the effect of incubation on the low strain Tensile moduli, high strain Tensile moduli, heel strain, yield strain, failure strain, heel stress, yield stress and failure stress respectively of scaffolds incubated in different conditions. Initially, there are no significant changes in the moduli (Figure 10:8, Figure 10:9), heel strain, yield strain or failure strain, (Figure 10:10 - Figure 10:12), heel stress, yield stress or failure stress (Figure 10:13 - Figure 10:15) of scaffolds incubated in medium-only. However, by Day 5 these scaffolds are too weak to test. In contrast, scaffolds incubated with FFTs show significant increases in Low Strain Tensile modulus (Figure 10:8) and High Strain Tensile modulus (Figure 10:9), reaching 231% and 313% of Day 0 values respectively by Day 26.

The heel stress, yield stress and failure stress (Figure 10:13-Figure 10:15) of FFT-seeded scaffolds also increase significantly over the course of the experiment, reaching 437%, 268%, and 230% of Day 1 values respectively by Day 26. However, incubation with FFTs does not significantly alter the heel strain, yield strain or failure strain of the FFT-seeded scaffolds (Figure 10:10, Figure 10:11 and Figure 10:12 respectively) over the course of the experiment.

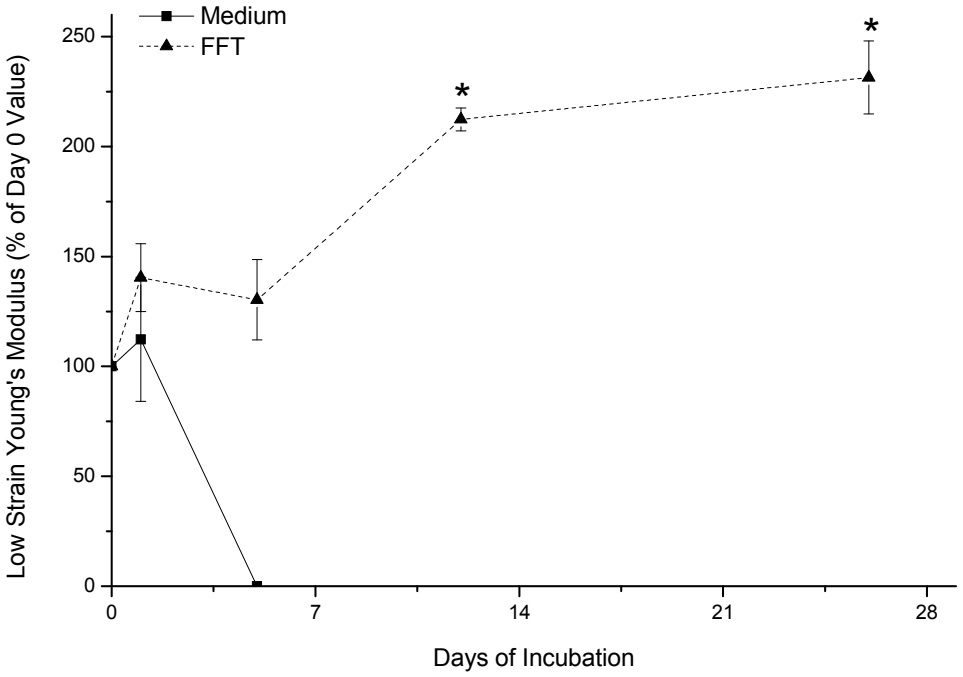

*Figure 10:8 Changing Low Strain Tensile modulus (EL) of scaffolds incubated in medium-only, and with FFT cells. *indicates significantly different ($p<0.05$) to Day 0 value. EH of medium-only scaffolds decreases rapidly and is negligible by Day 5, while EH of FFT-seeded scaffolds increases significantly over the course of the experiment.*

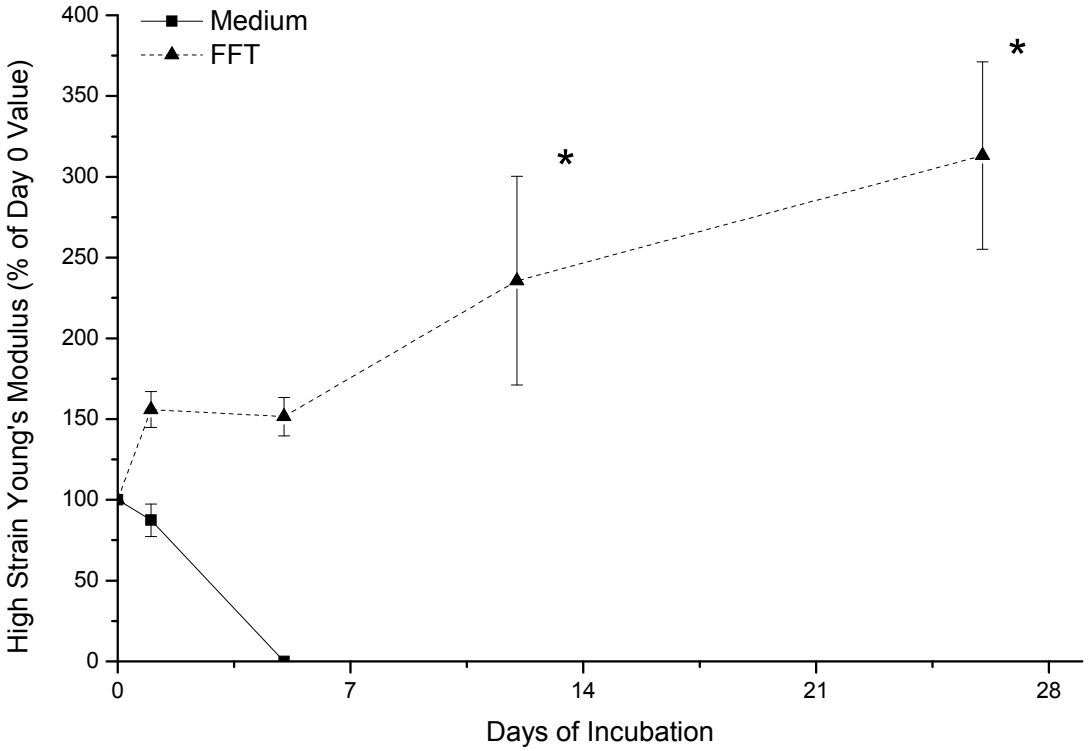

*Figure 10:9 Changing high strain tensile modulus (E_H) of scaffolds incubated in medium-only, and with FFT cells. *indicates significantly different ($p<0.05$) to Day 0 value. E_H of medium-only scaffolds decreases rapidly and is negligible by Day 5, while E_H of FFT-seeded scaffolds increases significantly over the course of the experiment.*

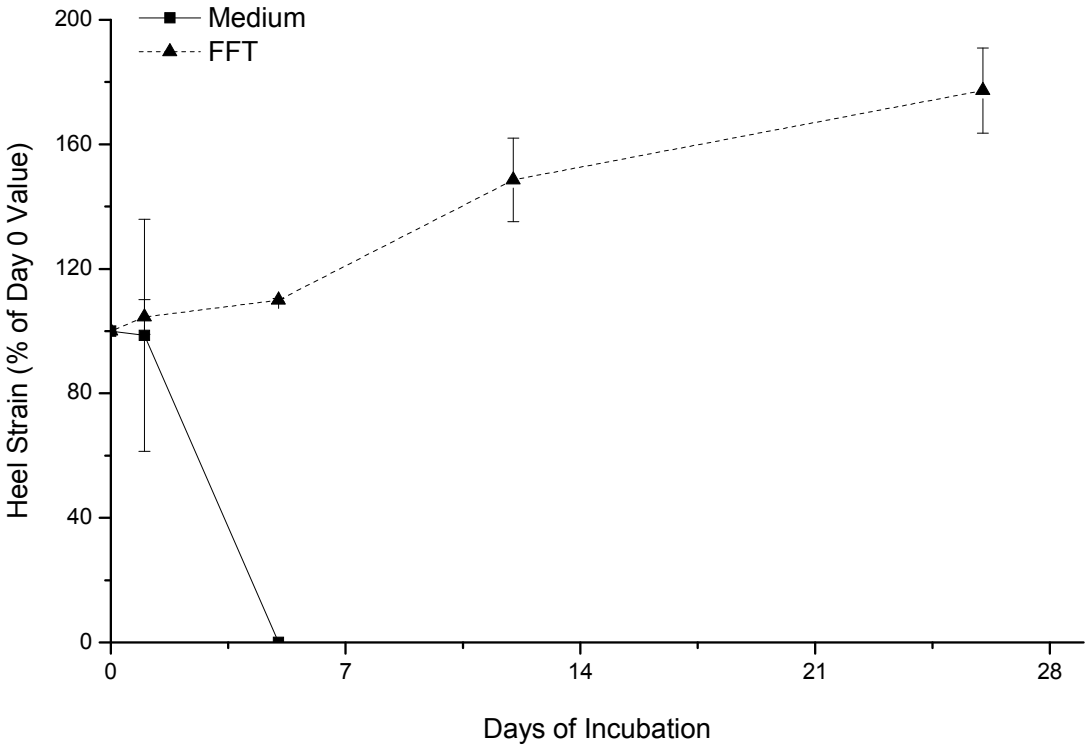

Figure 10:10 Changing Heel Strain (ε_H) of scaffolds incubated in medium-only, and with FFT cells. ε_H of medium-only scaffolds is negligible by Day 5, while ε_H of FFT-seeded scaffolds increases over the course of the experiment to an insignificant level.

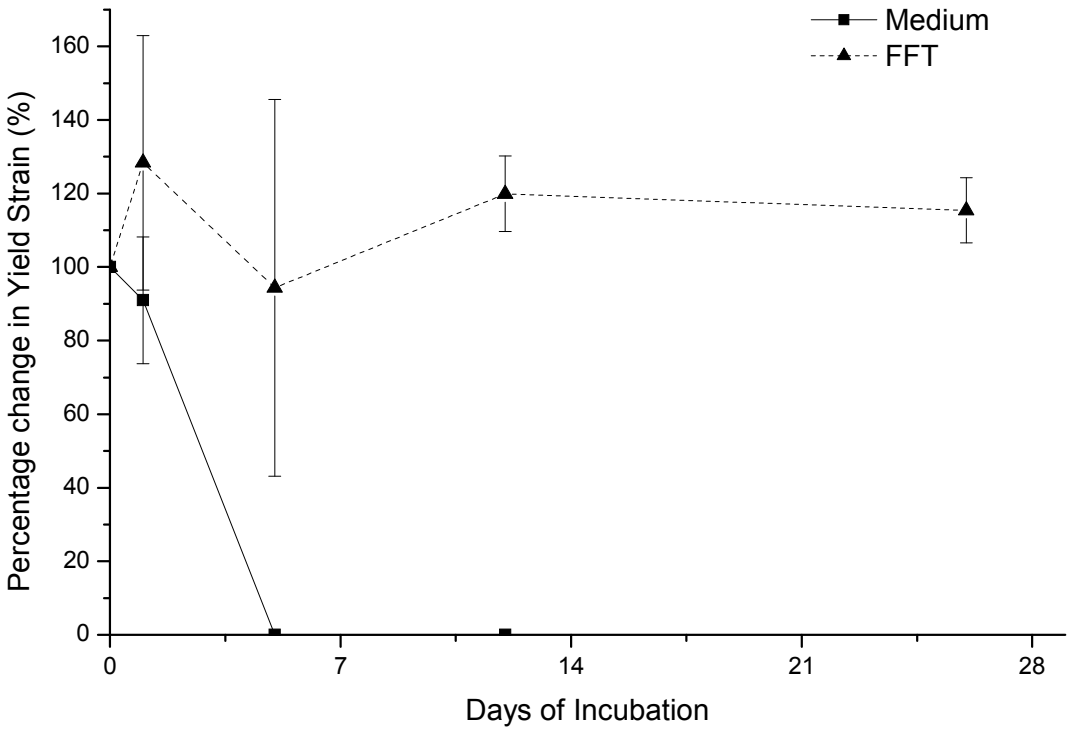

Figure 10:11 Changing yield strain (ε_Y), compared with Day 0, as a result of incubation in medium-only, or with FFT cells. By Day 5, ε_Y of medium-only scaffolds is negligible, while the ε_Y of FFT seeded scaffolds does not change significantly over the course of the experiment.

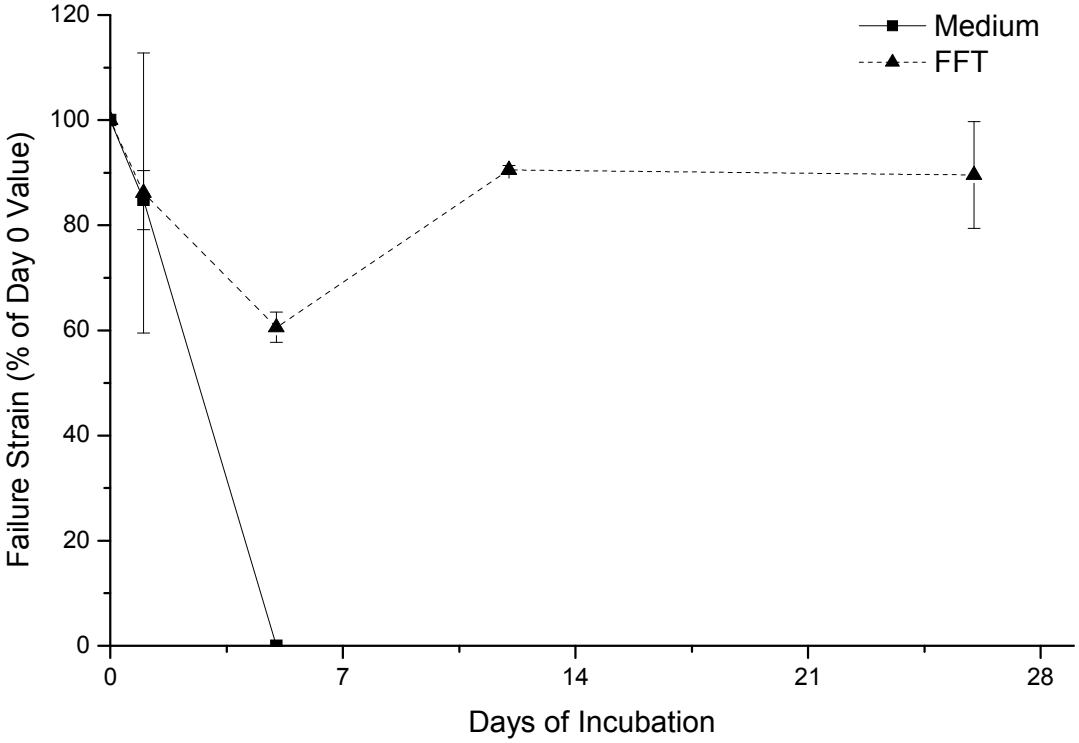

Figure 10:12 Changing failure strain (ε_F), compared with Day 0, as a result of incubation in medium-only, or with FFT cells. By Day 5, ε_F of medium-only scaffolds is un-measurable, while ε_F of FFT seeded scaffolds does not change significantly over the course of the experiment.

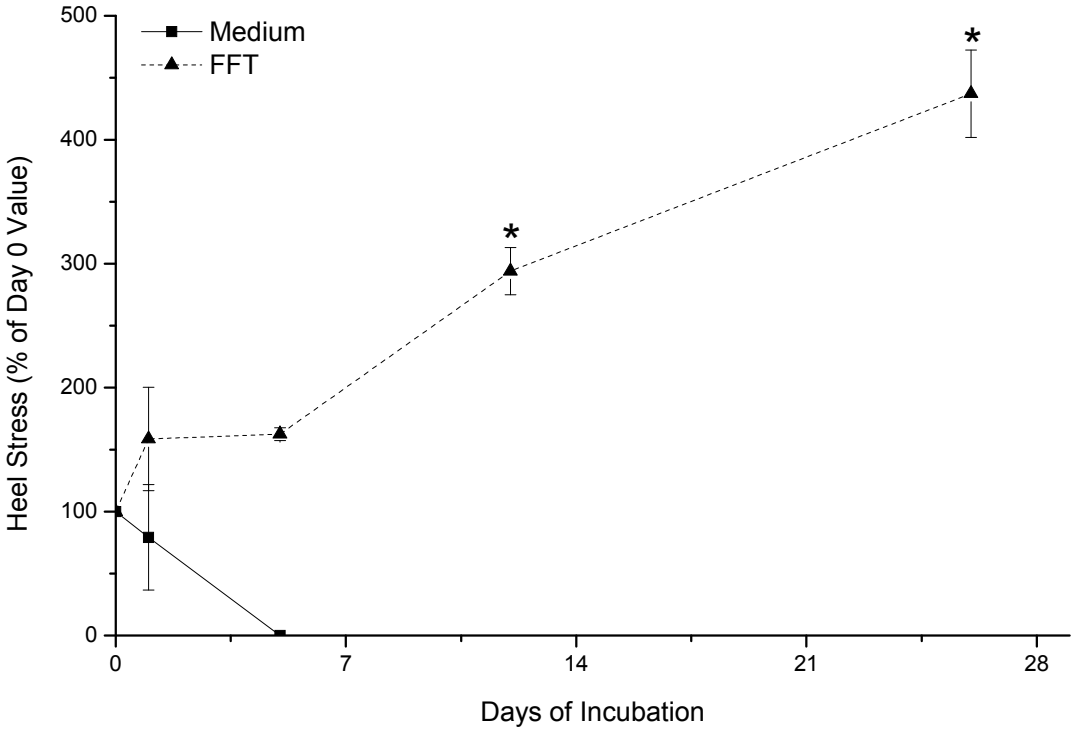

*Figure 10:13 Changing Heel stress (σ_H) of scaffolds incubated in medium-only, and with FFT cells. *indicates significantly different ($p<0.05$) to Day 0 value. σ_H of medium-only scaffolds decreases rapidly and is negligible by Day 5, while σ_H of FFT-seeded scaffolds increases significantly over the course of the experiment.*

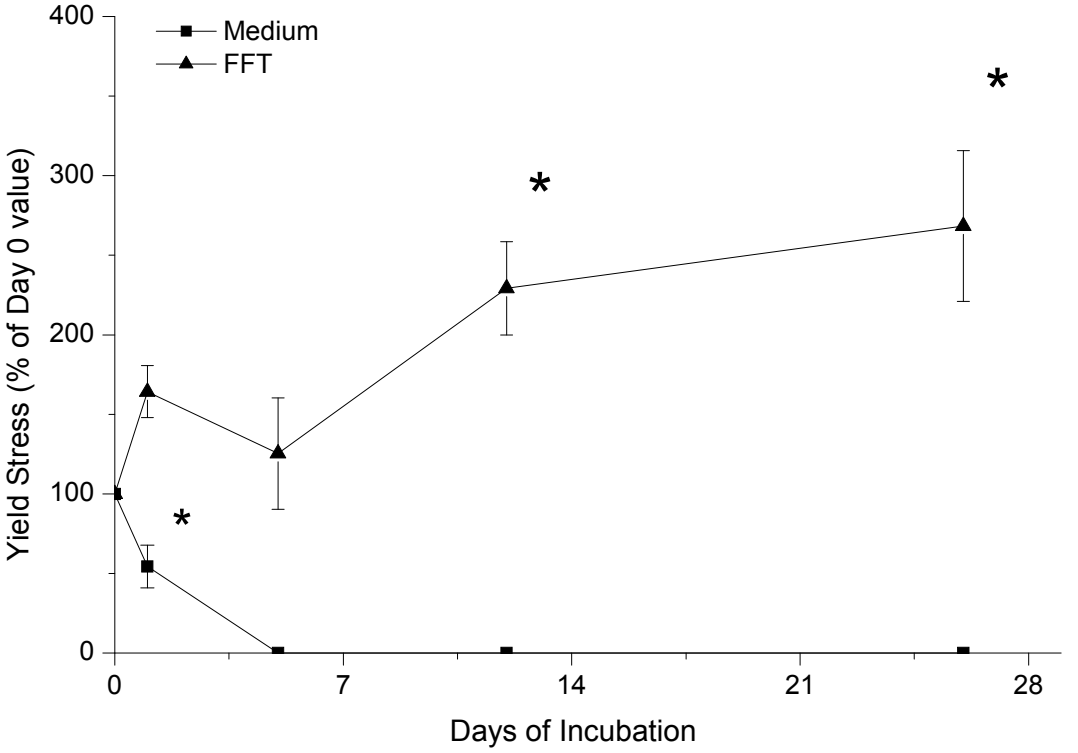

*Figure 10:14 Changing Yield Stress (σ_Y) of scaffolds incubated in medium-only, and with FFT cells. *indicates significantly different ($p<0.05$) to Day 0 value. σ_Y of medium-only scaffolds decreases rapidly and is negligible by Day 5, while σ_Y of FFT-seeded scaffolds increases significantly over the course of the experiment.*

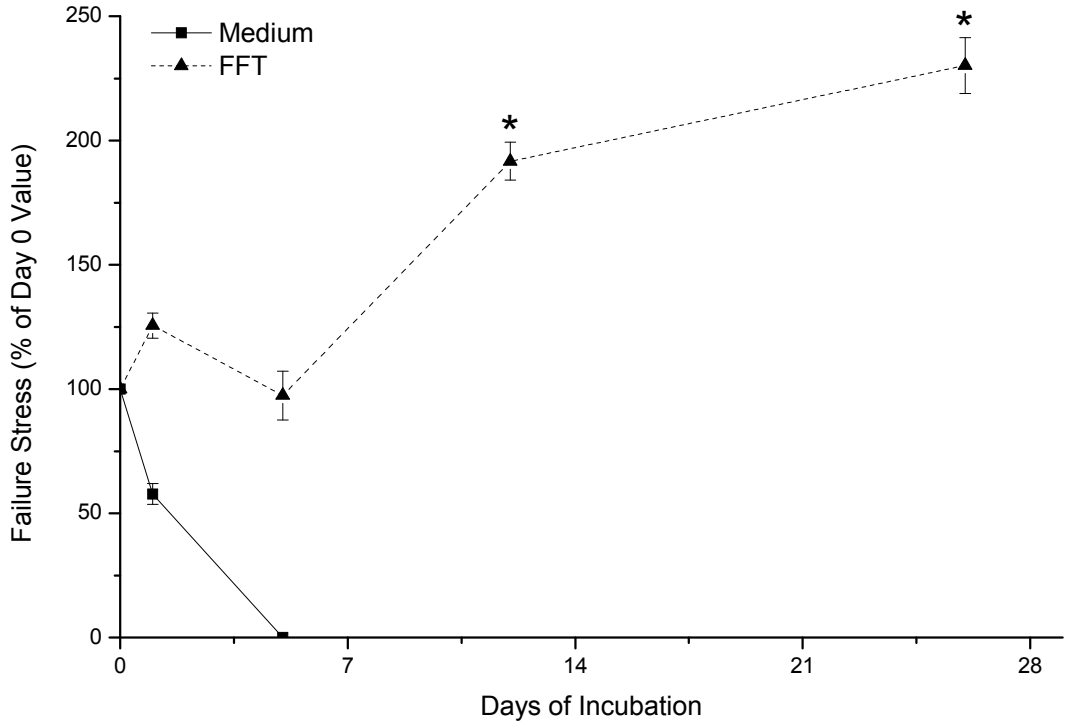

*Figure 10:15 Changing Failure Stress (σ_F) of scaffolds incubated in medium-only, and with FFT cells. *indicates significantly different ($p<0.05$) to Day 0 value. σ_F of medium-only scaffolds decreases rapidly and is negligible by Day 5, while σ_F of FFT-seeded scaffolds increases significantly over the course of the experiment.*

10.2.2.2 Material Changes

Figure 10:16 and Figure 10:17 show the denaturation temperature and FTIR spectra respectively of scaffolds incubated in different conditions. There are no significant changes in the denaturation temperature or FTIR peak wavenumbers of the scaffolds as a result of either incubation condition. However, there are differences in the FTIR spectra (Figure 10:17) of the scaffolds. The average spectrum for Day 26 medium-only does not change significantly compared to Day 1 unseeded scaffolds with the exception of a slight absorbance decrease and broadening of the Amide III peak. Conversely the Day 26 spectrum for FFT-seeded scaffolds exhibits increased Amide I and II peak absorbance compared with the Day 1 spectrum. As for the medium-only scaffolds, a broadening of the Amide III peak is seen.

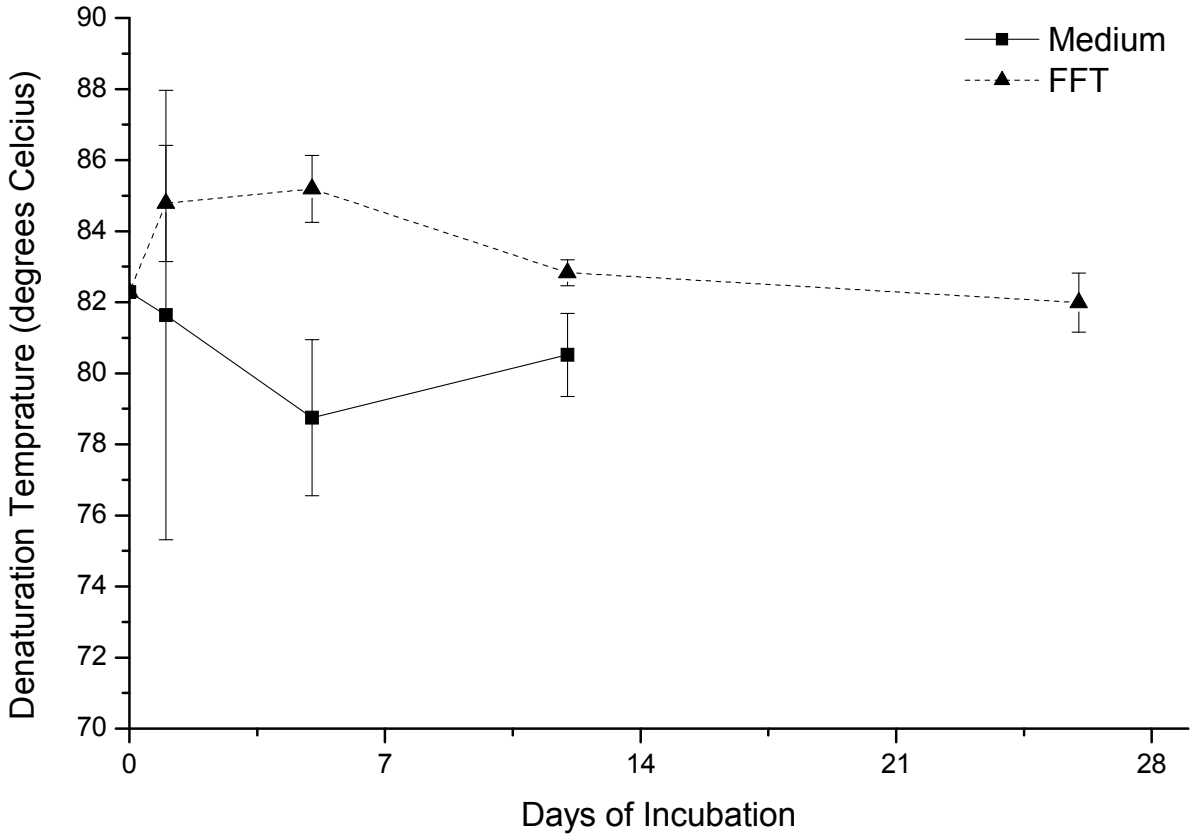

Figure 10:16 Changing denaturation temperature (D_T) of scaffolds after incubation in medium-only, and with FFT cells. By Day 26, scaffolds incubated in medium-only had degraded to such an extent that it was not possible to assess their D_T. However, there is no significant change in D_T of scaffolds throughout the course of the experiment, regardless of incubation condition.

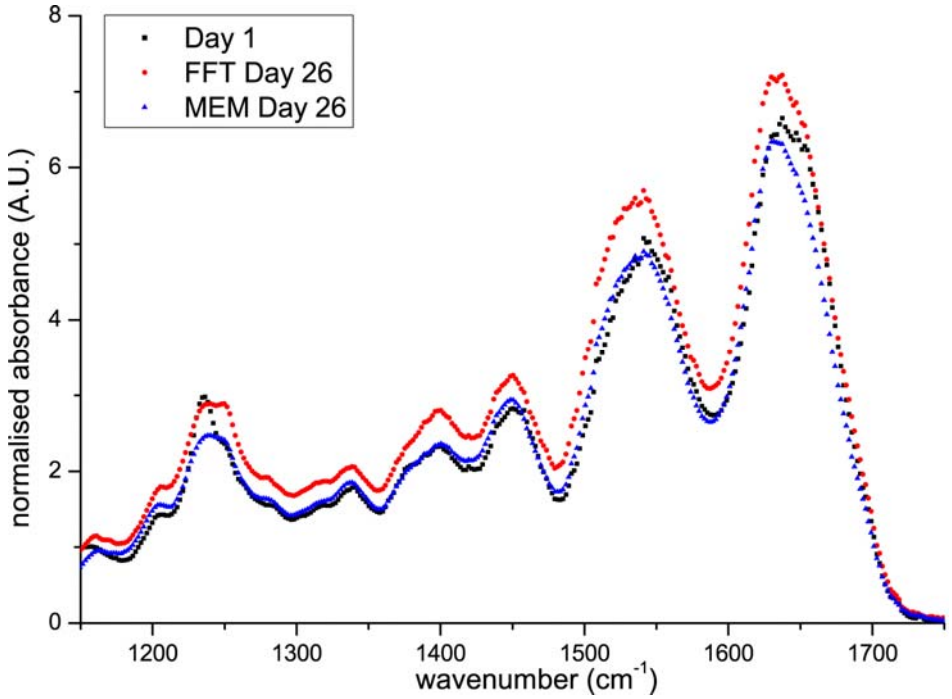

Figure 10:17 Average FTIR Spectra for scaffolds incubated in medium-only and with FFT cells in the fingerprint region (1150-1800cm-1). With the exception of a decrease in the Amide III peak, no significant change in amide peak absorbance is seen for medium-only scaffolds, while there are increases in Amide peak intensities for FFT-seeded scaffolds.

10.2.3 Culture Medium Changes

Figure 10:18 compares the changing culture medium content of sulfhydryl groups (-SH), indicative of cysteine amino acid concentration, and thus extent of scaffold degradation, for scaffolds incubated in different conditions. Sulfhydryl group concentration decrease by insignificant amounts for cell-seeded scaffolds but increase significantly for scaffolds incubated in medium only.

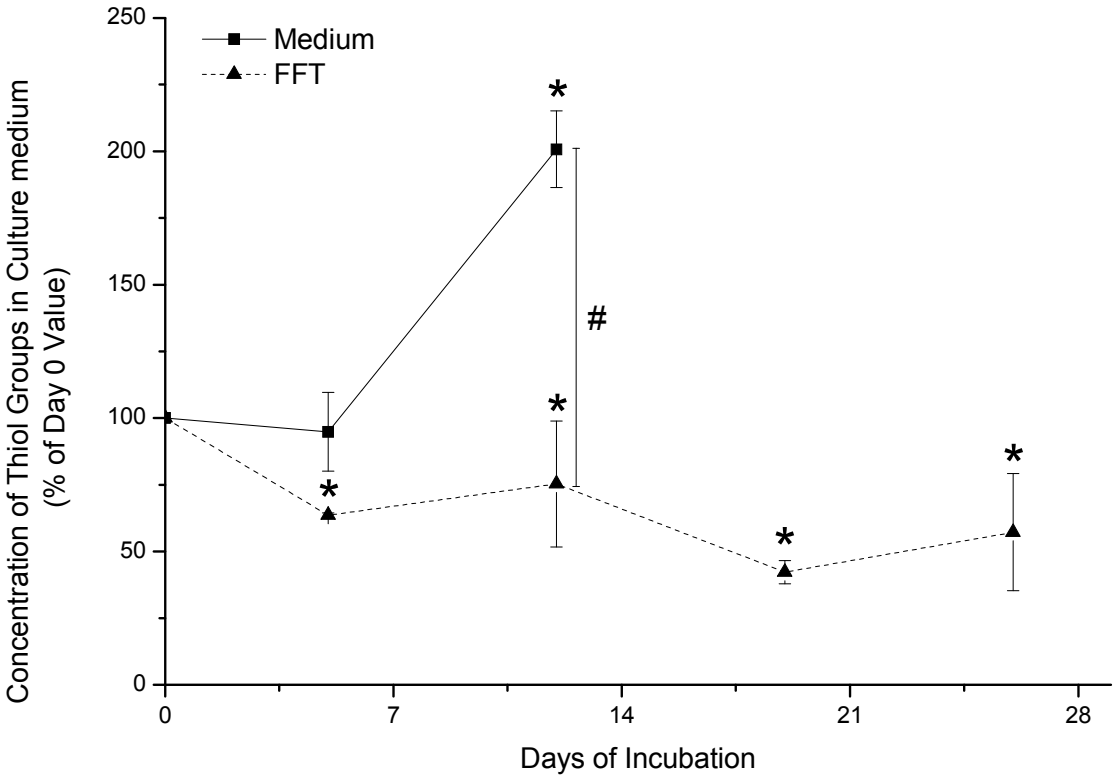

*Figure 10:18 Changing concentration of sulfhydryl groups (C_T) in culture medium after incubation in medium-only, and with FFT cells. *indicates a significant difference ($p<0.05$) to Day 0 value, $^{\#}$indicates a statistically significant difference ($p<0.05$) between results at a particular time point. There are significant decreases in C_T for scaffolds incubated with FFTs, while scaffolds incubated in medium-only exhibit significant increases in C_T by Day 12.*

10.3 DISCUSSION

10.3.1 Scaffold Suitability

Processing does not alter the intensity and position of the amide peaks of the scaffolds (Figure 10:3 pg. 174, and Table 10:1 pg. 175). It can therefore be concluded that processing does not alter their collagenous nature. With a high strain tensile modulus of 70.9kPa and a failure stress of 21.7 kPa (Table 10:2 pg. 176) the crosslinked scaffolds are stiffer and stronger than similar collagen scaffolds (e.g. [406]). However, they are less stiff and weaker than typical tendons and ligaments (wet tensile modulus 5-450MPa, wet UTS 2-50MPa [77, 430]). This is probably due to their high porosity, lack of structural hierarchy and low crosslinking density (indicated by their relatively low denaturation temperature, see Table 10:2 pg. 172) compared with soft tissues [431]).

Despite this, the scaffolds provide a suitable environment for 3D cell culture. The amount of viable biomass on collagen scaffolds as assessed using Alamar blue (Figure 10:4 pg. 177) follows the typical 'lag, log, lag' growth behaviour of tenocytes and fibroblasts cultured *in vitro*, only reaching a stationary phase after Day 13. This behaviour has been seen in previous studies of the *in vitro* behaviour of tenocytes from subscapularis tendon, supraspinatus tendon, Achilles tendon and foot flexor tendon (e.g. [432] and Figure 10:19). Hence the results indicate that the collagen scaffolds used in these experiments are not detrimental to cell proliferation.

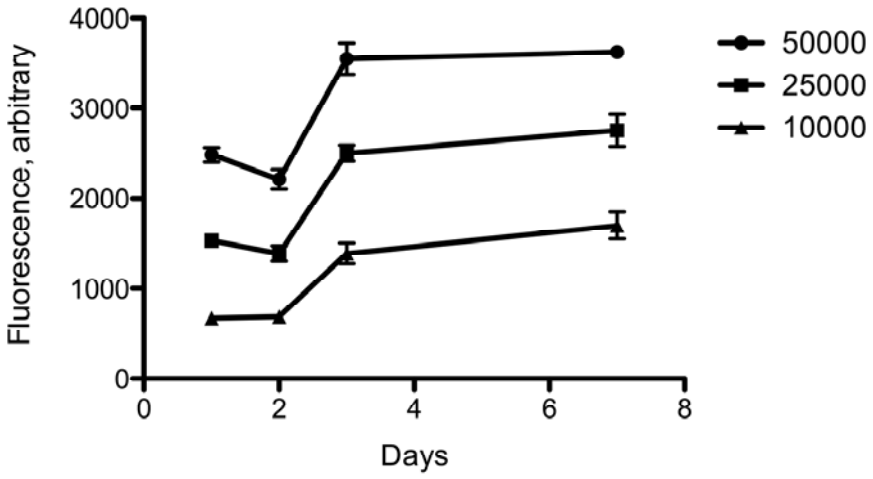

Figure 10:19 Changing amounts of viable biomass produced by rotator cuff tenocytes seeded in different densities as assessed by Alamar blue fluorescence. Cell behaviour shows the 'lag, log, lag' growth behaviour typical of tenocytes and fibroblasts cultured in vitro. These tenocytes were cultured in 96 well plates which have a smaller surface area; hence the second lag phase is reached more rapidly than in the current study. Graph courtesy of Dr. Osnat Hakimi.

Examination of the cell penetration profiles assessed using nuclear fast red-staining (Figure 10:5 pg. 6, and Figure 10:6 pg. 178) reveals that, despite concentrating 250-750μm from the scaffold edges, the cells are able to penetrate the scaffolds [433]. In agreement with the Alamar blue results (Figure 10:4 pg. 177) the penetration results also indicate that cell numbers increase significantly during the experiment. Therefore, the scaffolds appear to provide a suitable environment for 3D cell culture.

10.3.1.1 Mechanical Response

The results of mechanical testing suggest that scaffolds incubated in different conditions respond differently. The decreasing cross-sectional area (Figure 10:7 pg. 179) of scaffolds incubated in medium-only suggests that the scaffolds degrade rapidly in culture medium in the absence of cells. Conversely, seeding the scaffolds with cells appears to greatly reduce this medium-induced degradation; while the cross-sectional area of FFT-seeded scaffolds does decrease over the course of the experiment (Figure 10:7 pg. 179), this small decrease (approximately 15%) is probably the result of cell contraction [434, 435].

The results of the mechanical characterisation also indicate that proliferation of FFTs leads to significant improvements in the stress-bearing capabilities of the scaffolds; the low and high strain Tensile moduli (Figure 10:8 pg. 180, and Figure 10:9 pg. 181 respectively), heel stress, yield stress and failure stress (Figure 10:13 pg. 183, Figure 10:14 pg. 183 and Figure 10:15 pg. 184 respectively) of FFT-seeded scaffolds more than double their Day 0 values over 26 days. Thus it appears that, in addition to being able to protect the scaffolds from the rapid degradation caused by incubation in culture medium, FFT proliferation also improves the mechanical integrity of the scaffolds.

The scaffolds used in this study are porous, their properties depend on their relative density (density of structure divided by density of constituent material) [436]. Since no attempt was made to account for the effect of incubation on the porosity of the scaffolds, the mechanical measurements reported here are the *equivalent* properties of the structure, rather than the *actual* properties of the constituent material. Consequently, the mechanical changes reported here do not indicate material changes alone, but may also indicate structural changes. This phenomenon can be better understood by consideration of the's'-shaped stress-strain curve of a porous material.

Figure 10:20 presents a typical 's'-shaped stress strain curve produced when a porous material is tested under tension, together with pictorial representations of what is happening to the scaffold during testing, Table 10:3 outlines the definitions and origins of each different region on the graph in addition to the scaffold properties that affect these regions. Upon examination of these it can be seen that the mechanical behaviour of a porous material is significantly influenced by the porosity and internal architecture of the material. Changes in the mechanical response of a porous material are therefore likely to be related to changes in the porosity and internal architecture of the material. In other words, the increases in the mechanical properties of the FFT-seeded porous scaffolds presented here may be caused by changes in either the material properties of the constituent material, or the internal architecture of the scaffold itself. To investigate this further, the material properties of the scaffolds post-incubation were characterised (Section 10.2.2.2).

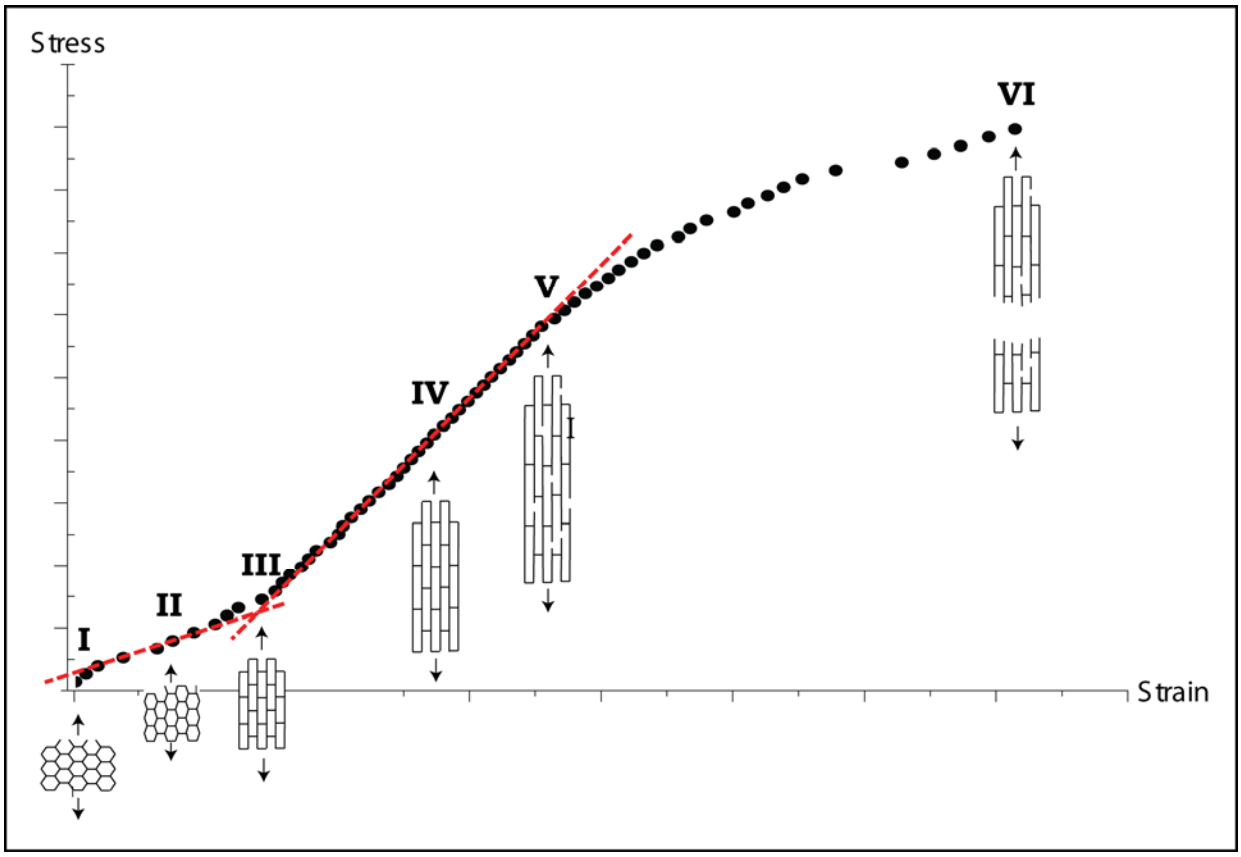

Figure 10:20 Pictorial depiction explaining how the deformation of a porous material under tensile load produces a stress-strain curve with a characteristic 's' shape.

Table 10:3 Explanation of the shape of a tensile stress-strain curve for a porous material

	Name	Characteristic Property	Definition	Influenced by	Comments
I	Neutral Point	n/a	Point at which the sample experiences no load	n/a	Rest position of the pores
II	Low Strain Linear Elastic Region	Low strain Tensile modulus, E_L	Pore walls that are not perpendicular to the primary stress axis want to align with the direction of applied stress. Resistance to the rotation provided by the walls perpendicular to the applied stress produces E_L	1. Internal angles of the pores 2. Cell wall thickness	
III	Heel Region	Heel strain, ε_H Heel stress, σ_H	Pore walls begin to align with the applied stress. Stiffness increases because the stress is now being applied directly to some of the pore walls.	1. Uniformity of pores, 2. Size of pores (smaller pores have less distance to travel and so align at much lower strains) 3. Ease of rotation of cell walls 4. Cell wall thickness 5. Tensile modulus of constituent material	If the pores are not uniform, the increase in stiffness will occur over a range of values, giving rise to a large heel region.
IV	High Strain Linear Elastic Region	High strain Tensile modulus, E_H	Stress is applied directly to the (now aligned) pore walls	1. Tensile modulus of constituent material 2. Pore wall thickness, 3. Uniformity of pore walls	Assumes no buckling of the pore walls aligned perpendicular to the applied stress
V	Yield Point	Yield strain, ε_Y Yield stress, σ_Y	Point at which pores begin to deform plastically and/or fail.	1. Yield Properties of constituent material 2. Failure Properties of constituent material, 3. Integrity and uniformity of pore walls	
VI	Failure Point	Failure strain, ε_F Failure stress, σ_F	Point of catastrophic failure when there are no intact cell walls remaining across the cross section of the sample	1. Failure Properties of constituent material	

10.3.1.2 Material Response

To further investigate the differing mechanical responses to incubation as discussed above (Section 10.3.1.1), the material properties of the scaffolds, as assessed by measurement of the scaffolds' denaturation temperature and FTIR spectra, were compared at different time points (Figure 10:16 pg. 185, and Figure 10:17 pg. 185 respectively). The results reveal that the changing mechanical properties are not caused by changes in the scaffolds' protein structure; the constant denaturation temperature of all scaffolds (see Figure 10:16 pg. 185) appears to suggests that the crosslinking density of the scaffolds does not change, while the lack of significant peak shifts in the FTIR spectra of these scaffolds (see Figure 10:17 pg. 3) reveals that there are no changes in the primary, secondary or tertiary structures of the proteins.

However, the FTIR spectra (Figure 10:17 pg. 185) do indicate differences in the amount of collagen present in the scaffolds, as indicated by changes in the amount of absorbance in the collagen fingerprint region. The average spectrum for Day 26 medium-only does not change significantly compared to Day 1 unseeded scaffolds with the exception of a slight decrease in the Amide III peak. This suggests that there are no significant compositional changes in these scaffolds. Conversely, the average spectrum for Day 26 FFT-seeded scaffolds exhibits increases in absorbance at the Amide I and Amide II peak positions. This indicates increased concentrations of collagen in the presence of FFTs [437] and suggests that, in addition to preventing the degradation of the scaffolds, seeding scaffolds with FFTs results in the deposition of increased amounts extracellular matrix.

To further investigate the behaviour of scaffolds incubated in different conditions, the sulfhydryl group (-SH) content of culture medium from FFT-seeded scaffolds and medium-only scaffolds was compared. Cysteine is a non-essential amino acid that contains sulfhydryl groups. Since it is found in type I collagen [429], collagen breakdown can be expected to release sulfhydryl groups to the culture medium. Despite the low sulfhydryl content of the type I collagen used in these experiments, a significant increase in sulfhydryl concentration was found in the culture medium aspirated from medium-only scaffolds (Figure 10:18 pg. 186). In agreement with the scaffold characterisation results discussed above, this suggests that large amounts of degradation are occurring when collagen scaffolds are incubated in culture medium only, and explains the rapid decreases in mechanical properties observed.

Conversely, the sulfhydroxyl concentration of medium aspirated from FFT-seeded scaffolds appears to decrease below background culture medium levels (Figure 10:18 pg. 186). This suggests that cells are significantly decreasing the rate of scaffold degradation and may even be absorbing any sulfhydryl-containing peptide fragments present in the culture medium either naturally or as products of degradation. This provides further evidence that the FFTs are able to both protect the scaffolds from degradation caused by culture medium and concurrently improve the scaffolds' mechanical properties by laying down new ECM.

The mechanism of rapid scaffold degradation in culture medium is not clear. A possible explanation is that, in the absence of cells, collagen degrades by hydrolysis in culture medium, releasing small peptide fragments to the culture medium [411]. Studies as early as 1960 were reporting that 'dilute organic acids or by various salts at neutral or slightly basic pH' [438] result in changing dissolution behaviour of collagen [439]. For example, Everaerts et al showed that, for scaffolds incubated in buffer, exposure to alkaline pH results in hydrolysation of the ester bonds (a small number of which are created during EDC/NHS crosslinking), producing a subsequent decrease in scaffold stiffness [440]. Thorough discussions of hydrolysation and degradation of collagen in the presence of various acids, bases, salts and solvents can be found in 'Treatise on Collagen' [441].

Unfortunately, whilst the incubation of collagen scaffolds with enzymes and cells is commonly reported in the literature, a thorough literature search has not revealed any studies that have presented data on the degradation of collagen exposed culture medium only. However, as Traub et al note, 'collagen exists naturally as a solid phase and usually cannot be taken into solution by any procedure not involving hydrolysis' [442]. It is possible that, in the absence of cells, changes in pH of the culture medium are driving the degradation of the scaffolds, hydrolyzing the collagen scaffolds and causing associated decreases in mechanical properties. Conversely, tenocytes should be able to digest these fragments, and therefore remove them from the system. This would produce a similar effect to that of dynamic flow which prevents autocatalysis through the removal of peptide fragments [397]. However, as the pH of incubation medium over the course of the experiment was not assessed the assertion that scaffolds degrade by hydrolysis in the absence of cells is speculative. The mechanisms underlying the changing properties of scaffolds incubated in medium and with cells should now be investigated.

10.4 SUMMARY, LIMITATIONS AND FURTHER WORK

The work presented in this chapter has provided evidence to support the hypothesis that tenocyte proliferation on collagen scaffolds alters the degradation behaviour of collagen scaffolds whilst improving scaffold mechanical properties. Specifically, tenocyte proliferation appears to slow the rate of scaffold degradation in culture medium, whilst increasing scaffold stiffness and strength over a 26-day incubation period. However, this investigation is limited by a number of factors.

Firstly, this study is limited by the difficulties associated with mechanically testing weak collagen scaffolds. Whilst extreme care has to be taken to eliminate clamp effects by excluding all samples that failed at the clamps, a more effective method might have been to test the samples in compression. Were this approach to have been chosen, however, it would have been more appropriate to seed the scaffolds with chondrocytes rather than with tenocytes. A future study investigating the effect of chondrocyte proliferation on the compressive mechanical properties of collagen scaffolds would be very interesting.

A second potential limitation of this study is the tenocyte source. The cells used in this study originate from a 75-year-old patient with decreased blood flow. However, as tendon is a relatively avascular tissue, decreased blood flow is unlikely to have a significant effect on the health of the tenocytes. Moreover, while a higher degree of senescent cells may be expected due to the patient's age and potential decreased mobility, these will have been eliminated during the passage and seeding processes. It is therefore not expected that tenocyte source will have a significant effect on the results presented here, although this should be investigated further. In particular further experimental investigations should assess the ability of tenocytes derived from damaged tissue to protect and modify collagen scaffolds, as this would be more relevant to the clinical problem [432].

The most important limitation of this study lies in the fact that it was designed to characterise the changing material properties (mechanical, compositional, structural) of scaffolds incubated under different conditions. As such this study has not investigated the underlying mechanisms of scaffold degradation by culture medium and the improvement of scaffold mechanical properties by tenocytes. To better understand the mechanisms by which cell proliferation protects against scaffold degradation,

further investigations into the behaviour of collagen in the absence and presence of cells, with a particular focus on the degradation mechanisms in the absence of cells, are strongly recommended.

Regardless of these limitations, however, this study highlights the important role cells play in the regulation of the properties of biological materials.

PART V

THESIS SUMMARY

Chapter Eleven

Conclusions and Further Work

Degenerative disorders of the rotator cuff tendons account for nearly 75% of all shoulder pain, causing considerable pain and morbidity. Improved understanding of tendon degeneration will guide the development of future diagnostic and treatments, and is therefore urgently needed. However, the aetiology and pathology of rotator cuff tendinopathy remain unclear. The work in this thesis has investigated the material adaptations of healthy and diseased tendons in order to explore the role of mechanical loading in rotator cuff aetiology and pathology.

The material adaptations of healthy bovine digital flexor and ovine infraspinatus tendons were characterised to gain insight into the adaptations of healthy wrap-around tendons in response to different loading environments (Chapter 4). The structural adaptations of healthy and delaminated cadaveric rotator cuffs were also mapped topographically and were compared with the mechanical environment predicted by finite element models (Chapter 3). The effects of age, tears, steroid injection and subacromial decompression surgery on the adaptations of cuff tendons were then characterised (Chapter 7 and Chapter 9). Finally, the effect of tendon cell proliferation on the mechanical properties and degradation behaviour of collagen scaffolds was studied (Chapter 10). Based on the results of these investigations a number of important conclusions can be drawn.

11.1 APPROPRIATE ANALYSIS TECHNIQUES

The results of Chapter 4 provide evidence that atomic force microscopy (AFM) and picrosirius red staining are highly suitable techniques for analysing the structural adaptations of formalin-fixed, wax-embedded tendon samples (see Chapter 4, Sections 4.2.2 and 4.2.3). The results also reveal that alcian blue staining is unsuitable for detailed studies of inter-fibre and inter-fascicle ground substance content, but that Raman spectroscopy is a promising technique for the analysis of inter-fibrillar ground substance content

(see Chapter 4, Section 4.2.1). Regarding micromechanical analysis, the results indicate that the use of AFM-indentation and nanoindentation to characterise small, glass-mounted tissue samples is not straightforward (see Chapter 4, Section 4.2.4).

Based on these findings, future studies should investigate alternative methods for assessment of *inter-fibre* and *inter-fascicle* ground substance content, with the aim of developing a simple, reproducible technique that provides a greater degree of precision and accuracy in such studies. Further investigation into Raman spectroscopy for the characterisation of *inter-fibrillar* ground substance content is also strongly recommended. Additional experimental investigations should also aim to establish appropriate methodologies and data analysis algorithms for AFM-indentation and nanoindentation studies. Such improved techniques would be immediately applicable to the study of tendon, and could provide valuable insight into the aetiology and pathology of tendinopathy as well as other soft tissues diseases.

11.2 MECHANICAL ENVIRONMENT AND MATERIAL ADAPTATIONS

The findings presented in Chapter 4 and Chapter 6 provide evidence to support the hypothesis that the mechanical environment of tendon significantly influences its material adaptations. Specifically, they demonstrate that tendon exposed to compressive, shear and tensile strains exhibits thinner, less aligned fibrils (Chapter 4, Section 4.2.3), a higher proportion of thinner fibres and shorter crimp lengths (Chapter 4, Section 4.2.2) and a higher proportion of ground substance (Chapter 4 Section 4.2.1) compared with regions of tendon exposed to tensile strains alone. In healthy rotator cuff tendons, the inhomogeneous loading environment causes the tendons to exhibit topographically inhomogeneous structural adaptations (Chapter 6, Sections 6.2.1 and 6.2.3), a characteristic that may pre-dispose the tendon to degeneration and tearing. Work presented in Chapter 7 also provides evidence that age plays a significant role in the structural adaptations of tendon. Specifically, tendon from older patients displays thicker fibrils, longer crimp lengths and a lower proportion of thinner fibres (Chapter 7, Sections 7.2.1 to 7.2.5). The effect of aging on the topographical variation in structural adaptations of the rotator cuff has not been investigated in the current study but is expected to be important.

Further work should now investigate the relationship between the structural adaptations of tendons and their associated mechanical properties in order to establish whether such adaptations are indeed pre-

disposing the cuff tendons to degeneration and tearing. The results of such studies could have important implications for the prevention and treatment of rotator cuff tendinopathy. The effect of age on the topographical variation in the structural adaptations of the cuff tendons and their ability to repair mechanical damage should also be investigated, as this may also play a critical role in rotator cuff tendinopathy.

11.3 DEGENERATIVE AND TORN TENDONS

The findings presented in Chapter 6 and Chapter 7 support the hypothesis that the presence and progression of rotator cuff tears is associated with increased levels of compressive and/or shear strain within the tendon. Specifically, tendons from a delaminated rotator cuff display a reduced degree of topographical variation of structural adaptation, and thinner, less aligned fibrils compared with macroscopically normal cuff tendons (Chapter 6, Section 6.2.1 to 6.2.3), while torn cuff tendons display thinner fibrils and shorter crimp lengths compared with control samples (Chapter 7, Section 7.2.1 and 7.2.5). These adaptations occur early in the disease progression, with partially torn tendons exhibiting significant structural differences compared with control samples (Chapter 7, Section 7.2). The findings also indicate that the adaptations are progressive with tear size (Chapter 7, Section 7.2) when age is included as a confounding factor, providing further evidence for the importance of age and compressive and/or shear loading in rotator cuff pathology.

Importantly, neither steroid injection not sub-acromial decompression significantly influence the structural adaptations on partially torn rotator cuff tendons (Chapter 9, Section 9.2). While this suggests that neither treatment is detrimental to tendon properties, it also indicates that neither treatment is able to reverse the pathological adaptations of degenerative and torn tendons in the time frame investigated in the current study. Further work is now needed to investigate the effect of the two interventions over a much longer timescale. Additionally, research presented here should be extended to include surgically repaired tissue, as very little is known regarding the effect of repair on the structural properties of torn rotator cuff tendons.

These findings have important clinical implications. In particular, they emphasis the urgent clinical need for pre-rupture diagnostic techniques capable of detecting of early pathological changes in the rotator cuff, in order that action can be taken to prevent further degeneration of the tissue. Concurrently, the results highlight the requirement for new and/or improved early interventions strategies that restore the healthy mechanical environment of the cuff tendons and reverse the initial pathological adaptations so as to prevent subsequent catastrophic, often irreparable, failure of the cuff tendons. Further work should now aim to establish biomarkers detectable early in the disease progression, possibly those linked to the regulation of the structural adaptations of tendon, which could be used as targets for novel therapies.

11.4 TENOCYTE PROLIFERATION ON COLLAGEN SCAFFOLDS

The findings presented in Chapter 10 demonstrate the influence of cellular proliferation on the properties of biological materials. Specifically, they demonstrate that tenocytes are able to alter both the degradation behaviour and mechanical properties of collagen scaffolds incubated *in vivo*, slowing the rate of degradation and increasing their mechanical properties (Chapter 10, Section 10.2.2). These findings have important implications for the viability of the tissue engineering approach, and also highlight the integral role cells play in the functional adaptation of biological materials.

As the research in Chapter 10 was designed solely to investigate the changing material properties of scaffolds incubated under different conditions, further work is now needed to evaluate the underlying mechanisms governing this behaviour. In particular, the work should be extended to study the ability of tenocytes derived from degenerated and torn rotator cuff tendon to protect and modify collagen scaffolds. This would be of considerable clinical relevance, and could provide further insight into the aetiology and pathology of rotator cuff tendinopathy.

Bibliography

1. Oxford Concise Colour Medical Dictionary, 1st edition (1996). E.A. Martin (Ed.). Oxford University Press, Oxford.
2. Marieb, E.N., (2001). Human Anatomy & Physiology, 5th edition. Edited by.Benjamin Cummings, San Francisco / London.
3. Yeovil Elbow and Shoulder Service (2009). Information for You after Your Operation: Anterior Stabilisation of the Shoulder. Published by Yeovil District Hospital, NHS Foundation Trust. Accessed on 05/05/11. Available from http://www.yeovilhospital.nhs.uk/Downloads/Patient%20information%20leaflets/Orthopaedics/Anterior-stabilisation-of-the-shoulder-post-op.pdf
4. Kujala, U.M., Sarna, S., and Kaprio, J., (2005). Cumulative Incidence of Achilles Tendon Rupture and Tendinopathy in Male Former Elite Athletes. **Clinical Journal of Sport Medicine** 15(3); p.133-5.
5. Kvist, M., (1991). Achilles Tendon Injuries. Submitted for the degree of PhD Thesis at University of Turku, Finland,.
6. Sein, M.L., Walton, J., Linklater, J., Appleyard, R., Kirkbride, B., Kuah, D., and Murrell, G.A., (2010). Shoulder Pain in Elite Swimmers: Primarily Due to Swim-Volume-Induced Supraspinatus Tendinopathy. **British Journal of Sports Medicine** 44(2); p.105-13.
7. Heinlein, S.A. and Cosgarea, A.J., (2010). Biomechanical Considerations in the Competitive Swimmer's Shoulder. **Sports Health: A Multidisciplinary Approach** 2(6); p.519-25.
8. Carroll, R., (1981). Tennis Elbow: Incidence in Local League Players. **British Journal of Sports Medicine** 15(4); p.250-6.
9. Nirschl, R.P., (1974). The Etiology and Treatment of Tennis Elbow. **Journal of Sports Medicine** 2(6); p.308-23.
10. Gruchow, H.W. and Pelletier, D., (1979). An Epidemiologic Study of Tennis Elbow. Incidence, Recurrence, and Effectiveness of Prevention Strategies. **America Journal of Sports Medicine** 7(4); p.234-8.
11. Cook, J.L., Khan, K.M., Harcourt, P.R., Kiss, Z.S., Fehrmann, M.W., Griffiths, L., and Wark, J.D., (1998). Patellar Tendon Ultrasonography in Asymptomatic Active Athletes Reveals Hypoechoic Regions: A Study of 320 Tendons. Victorian Institute of Sport Tendon Study Group. **Clinical Journal of Sport Medicine** 8(2); p.73-7.
12. Lian, O.B., Engebretsen, L., and Bahr, R., (2005). Prevalence of Jumper's Knee among Elite Athletes from Different Sports: A Cross-Sectional Study. **America Journal of Sports Medicine** 33(4); p.561-7.
13. Major, N.M. and Helms, C.A., (2002). Mr Imaging of the Knee: Findings in Asymptomatic Collegiate Basketball Players. **American Journal of Roentgenology** 179(3); p.641-4.
14. U. S. Department of Labor, Bureau of Labor Statistics., (2004). Incidence Rates for Nonfatal Occupational Injuries and Illnesses Involving Days Away from Work Per 10,000 Full-Time Workers for Selected Characteristics and Industry Division, United States, 2002. U.S. Department of Labor.
15. Jacobsson, L., Lindgarde, F., and Manthorpe, R., (1989). The Commonest Rheumatic Complaints of over Six Weeks' Duration in a Twelve-Month Period in a Defined Swedish Population. Prevalences and Relationships. **Scandinavian Journal of Rheumatology** 18(6); p.353-60.
16. Rolf, C. and Movin, T., (1997). Etiology, Histopathology, and Outcome of Surgery in Achillodynia. **Foot and Ankle International** 18(9); p.565-9.
17. Maffulli, N., Sharma, P., and Luscombe, K.L., (2004). Achilles Tendinopathy: Aetiology and Management. **Journal of the Royal Society of Medicine** 97(10); p.472-6.
18. Allander, E., (1974). Prevalence, Incidence, and Remission Rates of Some Common Rheumatic Diseases or Syndromes. **Scandinavian Journal of Rheumatology** 3(3); p.145-53.
19. Ostor, A.J., Richards, C.A., Prevost, A.T., Speed, C.A., and Hazleman, B.L., (2005). Diagnosis and Relation to General Health of Shoulder Disorders Presenting to Primary Care. **Rheumatology** 44(6); p.800-5.
20. Ozaki, J., Fujimoto, S., Nakagawa, Y., Masuhara, K., and Tamai, S., (1988). Tears of the Rotator Cuff of the Shoulder Associated with Pathological Changes in the Acromion. A Study in Cadavera. **Journal of Bone and Joint Surgery - American Version** 70(8); p.1224-30.

21. Yamamoto, A., Takagishi, K., Osawa, T., Yanagawa, T., Nakajima, D., Shitara, H., and Kobayashi, T., (2010). Prevalence and Risk Factors of a Rotator Cuff Tear in the General Population. **Journal of Shoulder and Elbow Surgery** 19(1); p.116-20.
22. Cotton, R.E. and Rideout, D.F., (1964). Tears of the Humeral Rotator Cuff; a Radiological and Pathological Necropsy Survey. **Journal of Bone and Joint Surgery - British Version** 46(2); p.314-28.
23. Tempelhof, S., Rupp, S., and Seil, R., (1999). Age-Related Prevalence of Rotator Cuff Tears in Asymptomatic Shoulders. **Journal of Shoulder and Elbow Surgery** 8(4); p.296-9.
24. Wilson, C.L. and Duff, G.L., (1943). Pathologic Study of Degeneration and Rupture of the Supraspinatus Tendon. **Archives of Surgery** 47(2); p.121-35.
25. Cofield, R.H., Parvizi, J., Hoffmeyer, P.J., Lanzer, W.L., Ilstrup, D.M., and Rowland, C.M., (2001). Surgical Repair of Chronic Rotator Cuff Tears. A Prospective Long-Term Study. **Journal of Bone and Joint Surgery - American Version** 83-A(1); p.71-7.
26. Hagberg, M. and Wegman, D.H., (1987). Prevalence Rates and Odds Ratios of Shoulder-Neck Diseases in Different Occupational Groups. **British Journal of Industrial Medicine** 44(9); p.602-10.
27. Arner, O., Lindholm, A., and Orell, S.R., (1959). Histologic Changes in Subcutaneous Rupture of the Achilles Tendon; a Study of 74 Cases. **Acta Chirurgica Scandinavica** 116(5-6); p.484-90.
28. Kannus, P. and Jozsa, L., (1991). Histopathological Changes Preceding Spontaneous Rupture of a Tendon. A Controlled Study of 891 Patients. **Journal of Bone and Joint Surgery - American Version** 73(10); p.1507-25.
29. Nobuhara, K., Hata, Y., and Komai, M., (1994). Surgical Procedure and Results of Repair of Massive Tears of the Rotator Cuff. **Clinical Orthopaedics and Related Research** 304(304); p.54-9.
30. Hashimoto, T., Nobuhara, K., and Hamada, T., (2003). Pathologic Evidence of Degeneration as a Primary Cause of Rotator Cuff Tear. **Clinical Orthopaedics and Related Research** 415(415); p.111-20.
31. Hashimoto, T., Nobuhara, K., and Hamada, T., (2003). Pathologic Evidence of Degeneration as a Primary Cause of Rotator Cuff Tear. **Clinical Orthopaedics & Related Research** 415(Journal Article); p.111-20.
32. Yuan, J., Murrell, G.A., Wei, A.Q., and Wang, M.X., (2002). Apoptosis in Rotator Cuff Tendonopathy. **Journal of Orthopaedic Research** 20(6); p.1372-9.
33. Sano, H., Wakabayashi, I., and Itoi, E., (2006). Stress Distribution in the Supraspinatus Tendon with Partial-Thickness Tears: An Analysis Using Two-Dimensional Finite Element Model. **Journal of Shoulder and Elbow Surgery** 15(1); p.100-05.
34. Wakabayashi, I., Itoi, E., Sano, H., Shibuya, Y., Sashi, R., Minagawa, H., and Kobayashi, M., (2003). Mechanical Environment of the Supraspinatus Tendon: A Two-Dimensional Finite Element Model Analysis. **Journal of Shoulder and Elbow Surgery** 12(6); p.612-7.
35. Adams, C.R., Baldwin, M.A., Laz, P.J., Rullkoetter, P.J., and Langenderfer, J.E., (2007). Effects of Rotator Cuff Tears on Muscle Moment Arms: A Computational Study. **Journal of Biomechanics** 40(15); p.3373-80.
36. Riley, G.P., Harrall, R.L., Constant, C.R., Chard, M.D., Cawston, T.E., and Hazleman, B.L., (1994). Glycosaminoglycans of Human Rotator Cuff Tendons: Changes with Age and in Chronic Rotator Cuff Tendinitis. **Annals of the Rheumatic Diseases** 53(6); p.367-76.
37. Parry, D.A.D., Barnes, G.R.G., and Craig, A.S., (1978). A Comparison of the Size Distribution of Collagen Fibrils in Connective Tissues as a Function of Age and a Possible Relation between Fibril Size Distribution and Mechanical Properties. **Proceedings of the Royal Society of London. Series B, Biological Sciences** 203(1152); p.305-21.
38. Feitosa, V., Vidal, B.C., and Pimentel, E.R., (2002). Optical Anisotropy of a Pig Tendon under Compression. **Journal of Anatomy** 200(Pt 1); p.105-11.
39. Fukuda, H., Hamada, K., and Yamanaka, K., (1990). Pathology and Pathogenesis of Bursal-Side Rotator Cuff Tears Viewed from En Bloc Histologic Sections. **Clinical Orthopaedics and Related Research** 254(254); p.75-80.
40. Lo, I.K., Marchuk, L.L., Hollinshead, R., Hart, D.A., and Frank, C.B., (2004). Matrix Metalloproteinase and Tissue Inhibitor of Matrix Metalloproteinase Mrna Levels Are Specifically Altered in Torn Rotator Cuff Tendons. **America Journal of Sports Medicine** 32(5); p.1223-9.
41. Schmutz, S., Fuchs, T., Regenfelder, F., Steinmann, P., Zumstein, M., and Fuchs, B., (2009). Expression of Atrophy Mrna Relates to Tendon Tear Size in Supraspinatus Muscle. **Clinical Orthopaedics and Related Research** 467(2); p.457-64.

42. Benjamin, M. and Ralphs, J.R., (1998). Fibrocartilage in Tendons and Ligaments — an Adaptation to Compressive Load. **Journal of Anatomy** 193(04); p.481-94.
43. Chaudhury, S., Holland, C., Porter, D., Tirlapur, U.K., Vollrath, F., and Carr, A.J., (2011). Torn Human Rotator Cuff Tendons Have Reduced Collagen Thermal Properties on Differential Scanning Calorimetry. **Journal of Orthopaedic Research** 29(12); p.1938-43.
44. Tilley, J.M.R., Carr, A.J., and Czernuszka, J.T., (2011). Atomic Force Microscopy of Bulk Tendon Samples: Affect of Location and Fixation on Tissue Ultrastructure. **Micron** 42(5); p.531-35.
45. Brewer, B.J., (1979). Aging of the Rotator Cuff. **America Journal of Sports Medicine** 7(2); p.102-10.
46. Bloom, D.E. and Canning, D., (2004). Global Demographic Change: Dimensions and Economic Significance. **National Bureau of Economic Research Working Paper Series** No. 10817(
47. König, H.E., Liebich, H.-G., and Bragulla, H., (2007). Veterinary Anatomy of Domestic Mammals : Textbook and Colour Atlas. Schattauer, Stuttgart; New York.
48. Martini, F.H., (1989). Articulations. In **Fundamentals of Anatomy and Physiology**. Edited by D.K. Brake Prentice Hall International, New Jersey.
49. Rumian, A.P., Wallace, A.L., and Birch, H.L., (2007). Tendons and Ligaments Are Anatomically Distinct but Overlap in Molecular and Morphological Features- a Comparative Study in an Ovine Model. **Journal of Orthopaedic Research** 25(4); p.458-64.
50. Woo, S.L., Debski, R.E., Zeminski, J., Abramowitch, S.D., Saw, S.S., and Fenwick, J.A., (2000). Injury and Repair of Ligaments and Tendons. **Annual Review of Biomedical Engineering** 2(2); p.83-118.
51. Amiel, D., Frank, C., Harwood, F., Fronek, J., and Akeson, W., (1983). Tendons and Ligaments: A Morphological and Biochemical Comparison. **Journal of Orthopaedic Research** 1(3); p.257-65.
52. Carpenter, J.E. and Hankenson, K.D., (2004). Animal Models of Tendon and Ligament Injuries for Tissue Engineering Applications. **Biomaterials** 25(9); p.1715-22.
53. Alberts, B., Bray, D., Lewis, J., Raff, M., Roberts, K., and Watson, J.D., (1994). Cell Junctions, Cell Adhesion, and the Extracellular Matrix. In **Molecular Biology of the Cell**. Edited by M. Robertson Garland Publishing, New York.
54. Cowin, S.C. and Doty, S.B., (2007). Collagen. In **Tissue Mechanics**. Edited by Springer, New Jersey.
55. Parry, D.A., (1988). The Molecular and Fibrillar Structure of Collagen and Its Relationship to the Mechanical Properties of Connective Tissue. **Biophysical Chemistry** 29(1-2); p.195-209.
56. Hukins, D.W.L., Leahy, J.C., and Mathias, K.J., (1999). Biomaterials: Defining the Mechanical Properties of Natural Tissues and Selection of Replacement Materials. **Journal of Materials Chemistry** 9(3); p.629-36.
57. Kadler, K.E., Holmes, D.F., Trotter, J.A., and Chapman, J.A., (1996). Collagen Fibril Formation. **Biochemical Journal** 316(1); p.1-11.
58. Diamant, J., Keller, A., Baer, E., Litt, M., and Arridge, R.G., (1972). Collagen; Ultrastructure and Its Relation to Mechanical Properties as a Function of Ageing. **Proceedings of the Royal Society of London. Series B, Containing papers of a Biological character** 180(60); p.293-315.
59. Funakoshi, T., Majima, T., Suenaga, N., Iwasaki, N., Yamane, S., and Minami, A., (2006). Rotator Cuff Regeneration Using Chitin Fabric as an Acellular Matrix. **Journal of Shoulder and Elbow Surgery** 15(1); p.112-8.
60. Fan, L., Sarkar, K., Franks, D.J., and Uhthoff, H.K., (1997). Estimation of Total Collagen and Types I and Iii Collagen in Canine Rotator Cuff Tendons. **Calcified Tissue International** 61(3); p.223-9.
61. Riley, G.P., Harrall, R.L., Constant, C.R., Chard, M.D., Cawston, T.E., and Hazleman, B.L., (1994). Tendon Degeneration and Chronic Shoulder Pain: Changes in the Collagen Composition of the Human Rotator Cuff Tendons in Rotator Cuff Tendinitis. **Annals of the Rheumatic Diseases** 53(6); p.359-66.
62. Hadjicostas, P.T., Soucacos, P.N., Koleganova, N., Krohmer, G., and Berger, I., (2008). Comparative and Morphological Analysis of Commonly Used Autografts for Anterior Cruciate Ligament Reconstruction with the Native Acl: An Electron, Microscopic and Morphologic Study. **Knee Surgery, Sports Traumatology, Arthroscopy** 16(12); p.1099-107.
63. Carvalho, H.F., Felisbino, S.L., Keene, D.R., and Vogel, K.G., (2006). Identification, Content, and Distribution of Type Vi Collagen in Bovine Tendons. **Cell and Tissue Research** 325(2); p.315-24.
64. Lakes, R., (1993). Materials with Structural Hierarchy. **Nature** 361(6412); p.511-15.
65. Kastelic, J., Galeski, A., and Baer, E., (1978). The Multicomposite Structure of Tendon. **Connective Tissue Research** 6(1); p.11-23.

66. Gupta, H.S., Seto, J., Krauss, S., Boesecke, P., and Screen, H.R., (2010). In Situ Multi-Level Analysis of Viscoelastic Deformation Mechanisms in Tendon Collagen. **Journal of Structural Biology** 169(2); p.183-91.
67. Sasaki, N. and Odajima, S., (1996). Elongation Mechanism of Collagen Fibrils and Force-Strain Relations of Tendon at Each Level of Structural Hierarchy. **Journal of Biomechanics** 29(9); p.1131-36.
68. Sasaki, N. and Odajimat, S., (1996). Stress-Strain Curve and Young's Modulus of a Collagen Molecule as Determined by the X-Ray Diffraction Technique. **Journal of Biomechanics** 29(5); p.655-58.
69. Screen, H.R.C., Lee, D.A., Bader, D.L., and Shelton, J.C., (2004). An Investigation into the Effects of the Hierarchical Structure of Tendon Fascicles on Micromechanical Properties. **Proceedings of the Institution of Mechanical Engineers Part H-Journal of Engineering in Medicine** 218(H2); p.109-19.
70. TheEngineeringToolbox, Elastic Properties and Young Modulus for Some Materials. Published by Accessed on. Available from
71. Kadler, K., (2004). Matrix Loading: Assembly of Extracellular Matrix Collagen Fibrils During Embryogenesis. **Birth Defects Research Part C: Embryo Today** 72(1); p.1-11.
72. Willett, T.L., Labow, R.S., Avery, N.C., and Lee, J.M., (2007). Increased Proteolysis of Collagen in an in Vitro Tensile Overload Tendon Model. **Annals of Biomedical Engineering** 35(11); p.1961-72.
73. Smith, J.R., (2011). The Changing Properties of Tendon: An Investigation Bridging the Gap between Mechanical Properties and Matrix Composition in Bovine Tendon. Submitted for the degree of MEng at University of Oxford.
74. Walker, L.B., Harris, E.H., and Benedict, J.V., (1964). Stress-Strain Relationship in Human Cadaveric Plantaris Tendon: A Preliminary Study. **Medical Electronics and Biological Engineering** 2(1); p.31-8.
75. Maganaris, C.N. and Paul, J.P., (1999). In Vivo Human Tendon Mechanical Properties. **J Physiol** 521 Pt 1(1); p.307-13.
76. Rigby, B.J., Hirai, N., Spikes, J.D., and Eyring, H., (1959). The Mechanical Properties of Rat Tail Tendon. **Journal of General Physiology** 43(2); p.265-83.
77. Kato, Y.P., Christiansen, D.L., Hahn, R.A., Shieh, S.J., Goldstein, J.D., and Silver, F.H., (1989). Mechanical Properties of Collagen Fibres: A Comparison of Reconstituted and Rat Tail Tendon Fibres. **Biomaterials** 10(1); p.38-42.
78. Pins, G.D. and Silver, F.H., (1995). A Self-Assembled Collagen Scaffold Suitable for Use in Soft and Hard Tissue Replacement. **Materials Science & Engineering C-Biomimetic Materials Sensors and Systems** 3(2); p.101-07.
79. Grant, C.A., Brockwell, D.J., Radford, S.E., and Thomson, N.H., (2009). Tuning the Elastic Modulus of Hydrated Collagen Fibrils. **Biophysical Journal** 97(11); p.2985-92.
80. Yang, L., van der Werf, K.O., Fitie, C.F., Bennink, M.L., Dijkstra, P.J., and Feijen, J., (2008). Mechanical Properties of Native and Cross-Linked Type I Collagen Fibrils. **Biophysical Journal** 94(6); p.2204-11.
81. van der Rijt, J.A.J., van der Werf, K.O., Bennink, M.L., Dijkstra, P.J., and Feijen, J., (2006). Micromechanical Testing of Individual Collagen Fibrils. **Macromolecular Bioscience** 6(9); p.697-702.
82. Wenger, M.P., Bozec, L., Horton, M.A., and Mesquida, P., (2007). Mechanical Properties of Collagen Fibrils. **Biophysical Journal** 93(4); p.1255-63.
83. Dourte, L.M., Kuntz, A.F., and Soslowsky, L.J., (2008). Twenty-Five Years of Tendon and Ligament Research. **Journal of Orthopaedic Research** 26(10); p.1297-305.
84. Baer, E., Hiltner, A., and Friedman, B., (1976). Relationship of the Ultrastructure and Mechanical Properties in Tendinous Collagen, a Highly Ordered Macromolecular Composite. **Polymer Mechanics** 11(6); p.896-904.
85. Hardingham, T.E. and Fosang, A.J., (1992). Proteoglycans: Many Forms and Many Functions. **Federation of American Societies for Experimental Biology J** 6(3); p.861-70.
86. Yoon, J.H. and Halper, J., (2005). Tendon Proteoglycans: Biochemistry and Function. **Journal of Musculoskeletal and Neuronal Interactions** 5(1); p.22-34.
87. Rigozzi, S., Müller, R., and Snedeker, J.G., (2009). Local Strain Measurement Reveals a Varied Regional Dependence of Tensile Tendon Mechanics on Glycosaminoglycan Content. **Journal of Biomechanics** 42(10); p.1547-52.

88. Vogel, K.G. and Meyers, A.B., (1999). Proteins in the Tensile Region of Adult Bovine Deep Flexor Tendon. **Clinical Orthopaedics and Related Research** 367(S1); p.S344-55.
89. Raspanti, M., Congiu, T., and Guizzardi, S., (2002). Structural Aspects of the Extracellular Matrix of the Tendon: An Atomic Force and Scanning Electron Microscopy Study. **Archives of Histology and Cytology** 65(1); p.37-43.
90. Ruoslahti, E., (1988). Structure and Biology of Proteoglycans. **Annual Review of Cell Biology** 4(1); p.229-55.
91. Vesentini, S., Redaelli, A., and Montevecchi, F.M., (2005). Estimation of the Binding Force of the Collagen Molecule-Decorin Core Protein Complex in Collagen Fibril. **Journal of Biomechanics** 38(3); p.433-43.
92. Scott, J., (1992). Supramolecular Organization of Extracellular Matrix Glycosaminoglycans, in Vitro and in the Tissues. **The FASEB Journal** 6(9); p.2639-45.
93. Scott, J.E., (1988). Proteoglycan-Fibrillar Collagen Interactions. **Biochemical Journal** 252(2); p.313-23.
94. Raspanti, M., Alessandrini, A., Ottani, V., and Ruggeri, A., (1997). Direct Visualization of Collagen-Bound Proteoglycans by Tapping-Mode Atomic Force Microscopy. **Journal of Structural Biology** 119(2); p.118-22.
95. Scott, J.E. and Orford, C.R., (1981). Dermatan Sulfate-Rich Proteoglycan Associates with Rat Tail Tendon Collagen at the D-Band in the Gap Region. **Biochemical Journal** 197(1); p.213-&.
96. Raspanti, M., Viola, M., Forlino, A., Tenni, R., Gruppi, C., and Tira, M.E., (2008). Glycosaminoglycans Show a Specific Periodic Interaction with Type I Collagen Fibrils. **Journal of Structural Biology** 164(1); p.134-39.
97. Kalamajski, S. and Oldberg, A., (2010). The Role of Small Leucine-Rich Proteoglycans in Collagen Fibrillogenesis. **Matrix Biology : Journal of the International Society for Matrix Biology** 29(4); p.248-53.
98. Cribb, A.M. and Scott, J.E., (1995). Tendon Response to Tensile Stress: An Ultrastructural Investigation of Collagen: Proteoglycan Interactions in Stressed Tendon. **Journal of Anatomy** 187(2); p.423-28.
99. Redaelli, A., Vesentini, S., Soncini, M., Vena, P., Mantero, S., and Montevecchi, F.M., (2003). Possible Role of Decorin Glycosaminoglycans in Fibril to Fibril Force Transfer in Relative Mature Tendons--a Computational Study from Molecular to Microstructural Level. **Journal of Biomechanics** 36(10); p.1555-69.
100. Vesentini, S., Redaelli, A., Soncini, M., Mantero, S., and Montevecchi, F.M., (2002). Glycosaminoglycan Stiffness Evaluation by Means of Molecular Mechanics Approach for Tendon Functional Analysis at **Molecular, Cellular and Tissue Engineering, 2002. Proceedings of the IEEE-EMBS Special Topic Conference on**,
101. Shen, Z.L., Kahn, H., Ballarini, R., and Eppell, S.J., (2011). Viscoelastic Properties of Isolated Collagen Fibrils. **Biophysical Journal** 100(12); p.3008-15.
102. Screen, H.R.C. and Evans, S.L., (2009). Measuring Strain Distributions in the Tendon Using Confocal Microscopy and Finite Elements. **Journal of Strain Analysis for Engineering Design** 44(5); p.327-35.
103. Screen, H.R., (2008). Investigating Load Relaxation Mechanics in Tendon. **Journal of the Mechanical Behavior of Biomedical Materials** 1(1); p.51-8.
104. Fratzl, P., Misof, K., Zizak, I., Rapp, G., Amenitsch, H., and Bernstorff, S., (1998). Fibrillar Structure and Mechanical Properties of Collagen. **Journal of Structural Biology** 122(1-2); p.119-22.
105. Screen, H.R.C., Bader, D.L., Lee, D.A., and Shelton, J.C., (2004). Local Strain Measurement within Tendon. **Strain** 40(4); p.157-63.
106. Fung, D.T., Sereysky, J.B., Basta-Pljakic, J., Laudier, D.M., Huq, R., Jepsen, K.J., Schaffler, M.B., and Flatow, E.L., (2010). Second Harmonic Generation Imaging and Fourier Transform Spectral Analysis Reveal Damage in Fatigue-Loaded Tendons. **Annals of Biomedical Engineering** 38(5); p.1741-51.
107. Fung, D.T., Wang, V.M., Andarawis-Puri, N., Basta-Pljakic, J., Li, Y., Laudier, D.M., Sun, H.B., Jepsen, K.J., Schaffler, M.B., and Flatow, E.L., (2010). Early Response to Tendon Fatigue Damage Accumulation in a Novel in Vivo Model. **Journal of Biomechanics** 43(2); p.274-9.
108. Fung, D.T., Wang, V.M., Laudier, D.M., Shine, J.H., Basta-Pljakic, J., Jepsen, K.J., Schaffler, M.B., and Flatow, E.L., (2009). Subrupture Tendon Fatigue Damage. **Journal of Orthopaedic Research** 27(2); p.264-73.

109. Screen, H.R., Chhaya, V.H., Greenwald, S.E., Bader, D.L., Lee, D.A., and Shelton, J.C., (2006). The Influence of Swelling and Matrix Degradation on the Microstructural Integrity of Tendon. **Acta Biomaterialia** 2(5); p.505-13.
110. Screen, H.R.C., Bader, D.L., Shelton, J.C., and Lee, D.A., (2002). Non-Collagenous Matrix Components Influence the Micro-Mechanical Environment of Tenocytes within Tendon Fascicles Subjected to Tensile Strain. **European Cells and Materials Vol.** 4(S1); p.41-42.
111. Fessel, G. and Snedeker, J.G., (2009). Evidence against Proteoglycan Mediated Collagen Fibril Load Transmission and Dynamic Viscoelasticity in Tendon. **Matrix Biology : Journal of the International Society for Matrix Biology** 28(8); p.503-10.
112. Legerlotz, K., Riley, G.P., and Screen, H.R., (2010). Specimen Dimensions Influence the Measurement of Material Properties in Tendon Fascicles. **Journal of Biomechanics** 43(12); p.2274-80.
113. Fessel, G. and Snedeker, J.G., (2011). Equivalent Stiffness after Glycosaminoglycan Depletion in Tendon--an Ultra-Structural Finite Element Model and Corresponding Experiments. **Journal of Theoretical Biology** 268(1); p.77-83.
114. Puxkandl, R., Zizak, I., Paris, O., Keckes, J., Tesch, W., Bernstorff, S., Purslow, P., and Fratzl, P., (2002). Viscoelastic Properties of Collagen: Synchrotron Radiation Investigations and Structural Model. **Philosophical transactions of the Royal Society of London. Series B, Biological sciences** 357(1418); p.191-7.
115. Doroski, D.M., Brink, K.S., and Temenoff, J.S., (2007). Techniques for Biological Characterization of Tissue-Engineered Tendon and Ligament. **Biomaterials** 28(2); p.187-202.
116. Kannus, P., (2000). Structure of the Tendon Connective Tissue. **Scandinavian Journal of Medicine and Science in Sports** 10(6); p.312-20.
117. Ge, Z., Yang, F., Goh, J.C., Ramakrishna, S., and Lee, E.H., (2006). Biomaterials and Scaffolds for Ligament Tissue Engineering. **Journal of Biomedical Materials Research - Part A** 77(3); p.639-52.
118. Ralphs, J.R., (2002). Cell Biology of Tendons. **European Cells and Materials** 4(Suppl.1); p.39-40.
119. McNeilly, C.M., Banes, A.J., Benjamin, M., and Ralphs, J.R., (1996). Tendon Cells in Vivo Form a Three Dimensional Network of Cell Processes Linked by Gap Junctions. **Journal of Anatomy** 189(3); p.593-600.
120. Wang, J.H. and Thampatty, B.P., (2006). An Introductory Review of Cell Mechanobiology. **Biomechanics and Modeling in Mechanobiology** 5(1); p.1-16.
121. Otsuka, K., Sodek, J., and Limeback, H.F., (1984). Collagenase Synthesis by Osteoblast-Like Cells. **Calcified Tissue International** 36(1); p.722-24.
122. Chakravarti, S., Magnuson, T., Lass, J.H., Jepsen, K.J., LaMantia, C., and Carroll, H., (1998). Lumican Regulates Collagen Fibril Assembly: Skin Fragility and Corneal Opacity in the Absence of Lumican. **Journal of Cell Biology** 141(5); p.1277-86.
123. Ezura, Y., Chakravarti, S., Oldberg, A., Chervoneva, I., and Birk, D.E., (2000). Differential Expression of Lumican and Fibromodulin Regulate Collagen Fibrillogenesis in Developing Mouse Tendons. **Journal of Cell Biology** 151(4); p.779-88.
124. Danielson, K.G., Baribault, H., Holmes, D.F., Graham, H., Kadler, K.E., and Iozzo, R.V., (1997). Targeted Disruption of Decorin Leads to Abnormal Collagen Fibril Morphology and Skin Fragility. **Journal of Cell Biology** 136(3); p.729-43.
125. Toole, B.P. and Lowther, D.A., (1968). The Effect of Chondroitin Sulphate-Protein on the Formation of Collagen Fibrils in Vitro. **Biochemical Journal** 109(5); p.857-66.
126. Vogel, K.G. and Trotter, J.A., (1987). The Effect of Proteoglycans on the Morphology of Collagen Fibrils Formed in Vitro. **Collagen and related Research** 7(2); p.105-14.
127. Kuc, I.M. and Scott, P.G., (1997). Increased Diameters of Collagen Fibrils Precipitated in Vitro in the Presence of Decorin from Various Connective Tissues. **Connective Tissue Research** 36(4); p.287-96.
128. Toole, B.P. and Lowther, D.A., (1968). Dermatan Sulfate-Protein: Isolation from and Interaction with Collagen. **Archives of Biochemistry and Biophysics** 128(3); p.567-78.
129. Zhang, G., Ezura, Y., Chervoneva, I., Robinson, P.S., Beason, D.P., Carine, E.T., Soslowsky, L.J., Iozzo, R.V., and Birk, D.E., (2006). Decorin Regulates Assembly of Collagen Fibrils and Acquisition of Biomechanical Properties During Tendon Development. **Journal of Cellular Biochemistry** 98(6); p.1436-49.
130. Robbins, J.R., Evanko, S.P., and Vogel, K.G., (1997). Mechanical Loading and Tgf-Beta Regulate Proteoglycan Synthesis in Tendon. **Archives of Biochemistry and Biophysics** 342(2); p.203-11.

131. Reed, C.C. and Iozzo, R.V., (2002). The Role of Decorin in Collagen Fibrillogenesis and Skin Homeostasis. **Glycoconjugate Journal** 19(4-5); p.249-55.
132. Lowther, D.A. and Natarajan, M., (1972). The Influence of Glycoprotein on Collagen Fibril Formation in the Presence of Chondroitin Sulphate Proteoglycan. **Biochemical Journal** 127(3); p.607-8.
133. Kuwaba, K., Kobayashi, M., Nomura, Y., Irie, S., and Koyama, Y., (2002). Size Control of Decorin Dermatan Sulfate During Remodeling of Collagen Fibrils in Healing Skin. **Journal of Dermatological Science** 29(3); p.185-94.
134. Vogel, K.G., Paulsson, M., and Heinegard, D., (1984). Specific Inhibition of Type I and Type Ii Collagen Fibrillogenesis by the Small Proteoglycan of Tendon. **Biochemical Journal** 223(3); p.587-97.
135. Chuen, F.S., Chuk, C.Y., Ping, W.Y., Nar, W.W., Kim, H.L., and Ming, C.K., (2004). Immunohistochemical Characterization of Cells in Adult Human Patellar Tendons. **Journal of Histochemistry and Cytochemistry** 52(9); p.1151-7.
136. Sharma, P. and Maffulli, N., (2005). Tendon Injury and Tendinopathy: Healing and Repair. **Journal of Bone and Joint Surgery - American Version** 87(1); p.187-202.
137. Rees, S.G., Flannery, C.R., Little, C.B., Hughes, C.E., Caterson, B., and Dent, C.M., (2000). Catabolism of Aggrecan, Decorin and Biglycan in Tendon. **Biochemical Journal** 350 Pt 1(1); p.181-8.
138. Gillis, C., Sharkey, N., Stover, S.M., Pool, R.R., Meagher, D.M., and Willits, N., (1995). Effect of Maturation and Aging on Material and Ultrasonographic Properties of Equine Superficial Digital Flexor Tendon. **American Journal of Veterinary Research** 56(10); p.1345-50.
139. Naresh, M.D. and Brodsky, B., (1992). X-Ray-Diffraction Studies on Human Tendon Show Age-Related-Changes in Collagen Packing. **Biochimica et Biophysica Acta** 1122(2); p.161-66.
140. Gillis, C., Pool, R.R., Meagher, D.M., Stover, S.M., Reiser, K., and Willits, N., (1997). Effect of Maturation and Aging on the Histomorphometric and Biochemical Characteristics of Equine Superficial Digital Flexor Tendon. **American Journal of Veterinary Research** 58(4); p.425-30.
141. Birch, H.L., Bailey, J.V., Bailey, A.J., and Goodship, A.E., (1999). Age-Related Changes to the Molecular and Cellular Components of Equine Flexor Tendons. **Equine Veterinary Journal** 31(5); p.391-6.
142. Tuite, D.J., Renstrom, P.A., and O'Brien, M., (1997). The Aging Tendon. **Scandinavian Journal of Medicine and Science in Sports** 7(2); p.72-7.
143. Wilmink, J., Wilson, A.M., and Goodship, A.E., (1992). Functional Significance of the Morphology and Micromechanics of Collagen Fibres in Relation to Partial Rupture of the Superficial Digital Flexor Tendon in Racehorses. **Research in Veterinary Science** 53(3); p.354-9.
144. Shadwick, R.E., (1990). Elastic Energy Storage in Tendons: Mechanical Differences Related to Function and Age. **Journal of Applied Physiology** 68(3); p.1033-40.
145. Lin, Y.L., Brama, P.A.J., Kiers, G.H., van Weeren, P.R., and DeGroot, J., (2005). Extracellular Matrix Compositon of the Equine Superficial Digital Flexor Tendon: Relationship with Age and Anatomical Site. **Journal of Veterinary Medicine Series a-Physiology Pathology Clinical Medicine** 52(7); p.333-38.
146. Williams, L.N., Elder, S.H., Horstemeyer, M.F., and Harbarger, D., (2008). Variation of Diameter Distribution, Number Density, and Area Fraction of Fibrils within Five Areas of the Rabbit Patellar Tendon. **Annals of Anatomy-Anatomischer Anzeiger** 190(5); p.442-51.
147. David A.D, P., (1988). The Molecular Fibrillar Structure of Collagen and Its Relationship to the Mechanical Properties of Connective Tissue. **Biophysical Chemistry** 29(1–2); p.195-209.
148. Merritt, J.S., Davies, H.M., Burvill, C., and Pandy, M.G., (2008). Influence of Muscle-Tendon Wrapping on Calculations of Joint Reaction Forces in the Equine Distal Forelimb. **Journal of Biomedicine and Biotechnology** 2008(Journal Article); p.165730.
149. Harrison, S.M., Whitton, R.C., Kawcak, C.E., Stover, S.M., and Pandy, M.G., (2010). Relationship between Muscle Forces, Joint Loading and Utilization of Elastic Strain Energy in Equine Locomotion. **Journal of Experimental Biology** 213(Pt 23); p.3998-4009.
150. Luo, Z.-P., Hsu, H.-C., Grabowski, J.J., Morrey, B.F., and An, K.-N., (1998). Mechanical Environment Associated with Rotator Cuff Tears. **Journal of Shoulder and Elbow Surgery** 7(6); p.616-20.
151. Giori, N.J., Beaupre, G.S., and Carter, D.R., (1993). Cellular-Shape and Pressure May Mediate Mechanical Control of Tissue Composition in Tendons. **Journal of Orthopaedic Research** 11(4); p.581-91.

152. Zobitz, M.E., Luo, Z.P., and An, K.N., (2001). Determination of the Compressive Material Properties of the Supraspinatus Tendon. **Journal of Biomechanical Engineering (Transactions of the ASME)** 123(1); p.47-51.
153. Huang, C.Y., Wang, V.M., Pawluk, R.J., Bucchieri, J.S., Levine, W.N., Bigliani, L.U., Mow, V.C., and Flatow, E.L., (2005). Inhomogeneous Mechanical Behavior of the Human Supraspinatus Tendon under Uniaxial Loading. **Journal of Orthopaedic Research** 23(4); p.924-30.
154. Vogel, K.G., Keller, E.J., Lenhoff, R.J., Campbell, K., and Koob, T.J., (1986). Proteoglycan Synthesis by Fibroblast Cultures Initiated from Regions of Adult Bovine Tendon Subjected to Different Mechanical Forces. **European Journal of Cell Biology** 41(1); p.102-12.
155. Feitosa, V.L.C., Reis, F.P., Esquisatto, M.A.M., Joazeiro, P.P., Vidal, B.C., and Pimentel, E.R., (2006). Comparative Ultrastructural Analysis of Different Regions of Two Digital Flexor Tendons of Pigs. **Micron** 37(6); p.518-25.
156. Vogel, K.G. and Heinegard, D., (1985). Characterization of Proteoglycans from Adult Bovine Tendon. **Journal of Biological Chemistry** 260(16); p.9298-306.
157. Kathryn, G.V. and Eugene, J.M.A.T., (1988). Keratan Sulfate Is a Component of Proteoglycans in the Compressed Region of Adult Bovine Flexor Tendon. **Journal of Orthopaedic Research** 6(3); p.434-42.
158. Gillard, G.C., Reilly, H.C., Bell-Booth, P.G., and Flint, M.H., (1979). The Influence of Mechanical Forces on the Glycosaminoglycan Content of the Rabbit Flexor Digitorum Profundus Tendon. **Connective Tissue Research** 7(1); p.37-46.
159. Vogel, K.G. and Peters, J.A., (2005). Histochemistry Defines a Proteogylcan-Rich Layer in Bovine Flexor Tendon Subjected to Bending. **Journal of Musculoskeletal Neuronal Interactions** 5(1); p.64-69.
160. Milz, S., Benjamin, M., and Putz, R., (2005). Molecular Parameters Indicating Adaptation to Mechanical Stress in Fibrous Connective Tissue. **Advances in Anatomy, Embryology and Cell Biology** 178(p.1-71.
161. Wren, T.A.L., Beaupre, G.S., and Carter, D.R., (2000). Mechanobiology of Tendon Adaptation to Compressive Loading through Fibrocartilaginous Metaplasia. **Journal of Rehabilitation Research and Development** 37(2); p.135-43.
162. Lee, S.B., Nakajima, T., Luo, Z.P., Zobitz, M.E., Chang, Y.W., and An, K.N., (2000). The Bursal and Articular Sides of the Supraspinatus Tendon Have a Different Compressive Stiffness. **Clinical Biomechanics** 15(4); p.241-47.
163. Merrilees, M.J. and Flint, M.H., (1980). Ultrastructural Study of Tension and Pressure Zones in a Rabbit Flexor Tendon. **American Journal of Anatomy** 157(1); p.87-106.
164. Feitosa, V.L., Reis, F.P., Esquisatto, M.A., Joazeiro, P.P., Vidal, B.C., and Pimentel, E.R., (2006). Comparative Ultrastructural Analysis of Different Regions of Two Digital Flexor Tendons of Pigs. **Micron** 37(6); p.518-25.
165. Gillard, G.C., Merrilees, M.J., Bell-Booth, P.G., Reilly, H.C., and Flint, M.H., (1977). The Proteoglycan Content and the Axial Periodicity of Collagen in Tendon. **Biochemical Journal** 163(1); p.145-51.
166. Koob, T.J. and Vogel, K.G., (1987). Site-Related Variations in Glycosaminoglycan Content and Swelling Properties of Bovine Flexor Tendon. **Journal of Orthopaedic Research** 5(3); p.414-24.
167. Benjamin, M., Qin, S., and Ralphs, J.R., (1995). Fibrocartilage Associated with Human Tendons and Their Pulleys. **Journal of Anatomy** 187(3); p.625-33.
168. Dawson, I.M.P., (1972). Fixation: What Should the Pathologist Do? **The Histochemical Journal** 4(4); p.381-85.
169. Hopwood, D., (1969). Fixatives and Fixation: A Review. **Histochemistry Journal** 1(4); p.323-60.
170. Prento, P., (1995). Glutaraldehyde for Electron Microscopy: A Practical Investigation of Commercial Glutaraldehydes and Glutaraldehyde-Storage Conditions. **Histochemistry Journal** 27(11); p.906-13.
171. Hayat, M.A., (1978). Principles and Techniques of Electron Microscopy: Biological Applications. Von Nostrand Reinhold Company, New York.
172. Hayat, M.A., (1986). Glutaraldehyde: Role in Electron Microscopy. **Micron and Microscopica Acta** 17(2); p.115-35.
173. Hopwood, D., (1972). Theoretical and Practical Aspects of Glutaraldehyde Fixation. **Histochemistry Journal** 4(4); p.267-303.

174. Pearse, A.G.E., (1968-72). Histochemistry, Theoretical and Applied, 3rd edition. Churchill Livingstone, London.
175. Cox, M.L., Schray, C.L., Luster, C.N., Stewart, Z.S., Korytko, P.J., KN, M.K., Paulauskis, J.D., and Dunstan, R.W., (2006). Assessment of Fixatives, Fixation, and Tissue Processing on Morphology and Rna Integrity. **Experimental and molecular pathology** 80(2); p.183-91.
176. Holt, S.J. and Hicks, R.M., (1961). Studies on Formalin Fixation for Electron Microscopy and Cytochemical Staining Purposes. **Journal of Biophysical and Biochemical Cytology** 11(1); p.31-45.
177. Hansen, P., Hassenkam, T., Svensson, R.B., Aagaard, P., Trappe, T., Haraldsson, B.T., Kjaer, M., and Magnusson, P., (2009). Glutaraldehyde Cross-Linking of Tendon--Mechanical Effects at the Level of the Tendon Fascicle and Fibril. **Connective Tissue Research** 50(4); p.211-22.
178. Jorge-Herrero, E., Fernandez, P., Turnay, J., Olmo, N., Calero, P., Garcia, R., Freile, I., and Castillo-Olivares, J.L., (1999). Influence of Different Chemical Cross-Linking Treatments on the Properties of Bovine Pericardium and Collagen. **Biomaterials** 20(6); p.539-45.
179. Quirinia, A. and Viidik, A., (1991). Freezing for Postmortal Storage Influences the Biomechanical Properties of Linear Skin Wounds. **Journal of Biomechanics** 24(9); p.819-23.
180. Ng, B.H., Chou, S.M., Lim, B.H., and Chong, A., (2005). The Changes in the Tensile Properties of Tendons after Freeze Storage in Saline Solution. **Proceedings of the Institution of Mechanical Engineers. Part H, Journal of Engineering in Medicine** 219(6); p.387-92.
181. Pek, Y.S., Spector, M., Yannas, I.V., and Gibson, L.J., (2004). Degradation of a Collagen-Chondroitin-6-Sulfate Matrix by Collagenase and by Chondroitinase. **Biomaterials** 25(3); p.473-82.
182. Tilley, J.M., Carr, A.J., and Czernuszka, J.T., (2011). Atomic Force Microscopy of Bulk Tendon Samples: Affect of Location and Fixation on Tissue Ultrastructure. **Micron** 42(5); p.531-5.
183. Blach, J.A., Watson, G.S., Busfield, W.K., and Myhra, S., (2002). Photo-Oxidative Degradation in Polyisoprene: Surface Characterization and Analysis by Atomic Force Microscopy. **Polymer International** 51(1); p.12-20.
184. Sneddon, I.N., (1965). The Relation between Load and Penetration in the Axisymmetric Boussinesq Problem for a Punch of Arbitrary Profile. **International Journal of Engineering Science** 3(1); p.47-57.
185. Oliver, W.C. and Pharr, G.M., (1992). Improved Technique for Determining Hardness and Elastic Modulus Using Load and Displacement Sensing Indentation Experiments. **Journal of Materials Research** 7(6); p.1564-80.
186. Pappas, D., Smith, B.W., and Winefordner, J.D., (2000). Raman Spectroscopy in Bioanalysis. **Talanta** 51(1); p.131-44.
187. Wang, Y.N., Galiotis, C., and Bader, D.L., (2000). Determination of Molecular Changes in Soft Tissues under Strain Using Laser Raman Microscopy. **Journal of Biomechanics** 33(4); p.483-86.
188. Krafft, C., (2004). Bioanalytical Applications of Raman Spectroscopy. **Analytical and Bioanalytical Chemistry** 378(1); p.60-2.
189. Krafft, C., Steiner, G., Beleites, C., and Salzer, R., (2009). Disease Recognition by Infrared and Raman Spectroscopy. **Journal of Biophotonics** 2(1-2); p.13-28.
190. Barry, B.W., Edwards, H.G.M., and Williams, A.C., (1992). Fourier-Transform Raman and Infrared Vibrational Study of Human Skin - Assignment of Spectral Bands. **Journal of Raman Spectroscopy** 23(11); p.641-45.
191. Diem, M., Romeo, M., Boydston-White, S., Miljkovic, M., and Matthaus, C., (2004). A Decade of Vibrational Micro-Spectroscopy of Human Cells and Tissue (1994-2004). **Analyst** 129(10); p.880-5.
192. Frushour, B.G. and Koenig, J.L., (1975). Raman Scattering of Collagen, Gelatin, and Elastin. **Biopolymers** 14(2); p.379-91.
193. Constantine, V.S. and Mowry, R.W., (1968). Selective Staining of Human Dermal Collagen. **The Journal of Investigative Dermatology** 50(5); p.419-23.
194. Junqueira, L., Bignolas, G., and Brentani, R., (1979). Picrosirius Staining Plus Polarization Microscopy, a Specific Method for Collagen Detection in Tissue Sections. **The Histochemical Journal** 11(4); p.447-55.
195. Constantine, V.S., (1969). A Combined Tissue Stain for the Selective Staining of Collagen, Elastic Fibers and Acidic Carbohydrates 1. **The Journal of Investigative Dermatology** 52(4); p.353-56.
196. Inoué, S., (2001). Polarization Microscopy. In **Current Protocols in Cell Biology**. John Wiley & Sons, Inc.,

197. Junqueira, L.C., Cossermelli, W., and Brentani, R., (1978). Differential Staining of Collagens Type I, Ii and Iii by Sirius Red and Polarization Microscopy. **Archivum Histologicum Japanicum** 41(3); p.267-74.
198. Vidal, B.D., (2003). Image Analysis of Tendon Helical Superstructure Using Interference and Polarized Light Microscopy. **Micron** 34(8); p.423-32.
199. Dayan, D., Hiss, Y., Hirshberg, A., Bubis, J.J., and Wolman, M., (1989). Are the Polarization Colors of Picrosirius Red-Stained Collagen Determined Only by the Diameter of the Fibers? **Histochemie** 93(1); p.27-9.
200. Rich, L.W., P.;, (2005). Collagen and Picrosirius Red Staining: A Polarised Light Assessment of Fibrillar Hue and Spatial Distribution. **Brazilian Journal of Morphological Sciences** 22(2); p.97-104.
201. Scott, J.E., Quintarelli, G., and Dellovo, M.C., (1964). The Chemical and Histochemical Properties of Alcian Blue. I. The Mechanism of Alcian Blue Staining. **Histochemie** 4(2); p.73-85.
202. Okuda, Y., Gorski, J.P., An, K.N., and Amadio, P.C., (1987). Biochemical, Histological, and Biomechanical Analyses of Canine Tendon. **Journal of Orthopaedic Research** 5(1); p.60-8.
203. Kiraly, K., Lapvetelainen, T., Arokoski, J., Torronen, K., Modis, L., Kiviranta, I., and Helminen, H.J., (1996). Application of Selected Cationic Dyes for the Semiquantitative Estimation of Glycosaminoglycans in Histological Sections of Articular Cartilage by Microspectrophotometry. **Histochemistry Journal** 28(8); p.577-90.
204. Meade, A.D., Clarke, C., Bonnier, F., Poon, K., Garcia, A., Knief, P., Ostrowska, K., Salford, L., Nawaz, H., Lyng, F.M., and Byrne, H.J., (2009). Functional and Pathological Analysis of Biological Systems Using Vibrational Spectroscopy with Chemometric and Heuristic Approaches at **Hyperspectral Image and Signal Processing: Evolution in Remote Sensing, 2009. WHISPERS '09. First Workshop on**, Grenoble, France.
205. Duygu, D.Y., Baykal, T., and Yildiz, K., (2009). Fourier Transform Infrared (Ft-Ir) Spectroscopy for Biological Studies. **Gazi University Journal of Science** 22(3); p.117-21.
206. Huang, Z., McWilliams, A., Lui, H., McLean, D.I., Lam, S., and Zeng, H., (2003). Near-Infrared Raman Spectroscopy for Optical Diagnosis of Lung Cancer. **International Journal of Cancer** 107(6); p.1047-52.
207. Krafft, C., Codrich, D., Pelizzo, G., and Sergo, V., (2008). Raman and Ftir Microscopic Imaging of Colon Tissue: A Comparative Study. **Journal of Biophotonics** 1(2); p.154-69.
208. Penteado, S.C., Fogazza, B.P., Carvalho Cda, S., Arisawa, E.A., Martins, M.A., Martin, A.A., and Martinho Hda, S., (2008). Diagnosis of Degenerative Lesions of Supraspinatus Rotator Cuff Tendons by Fourier Transform-Raman Spectroscopy. **Journal of Biomedical Optics** 13(1); p.014018.
209. Tromans, W.J., Horne, R.W., Gresham, G.A., and Bailey, A.J., (1963). Electron Microscope Studies on the Structure of Collagen Fibrils by Negative Staining. **Z Zellforsch Mikrosk Anat** 58(p.798-802.
210. Gotoh, T. and Sugi, Y., (1985). Electron-Microscopic Study of the Collagen Fibrils of the Rat Tail Tendon as Revealed by Freeze-Fracture and Freeze-Etching Techniques. **Cell and Tissue Research** 240(3); p.529-34.
211. Eyden, B. and Tzaphlidou, M., (2001). Structural Variations of Collagen in Normal and Pathological Tissues: Role of Electron Microscopy. **Micron** 32(3); p.287-300.
212. Kongsgaard, M., Qvortrup, K., Larsen, J., Aagaard, P., Doessing, S., Hansen, P., Kjaer, M., and Magnusson, S.P., (2010). Fibril Morphology and Tendon Mechanical Properties in Patellar Tendinopathy: Effects of Heavy Slow Resistance Training. **America Journal of Sports Medicine** 38(4); p.749-56.
213. Fotiadis, D., Scheuring, S., Muller, S.A., Engel, A., and Muller, D.J., (2002). Imaging and Manipulation of Biological Structures with the Afm. **Micron** 33(4); p.385-97.
214. Paige, M.F. and Goh, M.C., (2001). Ultrastructure and Assembly of Segmental Long Spacing Collagen Studied by Atomic Force Microscopy. **Micron** 32(3); p.355-61.
215. Gutsmann, T., Fantner, G.E., Kindt, J.H., Venturoni, M., Danielsen, S., and Hansma, P.K., (2004). Force Spectroscopy of Collagen Fibers to Investigate Their Mechanical Properties and Structural Organization. **Biophysical Journal** 86(5); p.3186-93.
216. Revenko, I., Sommer, F., Minh, D.T., Garrone, R., and Franc, J.-M., (1994). Atomic Force Microscopy Study of the Collagen Fibre Structure. **Biology of the Cell** 80(1); p.67-69.
217. Thalhammer, S., Heckl, W.M., Zink, A., and Nerlich, A.G., (2001). Atomic Force Microscopy for High Resolution Imaging of Collagen Fibrils - a New Technique to Investigate Collagen Structure in Historic Bone Tissues. **Journal of Archaeological Science** 28(10); p.1061-68.

218. Habelitz, S., Balooch, M., Marshall, S.J., Balooch, G., and Marshall, G.W., Jr., (2002). In Situ Atomic Force Microscopy of Partially Demineralized Human Dentin Collagen Fibrils. **Journal of Structural Biology** 138(3); p.227-36.
219. Hickey, D.S. and Hukins, D.W., (1979). Effect of Methods of Preservation on the Arrangement of Collagen Fibrils in Connective Tissue Matrices: An X-Ray Diffraction Study of Annulus Fibrosus. **Connective Tissue Research** 6(4); p.223-8.
220. Woo, S.L., Orlando, C.A., Camp, J.F., and Akeson, W.H., (1986). Effects of Postmortem Storage by Freezing on Ligament Tensile Behavior. **Journal of Biomechanics** 19(5); p.399-404.
221. Srinivasan, M., Sedmak, D., and Jewell, S., (2002). Effect of Fixatives and Tissue Processing on the Content and Integrity of Nucleic Acids. **American Journal of Pathology** 161(6); p.1961-71.
222. Pleshko, N.L., Boskey, A.L., and Mendelsohn, R., (1992). An Ft-Ir Microscopic Investigation of the Effects of Tissue Preservation on Bone. **Calcified Tissue International** 51(1); p.72-7.
223. Viidik, A. and Lewin, T., (1966). Changes in Tensile Strength Characteristics and Histology of Rabbit Ligaments Induced by Different Modes of Postmortal Storage. **Acta Orthop Scand** 37(2); p.141-55.
224. Mason, J. and O'Leary, T., (1991). Effects of Formaldehyde Fixation on Protein Secondary Structure: A Calorimetric and Infrared Spectroscopic Investigation. **J. Histochem. Cytochem.** 39(2); p.225-29.
225. Fox, C.H., Johnson, F.B., Whiting, J., and Roller, P.P., (1985). Formaldehyde Fixation. **Journal of Histochemistry and Cytochemistry** 33(8); p.845-53.
226. Sabatini, D.D., Bensch, K., and Barrnett, R.J., (1963). Cytochemistry and Electron Microscopy. The Preservation of Cellular Ultrastructure and Enzymatic Activity by Aldehyde Fixation. **Journal of Cell Biology** 17(1); p.19-58.
227. VARRIANO-MARSTON, E., DAVIS, E.A., HUTCHINSON, T.E., and GORDON, J., (1978). Postmortem Aging of Bovine Muscle: A Comparison of Two Preparation Techniques for Electron Microscopy. **Journal of Food Science** 43(3); p.680-83.
228. Scott, J.E., (1980). Collagen--Proteoglycan Interactions. Localization of Proteoglycans in Tendon by Electron Microscopy. **Biochemical Journal** 187(3); p.887-91.
229. Chaudhury, S., Holland, C., Vollrath, F., and Carr, A.J., (2011). Comparing Normal and Torn Rotator Cuff Tendons Using Dynamic Shear Analysis. **Journal of Bone and Joint Surgery - British Version** 93(7); p.942-8.
230. (2011). Handbook of Nanoindentation with Biological Applications, 1st Edition. Edited by M.L. Oyen. Pan Standford Publishing Pte. Ltd., Singapore.
231. Zhang, M., Zheng, Y.P., and Mak, A.F., (1997). Estimating the Effective Young's Modulus of Soft Tissues from Indentation Tests--Nonlinear Finite Element Analysis of Effects of Friction and Large Deformation. **Medical Engineering and Physics** 19(6); p.512-7.
232. Magonov, S.N. and Reneker, D.H., (1997). Characterization of Polymer Surfaces with Atomic Force Microscopy. **Annual Review of Materials Science** 27(p.175-222.
233. Liao, Q.Z., Huang, J.Y., Zhu, T., Xiong, C.Y., and Fang, J., (2010). A Hybrid Model to Determine Mechanical Properties of Soft Polymers by Nanoindentation. **Mechanics of Materials** 42(12); p.1043-47.
234. Charitidis, C., (2011). Nanoscale Deformation and Nanomechanical Properties of Soft Matter Study Cases: Polydimethylsiloxane, Cells and Tissues. **ISRN Nanotechnology** 2011(p.1-13.
235. Tomkoria, S., Masuda, K., and Mao, J., (2007). Nanomechanical Properties of Alginate-Recovered Chondrocyte Matrices for Cartilage Regeneration. **Proceedings of the Institution of Mechanical Engineers. Part H, Journal of Engineering in Medicine** 221(5); p.467-73.
236. Ebenstein, D.M. and Pruitt, L.A., (2006). Nanoindentation of Biological Materials. **Nano Today** 1(3); p.26-33.
237. Franke, O., Durst, K., Maier, V., Goken, M., Birkholz, T., Schneider, H., Hennig, F., and Gelse, K., (2007). Mechanical Properties of Hyaline and Repair Cartilage Studied by Nanoindentation. **Acta Biomaterialia** 3(6); p.873-81.
238. Stolz, M., Gottardi, R., Raiteri, R., Miot, S., Martin, I., Imer, R., Staufer, U., Raducanu, A., Duggelin, M., Baschong, W., Daniels, A.U., Friederich, N.F., Aszodi, A., and Aebi, U., (2009). Early Detection of Aging Cartilage and Osteoarthritis in Mice and Patient Samples Using Atomic Force Microscopy. **Nature Nanotechnology** 4(3); p.186-92.
239. Grant, C.A., Brockwell, D.J., Radford, S.E., and Thomson, N.H., (2008). Effects of Hydration on the Mechanical Response of Individual Collagen Fibrils. **Applied Physics Letters** 92(23);

240. Heim, A.J., Koob, T.J., and Matthews, W.G., (2007). Low Strain Nanomechanics of Collagen Fibrils. **Biomacromolecules** 8(11); p.3298-301.
241. Ebenstein, D.M., (2011). Nanoindentation of Soft Tissues and Other Biological Materials. In **Handbook of Nanindentation with Biological Applications**. Edited by M.L. Oyen Pan Stanford Publishing Pte. Ltd., Singapore.
242. Van Vliet, K., (2011). Instrumentation and Experimentation. In **Handbook of Nanoindentation with Biological Applications**. Edited by M.L. Oyen Pan Stanford Publishing Pte. Ltd., Singapore.
243. Akhtar, R., Schwarzer, N., Sherratt, M.J., Watson, R.E., Graham, H.K., Trafford, A.W., Mummery, P.M., and Derby, B., (2009). Nanoindentation of Histological Specimens: Mapping the Elastic Properties of Soft Tissues. **Journal of Materials Research** 24(3); p.638-46.
244. Chowdhury, S., Thomas, V., Dean, D., Catledge, S.A., and Vohra, Y.K., (2005). Nanoindentation on Porous Bioceramic Scaffolds for Bone Tissue Engineering. **Journal of Nanoscience and Nanotechnology** 5(11); p.1816-20.
245. Kaufman, J.D. and Klapperich, C.M., Nanomechanical Testing of Hydrated Biomaterials: Sample Preparation, Data Validation and Analysis at **Mechanical Properties of Bioinspired and Biological Materials as held at the 2004 MRS Fall Meeting; Boston, MA; USA; 29 Nov.-2 Dec. 2004**, 506 Keystone Drive, Warrendale, PA, 15086, USA, [URL:http://www.mrs.org/].
246. Oliver, W.C. and Pharr, G.M., (2004). Measurement of Hardness and Elastic Modulus by Instrumented Indentation: Advances in Understanding and Refinements to Methodology. **Journal of Materials Research** 19(1); p.3-20.
247. Oyen, M.L., (2011). Mechanics of Indentation. In **Handbook of Nanoindentation with Biological Applications**. Edited by M.L. Oyen Pan Stanford Publishing Pte. Ltd., Singapore.
248. Schwarzer, N., Chudoba, T., and Richter, F., (2006). Investigation of Ultra Thin Coatings Using Nanoindentation. **Surface & Coatings Technology** 200(18-19); p.5566-80.
249. Testing, C.I.A.M.S., (2012). Physical Characterization of Coated Surfaces Part I : Instrumented Indentation. In **Applications Bulletin**, M. Fuchs and Favaro, G., Editors. CH-2034 Peseux.
250. Bull, S.J., (2005). Nanoindentation of Coatings. **Journal of Physics D: Applied Physics** 38(24); p.R393.
251. Armstrong, D.E.J.P.C., (2012). Personal Communication
252. Malaviya, P., Butler, D.L., Boivin, G.P., Smith, F.N., Barry, F.P., Murphy, J.M., and Vogel, K.G., (2000). An in Vivo Model for Load-Modulated Remodeling in the Rabbit Flexor Tendon. **Journal of Orthopaedic Research** 18(1); p.116-25.
253. Berenson, M.C., Blevins, F.T., Plaas, A.H., and Vogel, K.G., (1996). Proteoglycans of Human Rotator Cuff Tendons. **Journal of Orthopaedic Research** 14(4); p.518-25.
254. Fallon, J., Blevins, F.T., Vogel, K., and Trotter, J., (2002). Functional Morphology of the Supraspinatus Tendon. **Journal of Orthopaedic Research** 20(5); p.920-6.
255. Plaas, A.H., Ison, A.L., and Ackland, J., (1989). Synthesis of Small Proteoglycans Substituted with Keratan Sulfate by Rabbit Articular Chondrocytes. **Journal of Biological Chemistry** 264(24); p.14447-54.
256. Sobue, M. and Takeuchi, J., (1979). Chondroitinase-Resistant Sulfated Glycosaminoglycans Synthesized by Cartilages of Chick Embryos and of Newborn Chickens and Rats. **Calcified Tissue International** 27(3); p.269-73.
257. Imhoff, A.B. and Ticker, J.B., (2003). Anatomy and Biomechanics of the Shoulder. In **An Atlas of Shoulder Arthroscopy**. Edited by F.H. Fu, Imhoff, A.B., and Ticker, J.B. London : Martin Dunitz, London.
258. Karlsson, D. and Peterson, B., (1992). Towards a Model for Force Predictions in the Human Shoulder. **Journal of Biomechanics** 25(2); p.189-99.
259. Allen, G.M., (2008). Shoulder Ultrasound Imaging-Integrating Anatomy, Biomechanics and Disease Processes. **European Journal of Radiology** 68(1); p.137-46.
260. Ha'eri, G.B., (1980). Ruptures of the Rotator Cuff. **Can Med Assoc J** 123(7); p.620-6.
261. Clark, J.M. and Harryman, D.T., 2nd, (1992). Tendons, Ligaments, and Capsule of the Rotator Cuff. Gross and Microscopic Anatomy. **Journal of Bone and Joint Surgery - American Version** 74(5); p.713-25.
262. Keating, J.F., Waterworth, P., Shaw-Dunn, J., and Crossan, J., (1993). The Relative Strengths of the Rotator Cuff Muscles. A Cadaver Study. **Journal of Bone and Joint Surgery - British Version** 75(1); p.137-40.

263. Turkelson, C.M. and Zhao, G., (2009). Musculoskeletal Conditions and Disorders: Occurrence and Healthcare Use in the United States. Published by Department of Research and Scientific Affairs, American Academy of Orthopaedic Surgeons. Accessed on. Available from
264. Murphy, R.J. and Carr, A.J., (2010). Shoulder Pain. **Clinical Evidence (Online)** 2010(
265. Chaudhury, S., Gwilym, S.E., Moser, J., and Carr, A.J., (2010). Surgical Options for Patients with Shoulder Pain. **Nature Reviews: Rheumatology** 6(4); p.217-26.
266. Schibany, N., Zehetgruber, H., Kainberger, F., Wurnig, C., Ba-Ssalamah, A., Herneth, A.M., Lang, T., Gruber, D., and Breitenseher, M.J., (2004). Rotator Cuff Tears in Asymptomatic Individuals: A Clinical and Ultrasonographic Screening Study. **European Journal of Radiology** 51(3); p.263-8.
267. Beaudreuil, J., Nizard, R., Thomas, T., Peyre, M., Liotard, J.P., Boileau, P., Marc, T., Dromard, C., Steyer, E., Bardin, T., Orcel, P., and Walch, G., (2009). Contribution of Clinical Tests to the Diagnosis of Rotator Cuff Disease: A Systematic Literature Review. **Joint Bone Spine** 76(1); p.15-9.
268. Itoi, E., Hsu, H.C., Carmichael, S.W., Morrey, B.F., and An, K.N., (1995). Morphology of the Torn Rotator Cuff. **Journal of Anatomy** 186(2); p.429-34.
269. Coleman, S.H., Fealy, S., Ehteshami, J.R., MacGillivray, J.D., Altchek, D.W., Warren, R.F., and Turner, A.S., (2003). Chronic Rotator Cuff Injury and Repair Model in Sheep. **Journal of Bone and Joint Surgery - American Version** 85-A(12); p.2391-402.
270. Barton, E.R., Gimbel, J.A., Williams, G.R., and Soslowsky, L.J., (2005). Rat Supraspinatus Muscle Atrophy after Tendon Detachment. **Journal of Orthopaedic Research** 23(2); p.259-65.
271. Steinbacher, P., Tauber, M., Kogler, S., Stoiber, W., Resch, H., and Sanger, A.M., (2010). Effects of Rotator Cuff Ruptures on the Cellular and Intracellular Composition of the Human Supraspinatus Muscle. **Tissue and Cell** 42(1); p.37-41.
272. Melis, B., Nemoz, C., and Walch, G., (2009). Muscle Fatty Infiltration in Rotator Cuff Tears: Descriptive Analysis of 1688 Cases. **Orthopaedics and Traumatology: Surgery and Research** 95(5); p.319-24.
273. Terrier, A., Reist, A., Vogel, A., and Farron, A., (2007). Effect of Supraspinatus Deficiency on Humerus Translation and Glenohumeral Contact Force During Abduction. **Clinical Biomechanics** 22(6); p.645-51.
274. Steenbrink, F., Meskers, C.G.M., Nelissen, R.G.H.H., and de Groot, J.H., (2010). The Relation between Increased Deltoid Activation and Adductor Muscle Activation Due to Glenohumeral Cuff Tears. **Journal of Biomechanics** 43(11); p.2049-54.
275. Williams, G.R., Jr., Rockwood, C.A., Jr., Bigliani, L.U., Iannotti, J.P., and Stanwood, W., (2004). Rotator Cuff Tears: Why Do We Repair Them? **Journal of Bone and Joint Surgery** 86(12); p.2764-76.
276. Watson, E.M. and Sonnabend, D.H., (2002). Outcome of Rotator Cuff Repair. **Journal of Shoulder and Elbow Surgery** 11(3); p.201-11.
277. Hawkins, R.J., Misamore, G.W., and Hobeika, P.E., (1985). Surgery for Full-Thickness Rotator-Cuff Tears. **Journal of Bone and Joint Surgery - American Version** 67(9); p.1349-55.
278. Steenbrink, F., de Groot, J.H., Veeger, H.E.J., Meskers, C.G.M., van de Sande, M.A.J., and Rozing, P.M., (2006). Pathological Muscle Activation Patterns in Patients with Massive Rotator Cuff Tears, with and without Subacromial Anaesthetics. **Manual Therapy** 11(3); p.231-37.
279. Derwin, K.A., Codsi, M.J., Milks, R.A., Baker, A.R., McCarron, J.A., and Iannotti, J.P., (2009). Rotator Cuff Repair Augmentation in a Canine Model with Use of a Woven Poly-L-Lactide Device. **Journal of Bone and Joint Surgery - American Version** 91(5); p.1159-71.
280. Huang, C.-Y., Wang, V.M., Pawluk, R.J., Bucchieri, J.S., Levine, W.N., Bigliani, L.U., Mow, V.C., and Flatow, E.L., (2005). Inhomogeneous Mechanical Behavior of the Human Supraspinatus Tendon under Uniaxial Loading. **Journal of Orthopaedic Research** 23(4); p.924-30.
281. Maman, E., Harris, C., White, L., Tomlinson, G., Shashank, M., and Boynton, E., (2009). Outcome of Nonoperative Treatment of Symptomatic Rotator Cuff Tears Monitored by Magnetic Resonance Imaging. **Journal of Bone and Joint Surgery - American Version** 91(8); p.1898-906.
282. Itoi, J. and Morioka, T., (2003). Surgical Treatment for Large and Massive Tears of the Rotator Cuff. **International Orthopaedics** 27(4); p.228-31.
283. Post, M., Silver, R., and Singh, M., (1983). Rotator Cuff Tear. Diagnosis and Treatment. **Clinical Orthopaedics and Related Research** 173(p.78-91.
284. DePalma, A.F., (2008). Surgical Anatomy of the Rotator Cuff and the Natural History of Degenerative Periarthritis. **Clinical Orthopaedics and Related Research** 466(3); p.543–51.

285. Wening, J.D., Hollis, R.F., Hughes, R.E., and Kuhn, J.E., (2002). Quantitative Morphology of Full Thickness Rotator Cuff Tears. **Clinical Anatomy** 15(1); p.18-22.
286. Gwilym, S.E., Watkins, B., Cooper, C.D., Harvie, P., Auplish, S., Pollard, T.C., Rees, J.L., and Carr, A.J., (2009). Genetic Influences in the Progression of Tears of the Rotator Cuff. **Journal of Bone and Joint Surgery - British Version** 91(7); p.915-7.
287. Xu, Y. and Murrell, G.A., (2008). The Basic Science of Tendinopathy. **Clinical Orthopaedics and Related Research** 466(7); p.1528-38.
288. Fehringer, E.V., Sun, J., VanOeveren, L.S., Keller, B.K., and Matsen, F.A., 3rd, (2008). Full-Thickness Rotator Cuff Tear Prevalence and Correlation with Function and Co-Morbidities in Patients Sixty-Five Years and Older. **Journal of Shoulder and Elbow Surgery** 17(6); p.881-5.
289. Bjorkenheim, J.M., Paavolainen, P., Ahovuo, J., and Slatis, P., (1988). Surgical Repair of the Rotator Cuff and Surrounding Tissues. Factors Influencing the Results. **Clinical Orthopaedics and Related Research** 236); p.148-53.
290. Longo, U.G., Oliva, F., Denaro, V., and Maffulli, N., (2008). Oxygen Species and Overuse Tendinopathy in Athletes. **Disabil Rehabil** 30(20-22); p.1563-71.
291. Luo, Z.P., Hsu, H.C., Grabowski, J.J., Morrey, B.F., and An, K.N., (1998). Mechanical Environment Associated with Rotator Cuff Tears. **Journal of Shoulder and Elbow Surgery** 7(6); p.616-20.
292. Seki, N., Itoi, E., Shibuya, Y., Wakabayashi, I., Sano, H., Sashi, R., Minagawa, H., Yamamoto, N., Abe, H., Kikuchi, K., Okada, K., and Shimada, Y., (2008). Mechanical Environment of the Supraspinatus Tendon: Three-Dimensional Finite Element Model Analysis. **Journal of Orthopaedic Science** 13(4); p.348-53.
293. Oh, J.H., Kim, J.Y., Lee, H.K., and Choi, J.A., (2010). Classification and Clinical Significance of Acromial Spur in Rotator Cuff Tear: Heel-Type Spur and Rotator Cuff Tear. **Clinical Orthopaedics and Related Research** 468(6); p.1542-50.
294. Hijioka, A., Suzuki, K., Nakamura, T., and Hojo, T., (1993). Degenerative Change and Rotator Cuff Tears. An Anatomical Study in 160 Shoulders of 80 Cadavers. **Archives of Orthopaedic and Trauma Surgery** 112(2); p.61-4.
295. Bigliani, L.U., Cordasco, F.A., McIlveen, S.J., and Musso, E.S., (1992). Operative Treatment of Failed Repairs of the Rotator Cuff. **Journal of Bone and Joint Surgery - American Version** 74(10); p.1505-15.
296. Neer, C.S., (1983). Impingement Lesions. **Clinical Orthopaedics and Related Research** 173); p.70-7.
297. Wang, J.C. and Shapiro, M.S., (1997). Changes in Acromial Morphology with Age. **Journal of Shoulder and Elbow Surgery** 6(1); p.55-9.
298. Hamid, N., Omid, R., Yamaguchi, K., Steger-May, K., Stobbs, G., and Keener, J.D., (2012). Relationship of Radiographic Acromial Characteristics and Rotator Cuff Disease: A Prospective Investigation of Clinical, Radiographic, and Sonographic Findings. **Journal of Shoulder and Elbow Surgery**. 10.1016/j.jse.2011.09.028
299. Bey, M.J., Ramsey, M.L., and Soslowsky, L.J., (2002). Intratendinous Strain Fields of the Supraspinatus Tendon: Effect of a Surgically Created Articular-Surface Rotator Cuff Tear. **Journal of Shoulder and Elbow Surgery** 11(6); p.562-9.
300. Reilly, P., Amis, A.A., Wallace, A.L., and Emery, R.J., (2003). Mechanical Factors in the Initiation and Propagation of Tears of the Rotator Cuff. Quantification of Strains of the Supraspinatus Tendon in Vitro. **Journal of Bone and Joint Surgery - British Version** 85(4); p.594-9.
301. Nakajima, T., Hughes, R.E., and An, K.N., (2004). Effects of Glenohumeral Rotations and Translations on Supraspinatus Tendon Morphology. **Clinical Biomechanics** 19(6); p.579-85.
302. Lake, S.P., Miller, K.S., Elliott, D.M., and Soslowsky, L.J., (2010). Tensile Properties and Fiber Alignment of Human Supraspinatus Tendon in the Transverse Direction Demonstrate Inhomogeneity, Nonlinearity, and Regional Isotropy. **Journal of Biomechanics** 43(4); p.727-32.
303. Szczesny, S.E., Liu, S.S., Peloquin, J., Elliott, D.M., and Soslowsky, L.J., (2012). Regional Material Properties of the Infraspinatus Tendon Differ from Those of the Supraspinatus. In **Orthopaedic Research Society Annual Meeting**, Orthopaedic Research Society, San Francisco.
304. Clark, J.M. and Harryman, D.T., (1992). Tendons, Ligaments, and Capsule of the Rotator Cuff. Gross and Microscopic Anatomy. **Journal of Bone and Joint Surgery** 74(5); p.713-25.
305. Vogel, K.G., (2003). Tendon Structure and Response to Changing Mechanical Load. **Journal of Musculoskeletal and Neuronal Interactions** 3(4); p.323-5; discussion 33-4.

306. Screen, H.R., Shelton, J.C., Chhaya, V.H., Kayser, M.V., Bader, D.L., and Lee, D.A., (2005). The Influence of Noncollagenous Matrix Components on the Micromechanical Environment of Tendon Fascicles. **Annals of Biomedical Engineering** 33(8); p.1090-9.
307. Nakajima, T., Rokuuma, N., Hamada, K., Tomatsu, T., and Fukuda, H., (1994). Histologic and Biomechanical Characteristics of the Supraspinatus Tendon: Reference to Rotator Cuff Tearing. **Journal of Shoulder and Elbow Surgery** 3(2); p.79-87.
308. Itoi, E., Berglund, L.J., Grabowski, J.J., Schultz, F.M., Growney, E.S., Morrey, B.F., and An, K.N., (1995). Tensile Properties of the Supraspinatus Tendon. **Journal of Orthopaedic Research** 13(4); p.578-84.
309. McGough, R.L., Debski, R.E., Taskiran, E., Fu, F.H., and Woo, S.L., (1996). Mechanical Properties of the Long Head of the Biceps Tendon. **Knee Surgery, Sports Traumatology, Arthroscopy** 3(4); p.226-9.
310. Rathbun, J.B. and Macnab, I., (1970). The Microvascular Pattern of the Rotator Cuff. **Journal of Bone and Joint Surgery - British Version** 52(3); p.540-53.
311. Ling, S.C., Chen, C.F., and Wan, R.X., (1990). A Study on the Vascular Supply of the Supraspinatus Tendon. **Surgical and Radiologic Anatomy** 12(3); p.161-5.
312. Adler, R.S., Fealy, S., Rudzki, J.R., Kadrmas, W., Verma, N.N., Pearle, A., Lyman, S., and Warren, R.F., (2008). Rotator Cuff in Asymptomatic Volunteers: Contrast-Enhanced Us Depiction of Intratendinous and Peritendinous Vascularity. **Radiology** 248(3); p.954-61.
313. Riley, G.P., Curry, V., DeGroot, J., van El, B., Verzijl, N., Hazleman, B.L., and Bank, R.A., (2002). Matrix Metalloproteinase Activities and Their Relationship with Collagen Remodelling in Tendon Pathology. **Matrix Biology : Journal of the International Society for Matrix Biology** 21(2); p.185-95.
314. Shirachi, I., Gotoh, M., Mitsui, Y., Yamada, T., Nakama, K., Kojima, K., Okawa, T., Higuchi, F., and Nagata, K., (2011). Collagen Production at the Edge of Ruptured Rotator Cuff Tendon Is Correlated with Postoperative Cuff Integrity. **Arthroscopy: The Journal of Arthroscopic & Related Surgery** 27(9); p.1173-79.
315. Cornell, H., Liang, M., Carr, A., and Hulley, P., (2009). Cell Shape Change and Actin Cytoskeleton Remodeling Drives Human Tenocytes Towards a Chondrocytic Phenotype. **Bone** 44(S1); p.148-48.
316. Matthews, T.J., Hand, G.C., Rees, J.L., Athanasou, N.A., and Carr, A.J., (2006). Pathology of the Torn Rotator Cuff Tendon. Reduction in Potential for Repair as Tear Size Increases. **Journal of Bone and Joint Surgery - British Version** 88(4); p.489-95.
317. Tillander, B., Franzen, L., and Norlin, R., (2002). Fibronectin, Mmp-1 and Histologic Changes in Rotator Cuff Disease. **Journal of Orthopaedic Research** 20(6); p.1358-64.
318. Benson, R.T., McDonnell, S.M., Knowles, H.J., Rees, J.L., Carr, A.J., and Hulley, P.A., (2010). Tendinopathy and Tears of the Rotator Cuff Are Associated with Hypoxia and Apoptosis. **Journal of Bone and Joint Surgery - British Version** 92(3); p.448-53.
319. Riley, G.P., Harrall, R.L., Cawston, T.E., Hazleman, B.L., and Mackie, E.J., (1996). Tenascin-C and Human Tendon Degeneration. **American Journal of Pathology** 149(3); p.933-43.
320. Gimbel, J.A., Van Kleunen, J.P., Mehta, S., Perry, S.M., Williams, G.R., and Soslowsky, L.J., (2004). Supraspinatus Tendon Organizational and Mechanical Properties in a Chronic Rotator Cuff Tear Animal Model. **Journal of Biomechanics** 37(5); p.739-49.
321. Yang, S., Park, H.S., Flores, S., Levin, S.D., Makhsous, M., Lin, F., Koh, J., Nuber, G., and Zhang, L.Q., (2009). Biomechanical Analysis of Bursal-Sided Partial Thickness Rotator Cuff Tears. **Journal of Shoulder and Elbow Surgery** 18(3); p.379-85.
322. Andarawis-Puri, N., Ricchetti, E.T., and Soslowsky, L.J., (2009). Interaction between the Supraspinatus and Infraspinatus Tendons: Effect of Anterior Supraspinatus Tendon Full-Thickness Tears on Infraspinatus Tendon Strain. **America Journal of Sports Medicine** 37(9); p.1831-9.
323. Lo, I.K., Boorman, R., Marchuk, L., Hollinshead, R., Hart, D.A., and Frank, C.B., (2005). Matrix Molecule Mrna Levels in the Bursa and Rotator Cuff of Patients with Full-Thickness Rotator Cuff Tears. **Arthroscopy: The Journal of Arthroscopic & Related Surgery** 21(6); p.645-51.
324. Sano, H., Ishii, H., Trudel, G., and Uhthoff, H.K., (1999). Histologic Evidence of Degeneration at the Insertion of 3 Rotator Cuff Tendons: A Comparative Study with Human Cadaveric Shoulders. **Journal of Shoulder and Elbow Surgery** 8(6); p.574-79.
325. Shindle, M.K., Chen, C.C.T., Robertson, C., DiTullio, A.E., Paulus, M.C., Clinton, C.M., Cordasco, F.A., Rodeo, S.A., and Warren, R.F., (2011). Full-Thickness Supraspinatus Tears Are Associated

with More Synovial Inflammation and Tissue Degeneration Than Partial-Thickness Tears. **Journal of Shoulder and Elbow Surgery** 20(6); p.917-27.

326. Sano, H., Ishii, H., Yeadon, A., Backman, D.S., Brunet, J.A., and Uhthoff, H.K., (1997). Degeneration at the Insertion Weakens the Tensile Strength of the Supraspinatus Tendon: A Comparative Mechanical and Histologic Study of the Bone-Tendon Complex. **Journal of Orthopaedic Research** 15(5); p.719-26.
327. Doughty, M.J. and Bergmanson, J.P., (2005). Resolution and Reproducibility of Measures of the Diameter of Small Collagen Fibrils by Transmission Electron Microscopy--Application to the Rabbit Corneal Stroma. **Micron** 36(4); p.331-43.
328. Lake, S.P., Sheth, P.M., O'Neil, A.M., Raghupathy, R., and Barocas, V.H., (2012). Highly Inhomogeneous Spatial Properties of Human Supraspinatus Tendon Quantified Via Biaxial Mechanical Testing and Anisotropic Inverse Mechanics. In **Orthopaedic Research Society Annual Meeting**, Orthopaedic Research Centre, San Fancisco, CA, USA.
329. Magnusson, S.P., Qvortrup, K., Larsen, J.O., Rosager, S., Hanson, P., Aagaard, P., Krogsgaard, M., and Kjaer, M., (2002). Collagen Fibril Size and Crimp Morphology in Ruptured and Intact Achilles Tendons. **Matrix Biology : Journal of the International Society for Matrix Biology** 21(4); p.369-77.
330. Ploetz, E., (1938). Funktioneller Bau Und Funktionelle Anpassung Der Gleitsehnen. **Z. Orthop** 67(p.212-34.
331. Dennis, A., (2007). Photo-Bleaching and Automatic Baseline Correction for Raman Spectroscopy. Published by PerkinElmer, Inc. Accessed on. Available from
332. Cabassi, F., Casu, B., and Perlin, A.S., (1978). Infrared Absorption and Raman Scattering of Sulfate Groups of Heparin and Related Glycosaminoglycans in Aqueous-Solution. **Carbohydrate Research** 63(Jun); p.1-11.
333. Silver, F.H., Freeman, J.W., and Seehra, G.P., (2003). Collagen Self-Assembly and the Development of Tendon Mechanical Properties. **Journal of Biomechanics** 36(10); p.1529-53.
334. Bank, R.A., TeKoppele, J.M., Oostingh, G., Hazleman, B.L., and Riley, G.P., (1999). Lysylhydroxylation and Non-Reducible Crosslinking of Human Supraspinatus Tendon Collagen: Changes with Age and in Chronic Rotator Cuff Tendinitis. **Annals of the Rheumatic Diseases** 58(1); p.35-41.
335. Andarawis-Puri, N., Ricchetti, E.T., and Soslowsky, L.J., (2009). Rotator Cuff Tendon Strain Correlates with Tear Propagation. **Journal of Biomechanics** 42(2); p.158-63.
336. Longo, U.G., Franceschi, F., Ruzzini, L., Rabitti, C., Morini, S., Maffulli, N., Forriol, F., and Denaro, V., (2007). Light Microscopic Histology of Supraspinatus Tendon Ruptures. **Knee Surgery, Sports Traumatology, Arthroscopy** 15(11); p.1390-4.
337. Riley, G.P., Harrall, R.L., Constant, C.R., Chard, M.D., Cawston, T.E., and Hazleman, B.L., (1994). Tendon Degeneration and Chronic Shoulder Pain: Changes in the Collagen Composition of the Human Rotator Cuff Tendons in Rotator Cuff Tendinitis. **Annals of the Rheumatic Diseases** 53(6); p.359-66.
338. Samiric, T., Parkinson, J., Ilic, M.Z., Cook, J., Feller, J.A., and Handley, C.J., (2009). Changes in the Composition of the Extracellular Matrix in Patellar Tendinopathy. **Matrix Biology : Journal of the International Society for Matrix Biology** 28(4); p.230-6.
339. Jarvinen, T.A., Jarvinen, T.L., Kannus, P., Jozsa, L., and Jarvinen, M., (2004). Collagen Fibres of the Spontaneously Ruptured Human Tendons Display Decreased Thickness and Crimp Angle. **Journal of Orthopaedic Research** 22(6); p.1303-9.
340. Jozsa, L. and Kannus, P., (1997). Histopathological Findings in Spontaneous Tendon Ruptures. **Scandinavian Journal of Medicine and Science in Sports** 7(2); p.113-8.
341. Chaudhury, S., Dicko, C., Burgess, M., Vollrath, F., and Carr, A.J., (2011). Fourier Transform Infrared Spectroscopic Analysis of Normal and Torn Rotator-Cuff Tendons. **Journal of Bone and Joint Surgery - British Version** 93(3); p.370-7.
342. Fallon, K., Purdam, C., Cook, J., and Lovell, G., (2008). A ''Polypill'' for Acute Tendon Pain in Athletes with Tendinopathy? **Journal of Science and Medicine in Sport** 11(3); p.235-38.
343. Wei, A.S., Callaci, J.J., Juknelis, D., Marra, G., Tonino, P., Freedman, K.B., and Wezeman, F.H., (2006). The Effect of Corticosteroid on Collagen Expression in Injured Rotator Cuff Tendon. **Journal of Bone and Joint Surgery - American Version** 88(6); p.1331-8.
344. Mikolyzk, D.K., Wei, A.S., Tonino, P., Marra, G., Williams, D.A., Himes, R.D., Wezeman, F.H., and Callaci, J.J., (2009). Effect of Corticosteroids on the Biomechanical Strength of Rat Rotator Cuff Tendon. **Journal of Bone and Joint Surgery - American Version** 91(5); p.1172-80.

345. Poulsen, R.C., Carr, A.J., and Hulley, P.A., (2011). Protection against Glucocorticoid-Induced Damage in Human Tenocytes by Modulation of Erk, Akt, and Forkhead Signaling. **Endocrinology** 152(2); p.503-14.
346. Poulsen, R.C., Carr, A.J., and Hulley, P.A., (2011). Protection against Glucocorticoid-Induced Damage in Human Tenocytes by Modulation of Erk, Akt, and Forkhead Signaling. **Endocrinology** 152(2); p.503-14.
347. Akpinar, S., Hersekli, M.A., Demirors, H., Tandogan, R.N., and Kayaselcuk, F., (2002). Effects of Methylprednisolone and Betamethasone Injections on the Rotator Cuff: An Experimental Study in Rats. **Advances in Therapy** 19(4); p.194-201.
348. Tillander, B., Franzen, L.E., Karlsson, M.H., and Norlin, R., (1999). Effect of Steroid Injections on the Rotator Cuff: An Experimental Study in Rats. **Journal of Shoulder and Elbow Surgery** 8(3); p.271-4.
349. Kapetanos, G., (1982). The Effect of the Local Corticosteroids on the Healing and Biomechanical Properties of the Partially Injured Tendon. **Clinical Orthopaedics and Related Research** 163(p.170-9.
350. Rockwood, C.A., Jr., Williams, G.R., Jr., and Burkhead, W.Z., Jr., (1995). Debridement of Degenerative, Irreparable Lesions of the Rotator Cuff. **Journal of Bone and Joint Surgery - American Version** 77(6); p.857-66.
351. Gartsman, G.M. and Milne, J.C., (1995). Articular Surface Partial-Thickness Rotator Cuff Tears. **Journal of Shoulder and Elbow Surgery** 4(6); p.409-15.
352. Ellman, H., Kay, S.P., and Wirth, M., (1993). Arthroscopic Treatment of Full-Thickness Rotator Cuff Tears: 2- to 7-Year Follow-up Study. **Arthroscopy: The Journal of Arthroscopic & Related Surgery** 9(2); p.195-200.
353. Brox, J.I., Staff, P.H., Ljunggren, A.E., and Brevik, J.I., (1993). Arthroscopic Surgery Compared with Supervised Exercises in Patients with Rotator Cuff Disease (Stage Ii Impingement Syndrome). **British Medical Journal** 307(6909); p.899-903.
354. Dines, D.M., Moynihan, D.P., Dines, J.S., and McCann, P., (2006). Irreparable Rotator Cuff Tears: What to Do and When to Do It; the Surgeon's Dilemma. **Journal of Bone and Joint Surgery-American Volume** 88A(10); p.2294-302.
355. Harryman, D.T., 2nd, Mack, L.A., Wang, K.Y., Jackins, S.E., Richardson, M.L., and Matsen, F.A., 3rd, (1991). Repairs of the Rotator Cuff. Correlation of Functional Results with Integrity of the Cuff. **Journal of Bone and Joint Surgery - American Version** 73(7); p.982-9.
356. Bishop, J., Klepps, S., Lo, I.K., Bird, J., Gladstone, J.N., and Flatow, E.L., (2006). Cuff Integrity after Arthroscopic Versus Open Rotator Cuff Repair: A Prospective Study. **Journal of Shoulder and Elbow Surgery** 15(3); p.290-9.
357. Bedi, A., Dines, J., Warren, R.F., and Dines, D.M., (2010). Massive Tears of the Rotator Cuff. **Journal of Bone and Joint Surgery - American Version** 92(9); p.1894-908.
358. Galatz, L.M., Rothermich, S.Y., Zaegel, M., Silva, M.J., Havlioglu, N., and Thomopoulos, S., (2005). Delayed Repair of Tendon to Bone Injuries Leads to Decreased Biomechanical Properties and Bone Loss. **Journal of Orthopaedic Research** 23(6); p.1441-7.
359. Gerber, C., Schneeberger, A.G., Beck, M., and Schlegel, U., (1994). Mechanical Strength of Repairs of the Rotator Cuff. **Journal of Bone and Joint Surgery - British Version** 76(3); p.371-80.
360. Duquin, T.R., Buyea, C., and Bisson, L.J., (2010). Which Method of Rotator Cuff Repair Leads to the Highest Rate of Structural Healing? **The American Journal of Sports Medicine** 38(4); p.835-41.
361. MacGillivray, J.D., Fealy, S., Terry, M.A., Koh, J.L., Nixon, A.J., and Warren, R.F., (2006). Biomechanical Evaluation of a Rotator Cuff Defect Model Augmented with a Bioresorbable Scaffold in Goats. **Journal of Shoulder and Elbow Surgery** 15(5); p.639-44.
362. Gerber, C., Fuchs, B., and Hodler, J., (2000). The Results of Repair of Massive Tears of the Rotator Cuff. **Journal of Bone and Joint Surgery - American Version** 82(4); p.505-15.
363. Ma, C.B., MacGillivray, J.D., Clabeaux, J., Lee, S., and Otis, J.C., (2004). Biomechanical Evaluation of Arthroscopic Rotator Cuff Stitches. **Journal of Bone and Joint Surgery - American Version** 86-A(6); p.1211-6.
364. Schneeberger, A.G., von Roll, A., Kalberer, F., Jacob, H.A., and Gerber, C., (2002). Mechanical Strength of Arthroscopic Rotator Cuff Repair Techniques: An in Vitro Study. **Journal of Bone and Joint Surgery - American Version** 84-A(12); p.2152-60.
365. Cummins, C.A. and Murrell, G.A., (2003). Mode of Failure for Rotator Cuff Repair with Suture Anchors Identified at Revision Surgery. **Journal of Shoulder and Elbow Surgery** 12(2); p.128-33.

366. Mura, N., O'Driscoll, S.W., Zobitz, M.E., Heers, G., and An, K.N., (2003). Biomechanical Effect of Patch Graft for Large Rotator Cuff Tears: A Cadaver Study. **Clinical Orthopaedics and Related Research** 415(415); p.131-8.
367. Paulos, L.E., Rosenberg, T.D., Grewe, S.R., Tearse, D.S., and Beck, C.L., (1992). The Gore-Tex Anterior Cruciate Ligament Prosthesis. A Long-Term Followup. **America Journal of Sports Medicine** 20(3); p.246-52.
368. Chen, X., Qi, Y.Y., Wang, L.L., Yin, Z., Yin, G.L., Zou, X.H., and Ouyang, H.W., (2008). Ligament Regeneration Using a Knitted Silk Scaffold Combined with Collagen Matrix. **Biomaterials** 29(27); p.3683-92.
369. Grood, E.S. and Noyes, F.R., (1976). Cruciate Ligament Prosthesis: Strength, Creep, and Fatigue Properties. **Journal of Bone and Joint Surgery - American Version** 58(8); p.1083-8.
370. Ozaki, J., Fujimoto, S., Masuhara, K., Tamai, S., and Yoshimoto, S., (1986). Reconstruction of Chronic Massive Rotator Cuff Tears with Synthetic Materials. **Clinical Orthopaedics and Related Research** 202(p.173-83.
371. Kimura, A., Aoki, M., Fukushima, S., Ishii, S., and Yamakoshi, K., (2003). Reconstruction of a Defect of the Rotator Cuff with Polytetrafluoroethylene Felt Graft. Recovery of Tensile Strength and Histocompatibility in an Animal Model. **Journal of Bone and Joint Surgery - British Version** 85(2); p.282-7.
372. She, Z., Jin, C., Huang, Z., Zhang, B., Feng, Q., and Xu, Y., (2008). Silk Fibroin/Chitosan Scaffold: Preparation, Characterization, and Culture with Hepg2 Cell. **Journal of Materials Science. Materials in Medicine** 19(12); p.3545-53.
373. Wahl, D.A., (2007). Collagen-Hydroxyapatite Scaffolds for Bone Tissue Engineering. Submitted for the degree of Dissertation/Thesis at
374. Guidoin, M.-F., Marois, Y., Bejui, J., Poddevin, N., King, M.W., and Guidoin, R., (2000). Analysis of Retrieved Polymer Fiber Based Replacements for the Acl. **Biomaterials** 21(23); p.2461-74.
375. Horan, R.L., Antle, K., Collette, A.L., Wang, Y., Huang, J., Moreau, J.E., Volloch, V., Kaplan, D.L., and Altman, G.H., (2005). In Vitro Degradation of Silk Fibroin. **Biomaterials** 26(17); p.3385-93.
376. Turner, I.G. and Thomas, N.P., (1990). Comparative Analysis of Four Types of Synthetic Anterior Cruciate Ligament Replacement in the Goat--in Vivo Histological and Mechanical Findings. **Biomaterials** 11(5); p.321-29.
377. Ling, H.Y., Angeles, J.G., and Horodyski, M.B., (2009). Biomechanics of Latissimus Dorsi Transfer for Irreparable Posterosuperior Rotator Cuff Tears. **Clinical Biomechanics** 24(3); p.261-6.
378. Clancy, W.G., Jr., Narechania, R.G., Rosenberg, T.D., Gmeiner, J.G., Wisnefske, D.D., and Lange, T.A., (1981). Anterior and Posterior Cruciate Ligament Reconstruction in Rhesus Monkeys. **Journal of Bone and Joint Surgery - American Version** 63(8); p.1270-84.
379. Arnoczky, S.P., Tarvin, G.B., and Marshall, J.L., (1982). Anterior Cruciate Ligament Replacement Using Patellar Tendon - an Evaluation of Graft Revascularization in the Dog. **Journal of Bone and Joint Surgery-American Volume** 64(2); p.217-24.
380. Magermans, D.J., Chadwick, E.K., Veeger, H.E., van der Helm, F.C., and Rozing, P.M., (2004). Biomechanical Analysis of Tendon Transfers for Massive Rotator Cuff Tears. **Clinical Biomechanics** 19(4); p.350-7.
381. Dopirak, R., Bond, J.L., and Snyder, S.J., (2007). Arthroscopic Total Rotator Cuff Replacement with an Acellular Human Dermal Allograft Matrix. **International Journal of Shoulder Surgery** 1(Journal Article); p.7-15.
382. Dejardin, L.M., Arnoczky, S.P., Ewers, B.J., Haut, R.C., and Clarke, R.B., (2001). Tissue-Engineered Rotator Cuff Tendon Using Porcine Small Intestine Submucosa - Histologic and Mechanical Evaluation in Dogs. **American Journal of Sports Medicine** 29(2); p.175-84.
383. Fini, M., Torricelli, P., Giavaresi, G., Rotini, R., Castagna, A., and Giardino, R., (2007). In Vitro Study Comparing Two Collageneous Membranes in View of Their Clinical Application for Rotator Cuff Tendon Regeneration. **Journal of Orthopaedic Research** 25(1); p.98-107.
384. Badhe, S.P., Lawrence, T.M., Smith, F.D., and Lunn, P.G., (2008). An Assessment of Porcine Dermal Xenograft as an Augmentation Graft in the Treatment of Extensive Rotator Cuff Tears. **Journal of Shoulder and Elbow Surgery** 17(S1); p.35-39.
385. Bond, J.L., Dopirak, R.M., Higgins, J., Burns, J., and Snyder, S.J., (2008). Arthroscopic Replacement of Massive, Irreparable Rotator Cuff Tears Using a Graftjacket Allograft: Technique and Preliminary Results. **Arthroscopy: The Journal of Arthroscopic & Related Surgery** 24(4); p.403-09.

386. Liden, B.A. and Simmons, M., (2009). Histologic Evaluation of a 6-Month Graftjacket Matrix Biopsy Used for Achilles Tendon Augmentation. **Journal of the American Podiatric Medical Association** 99(2); p.104-07.
387. Badylak, S.F., (2004). Xenogeneic Extracellular Matrix as a Scaffold for Tissue Reconstruction. **Transplant Immunology** 12(3-4); p.367-77.
388. Sclamberg, S.G., Tibone, J.E., Itamura, J.M., and Kasraeian, S., (2004). Six-Month Magnetic Resonance Imaging Follow-up of Large and Massive Rotator Cuff Repairs Reinforced with Porcine Small Intestinal Submucosa. **Journal of Shoulder and Elbow Surgery** 13(5); p.538-41.
389. Walton, J.R., Bowman, N.K., Khatib, Y., Linklater, J., and Murrell, G.A.C., (2007). Restore Orthobiologic Implant: Not Recommended for Augmentation of Rotator Cuff Repairs. **Journal of Bone and Joint Surgery** 89(4); p.786-91.
390. Schlegel, T.F., Hawkins, R.J., Lewis, C.W., Motta, T., and Turner, A.S., (2006). The Effects of Augmentation with Swine Small Intestine Submucosa on Tendon Healing under Tension: Histologic and Mechanical Evaluations in Sheep. **America Journal of Sports Medicine** 34(2); p.275-80.
391. MacBride, J., (2006). Materials for Cartilage Engineering Scaffolds. Submitted for the degree of MEng at University of Oxford.
392. Badylak, S.F. and Gilbert, T.W., (2008). Immune Response to Biologic Scaffold Materials. **Seminars in Immunology** 20(2); p.109-16.
393. Geiger, M., Li, R.H., and Friess, W., (2003). Collagen Sponges for Bone Regeneration with Rhbmp-2. **Advanced Drug Delivery Reviews** 55(12); p.1613-29.
394. Gopferich, A., (1996). Mechanisms of Polymer Degradation and Erosion. **Biomaterials** 17(2); p.103-14.
395. Sengers, B.G., Taylor, M., Please, C.P., and Oreffo, R.O., (2007). Computational Modelling of Cell Spreading and Tissue Regeneration in Porous Scaffolds. **Biomaterials** 28(10); p.1926-40.
396. Guo, C., Sheng, X.B., Chu, C.L., Dong, Y.S., Pu, Y.P., and Lin, P.H., (2009). A Cellular Automaton Simulation of the Degradation of Porous Polylactide Scaffold: I. Effect of Porosity. **Materials Science & Engineering C-Materials for Biological Applications** 29(6); p.1950-58.
397. Agrawal, C.M., McKinney, J.S., Lanctot, D., and Athanasiou, K.A., (2000). Effects of Fluid Flow on the in Vitro Degradation Kinetics of Biodegradable Scaffolds for Tissue Engineering. **Biomaterials** 21(23); p.2443-52.
398. Mainil-Varlet, P., Cordey, J., and Gogolewski, S., (1997). Resorbable Polymeric Inserts as a Means of Enhancing Fixation of Fractures of Porotic Bones : I. Stability of Mechanical Properties and Viscoelasticity of the Inserts Aged in Vitro. **Biomaterials** 18(4); p.289-93.
399. Pistner, H., Bendix, D.R., Muhling, J., and Reuther, J.F., (1993). Poly(L-Lactide): A Long-Term Degradation Study in Vivo. Part Iii. Analytical Characterization. **Biomaterials** 14(4); p.291-8.
400. Wu, L. and Ding, J., (2005). Effects of Porosity and Pore Size on in Vitro Degradation of Three-Dimensional Porous Poly(D,L-Lactide-Co-Glycolide) Scaffolds for Tissue Engineering. **Journal of Biomedical Materials Research - Part A** 75(4); p.767-77.
401. Hutmacher, D.W., (2000). Scaffolds in Tissue Engineering Bone and Cartilage. **Biomaterials** 21(24); p.2529-43.
402. Yahyouche, A., Zhidao, X., Czernuszka, J.T., and Clover, A.J.P., (2011). Macrophage-Mediated Degradation of Crosslinked Collagen Scaffolds. **Acta Biomaterialia** 7(1); p.278-86.
403. Shea, K.P., McCarthy, M.B., Ledgard, F., Arciero, C., Chowaniec, D., and Mazzocca, A.D., (2010). Human Tendon Cell Response to Seven Commercially Available Extracellular Matrix Materials: An in Vitro Study. **Arthroscopy: The Journal of Arthroscopic & Related Surgery** 26(9); p.1181-8.
404. Stoll, C., John, T., Endres, M., Rosen, C., Kaps, C., Kohl, B., Sittinger, M., Ertel, W., and Schulze-Tanzil, G., (2010). Extracellular Matrix Expression of Human Tenocytes in Three-Dimensional Air-Liquid and Plga Cultures Compared with Tendon Tissue: Implications for Tendon Tissue Engineering. **Journal of Orthopaedic Research** 28(9); p.1170-7.
405. Charulatha, V. and Rajaram, A., (2003). Influence of Different Crosslinking Treatments on the Physical Properties of Collagen Membranes. **Biomaterials** 24(5); p.759-67.
406. Oliveira, S.M., Ringshia, R.A., Legeros, R.Z., Clark, E., Yost, M.J., Terracio, L., and Teixeira, C.C., (2010). An Improved Collagen Scaffold for Skeletal Regeneration. **Journal of Biomedical Materials Research - Part A** 94(2); p.371-9.

407. Haugh, M.G., Murphy, C.M., McKiernan, R.C., Altenbuchner, C., and O'Brien, F.J., (2011). Crosslinking and Mechanical Properties Significantly Influence Cell Attachment, Proliferation, and Migration within Collagen Glycosaminoglycan Scaffolds. **Tissue Eng Part A** 17(9-10); p.1201-8.
408. Cao, D., Liu, W., Wei, X., Xu, F., Cui, L., and Cao, Y., (2006). In Vitro Tendon Engineering with Avian Tenocytes and Polyglycolic Acids: A Preliminary Report. **Tissue Engineering** 12(5); p.1369-77.
409. Chen, G., Liu, D., Maruyama, N., Ohgushi, H., Tanaka, J., and Tateishi, T., (2004). Cell Adhesion of Bone Marrow Cells, Chondrocytes, Ligament Cells and Synovial Cells on a Plga-Collagen Hybrid Mesh. **Materials Science and Engineering: C** 24(6-8); p.867-73.
410. Powell, H.M. and Boyce, S.T., (2006). Edc Cross-Linking Improves Skin Substitute Strength and Stability. **Biomaterials** 27(34); p.5821-7.
411. Willows, A., Fan, Q., Ismail, F., Vaz, C.M., Tomlins, P.E., Mikhalovska, L.I., Mikhalovsky, S.V., James, S.L., Vadgama, P., and Wasikiewicz, J., (2008). Assessment of Tissue Scaffold Degradation Using Electrochemical Techniques. **Acta Biomaterialia** 4(3); p.686-96.
412. Mazzocca, A.D., McCarthy, M.B., Arciero, C., Jhaveri, A., Obopilwe, E., Rincon, L., Wyman, J., Gronowicz, G.A., and Arciero, R.A., (2007). Tendon and Bone Responses to a Collagen-Coated Suture Material. **Journal of Shoulder and Elbow Surgery** 16(S5); p.S222-30.
413. Kanematsu, A., Yamamoto, S., Ozeki, M., Noguchi, T., Kanatani, I., Ogawa, O., and Tabata, Y., (2004). Collagenous Matrices as Release Carriers of Exogenous Growth Factors. **Biomaterials** 25(18); p.4513-20.
414. Olde Damink, L.H.H., Dijkstra, h, P.J., Luyn, h, M.J.A.v., Wachem, and h, P.B.v., (1995). Crosslinking of Dermal Sheep Collagen Using Hexamethylene Diisocyanate. **Journal of Materials Science: Materials in Medicine** 6(7); p.429-34.
415. Olde Damink, L.H.H., Dijkstra, P.J., van Luyn, M.J.A., van Wachem, P.B., Nieuwenhuis, P., and Feijen, J., (1996). In Vitro Degradation of Dermal Sheep Collagen Cross-Linked Using a Water-Soluble Carbodiimide. **Biomaterials** 17(7); p.679-84.
416. Wolfgang, F., (1998). Collagen – Biomaterial for Drug Delivery. **European Journal of Pharmaceutics and Biopharmaceutics** 45(2); p.113-36.
417. Olde Damink, L.H.H., Dijkstra, P.J., Luyn, M.J.A., and van Wachem, P.B., (1995). Glutaraldehyde as a Crosslinking Agent for Collagen-Based Biomaterials. **Journal of Materials Science: Materials in Medicine** 6(8); p.460-72.
418. Bitar, M., Brown, R.A., Salih, V., Kidane, A.G., Knowles, J.C., and Nazhat, S.N., (2008). Effect of Cell Density on Osteoblastic Differentiation and Matrix Degradation of Biomimetic Dense Collagen Scaffolds. **Biomacromolecules** 9(1); p.129-35.
419. Kato, Y.P., Dunn, M.G., Zawadsky, J.P., Tria, A.J., and Silver, F.H., (1991). Regeneration of Achilles Tendon with a Collagen Tendon Prosthesis. Results of a One-Year Implantation Study. **Journal of Bone and Joint Surgery - American Version** 73(4); p.561-74.
420. Goldstein, J.D., Tria, A.J., Zawadsky, J.P., Kato, Y.P., Christiansen, D., and Silver, F.H., (1989). Development of a Reconstituted Collagen Tendon Prosthesis. A Preliminary Implantation Study. **Journal of Bone and Joint Surgery - American Version** 71(8); p.1183-91.
421. Awad, H.A., Butler, D.L., Boivin, G.P., Smith, F.N., Malaviya, P., Huibregtse, B., and Caplan, A.I., (1999). Autologous Mesenchymal Stem Cell-Mediated Repair of Tendon. **Tissue Eng** 5(3); p.267-77.
422. Lamberti, P.M. and Wezeman, F.H., (2002). Biologic Behavior of an in Vitro Hydrated Collagen Gel-Human Tenocyte Tendon Model. **Clinical Orthopaedics and Related Research** 397(p.414-23.
423. Grinnell, F. and Lamke, C.R., (1984). Reorganization of Hydrated Collagen Lattices by Human Skin Fibroblasts. **Journal of Cell Science** 66(1); p.51-63.
424. Gigante, A., Cesari, E., Busilacchi, A., Manzotti, S., Kyriakidou, K., Greco, F., Di Primio, R., and Mattioli-Belmonte, M., (2009). Collagen I Membranes for Tendon Repair: Effect of Collagen Fiber Orientation on Cell Behavior. **Journal of Orthopaedic Research** 27(6); p.826-32.
425. Zhong, S., Teo, W.E., Zhu, X., Beuerman, R.W., Ramakrishna, S., and Yung, L.Y., (2006). An Aligned Nanofibrous Collagen Scaffold by Electrospinning and Its Effects on in Vitro Fibroblast Culture. **Journal of Biomedical Materials Research - Part A** 79(3); p.456-63.
426. Yao, L., Bestwick, C.S., Bestwick, L.A., Maffulli, N., and Aspden, R.M., (2006). Phenotypic Drift in Human Tenocyte Culture. **Tissue Eng** 12(7); p.1843-9.
427. Sachlos, E., Reis, N., Ainsley, C., Derby, B., and Czernuszka, J.T., (2003). Novel Collagen Scaffolds with Predefined Internal Morphology Made by Solid Freeform Fabrication. **Biomaterials** 24(8); p.1487-97.

428. Byth, H.A., McHunu, B.I., Dubery, I.A., and Bornman, L., (2001). Assessment of a Simple, Non-Toxic Alamar Blue Cell Survival Assay to Monitor Tomato Cell Viability. **Phytochem Anal** 12(5); p.340-6.
429. Graham, C.E., Waitkoff, H.K., and Hier, S.W., (1949). The Amino Acid Content of Some Scleroproteins. **Journal of Biological Chemistry** 177(2); p.529-32.
430. Moore, S.M., McMahon, P.J., Azemi, E., and Debski, R.E., (2005). Bi-Directional Mechanical Properties of the Posterior Region of the Glenohumeral Capsule. **Journal of Biomechanics** 38(6); p.1365-9.
431. Bigi, A., Cojazzi, G., Roveri, N., and Koch, M.H.J., (1987). Differential Scanning Calorimetry and X-Ray-Diffraction Study of Tendon Collagen Thermal-Denaturation. **International Journal of Biological Macromolecules** 9(6); p.363-67.
432. Hakimi, O., Chaudhury, S., Murphy, R., and Carr, A., (2012). Differential Growth on Sutures of Tendon Cells Derived from Torn Human Rotator Cuff. **Journal of biomedical materials research. Part B, Applied biomaterials** 100(3); p.685-92.
433. Martini, F.H., (1998). Fundamentals of Anatomy and Physiology, 4th edition. Edited by D.K. Brake.Prentice Hall, Inc., New Jersey.
434. Vernon, R.B. and Gooden, M.D., (2002). An Improved Method for the Collagen Gel Contraction Assay. **In vitro cellular & developmental biology - Animal** 38(2); p.97-101.
435. Schulz Torres, D., M. Freyman, T., Yannas, I.V., and Spector, M., (2000). Tendon Cell Contraction of Collagen–Gag Matrices in Vitro: Effect of Cross-Linking. **Biomaterials** 21(15); p.1607-19.
436. Gibson, L.J., (1988). Cellular Solids : Structure & Properties. Edited by M.F. Ashby. Oxford : Pergamon Press, Oxford.
437. Gough, K.M., Zelinski, D., Wiens, R., Rak, M., and Dixon, I.M.C., (2003). Fourier Transform Infrared Evaluation of Microscopic Scarring in the Cardiomyopathic Heart: Effect of Chronic At1 Suppression. **Analytical Biochemistry** 316(2); p.232-42.
438. Veiz, A., (1967). Intact Collagen. In **Treatise on Collagen**. Edited by G.N. Ramachandran Academic Press, London.
439. Elden, H.R. and Boucek, R.J., (1960). The Successive-Extraction of Collagen from Hide Powder. **Journal of Colloid Science** 15(2); p.97-104.
440. Everaerts, F., Torrianni, M., Hendriks, M., and Feijen, J., (2007). Quantification of Carboxyl Groups in Carbodiimide Cross-Linked Collagen Sponges. **Journal of Biomedical Materials Research - Part A** 83(4); p.1176-83.
441. Ramachandran, G.N. and Gould, B.S., (1967-1968). Treatise on Collagen. Edited by.Academic Press, London.
442. Traub, W. and Piez, K.A., (1971). The Chemistry and Structure of Collagen. In **Advances in Protein Chemistry**. Edited by J.T.E. C.B. Anfinsen and Frederic, M.R. Academic Press,

Appendix

Macro for Colour Thresholding Analysis in ImageJ, courtesy of Dr. D. Haley

```
//To be run on a stack of RGB images.
run("Threshold Colour");
// Threshold Colour v1.12a------
// Autogenerated macro, single images only!
// G. Landini 27/Sep/2010.
//
min=newArray(3);
max=newArray(3);
filter=newArray(3);
a=getTitle();
run("HSB Stack");
run("Convert Stack to Images");
selectWindow("Hue");
rename("0");
selectWindow("Saturation");
rename("1");
selectWindow("Brightness");
rename("2");
min[0]=131;
max[0]=168;
filter[0]="pass";
min[1]=0;
max[1]=255;
filter[1]="pass";
min[2]=0;
max[2]=255;
filter[2]="pass";
for (i=0;i<3;i++){
  selectWindow(""+i);
  setThreshold(min[i], max[i]);
  run("Convert to Mask");
  if (filter[i]=="stop")  run("Invert");
}
imageCalculator("AND create", "0","1");
imageCalculator("AND create", "Result of 0","2");
for (i=0;i<3;i++){
  selectWindow(""+i);
  close();
}
selectWindow("Result of 0");
close();
selectWindow("Result of Result of 0");
rename(a);

// Threshold Colour ------------
run("Make Binary");
run("Measure");
run("Open Next");
```